

Gasification of algal biomass in supercritical water with the potential of energy and nutrients recovery

zur Erlangung des akademischen Grades eines
Doktors der Ingenieurwissenschaften (Dr.-Ing.)

von der KIT-Fakultät für Chemieingenieurwesen und Verfahrenstechnik
des Karlsruher Instituts für Technologie (KIT)
genehmigte

DISSERTATION

von

M.Sc. Sherif H.N. Elsayed
aus Kairo, Ägypten

Tag der mündlichen Prüfung: 30.10.2019

Erstgutachter: Prof. Dr.-Ing. Jörg Sauer

Zweitgutachter: Prof. Dr.-Ing. Michael Türk

Acknowledgment

I am showing my deep gratitude to Dr. Nikolaos Boukis for his constant support over the past years, since I was admitted to doctoral studies at Karlsruhe Institute of Technology (KIT) and became part of his work group. I ultimately appreciate the valuable opportunity he granted me to work in an excellent scientific environment and develop my academic as well as my technical skills. From him and given his expertise in the field of hydrothermal conversion, I learned many aspects which have been useful to understand. I consider our discussions as the most interesting point of my work at KIT. Moreover, I take the chance to sincerely thank Prof. Dr.-Ing. Jörg Sauer for supervising my work, his friendly attitude, commitment and for his continuous willingness to cooperate whenever possible.

The laboratory assistance of Ms. Elena Hauer and Mr. Karl Weiss cannot be disregarded. Therefore, I would like to praise them for the efforts they exerted to keep everything related to the experimental work in a good order. In addition, I want to acknowledge the vital role of the analytics department at the institute of Catalysis Research and Technology (IKFT) with regards to samples analyses and keeping the work progress at a decent level. Also, I would like to thank David Böning for his assistance with initiating process simulation, Chiara Boscagli and Manuel Gentzen for being helpful with the analysis of additional samples. The experimental activities leading to this work was conducted in cooperation with the project partner represented by Dr. Marin Kerner from Strategic Science Consult GmbH and Dominik Patzelt in the University of Hamburg, using the financial aid of the Agency for Renewable Resources (FNR) – funding code 22407012, so I acknowledge their role in this context.

If I am to express my gratitude to someone for the rest of my life, this would be my parents and family back home in Maadi/Cairo, who supported me unconditionally and are still doing. Thank you very much from the bottom of my heart for your tremendous love and outstanding backup, ever since I moved to Germany to find my own path in life. Last but not least, I would like to show my appreciation to Barbara Gadinger and her loving family. It has been my pleasure getting to know you. Your kindness over the past years has been remarkable.

Sherif Hanafy Nasr Elsayed
شريف حنفي نصر السيد
May 2019

Summary

Some of the efforts which have been made to investigate the gasification of biomass in supercritical water are presented in this work. The work is basically motivated by the increasing demand for energy worldwide and the limitations that fossil fuels currently have in terms of existence, long-term availability, supply as well as their negative impact on the environment. The exploitation of renewable energies should be the adopted trend and the shift to abundant sources such as biomass is continuously increasing. Several strategies and roadmaps have been suggested to push forward in this direction in the coming decades.

As a renewable energy source, microalgae have shown a good capability of rapid growth and biomass productivity due to their simple structure and direct utilization of light. Therefore, several configurations of closed systems or Photobioreactors have been developed to implement in outdoor cultivation of algal cells under controlled conditions (e.g. mixing, nutrients and air supply) using sunlight. In this context, the algal biomass of the species *A. obliquus* was used as the feedstock for gasification under supercritical conditions due to its reported high biomass productivity. The biomass was cultivated outdoors through the project partner in Hamburg (Strategic Science Consult GmbH) within flat-panel Photobioreactors using a pilot unit as well as the novel façade structure of the BIQ-House. These research activities were conducted in the framework of the project PHYKON (*Prototyp zur hydrothermalen Konversion*, funding code 22407012) that is supported by the Agency for Renewable Resources (FNR).

On the other hand, the hydrothermal conversion processes have been the focus of many workgroups in the recent decades. This is supported by a number of advantages that are not available through classical conversional processes. Processing biomass in its already-existing moisture or water content is a major benefit under supercritical conditions, eliminating the need to dry biomass, which is an energy-consuming step, and exploiting the changed properties of water such as density and viscosity at elevated temperatures and pressures. The unique properties of the water molecule above its critical point ($T > 374\text{ °C}$, $P > 22.1\text{ MPa}$) helps creating a reactive medium that enables the decomposition and conversion of any organic materials in wet biomass streams with their various sources and compositions.

Considering supercritical water gasification (SCWG) in this study, a combustible gas mixture which contains mainly hydrogen (H_2), carbon dioxide (CO_2), methane (CH_4) as well as ethane (C_2H_6) is the major product. The scope of work was to conduct the gasification of algal biomass under supercritical conditions, and investigate the influence of major process variables such as temperature and feed concentration on the system performance. This was experimentally realized on continuous operation using three laboratory units with tubular reactors. Given the operation of these units, the process of SCWG consists mainly of three zones; feed pre-heating, reaction and phase separation.

System performance was evaluated in terms of the carbon gasification efficiency (CGE), the composition of the product gas as well as the quality of the residual water stream (e.g. its content of total organic carbon, TOC) leaving the process after conversion. The availability of inorganic nutrients, being part of the wet biomass prior to SCWG, was investigated in both the aqueous and solid phases resulting from the process. The distribution and recovery of these inorganic elements was also evaluated based on the system configurations presented in this work.

The influence of the reactor temperature was experimentally determined in the range of 600–690 °C, whereas the feed concentration was varied between 2.5 and 20 wt% total solids at the highest temperature. The operating pressure was kept in most of the experiments at 28 MPa. An alkali metal salt (K_2CO_3 or $KHCO_3$) was used as a homogeneous catalyst in a concentration (K^+) of 1500 ppm. This concentration was varied in some experiments, reaching up to 3000 ppm, to evaluate the influence of salt addition on system performance. The mean residence time for the entire experiments was in the range of 1 to 4 minutes, depending on the corresponding flow rates (set between 0.2 and 1 $kg \cdot h^{-1}$), operating conditions and reactor volume (~ 0.2, 0.3 and 0.4 liter).

High carbon gasification efficiency, a maximum value of 96.4%, was calculated from the experimental work using a biomass concentration of 2.5 wt% (figure S1). The efficiency decreased noticeably (to 82%) upon introducing the highest concentration (20 wt%). Extended continuous operation over two days (50 hours) was successfully achieved. Increased hydrogen yield was observed during the experiments, when higher temperature and lower feed concentrations were set. To the contrary, the yield of combustible hydrocarbons, mainly methane and ethane, was clearly higher at lower temperatures and higher feed concentrations.

These findings related to the yield of H₂ and CH₄ come in accordance with several previous works (refer to ch. 4.4 and 4.5) and are also supported by a thermodynamic basis. Moreover, the contribution of water molecules to the overall gas production at diluted concentrations was distinguished and it confirms the reactive role of water under supercritical conditions.

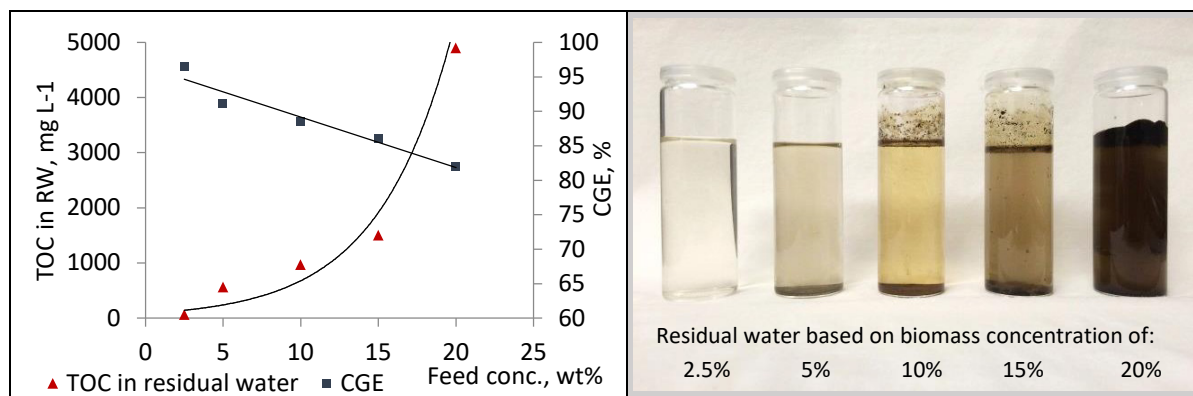


Figure S1 - Influence of feed concentration on carbon gasification efficiency and the TOC levels in the residual water – Operating conditions: T = 690 °C, P = 280 bar (data from LUII)

A further finding was the contribution of purging or flushing the units with water after each experiment on hot and cold basis to the net recovery of inorganic residues. Solids precipitation, including valuable elements such as phosphorus, is a major challenge associated with biomass in SCWG. A major fraction of phosphorous tended to migrate to the solid phase during operation, a phenomenon related to low solubility in the supercritical regime that was reported in earlier works. A total recovery up to 89% of phosphorus was achieved, of which up to 62% was found in the solid phase. About 94% of potassium was recovered and the purging contributed in gaining a major fraction in the aqueous phase. The recovery percentages of micro-nutrients at optimum conditions were (Mg: 84.5%, Ca: 79.2%, Si: 64.7% and S: 64.5%), with Mg and Ca being detected in higher amounts in the solid phase.

Utilizing the aqueous phase of SCWG including its content of inorganic elements serves a crucial role for recycling natural resources. Around 95% of the total nitrogen content in the algal biomass can be recovered after SCWG in the aqueous form and be potentially used for algal growth, reducing the cost of the fresh nutrients. For this purpose, the residual water was applied a culture medium for the algal growth indoors on a lab-scale using artificial illumination. The residual water was tested first in the raw state as well as after treatment using two techniques. The first treatment technique is done via activated carbon filtration and the second is through an ultraviolet (UV) light treatment. Growth inhibition was observed and

referred to the existence of potentially-toxic substances which evolved during gasification as side products or unreacted intermediates. Upon treatment, these toxic substances were eliminated and the cultivation was made possible.

Process simulation with the aid of the software *Aspen Plus* was also conducted in this work. The goal of simulation was to evaluate the influence of the temperature and feed concentration on the composition of the gaseous species and compare the results with those obtained from the experimental work. A broader range of temperatures (450 - 750 °C) and feed concentrations (2.5 - 25 wt%) was applied in the simulated models. The hydrothermal gasification as well as the gas compositions were mainly calculated via the reactor model (R-Gibbs), which applies the minimization of the Gibbs free energy. The produced data showed comparable trends to the experimental results, especially regarding the composition of hydrogen and methane. An example of the effect of feed concentration on the composition of the major produced gaseous species is shown below in figure S2 for both model-based and experimental results.

In addition, a useful quantitative analysis of the basic energy requirements of SCWG (e.g. thermal energy, power consumption for pumping) was obtained at different operating conditions. The thermal energy recovery of the hot product stream was found to have a major significance in the process, as it represents the highest share of the total thermal energies which is necessary for maintaining a good efficiency.

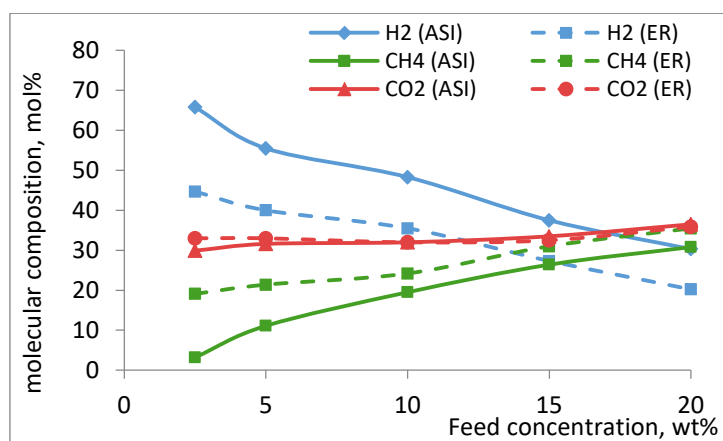


Figure S2 – Influence of feedstock concentration on the composition of the major components in the produced gas based on a simulated feedstock model (ASI) and experimental results (ER)

[Conditions: P = 280 bar, feed conc. 10 wt%]

As part of the proposal included in the framework of the project PHYKON, a basic concept which aims at coupling algal cultivation and supercritical water gasification was initiated. The concept is demonstrated below in figure S3. In this scheme, all energy and material streams are utilized according to the specific needs of each process. These streams include the residual water of SCWG as well as the inorganic nutrients that are needed for the growth of microalgae. The gaseous stream of SCWG consists of a combustible gas mixture along with carbon dioxide. Carbon dioxide, produced at high pressure, can be separated and used as the main carbon source for algal cultivation. A fraction of the combustible gas mixture can be thermally utilized to supply any make-up heat required within the system and the exhaust gas would then increase the share of CO₂ contribution for cultivation.

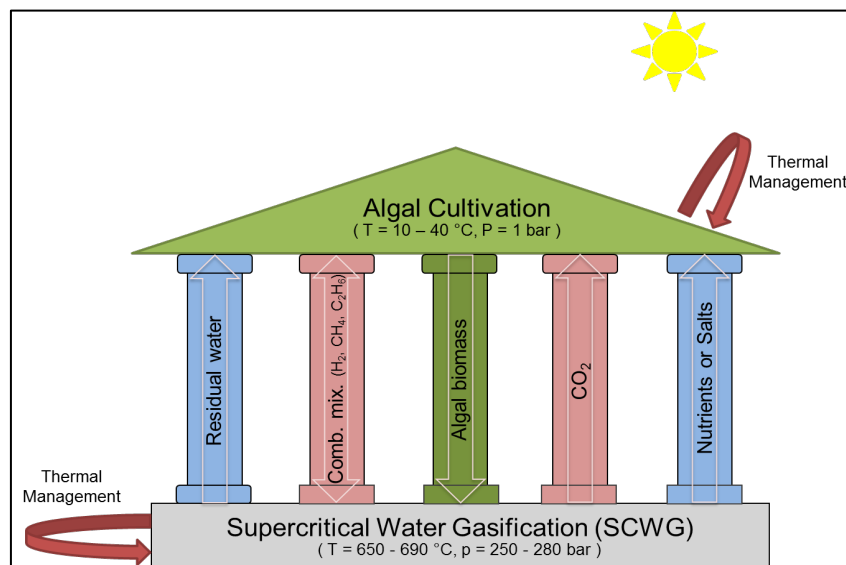


Figure S3 – A proposed concept for coupling algal cultivation and supercritical water gasification taking into account energy and nutrients recovery

Thermal management is also present in the integrated system. The excess thermal energy from sunlight in the case of cultivation or the heating required to maintain the operation of SCWG can be utilized by the means of circulating (heat exchange) or storing for use at a later point for cultivation during cold days. In the framework of this study, some work packages have been conducted on the road to address the aforementioned concept. This includes the two core processes (outdoor cultivation and supercritical water gasification), as well as the application of the residual water as the cultivation medium for the growth of microalgae.

Zusammenfassung

In der vorliegenden Dissertation wurde die Vergasung von Mikroalgen in überkritischem Wasser untersucht. Die Relevanz der Arbeit ergibt sich aus dem weltweit steigenden Energiebedarf und der beschränkten Verfügbarkeit von fossilen Brennstoffen. Außerdem können durch den Einsatz von erneuerbaren Energiequellen die negativen Auswirkungen der fossilen Brennstoffe auf die Umwelt reduziert werden. Die Nutzung erneuerbarer Energien sollte selbstverständlich werden. Dafür spricht, dass die Verlagerung hinzu reichlich regenerativen Quellen, wie z. B. der Biomasse, kontinuierlich zunimmt. Es wurden bereits auf verschiedenen Ebenen Strategien und Pläne vereinbart, um den Fortschritt in den kommenden Jahrzehnten zu garantieren.

Mikroalgen haben als eine erneuerbare Energiequelle ein großes Potential, aufgrund ihrer einfachen Struktur und der direkten Nutzung von Licht, sowie der guten Wachstumsgeschwindigkeit und der Biomasseproduktivität. Daher wurden verschiedene geschlossene Kultivierungssystemen oder Photobioreaktoren entwickelt, um die Kultivierung im Freien unter Verwendung von Sonnenlicht und kontrollierten Bedingungen (Mischen, Nährstoffe- und Luftzufuhr) durchzuführen. In diesem Zusammenhang wurde die Mikroalgen *A. obliquus* als Edukt für die Vergasung unter überkritischen Bedingungen eingesetzt. Die Algenbiomasse wurde durch den Projektpartner in Hamburg (Strategic Science Consult GmbH) in Flat-Panel-Photobioreaktoren in einer Pilotanlage sowie der neuartigen Fassade des BIQ-Hauses kultiviert. Diese Forschungsarbeiten wurden im Rahmen des von der Fachagentur Nachwachsende Rohstoffe (FNR) geförderten Projekts PHYKON (Prototyp zur hydrothermalen Konversion, Förderkennzeichen 22407012) durchgeführt.

In den letzten Jahrzehnten ist die hydrothermale Konversion der Schwerpunkt vieler Arbeitsgruppen weltweit gewesen. Dies ist auf mehrere Vorteile zurückzuführen, die durch die klassischen Verfahren nicht erreicht werden können. Der größte Vorteil des Verfahrens besteht darin, dass die Biomasse unter überkritischen Bedingungen im nassen Zustand bearbeitet werden kann. Eine Trocknung der Biomasse ist daher nicht notwendig, wodurch wiederum Energie eingespart werden kann. Zudem werden die besonderen Eigenschaften von Wasser, wie z. B. Dichte und Viskosität, bei erhöhter Temperatur und bei erhöhtem Druck genutzt. Die Eigenschaften der Wassermoleküle im überkritischen Bereich ($T > 374 \text{ °C}$, $P > 22,1 \text{ MPa}$) tragen zur Schaffung eines reaktiven Mediums bei, das den Abbau von organischen Substanzen ermöglicht.

Bei der Vergasung in überkritischem Wasser (SCWG) ist das Produkt ein brennbares Gasgemisch, das hauptsächlich Wasserstoff, Kohlenstoffdioxid, Methan und Ethan enthält. Im Rahmen der experimentellen Arbeiten wurde die Vergasung von Algenbiomasse unter überkritischen Bedingungen durchgeführt und der Einfluss der Hauptprozessvariable (Temperatur und Feedkonzentration) auf die Systemleistung untersucht. Die Untersuchungen wurden im kontinuierlichen Betrieb in drei Laboranlagen mit Rohrreaktoren realisiert. Der Kern des Prozesses besteht aus drei Bereichen; Feed-Vorwärmung, Reaktion und Phasentrennung.

Die Systemleistung wurde in Bezug auf die Menge und Zusammensetzung des Produktgases untersucht; sowie auf die Qualität des Prozessabwassers (z. B. gesamter organischer Kohlenstoff, TOC) nach der Vergasung. Die Verfügbarkeit von anorganischen Elementen, die vor der SCWG Bestandteil der nassen Biomasse waren, wurde sowohl in der aus dem Prozess entstandenen wässrigen als auch in der Feststoff- Phase bewertet. Die Verteilung sowie die Gewinnung dieser anorganischen Nährstoffe wurde ebenfalls anhand der eingesetzten Anlagenkonfigurationen untersucht.

Der Einfluss der Reaktortemperatur wurde im Bereich von 600-690 °C untersucht. Bei der höchsten Temperatur wurde die Konzentration der Biomasse zwischen 2,5 und 20 Gew.% variiert. Der Betriebsdruck wurde meistens bei 28 MPa gehalten. Ein Alkalisalz (K_2CO_3 oder $KHCO_3$) wurde als homogener Katalysator in einer Konzentration (K^+) von 1500 ppm verwendet. Die Konzentration von K^+ wurde in einigen Versuche variiert (bis maximal 3000 ppm), um den Einfluss der Salzzugabe auf den Prozess zu bewerten. Die mittlere Verweilzeit für die gesamten Experimente lag im Bereich von 1 bis 4 Minuten, abhängig von dem entsprechenden Durchfluss (min. / max. $\sim 0,2 / 1 \text{ kg}\cdot\text{h}^{-1}$), den Betriebsbedingungen und dem Reaktorvolumen ($\sim 0,2; 0,3$ und $0,4 \text{ l}$).

Experimentell wurde bei einer Biomassekonzentration von 2,5 Gew.% ein maximaler Kohlenstoff-Vergasungsumsatz (CGE) von 96,4% berechnet (s. Abb. S1). Die CGE sank signifikant ab (auf 82%) wenn die höchste Konzentration (20 Gew.%) genutzt wurde. Ein kontinuierlicher Betrieb über zwei Tage (50 Stunden) wurde erfolgreich durchgeführt. Bei höheren Temperaturen und niedrigeren Feedkonzentrationen wurde eine höhere Wasserstoffausbeute erzielt. Dagegen war die Menge an brennbaren Kohlenwasserstoffen, hauptsächlich Methan und Ethan, bei niedrigeren Temperaturen und höheren Feedkonzentrationen deutlich höher.

Diese Ergebnisse, bezogen auf die Wasserstoff- und Methanausbeute, decken sich mit denen einiger früherer Arbeiten (vgl. Kap. 4.4 und 4.5) und werden auf der Basis der Thermodynamik gestützt. Dazu kommt, dass einen deutlichen Beitrag der Wassermoleküle zu der gesamten Gasproduktion bei niedrigen Konzentrationen gab. So wurde die Reaktionsfähigkeit von Wasser unter überkritischen Bedingungen verdeutlicht.

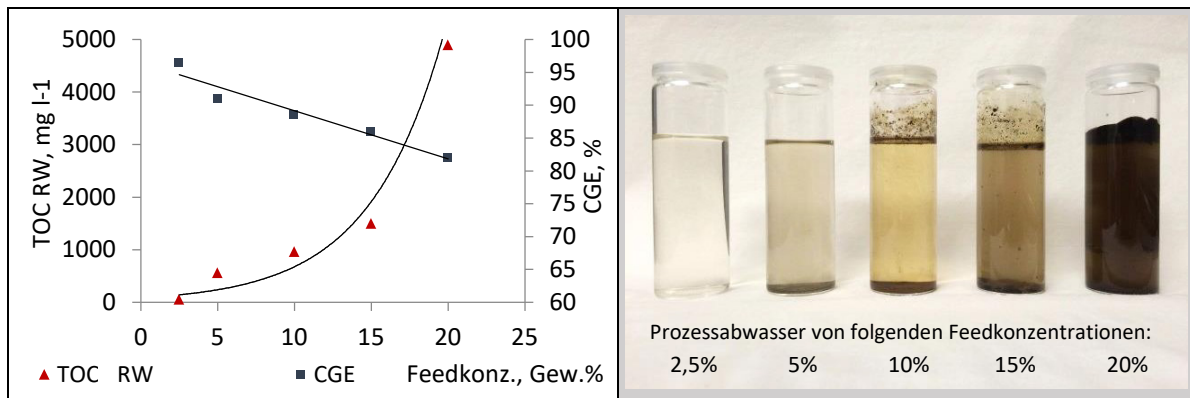


Abbildung S1 – Einfluss der Feedkonzentration auf die CGE und den gesamten organischen Kohlestoffgehalt (TOC) im Prozessabwasser (RW) – Betriebsbedingungen: T = 690°C, P= 280 bar (LUII)

Eine weitere Feststellung war der Beitrag des Spülens mit Wasser in heißem und kaltem Zustand nach jedem Versuch. Dadurch konnten anorganische Rückstände aus dem System wiedergewonnen werden. Die Ablagerung von Feststoffen, einschließlich wertvoller Elemente wie Phosphor, ist eine große Herausforderung bei der SCWG. Der Großteil des Phosphors tendierte dazu, in eine feste Form überzugehen. Dieses Phänomen, welches bereits in früheren Arbeiten beschrieben wurde, hängt mit der geringen Löslichkeit im überkritischen Bereich zusammen. Es wurde eine Wiedergewinnung des Phosphors bis zu 89% erreicht, wovon 62% im festen Zustand gewonnen wurde. Bis zu 94% des Kaliums wurden wiedergewonnen, wobei das Spülen dabei half den Großteil davon in der wässrigen Phase zu überführen.

Die Wiedergewinnung von Mikronährstoffen unter optimalen Bedingungen erzielte folgende Erträge: Mg: 84,5%, Ca: 79,2%, Si: 64,7% und S: 64,5%), wobei Mg und Ca in der festen Phase in höherem Mengen festgestellt wurden. Die Nutzung der wässrigen Phase von SCWG spielt aufgrund des Gehalts an anorganischen Elementen eine wichtige Rolle beim Recycling natürlicher Ressourcen. Es wurden etwa 95% des gesamten Stickstoffgehalts in der Algenbiomasse, nach SCWG, in wässriger Form wiedergewonnen und potenziell für das

Algenwachstum verwendet. Dadurch ist es möglich, die Kosten für die benötigten frischen Nährstoffe zu reduzieren und die Umweltbilanz des Verfahrens zu erhöhen.

Zu diesem Zweck wurde dem Prozessabwasser ein Kulturmedium für das Algenwachstum im Labor mit künstlicher Beleuchtung zugeführt. Das Prozessabwasser wurde sowohl im Rohzustand als auch nach der Behandlung mit zwei Methoden getestet. Zuerst wurde die Aktivkohlefiltration angewendet und dann die ultraviolette (UV-) Bestrahlung als zweite Behandlungsmethode. Die Wachstumshemmung der Mikroalgen wurde durch die Existenz potentiell toxischer Substanzen, die während der Vergasung als Nebenprodukte oder nicht umgesetzte Zwischenprodukte entstanden, verursacht. Bei der Behandlung wurden diese toxischen Substanzen entfernt und die Algenkultivierung im Prozessabwasser war möglich.

Die Prozesssimulation mit Hilfe der Software *Aspen Plus* wurde im Zuge dieser Arbeit durchgeführt. Ziel der Simulation war es, den Einfluss von Temperatur und Feedkonzentration auf die Vergasungsprodukte zu bewerten und die Ergebnisse mit denen der Laborversuche zu vergleichen. In den Modellen wurden ein breiter Bereich von Temperaturen (450 - 750 °C) und Feedkonzentrationen (2,5 - 25 Gew.%) angewendet. Die hydrothermale Vergasung sowie die Gaszusammensetzungen wurden hauptsächlich mit Hilfe des Reaktormodells (R-Gibbs) und durch die Minimierung der Gibbs-Energie berechnet. Die Ergebnisse zeigten vergleichbare Trends zu den experimentellen Ergebnissen, insbesondere hinsichtlich der Zusammensetzung von Wasserstoff und Methan.

Ein Beispiel für den Einfluss der Feedkonzentration auf die Zusammensetzung der produzierten Gase wird in Abbildung S2 dargestellt. In dieser Abbildung sind sowohl die modellgestützten, als auch die experimentellen Ergebnisse dargestellt. Zusätzlich wurde eine quantitative Analyse in Bezug des grundlegenden Energiebedarfs von SCWG (z. B. thermische Energie, Energieverbrauch von Pumpen) bei verschiedenen Betriebsbedingungen durchgeführt. Die thermische Energierückgewinnung des heißen Produktstroms hat eine erhebliche Bedeutung in diesem Prozess, da sie den größten Anteil daran hat, einen hohen thermischen Wirkungsgrad zu erreichen.

Im Rahmen des Projektes PHYKON wurde ein Grundkonzept zur Kopplung von Algenkultivierung und SCWG initiiert. Das Konzept wird nachfolgend in Abbildung S3 dargestellt. In diesem Schema werden alle Energie- und Stoffströme nach Bedarf jedes Prozesses genutzt. Diese Ströme umfassen das Prozessabwasser von SCWG und die

anorganischen Nährstoffe, die für das Wachstum von Mikroalgen benötigt werden. Der gasförmige Strom von SCWG besteht aus einer brennbaren Mischung und Kohlenstoffdioxid. Kohlenstoffdioxid, das unter hohem Druck produziert wird, kann abgetrennt und als die Haupt-Kohlenstoffquelle für die Algenkultivierung verwendet werden. Ein Bruchteil des brennbaren Gasgemisches kann thermisch genutzt werden, um die erforderliche Zusatzwärme innerhalb des Systems zu liefern. Zudem würde sich durch das Abgas ebenfalls der Anteil des CO₂-Beitrags für die Kultivierung erhöhen.

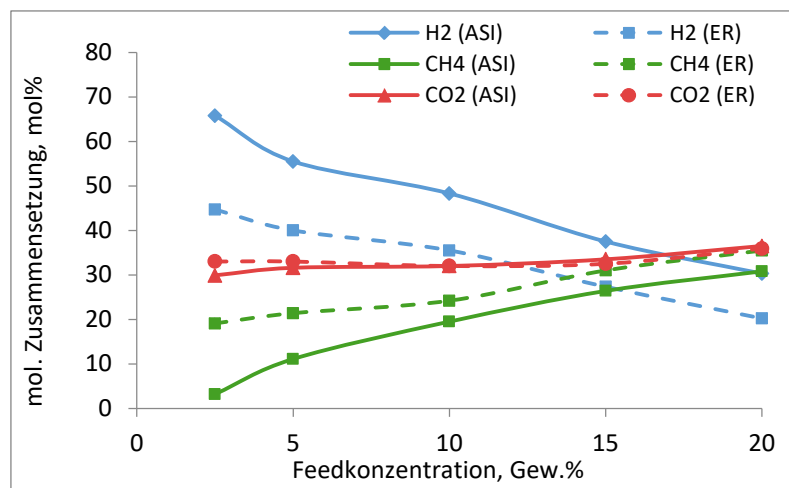


Abbildung S2 – Einfluss der Feedkonzentration auf die Zusammensetzung der Hauptkomponenten des Produktgases basierend auf einem simulierten Feed-Model (ASI) und Laborversuche (ER) [Betriebsbedingungen: P = 280 bar, Feedkonz. 10 Gew.%]

Das Wärmemanagement ist auch im integrierten System vorhanden. Die überschüssige Wärme, die durch Sonnenlicht im Falle der Kultivierung gewonnen wird, kann mittels Speichern zur Verwendung für einen späteren Zeitpunkt der Kultivierung (z. B. während kalter Tage) genutzt werden. Durch Wärmeaustausch kann die Wärme aus den heißen Strömen für den Betrieb von SCWG genutzt werden. Im Rahmen dieser Studie wurden einige Arbeitspakete zur Beurteilung des oben genannten Konzeptes durchgeführt. Dazu gehören die beiden Kernprozesse (Algenkultivierung und die Vergasung in überkritischem Wasser) sowie der Einsatz von Prozessabwasser als Kultivierungsmedium für das Algenwachstum.

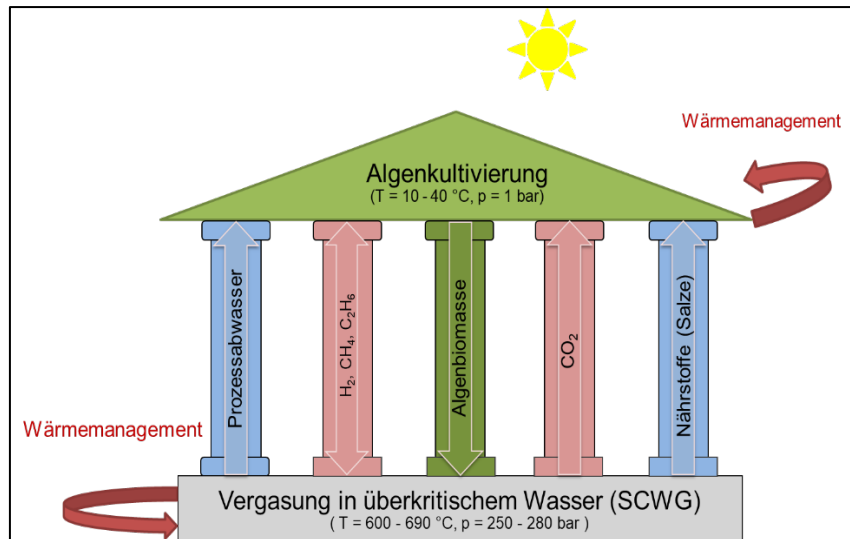


Abbildung S3 – Ein vorgeschlagenes Konzept zur Kopplung von Algenkultivierung und SCWG unter Berücksichtigung der Energie- und Nährstoffgewinnung

Content

Section	Page
▪ Acknowledgment	iii
▪ Summary	iv
▪ Zusammenfassung (Summary in German)	ix
▪ Content	xv
▪ List of tables	xviii
▪ List of figures	xix
▪ Nomenclature	xxi
01. Introduction	1
1.1. Energy supply and demand	1
1.2. Environmental concerns associated with fossil fuel	3
1.3. Renewables as an alternative source of energy	4
1.4. Biomass as a renewable feedstock for energy production	6
1.5. Microalgae as a biomass candidate	7
1.5.1. General overview	7
1.5.2. Cultivation techniques	7
1.5.3. Process parameters for algal cultivation	8
1.6. Typical biomass conversion processes	10
1.6.1. Combustion	10
1.6.2. Pyrolysis	10
1.6.3. Gasification	11
1.6.4. Biochemical conversion	11
1.7. Hydrothermal conversion	12
1.7.1. Hydrothermal Carbonization (HTC)	12
1.7.2. Hydrothermal liquefaction (HTL)	12
1.7.3. Supercritical water gasification (SCWG)	13
1.7.4. Reaction pathways of biomass in near- and supercritical water	15
1.7.5. The catalytic role of salts	18
1.8. References (Ch. 1)	20
02. Literature and Technology Review	26
2.1. Introduction	26
2.2. Feedstock materials and process objectives	26
2.3. Exploitation of algal biomass	29
2.3.1. Hydrothermal carbonization	29
2.3.2. Hydrothermal liquefaction	29
2.3.3. Gasification in supercritical water	30
2.4. Treatment of sewage sludge	35
2.5. Toward process development	37
2.5.1. Slurry pumping	37
2.5.2. Recycling of natural resources	40
2.5.3. System corrosion	43
2.6. References (Ch. 2)	46

03. Materials and Methods	51
3.1. Overview	51
3.2. Biomass production	51
3.3. Feed preparation	54
3.4. Process performance and product analysis	55
3.5. Growth of microalgae using the residual water from gasification	56
3.6. Experimental setup (Supercritical water gasification)	57
3.6.1. Laboratory unit (I)	57
3.6.2. Laboratory unit (II)	58
3.6.3. Laboratory unit (III)	59
3.7. Pre-testing and system startup	60
3.8. Heat supply and temperature control	60
3.9. References (Ch. 3)	62
04. Results and Discussion	63
4.1. Summary of the results from the first laboratory unit I (LUI)	63
4.2. Summary of the results from the second laboratory unit II (LUII)	64
4.3. Summary of the results from the third laboratory unit III (LUIII)	65
4.4. Influence of temperature	66
4.5. Influence of biomass concentration	69
4.6. Influence of dissolved salts addition	73
4.7. Influence of residence time	75
4.8. Assessment of the aqueous phase and the potential of effluent utilization	78
4.9. Cultivation of microalgae using the residual water of gasification	82
4.10. Carbon distribution in the gasification products	83
4.11. Recovery of the nutrients after gasification	85
4.12. References (Ch. 4)	90
05. Process Simulation	92
5.1. Solution strategy	92
5.2. Feedstock decomposition	93
5.3. Algal biomass simulant	94
5.4. Thermodynamic equilibrium	95
5.5. Process Configuration	98
5.6. Results and discussion (Process simulation)	101
5.6.1. Influence of reaction temperature	102
5.6.2. Influence of feed concentration	104
5.6.3. Gasification quotient	105
5.6.4. Energy assessment	107
5.6.5. Overall process efficiency	111
5.7. References (Ch. 5)	113
06. Conclusions and prospects for future works	114

07. List of scientific contributions	117
08. Appendix	118
8.1. Thermo-physical properties of water under sub- and supercritical conditions	118
8.2. Cultivation systems	119
8.3. BIQ house modules	120
8.4. Methods applied for samples analysis	121
8.5. Significance of feed mixing	122
8.6. Analysis of the calorific value of the algal biomass:	123
8.7. Supercritical water gasification of a model solution (Ethanol) at different concentrations	124
8.8. Quality of the residual water from SCWG	125
8.9. Conductivity of the salt brine	126
8.10. Energy content of the gas product from SCWG	127
8.11. Analysis of a complex intermediate of hydrothermal conversion	128
8.12. Analysis of a solid particle using X-ray diffraction (XRD)	130
8.13. Determination of the gas composition	131
8.14. Elemental mapping using scanning electron microscopy (SEM)	132
8.15. Salt extraction mechanisms during supercritical water gasification	133
8.16. Recovery of the micro-nutrients from supercritical water gasification	134
8.17. Process Simulation using Aspen Plus (Selected database components)	135
8.18. Calculation of water properties	136
8.19. Reaction intermediates in the residual water	137
8.20. Coupling algal cultivation and SCWG	138
8.20.1 Conceptual basis	138
8.20.2 Biomass Productivity	140
8.20.3 Layout of the cultivation system	141
8.21. References (Appendix)	143

List of Tables

	Title	Page
Table 1.1	Basic gasification reactions possibly occurring during hydrothermal conversion of biomass	17
Table 2.1	Different types of biomass and some of their basic analyses	28
Table 2.2	Summary of selected works in the field of hydrothermal gasification of algal feedstock	45
Table 3.1	The composition of the nutrient applied for algal cultivation	53
Table 3.2	Elemental composition of the algal biomass feedstock to gasification	54
Table 4.1	Summary of the experimental conditions and obtained results from LUI	63
Table 4.2	Summary of the experimental conditions and obtained results from LUII	64
Table 4.3	Summary of the experimental conditions and obtained results from LUIII	65
Table 4.4	The share of carbon in the aqueous phase of supercritical water gasification	72
Table 4.5	List of existing compounds in the residual water of SCWG	79
Table 4.6	Influence of activated carbon filtration and ultraviolet treatment of the residual water on the phenol index, total carbon (TC) and total nitrogen (TN)	80
Table 4.7	Solid residues from supercritical water gasification and their elemental composition	88
Table 5.1	A combination of conventional compounds achieving similar weight percentage of the basic elements in microalgae	94
Table 5.2	Energy requirements at different temperatures for the two feed types applied (Calculations apply for: 100 kg.h ⁻¹ Feed input, feed conc. = 10 wt%, P = 280 bar).	109
Table 5.3	Energy requirements at different feed concentrations for the two feed types applied (Calculations apply for: 100 kg.h ⁻¹ Feed input, T = 650 °C, P = 280 bar).	109
Table 5.4	Suggested reaction scheme with the corresponding molar conversion for ASI model	112
Table A1.1	Qualitative Comparison between open cultivations systems and Photobioreactors	119
Table A3.1	The methods applied for the analysis of the solid and liquid samples from supercritical water gasification	121
Table A3.2	Elemental analysis of a dried algal biomass sample	123
Table A3.3	Determination of the calorific value of the algal biomass	123
Table A4.1	Summary of the pre-experiments conducted with an ethanol solution	124
Table A4.2	List of the qualitatively detected substances in the aqueous phase of SCWG and the influence of the two treatment methods applied on the removal of these substances	125
Table A4.3	Energy content of the gas product from SCWG [Data from LUII]	127
Table A4.4	Retention time of the chromatogram with possible assignment of few compounds	129
Table A4.5	Chemical formulas matching the structures detected in the XRD analysis	130
Table A4.6	Retention time, composition and component detection based on gas chromatography	131
Table A4.7	Results of the SEM analysis (weight & atomic percentages of the detected elements)	132
Table A5.1	List of the components which were selected from the Aspen database for process simulation	135
Table A5.2	Three properties of water under near and supercritical conditions, given by two references of calculations (NIST and IAPWS) at a pressure of 280 bar	136
Table A5.3	List of the reaction intermediates found in the residual water of gasification	137
Table A6.1	Scenarios based on two biomass productivities and different SCWG throughputs	141

List of Figures

	Title	Page
Fig. S1	Figure S1 - Influence of feed concentration on carbon gasification efficiency and the TOC levels in the residual water	vi
Fig. S2	Figure S2 – Influence of feedstock concentration on the composition of the major components in the produced gas based on a simulated feedstock model (ASI) and experimental results (ER)	vii
Fig. S3	A proposed concept for coupling algal cultivation and supercritical water gasification taking into account energy and nutrients recovery	viii
Abb. S1	Einfluss der Feedkonzentration auf die CGE und den gesamten organischen Kohlestoffgehalt (TOC) im Prozessabwasser	xi
Abb. S2	Einfluss der Feedkonzentration auf die Zusammensetzung der Hauptkomponenten des Produktgases basierend auf einem simulierten Feed-Model (ASI) und Laborversuche (ER)	xiii
Abb. S3	Ein vorgeschlagenes Konzept zur Kopplung von Algenkultivierung und SCWG unter Berücksichtigung der Energie- und Nährstoffgewinnung	xiv
Fig. 1.1	Global energy consumption between 1990 and 2015 (in million tons oil equivalent)	1
Fig. 1.2	Price fluctuation of crude oil (Europe Brent Spot) between 1997 and 2017	2
Fig. 1.3	Annual average global concentrations of CO ₂ in the atmosphere over time and the relevant temperature anomalies	3
Fig. 1.4	Primary energy consumption by source, the ratio of domestic supply to imports and relative shares in 2015, for Germany in 2005 and 2015	4
Fig. 1.5	Global energy supply from renewables in 2015	6
Fig. 1.6	Spectral distribution of solar irradiance	8
Fig. 1.7	Simplified Phase diagram of water	13
Fig. 1.8	Effect of temperature on water properties including density, dielectric constant, dynamic viscosity and specific heat capacity at P = 280 bar	14
Fig. 1.9	A Simplified reaction scheme of biomass conversion in sub- and supercritical water starting from cellulose and identified by key compounds	16
Fig. 1.10	A suggested mechanism for the catalyzed water-gas shift reaction in high temperature pressurized aqueous systems involving a dissolved salt	19
Fig. 2.1	Basic sub-processes involved in hydrothermal gasification (HTG)	34
Fig. 2.2	Illustrative sketch of <i>Feluwa</i> 's hose diaphragm pump	38
Fig. 2.3	Viscosity of different concentrations of milled sec. sludge at different shear rates	39
Fig. 3.1	The novel construction (BIQ house) in Hamburg-Wilhelmsburg	52
Fig. 3.2	Microalgae in the form of slurry (left) and as dried biomass (right)	54
Fig. 3.3	Simplified flow diagram of laboratory unit I with system and process conditions	57
Fig. 3.4	Simplified flow diagram of laboratory unit II with system and process conditions	58
Fig. 3.5	Simplified flow diagram of laboratory unit III with system and process conditions	59
Fig. 3.6	Inner and outer temperature measurements for one of the tubular reactors (LUI)	60
Fig. 3.7	Inner and outer temperature measurement along the preheater in LUIII	61
Fig. 4.1	Influence of temperature on the carbon gasification efficiency (CGE) and the TOC concentration in the residual water – data from LUI	66
Fig. 4.2	Influence of temperature on the carbon gasification efficiency (CGE) and the TOC levels in the residual water – data from LUI	67
Fig. 4.3	Influence of temperature on the gas yield (data from LUII)	68
Fig. 4.4	Influence of biomass concentration on CGE and the TOC levels in the residual water (data from LUII)	69
Fig. 4.5	Influence of biomass concentration on the molar yield of the major gas components at different biomass concentrations (data from LUII)	70
Fig. 4.6	Influence of the dissolved salts addition on the carbon gasification efficiency and	73

	the TOC concentrations in the residual water (data from LUIII)	
Fig. 4.7	Influence the of dissolved salt addition on the yield of the major gas components (data from LUIII)	74
Fig. 4.8	Influence of residence time on the yield of the major gas components (Data from LUIII)	76
Fig. 4.9	Random samples of the residual water resulting from supercritical water gasification	78
Fig. 4.10	Distribution of (a) ionic phosphorus and (b) nitrogen in the aqueous phase of gasification, between the residual water and salt brine (data from LUII)	78
Fig. 4.11	Compared to a standard medium, the growth of <i>A. obliquus</i> in different batches of residual water from SCWG [a] and the effect of RW treatment on the algal growth [b]	82
Fig. 4.12	Distribution of total carbon among the output streams of gasification from: [a] LUII and [b] LUIII	83
Fig. 4.13	Elemental distribution of the inorganic nutrients in the algal biomass	85
Fig. 4.14	Distribution and recovery of the macro-nutrients (N, P and K) from the gasification products from: [a] LUII and [b] LUIII	86
Fig. 4.15	Major contributions of purging to the recovery of N, P and K from supercritical water gasification for: [a] LUII and [b] LUIII	88
Fig. 5.1	Feed decomposition to simpler molecules in the R-Yield reactor model	93
Fig. 5.2	Two suggested conceptual process schemes for the gasification of algal biomass in supercritical water	100
Fig. 5.3	Gas composition from gasification under supercritical conditions for four feed types compared to experimental results	101
Fig. 5.4	Influence of reaction temperature on the composition of the major components in the produced gas for the two models based on FDE and ASI	102
Fig. 5.5	Influence of feed concentration on the composition of the major components in the product gas, compared to experimental results (ER), for the two models based on FDE and ASI	104
Fig. 5.6	Variation of gasification quotient versus temperature and feed concentration	106
Fig. 5.7	Example of the duty shares (power) of supercritical water gasification (ASI model)	107
Fig. 5.8	Overall process steps for the gasification of biomass in supercritical water	110
Fig. 5.9	Overall process efficiency at different feed concentrations [a] and temperatures [b] of the R-Gibbs models (for FDE and ASI) compared to the R-Stoich. model using ASI	112
Fig. A1.1	Major changes which occur to water around the critical point at different pressures	118
Fig. A3.1	Façade elements of the BIQ house: the flat panels reactor modules (PBR)	120
Fig. A3.2	Particles settling without feed mixing at different concentrations after 100 hours	122
Fig. A4.1	Measurements of the conductivity of some samples of the salt brine resulting from supercritical water gasification of algal biomass (LU II)	126
Fig. A4.2	[a] GC-MS chromatogram (with indicated retention time) of a sample extracted from LUIII in the preheating section at a temperature of 390 °C and [b] fragmentation peaks of the compound detected at 22.13 min of retention time.	128
Fig. A4.3	X-ray diffraction analysis of a solid sample extracted after SCWG [Data from LUI]	130
Fig. A4.4	Gas chromatogram [Exp. code ESL13-G7] [Date from LUIII]	131
Fig. A4.5	Elemental mapping using scanning electron microscope (SEM) [Data from LUI]	132
Fig. A4.6	Extraction of inorganic constituents during supercritical water gasification	133
Fig. A4.7	Distribution and recovery of the micro-nutrients (S, Mg, Ca and Si) from the gasification products for: [a] LUII and [b] LUIII	134
Fig. A6.1	Schematic representation of integrating algal cultivation and supercritical water gasification with the potential of nutrients and energy recovery	138
Fig. A6.2	Arrangement of flat panels for large scale cultivation of microalgae	142

Nomenclature

Symbols

c	[mol%]	Concentration
f	[MPa]	Fugacity
G	[J]	Gibbs free Energy
ΔH	[J.mol ⁻¹]	Molar reaction enthalpy
K_{ij}	[-]	Interaction parameter (mixing rules for EoS calculations)
M	[kg.mol ⁻¹]	Molar mass of carbon
m	[kg]	Mass
n	[-]	Total number of moles produced
P	[MPa]	Pressure
R	[J.mol ⁻¹ . K ⁻¹]	Universal gas constant
S	[J.K ⁻¹]	Entropy
T	[°C]	Temperature
V	[m ³]	Volume
w	[-]	Weight fraction of total organic carbon in feed
w	[-]	Eccentric factor (PR-EoS)
Z	[-]	Compressibility factor
α	[-]	Number of carbon atoms in a component i
τ	[s]	Residence time
μ	[J.mol ⁻¹]	Chemical Potential
Φ	[-]	Fugacity coefficient

Sub- and Superscripts

i	Any given component of the produced gas
x	H/C molar ratio
y	O/C molar ratio
$^{\circ}$	Reference conditions or degree (C), depending on the context

Abbreviations

AC / ACF	Activated carbon / Activated carbon filtration
AS	Algal simulant
AFE	Ash forming elements
BPR	Backpressure regulator
BIQ	Bio-intelligent quotient
CGE	Carbon gasification efficiency
CDW	Cell dry weight
CHP	Combined heat and power
CY	Carbon yield
DM	Dry matter
ECE	Energy conversion efficiency
EDX / EDXS	Energy-dispersive x-ray spectroscopy
ER	Experimental results
FDE	Feed decomposition to basic element
FE-SEM	Field emission scanning electron microscope
FRS	Feed reforming to syngas
GC-MS	Gas chromatography-mass spectrometry

GE	Gasification efficiency
Gew.%	German for: weight percent (<i>Gewichtsprozent</i>)
GJ	Gigajoule
GQ	Gasification quotient
HHV	Higher heating value
HTG / HTL / HTC	Hydrothermal gasification / liquefaction / carbonization
HPLC	High performance liquid chromatography
IAPWS	International association for the properties of water and steam
ICP-OES	Inductively coupled plasma-optical emission spectrometry
ID	Internal diameter
LHV	Lower heating value
LSG	laminated safety glass
KJ	Kilojoule
L	Length
LU	Laboratory unit
MM	Molar mass
MTOE	Million tons oil equivalent
OD	Optical density
PAR	Photosynthetically active radiation
PBR	Photo-bioreactor
PC	Progressive cavity (pump type)
PENG-ROB	Peng-Robinson
PNNL	The Pacific Northwest National Laboratory
PR-EoS	Peng-Robinson equation of state
ppm	Parts per million
PVB	polyvinyl butyral
RW	Residual water
RT	Residence time or Reaction time
SB	Salt brine
SCC	Stress corrosion cracking
SCWG / SCWO	Supercritical water gasification / oxidation
SEM	Scanning electron microscope
TIC	Total inorganic carbon
TN (TN _b)	Total nitrogen (Total bounded nitrogen)
TOC	Total organic carbon
TS	Total solids
TWR	Transpiring wall reactor
UV	Ultraviolet
vol%	Volume percent
wt%	Weight percent
XRD	X-ray diffraction

1. Introduction

1.1. Energy supply and demand

The increasing demand for energy with the growing population continues to form an escalating problem during the recent decades. This is in particular the case, especially with the major dependence on common sources, demonstrated in figure 1.1, for energy generation worldwide. To date, fossil fuels including coal, natural gas and oil represent the major sources of energy supply that are used to produce heat and power for heating, cooking, electricity generation as well as transportation. According to statistics conducted by various sources, the global energy consumption has exceeded 13 billion tons of oil equivalent by the end of 2015.

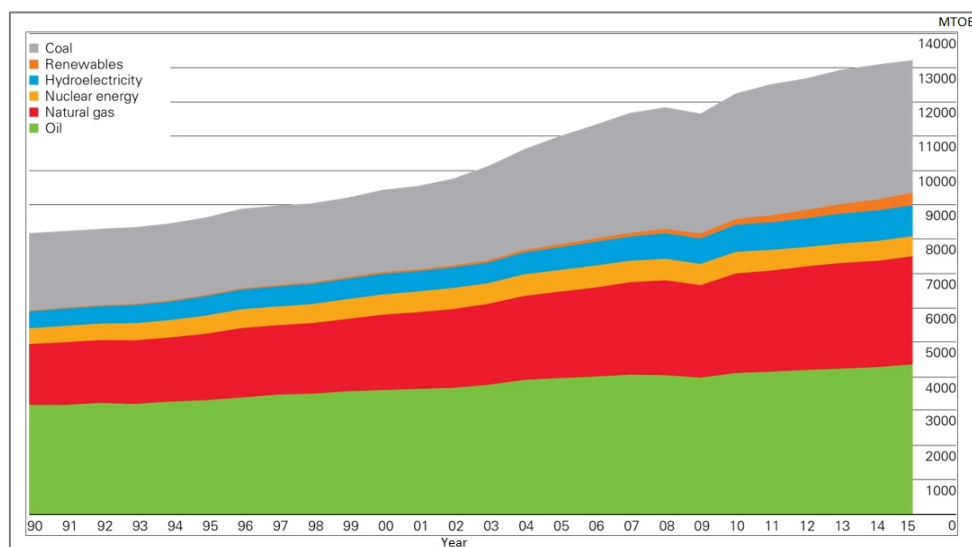


Figure 1.1 – Global energy consumption between 1990 and 2015 (in million tons oil equivalent)¹

According to the information forming the graph above, this number reflects a significant increase, approximately 50%, given the consumption in 1990. On the other hand, the availability of fossil fuel in terms of existence and cost is not present everywhere at the same extent. It rather depends on a number of factors or circumstances such as major global or geopolitical events, which are not necessarily related to the fuel's absolute availability in a certain location. For example, the oil crises in the modern history started in the seventies of the last century, particularly in 1973 and 1979. The spark for the crises was the political disputes in the Middle East, which resulted in a sharp cut-off of oil supplies by major producers at the time.

¹ Source: BP Statistical Review of World Energy 2016

Such a situation led to a rapid increase in oil prices to a high record, rising from \$3.6 per barrel annual average crude oil in 1973 to over \$37 by the end of this decade². The steep increase during the first half of 2008 was the outcome of a significant shortage in the market supply fueled by various incidents in some countries including Venezuela, Nigeria and Iraq³. This resulted in an increase that is accelerated by the rising market demand back then. In the same year, the global economic recession caused the demand for energy to drop off, leading the oil prices to fall from about \$133 to \$40 per barrel between mid- and end of the year respectively⁴, before they relatively stabilize in 2009. A reflection of the price fluctuation is demonstrated in figure 1.2 which shows the average price of the Europe Brent Spot Price over twenty years.

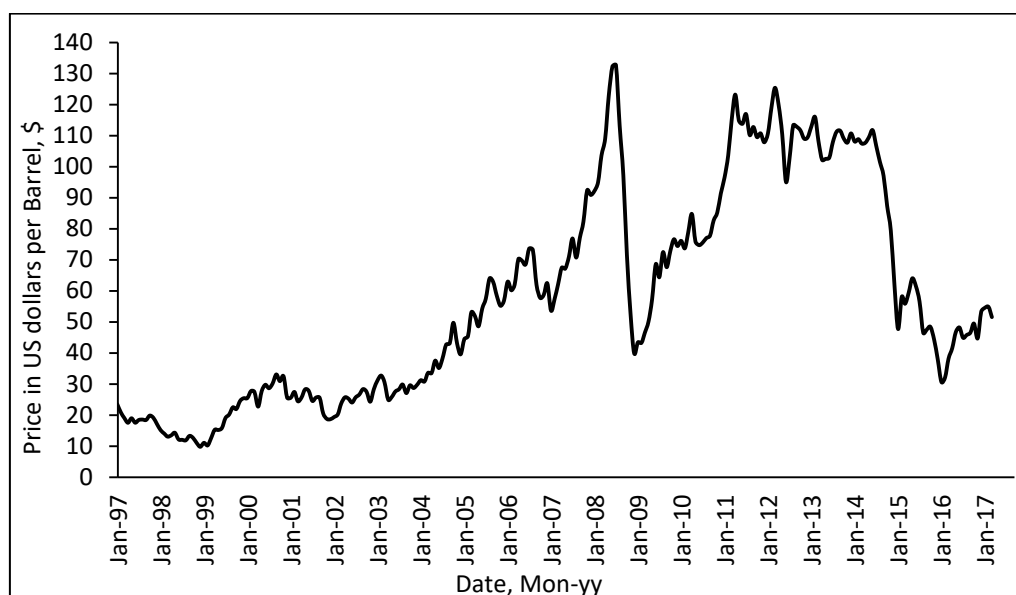


Figure 1.2 – Price fluctuation of crude oil (Europe Brent Spot) between 1997 and 2017 ⁴

On the contrary, an opposite trend occurred when oil prices dropped to low-record values in 1998 (below \$10) and 2014 (below \$50). The reason for the decrease in 1998 was the excess amounts available in the market due to oversupply accompanied by economic recession in East Asia. This caused a major decline in oil demands. In 2014, the increased shale oil production in the United States and the maintained levels of production by OPEC led to the decrease in oil prices. This created a severe pull-back of investments in the oil and gas sectors [Clayton 2015, Dalarossa 2014], followed by a huge wave of job layoff in these fields worldwide.

² Source: InflationData, historical crude oil prices (<https://inflationdata.com>)

³ Source: Resources for the future: (<http://www.rff.org/blog/2009/2008-oil-price-shock-markets-or-mayhem>)

⁴ Source: U.S. Energy Information Administration – Spot prices of crude oils and products

1.2. Environmental concerns associated with fossil fuel

The consumption of fossil fuel results in the release of carbon dioxide. The presence of such a greenhouse gas in earth's atmosphere has become a concern which is directly reflected through the climate change phenomena or global warming. Greenhouse gases such as water vapor, ozone and CO₂ exist in the earth's atmosphere to help keeping its temperatures warm enough to sustain life. This takes place by absorbing and emitting some the solar radiation in the infrared range. However, any deviation from certain concentration of greenhouse gases in the atmosphere will affect the balance of the ecosystem. Ideally, the amount of greenhouses gases is maintained in a certain balance within the atmosphere. The increase of CO₂ levels in the atmosphere has started with the industrial revolution in the eighteenth of the last century. It continues in the recent time due to the increasing anthropogenic activities, mainly related to fossil fuel burning for electricity generation, transportation and industrial processes, beside the change of land use such as deforestation [Quéré *et al.* 2013]. Therefore, CO₂ has been continuously added to the atmosphere at an increasing rate ever since as concluded from figure 1.3, leading global warming that is recognized by a temperature increase relative to average values of previous years (i.e. anomaly).

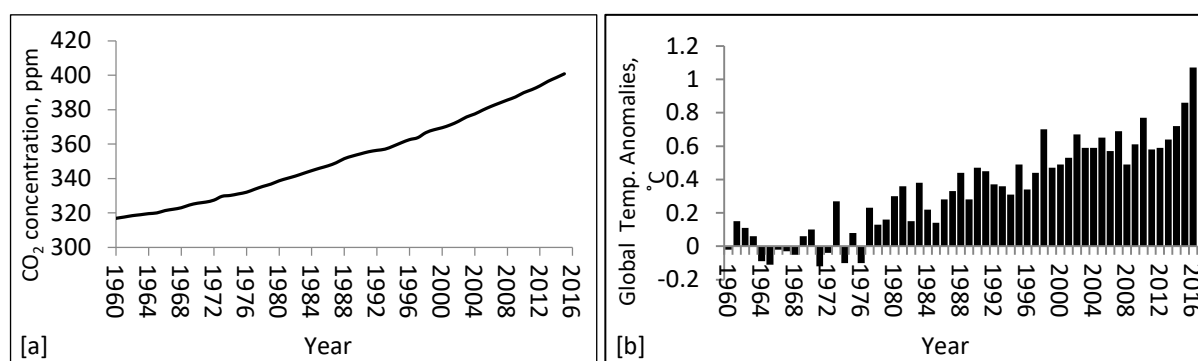


Figure 1.3 – Annual average global concentrations of CO₂ in the atmosphere over time [a] and the corresponding temperature anomalies [b] [Source: Environmental protection Agency (EPA) 2016 - Climate Change Indicators, Quéré *et al.* 2013]

The global atmospheric concentrations of CO₂ have exceeded 400 ppm as of 2015 compared to 317 ppm in 1960. The majority of the warmest years since 1880 have occurred since 2001, having 2016 as the warmest on record. As a result, continuous loss of land ice and consequent rise of sea level occurs. The impact of these ascending trends creates a threat to the ecosystems and biodiversity, which is alarming enough to reconsider the way energy sources are handled.

1.3. Renewables as an alternative source of energy

The search for alternatives to fossil fuel continues in several directions. In the recent decades, the exploitation of various renewable sources of energy, which possess no risk on the environment, has been the focus of many organizations worldwide. The reason for the transition is the fact that fuels that stem from renewable sources (ex.: plants or micro-organisms) produces CO₂ which does not alter the balance of greenhouse gases in the biosphere [Cherubini et al. 2011].

On the contrary to fossil fuels, of which their carbon content, was absent from the biosphere’s natural cycle for millions of years and therefore cannot be balanced by photosynthesis. An example of the efforts made for the transition to more dependence on renewable energies is portrayed in figure 1.4. In the figure, a summary of the primary energy consumption in metric tons of carbon equivalent (MTCE) in Germany, categorized by fuel source, the ratio of domestic supply to imports as well as relative shares in 2015, over a time span of ten years.

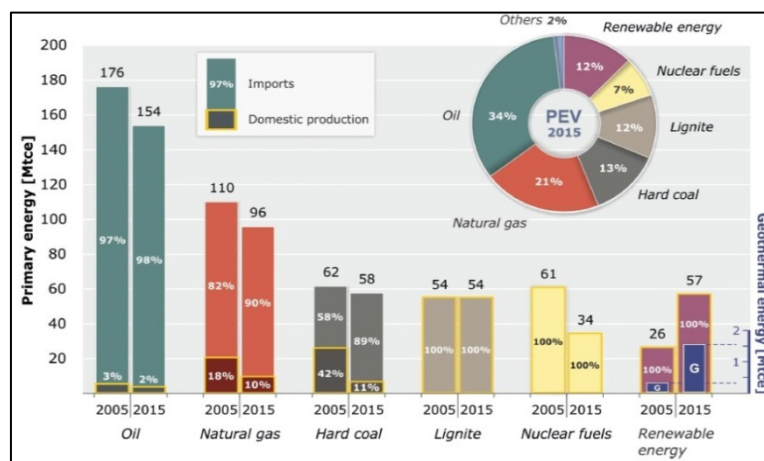


Figure 1.4 – Primary energy consumption by source, the ratio of domestic supply to imports and relative shares in 2015, for Germany in 2005 and 2015⁵

According to statistics, the majority (about 80%) of the energy consumption in Germany is based on imported fossil fuel, typically crude oil, hard coal, lignite and natural gas. Nevertheless, the overall descending trend of total consumption and the increase in the share of renewables is obvious and continuing to rise through the next years. In terms of power generation, renewables (Mainly wind, biomass and solar PV) have contributed to around 30% of the total power consumption from all sources by 2016⁵.

⁵ Source: Bundesanstalt für Geowissenschaften und Rohstoffe (BGR) - Energy Study 2016. Reserves, resources & availability of energy resources

In Europe, the goal to increase the dependence on renewable sources, as a step to secure energy sufficiency and challenge climate change, has taken a major step forward and become embedded through the National Renewable Energy Action Plan (NREAP) submitted by members of the European Union (EU) in 2010. The plan, set by the renewable energy directive, has urged the EU members to reach 20% of the total energy consumption from renewable sources by 2020 [EREC 2011, world energy resources 2016]. Moreover, an agreement on a framework to increase the use of renewable sources for energy consumption has been made in 2014. The plan, set for 2030, aims at the reliance on renewables up to 27% of total energy consumption, with a target to reduce the greenhouse gas by 40% referenced to the levels of 1990 [Danish Energy Agency 2015]. Another EU roadmap was formulated and suggested a 60% reduction in greenhouse gas emissions by 2040 and 80% by 2050, both with respect to the 1990 levels [EU Commission: 2050 low-carbon economy].

Globally, various statistics regarding the status of renewable energies and their distribution in the different energy sectors are produced on regular basis. The information available in a number of energy statistics reports usually provide an inclusive insight with regards to the share of renewables in power generation, primary or final energy consumption. In general, energy can be derived using different technologies from various renewable and abundant sources in nature. Examples include biomass, wind, hydropower, geothermal as well as solar-based heat and power generation. According to a global status report of renewables [REN21 2017], the energy produced through renewable sources accounted for 19.3% of global final energy consumption in 2015.

Energy from biomass as well as hydropower account for the majority of energy consumption from renewables. The federal institute for geosciences and natural resources indicated that renewable sources such as hydropower and solid biomass covered about 14% of primary energy consumption worldwide [BGR 2016, renewable information overview 2017]. Based on the energy resources report issued in 2016 by the world energy council, hydropower supplied 71% of the electricity generated from renewables and 16.4% of all sources globally, with a power capacity of approximately 1,064 GW [World energy resources 2016].

1.4. Biomass as a renewable feedstock for energy production

The term "biomass" describes a broad range of organic lignocellulosic materials that are either available in nature or produced by human activities. Unlike fossil fuels, biomass does not undergo any geological transformations and thus, can be readily used for direct energy production (e.g. burning) or converted to different forms of biofuels such as biodiesel or bioethanol. Biomass is the fourth largest energy supply worldwide after oil, coal and natural gas. It supplies about 35% of energy in developing countries as a whole and over 90% of the total energy used as traditional fuels in many of these countries [Küçük and Demirbas 1997].

Energy from biomass, or "bioenergy", can stem from several sources including agricultural or crop residues (e.g. seeds, straw, husk and bagasse), forestry as well as municipal wastes such as sewage sludge. The distribution of renewable sources and their shares in the global energy supply in 2015 is illustrated in figure 1.5. Solid biofuel, including wood and charcoal, is the most common type of biomass that is widely used as a major source of heating and for cooking in both rural and developing countries.

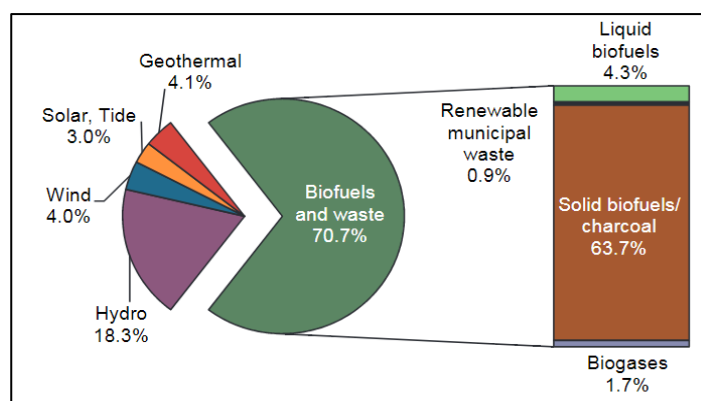


Figure 1.5 – Global energy supply from renewables in 2015 [Source: Renewables Information overview 2017]

As indicated in the figure above, the entire share of biomass in the 2015 global energy supply from renewables was about 71%. Other sources such as hydropower, wind, solar, tide, and geothermal accounted for the remaining shares of total renewables. Woody biomass provides around 90% of the global primary energy which is annually supplied from all sources of biomass. The share of forest biomass in global primary energy supply is approximately 56 EJ, which makes over 10% of the entire energy supplied annually according to the 2016 report of the world energy council [World energy resources 2016].

1.5. Microalgae as a biomass candidate ⁶

1.5.1. General overview

Microalgae represent a broad group of unicellular photosynthetic micro-organisms with a simple structure compared to complex higher plants [Chisti 2008]. They utilize sunlight and a carbon source, grow rapidly and accumulate several useful molecules [Morweiser et al. 2010, Chisti 2007] such as carbohydrates, proteins and lipids, in the form of biomass. Like plants, microalgae have some basic needs for growth including light, water, and nutrition. Additionally, certain conditions for growth should be available, depending on each species, to maintain life. Microalgae can grow in fresh water. They also grow in saline water such as natural seawater that contains over 50 inorganic elements [Andersen 2005]. Wastewater containing nitrogenous and phosphorous compounds can be a medium for growing microalgae too. By utilizing wastewater streams for algal growth, organic constituents from municipal and industrial wastewater can be removed as a mean of water treatment to improve water quality, decrease its load of organics and heavy metals [Hena et al. 2015].

1.5.2. Cultivation techniques

Algal cultivation is usually conducted under photo-autotrophic, -heterotrophic or mixotrophic conditions. The difference between the three modes is the way energy and carbon consumed during metabolism. Cultivating microalgae under autotrophic conditions can be advantageous due to the consumption of CO₂ which can be supplied from different sources such as industrial power plants. Photo-heterotrophic cultivation occurs when carbon requirements can be fulfilled by organic compounds [Lee 2007]. Here, algal growth can be achieved not only in the presence of light but also during dark periods (chemo-heterotrophic). The main advantage of this technique is the potential of obtaining high biomass concentrations and overcoming the problems associated with limited light on large scale during autotrophic cultivation [Huang et al. 2010]. However, the main challenge related to this method is the availability and cost of the organic compounds used for growth. A combination of both methods is called mixo-trophic, where different sources of energy and carbon can be consumed for growth [Perez-Garcia et al. 2011].

⁶ Parts of this section appeared in the thesis work (Scale-up studies of algal growth and hydrogen production using *Chlamydomonas reinhardtii* in closed Photobioreactors) – Sherif Elsayed, Otto-von-Guericke University Magdeburg, Faculty of Process and Systems Engineering, May 2012

1.5.3. Process parameters for algal cultivation

Light is the major parameter which affects the cultivation of microalgae. Basically, the growth of microalgae should be controlled by light, because when light is the only limiting factor, algal productivity then becomes proportional to the photosynthetic conversion efficiency (PCE) [Richmond *et al.* 2003]. The major criteria which govern light utilization by microalgae are related to the light source, intensity and the levels of exposure by the algal cells.

Light is naturally available from the sun for outdoor cultivation. Figure 1.6 shows the spectral distribution of sunlight (250 – 3000 nm) and the corresponding irradiance. The spectral range (400 – 740 nm) which microalgae and other plants utilize for photosynthesis is defined as the photosynthetically active radiation (PAR). Beside the light source, the intensity or irradiance power of light plays an important role in the growth process, leading to light limitation, saturation and photo-inhibition can be distinguished. Regarding exposure, light can be available during cultivation in a continuous or discontinuous manner. Continuous illumination is widely used for indoor experiments. Discontinuous light regimes include natural or simulated day-night cycles based on growth requirements.

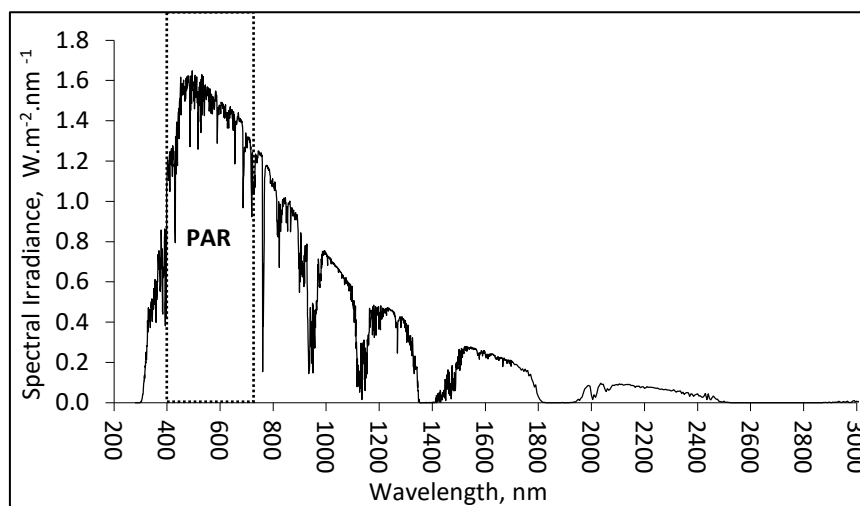


Figure 1.6 – Spectral distribution of solar irradiance [Source: ASTM]

The availability of nutrients is important for the growth of microalgae and forming complex molecules. There are specific elements which are essential for the metabolic activities. Beside carbon and hydrogen which are considered to be the backbone of any chemical energetic molecule, primary growth elements (Macro-nutrients) are nitrogen and phosphorus.

Minor elements that are necessary for growth are calcium, magnesium, sulphur, sodium and potassium. Additionally, other elements which are required in trace amounts (Micro-nutrients) include manganese, copper, iron, zinc and cobalt [Horne and Goldman 1994]. Nutrients usually exist within the culture volume in the dissolved form.

Gases needed by microalgae (CO_2 and O_2) are practically introduced to the culture volume through bubbling or gas diffusion membranes. The continuous uptake and discharge of gases is important for the cultures to maintain a certain degree of physiological balance and keep its metabolic activities at a stable level. CO_2 is found in the atmosphere in a partial pressure of 0.04 kPa (0.04 vol.%), which is not sufficient to backup successful cultivation due to diffusion limitation. Therefore, a minimum utilizable level in the range 0.1 – 0.2 kPa should be available for the culture [Doucha et al. 2005]. A calculation of the CO_2 demand of microalgae can be done based on the stoichiometry of photosynthesis and biomass formed [Posten 2009], indicating that an amount of around 1.7 g CO_2 per 1 g biomass is necessary. Generally, a major group of microalgae grow under neutral pH levels [Qiang et al. 1998], whereas an optimal pH range for growth can be species-specific. The relation between CO_2 and pH is related to the chemical equilibrium between CO_2 , H_2CO_3 , HCO_3^{-1} and CO_3^{-2} in the culture. Further CO_2 addition requires the pH of the medium to be continuously buffered.

Temperature is a major factor which regulates cellular and morphological responses of microalgae [Munoz and Guieysse 2006]. An optimal temperature for cultivation varies in a certain range that can be species-specific and a function of other cultivation conditions. Generally, the temperature range which a broad group of microalgae tolerate lies between 10 and 40 °C, with an optimum value for several species in the range of 20 – 30 °C [Singh and Singh 2015]. Outdoor cultivation at cold locations usually leads to growth limitation. The culture's temperature should be carefully regulated to keep a suitable environment for growth and productivity. This can be done using heat transfer circuits which provide hot or cold water across the outer surfaces of the cultivation system, or submerged coils to control the temperature within the culture volume. Cultivating microalgae at places with cold or severe conditions (ex.: heavy rains or strong winds) can be successful by implementing a greenhouse.

1.6. Typical biomass conversion processes

Numerous forms of biomass such as wood, organic wastes and crop residue undergo conversion to solid, liquid and gaseous products through several processes. Whether these processes are designated as treatment, upgrade or conversion, the aim is to obtain a product that has a simpler form and higher energy-density. Depending on the process type, three conversion technologies can be distinguished. These technologies are based on thermochemical, biological and chemical processes. For example, thermal energy or a wide range of fuels can be produced from thermochemical processes such as combustion, pyrolysis or gasification.

1.6.1. Combustion

Thermochemical processes rely in the first place on applying thermal energy or temperature followed by a chemical and physical conversion of the feed material. In the presence of an oxidant such as air, direct combustion or burning is the simplest method to obtain energy from biomass. Combustion has the highest temperature range compared to other conversion processes. The main product is a mixture of CO₂, water vapor with some solid residues depending on the feedstock nature. Combustion produces the majority of energy generated from biomass for heating, cooking as well as electricity generation.

1.6.2. Pyrolysis

This type of biomass conversion takes place in an oxygen-free environment. Pyrolysis typically occurs within temperatures in the range of 300 – 700 °C. During pyrolysis, the biomass is decomposed and converted into a liquid phase (tar, liquid hydrocarbons or bio-crude), solid phase (char) as well as gaseous phase (water vapor, gases or volatiles). Torrefaction can be considered as a mild form of Pyrolysis which starts at lower temperatures (around 200 – 320 °C). During torrefaction, the moisture content of biomass is released along with some volatiles. Other complex structures such as cellulose, hemicellulose or lignin are partially decomposed to volatile compounds [Bates and Ghoniem 2012]. The main product of torrefaction is a dry solid material that is defined as bio-coal.

1.6.3. Gasification

The term gasification can be used as a general description for combustion, or an inter-stage of pyrolysis for instance. However, the process dedicated for gasification mainly occurs when biomass is converted at higher temperatures (ex.: 700 – 1200 °C) in an oxygen-deficient environment. The product is then a mixture of gaseous compounds (ex.: H₂, CO, CO₂, CH₄) along with other solid constituents such as char or ash. Gasification includes a series of homogeneous and heterogeneous reactions such as decomposition, partial combustion, reduction and reforming between the different gaseous species, volatiles and carbon. The reactions take place in the different zones of a gasifier built-up in certain setups (fixed bed, fluidized bed, entrained flow) and operation mechanisms, depending on the feedstock nature. Steam can be used solely or with air to achieve the conversion. When steam is used, the yield of H₂ and CO₂ increases due to the water-gas shift reaction [Devi *et al.* 2003].

1.6.4. Biochemical conversion

A number of non-thermal processes for the utilization of biomass feedstocks are implemented for producing several energetic molecules. Biomass can be converted biochemically to liquid fuel such as biogas and bioethanol using micro-organisms. The use of yeast for the production of bioethanol is one example. Bioethanol can be produced from starchy or lignocellulosic biomass through hydrolysis followed by fermentation and product recovery [Verardi *et al.* 2012]. Hydrolysis results in the formation of fermentable sugars and it is usually performed catalytically via an acid or enzyme [Galbe & Zacchi 2002].

Another process is the anaerobic digestion, where the use of microorganisms is conducted to break down the organic biodegradable materials of biomass (e.g. crop residues or manure). Several types of bacteria are used to decompose carbohydrates (hydrolysis) into digestible forms that are further degraded to CO₂, H₂, NH₄⁺ and organic acids, before methane or biogas is obtained. The remaining solid residues (digestate) can be used as an organic fertilizer [Giuntoli *et al.* 2016] or for animal bedding [Zhang *et al.* 2015]. Other techniques such as dark and photo-fermentation can be used for the production of H₂ from biomass through fermentative pathways using anaerobic microorganisms [Hallenbeck 2011], but these processes are relatively complex and a significant improvement in their conversion efficiency needs to be realized [Chong *et al.* 2009].

1.7. Hydrothermal conversion

Typically, thermochemical conversion processes (Combustion, pyrolysis and gasification) involve the operation at atmospheric or low pressure as a common practice. As higher pressure (> 10 bar) is applied and in the presence of water or biomass's moisture content, the process chemistry changes and other conversion mechanisms can be conducted at different combinations of temperature and pressure. These processes are referred to as hydrothermal processes. Based on the product desired from each process, they are mainly categorized in carbonization, liquefaction or gasification.

1.7.1. Hydrothermal Carbonization (HTC)

This process is conducted in the temperature range of $170 - 260$ °C. The operating pressure ranges from below 20 bar [Heilmann *et al.* 2010] up to 50 bar [Basso *et al.* 2016] depending on the temperature applied, to keep the moisture content of biomass from evaporation. The residence time inside the system can vary from 20 – 30 minutes to several hours [Liu and Balasubramanian 2014, Erlach *et al.* 2012] according to feedstock nature and the scope of operation. Hydrothermal carbonization might be seen or referred to in literature as wet torrefaction due to the production of biochar in both processes. In HTC, biomass reacts with the hot pressurized water in a series of complex chemical reactions to produce a biochar. A liquid fraction containing reaction intermediates such as furfurals and organic acids can be obtained as a byproduct with the release of carbon dioxide [Kambo and Dutta 2015].

1.7.2. Hydrothermal liquefaction (HTL)

Wet biomass can be converted through hydrothermal liquefaction (HTL) into an oil product or a so-called bio-crude with relatively high heating value, along with water-soluble compounds, solid residues and gas fraction [Toor *et al.* 2011]. The temperature and pressure at which liquefaction is conducted ranges between $280 - 370$ °C and $100 - 250$ bar respectively [Behrendt *et al.* 2008] with a residence time in the minutes-range. During HTL, the complex structure of biomass is decomposed into unstable fragments of lighter molecules using a suitable catalyst or sometimes non-catalytically [Biller *et al.* 2011]. These unstable fragments are reactive and they re-polymerize forming oily and stable compounds with proper molecular weights [Molten *et al.* 1983]. The separation of the liquefaction products plays a significant role in the overall process assessment. Using physical methods (filtration and decanting) as well as solvent chemical extraction, the solid residues, different fractions of

bio-crude and the aqueous phase can be separated [Jazrawi *et al.* 2013, Valdez *et al.* 2012]. So far, the bio-crude obtained from HTL cannot directly be used as biofuel for transportation. Further upgrading to reduce the nitrogen, sulphur and oxygen content of the bio-crude is necessary [Barreiro *et al.* 2013].

1.7.3. Supercritical water gasification (SCWG)

Gasification in supercritical water or hydrothermal gasification (HTG) features the highest temperature and pressure among other hydrothermal conversion processes. Figure 1.7 shows a simplified phase diagram of water as a function of temperature and pressure. Above its critical point ($T = 647$ K and $P = 221$ bar), the boundary between liquid and vapor vanishes. This state is then referred to as supercritical. Under these extreme conditions, the water molecule comprises unique properties of both its gaseous and liquid states [Beslin *et al.* 1998, Shaw *et al.* 1991].

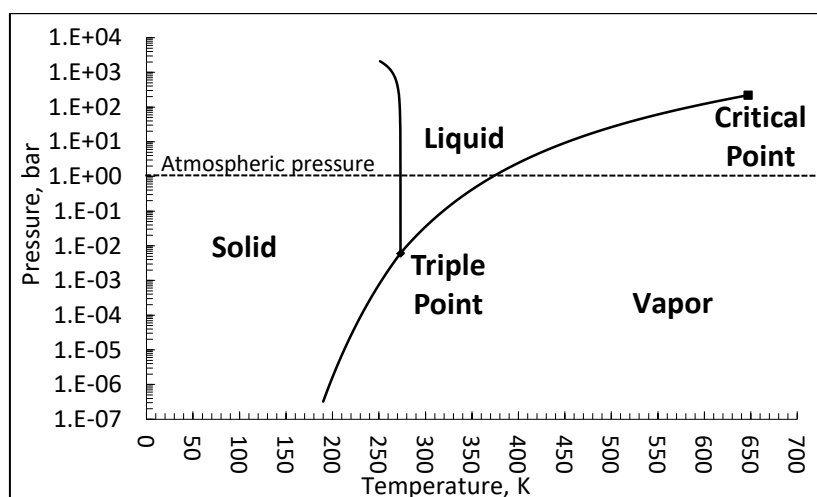


Figure 1.7 – Simplified Phase diagram of water [Modified from: 1998 ChemicalLogic Corporation]

As the critical point is approached, a major decrease of density occurs. In conjunction, the viscosity and diffusivity of water tend to have values comparable to those of gases. As a medium for gasification, this ensures good transport properties (no mass transfer limitation) and rapid reaction kinetics [Calzavara *et al.* 2004, Williams *et al.* 2006, Erkonak *et al.* 2008], allowing for high conversion. In addition, the dielectric constant decreases sharply in this region and water behaves like a non-polar molecule that is capable of diluting and dissolving organic materials [Kıpçak *et al.* 2011].

As a result, char formation is suppressed when gasification takes place in supercritical water [Modell 1985, Matsumura et al. 2005, Furusawa et al. 2007, Yanik et al. 2007]. Figure 1.8 demonstrates the changes which occur to some of water properties such as density, dynamic viscosity, isobaric heat capacity and dielectric constant upon reaching the critical point at a supercritical pressure of 280 bar. The isobaric heat capacity (C_p) tends to infinity around the critical point compared to its normal values. The peak in C_p can be thought of as mean to indicate the high energy demand around this region, given a zero latent heat of vaporization [Yakaboylu et al. 2015]. The varying properties in the sub- and super-critical vicinity give an opportunity for a flexible operation by tuning temperature and pressure to achieve desired mechanisms and reach better process control.

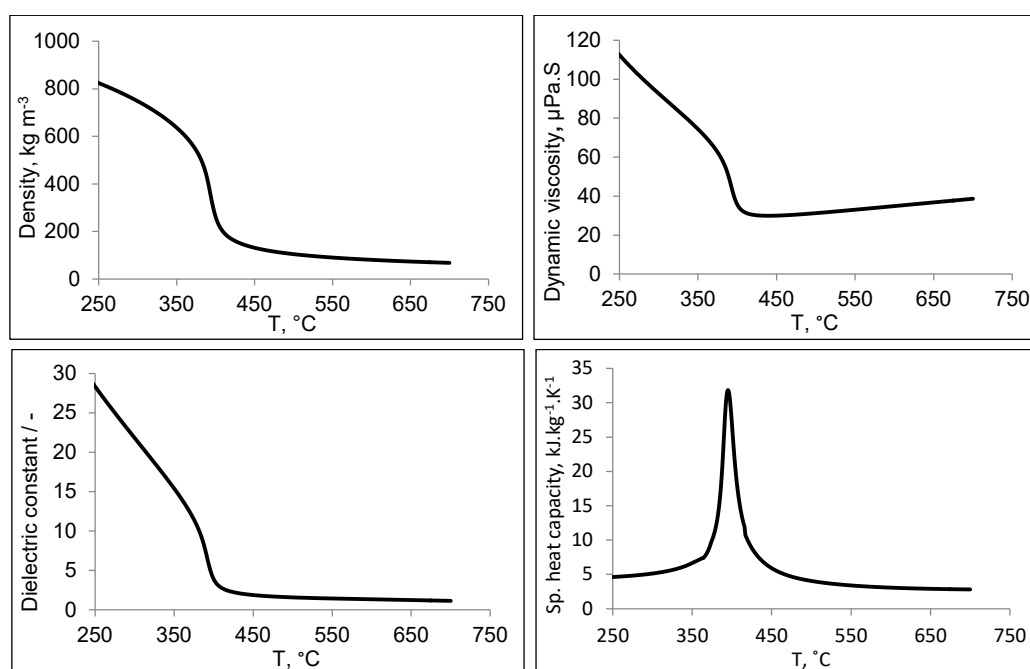


Figure 1.8 – Effect of temperature on water properties including density, dielectric constant, dynamic viscosity and specific heat capacity at P = 280 bar [Source: IAPWS]

Water molecules can act as a catalyst for acidic or basic reactions following the concentration of H_3O^+ or OH^- ions respectively [Akiya and Savage 2002, Kruse and Dinjus 2007, Brunner 2009]. At high densities, the ionic product (K_w) of water is high. Aqueous phase reactions such as biomass hydrolysis [Guo et al. 2007] preferably occur. On the other hand, the ionic product is minimized as the density of water sharply decreases under supercritical conditions, a case that promotes free radical reactions which are necessary to form gases such as hydrogen and methane [Kruse and Gawlik 2003, Sinag et al. 2003].

Processing biomass in high moisture content (> 80 wt%) in supercritical water promotes the unique and reactive role of water and eliminates the energy-consuming dewatering or drying prior to traditional gasification processes [Boukris *et al.* 2007]. Moreover, fast reaction kinetics lead to a shorter residence time within the system and hence, less space would be needed to construct these systems if a comparison with biological treatment processes is made [Crocker 2010].

1.7.4. Reaction pathways of biomass in near- and supercritical water

Basically, the decomposition of biomass leads to the formation of simpler molecules as an initial step. These molecules are considered to be the reaction intermediates or the starting point for further dissociation regardless of the reactions pathway. The speed, at which these reactions proceed are ideally governed by certain kinetics. The definition of detailed reaction kinetics under near- and supercritical conditions is not perfectly understood. This is due to the nature of the feedstock materials and consequently, the numerous intermediates which are present in the reaction medium at these conditions. Having a better understanding of reaction kinetics for hydrothermal conversion would definitely contribute to improving the process, for example by preventing the formation of unwanted reaction species or finding process conditions, at which certain reactions are favored.

Simplified reaction schemes were suggested in several works addressing hydrothermal conversion. A kinetic model for the gasification of the algal species *Nannochloropsis sp.* in supercritical water was discussed [Guan *et al.* 2012], in which certain reaction pathways starting with two types of lumped intermediates were proposed. These two intermediates suggested were categorized based on their reactivity in the medium or the speed of their decomposition. First order kinetics was assumed for simplicity and due to the lack of other information which contradicts this suggestion. The work concluded that the formation of gaseous species was mainly associated with the decomposition of the fast-reacting intermediates. There, and based on an experimental analysis of their earlier work, a reaction intermediate such as Hexadecane was found to be rapidly reacting to form gases. From the model they proposed, it was also stated that the rate of hydrogen production from steam reforming was clearly appreciable if compared to that which is generated directly from the intermediates decomposition.

A higher gas yield was predicted through the model upon increasing temperature. Moreover, the work presented a step for the conversion of these intermediates to solid products such as char and assumed it to be a stable product, i.e. having a low reactivity which makes it unlikely to undergo further conversion compared to gasification of intermediates. Other works have addressed the same topic and designed kinetic expressions which mainly proposed simplified reaction schemes supporting the first order behavior. These works involved different organic feedstock materials such as glucose [Kabyemela *et al.* 1997] as the building unit or starting material of cellulose, indole [Guo *et al.* 2013], methanol [Castello and Fiori 2012] and glycerol [Guo *et al.* 2013].

Unlike standard or model chemical compounds, the composition of biomass is rather complex. This is due to its structure that is based on cellulose, hemi-cellulose and lignin. For simplification, the reactions included in hydrothermal conversion of biomass at near- and supercritical can be categorized in two major groups. The first group includes hydrolysis or steam reforming, where biomass is decomposed and several liquid reactions intermediates are formed (liquefaction). The second group (gasification) is dominant when temperature exceeds the critical point and is associated with the formation of gaseous species.

Figure 1.9 shows another simplified form of a suggested reaction scheme which can describe the conversion of biomass, starting from cellulose, in sub- and supercritical water using certain key compounds. Such a conversion scheme was presented by Kruse *et al.* in several works which are based on experimental results and was adopted later in further publications.

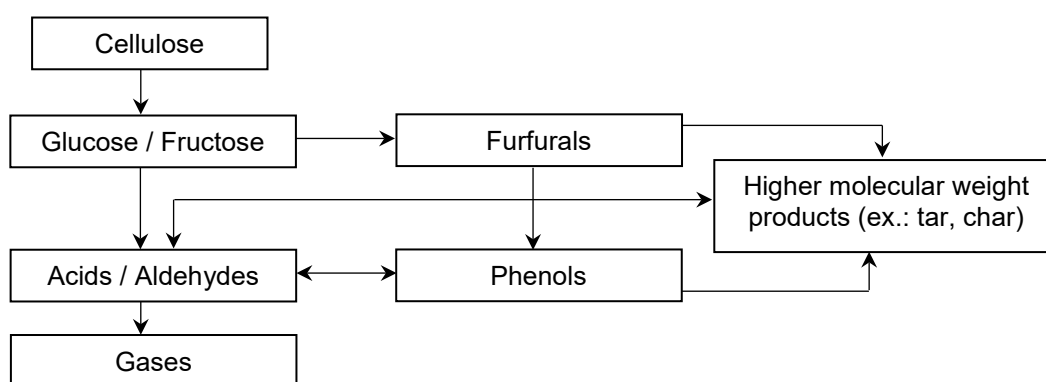


Figure 1.9 – A Simplified reaction scheme of biomass conversion in sub- and supercritical water starting from cellulose and identified by key compounds. [Source: Kruse *et al.* 2003]

According to the scheme, the breakdown of the large or long-chain molecules precedes the decomposition of sugars to molecules of a shorter chain such as aldehydes, alcohols or organic acids. Cellulose hydrolysis or reforming occurs rapidly, with water accelerating the decomposition of biomass structure to smaller units of sugars [Sasaki et al. 1998, Kruse and Dinjus 2007]. This decomposition occurs completely under sub-critical conditions [Minowa et al. 1998]. Simultaneously, parallel or competing reactions would lead to dehydration to different derivatives of furfurals and phenolic compounds [Kruse et al. 2003]. These types of substances react further to produce a mixture of gaseous products under supercritical conditions. As stated earlier, high molecular weight products such as solids depositing in the form of tar and char may also be formed due to extended polymerization of the existing intermediates [Rönnlund et al. 2011, Kruse and Denjuis 2007].

Due to the large number of intermediates and reaction pathways involved in the hydrothermal conversion, it is a difficult task to list such reactions in full details. However, the overall equations listed below in table 1.1 give an overview on some fundamental reactions occurring in the conversion medium. A crucial reaction in SCWG is the hydrolysis or steam reforming of the organic substance to obtain carbon monoxide and hydrogen (Eq. 1.1). A general formula of a key compound ($C H_x O_y$) which can describe biomass or other organic chemicals was adopted in several works for simplicity. The subscripts (x) and (y) indicate the H/C and O/C molar ratio respectively.

Table 1.1 – Basic gasification reactions possibly occurring during hydrothermal conversion of biomass [Source: Susanti et al. 2010, Rönnlund et al. 2011]

Reaction	Reaction no.	ΔH_r^0 (298K) kJ.mol ⁻¹	Description
$CH_xO_y + (1 - y) H_2O \rightarrow CO + (1 - y + [(x/2)]) H_2$	1.1	+ ve*	Reforming or decomposition
$CO + H_2O \leftrightarrow CO_2 + H_2$	1.2	- 41.2	Water-gas shift reaction
$CO + 3 H_2 \leftrightarrow CH_4 + H_2O$	1.3	- 206.2	CO Methanation
$CO_2 + 4 H_2 \leftrightarrow CH_4 + 2 H_2O$	1.4	- 165	CO ₂ Methanation
$C + CO_2 \leftrightarrow 2 CO$	1.5	+172.5	Boudouard equilibrium
$CO + H_2 \leftrightarrow C + H_2O$	1.6	- 131.3	CO-hydrogenation
$CO_2 + 2 H_2 \leftrightarrow C + 2 H_2O$	1.7	- 90.1	CO ₂ hydrogenation
$C_nH_{2n} + H_2 \leftrightarrow C_nH_{2n+2}$	1.8	- ve*	Alkene hydrogenation

* The +v and -ve sign indicate endothermic and exothermic reactions respectively.

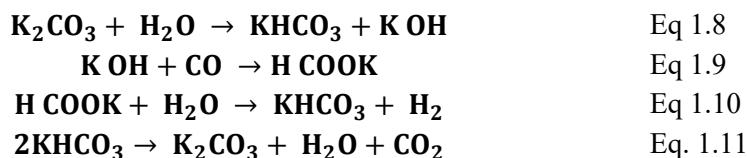
This general reaction is endothermic, since energy is required to break-up the starting molecule. More energy is needed for decomposition as the chain length of the organic molecule increases. For example, the reaction enthalpies of reforming some model compounds used in hydrothermal gasification, such as methanol and isooctane to syngas are 91.7 and 1274.5 KJ.mol⁻¹ respectively [Boukris *et al.* 2003, Susanti *et al.* 2010]. After decomposition, other reactions occur such as the water-gas shift reaction, from which hydrogen and carbon dioxide are released. The formation of methane is achieved by the methanation of CO and CO₂ via reacting both gaseous species with hydrogen. These three reactions (Eq. 1.2 - 1.4) are energy-releasing, i.e. exothermic. Other reactions would possibly occur, resulting in the formation of light hydrocarbons (ex.: ethane, propane) or even coke in some cases from reduction or hydrogenation reactions.

1.7.5. The catalytic role of salts

One factor which plays a role during hydrothermal or supercritical water gasification is the existence of dissolved salts within the reaction medium. Certain amounts of an alkali metal such as potassium carbonate or bicarbonate (K₂CO₃, KHCO₃) can be added by dissolving in a model compound or a slurry biomass feedstock. This addition enables the dissolved salt to act as a homogeneous catalyst that favors some reactions over others. Based on previous works, the existence of such salts in the feedstock proved to have their catalytic activity through forming a reaction mechanism which promotes the production of gaseous species such as hydrogen. These mechanisms, however, were proposed in literature as proposed schemes and are mentioned here as a possible explanation for the changes taking place. Also, other works reported that the addition of a salt like K₂CO₃ suppresses the formation of coke or char [e.g. *Matsumura et al.* 2005] and leads to an improvement in gasification efficiency [e.g. *Schmieder et al.* 2000].

Elliott et al. 1983 discussed a mechanism for the decomposition of K₂CO₃ in high temperature pressurized systems. The work credited the alkali catalysis of the water-gas shift reaction in aqueous solutions to the works of *Yoneda et al.* 1943a,b and 1944a,b. The mechanism, represented with the following equations below, includes both the formation and decomposition of a formate salt intermediate in a solution containing dissolved K₂CO₃. As a result, the equilibrium of the water-gas shift reaction moves towards H₂ production and CO₂. In the first step (Eq. 1.8), K₂CO₃ is hydrolyzed and converted to KHCO₃ in the aqueous medium.

The ionization of the salt promotes the formation of potassium formate (Eq. 1.9). As a result and given the decomposition of formate (Eq. 1.10) with the regeneration of bicarbonate (Eq. 1.11), H₂ and CO₂ are generated. The water-gas shift reaction is simply the summation of these reactions. According to the mechanism, an increase in both CO₂ and H₂ concentrations are expected by the addition of such a catalyst.



Such a mechanism was also highlighted in later works [e.g. *Onsager 1996, Sinag et al. 2003, Yanik et al. 2008*]. Nevertheless, the work of *Elliott et al. 1983* provided a criticism for this a mechanism based on their experimental work, indicating no evidence of bicarbonate formation from Eq. 1.10. Instead, a modified mechanism for the catalysis of the water-gas shift reaction was proposed (fig. 1.10), through which formaldehyde, formate and hydroxide ions (OH⁻) are formed as intermediates.

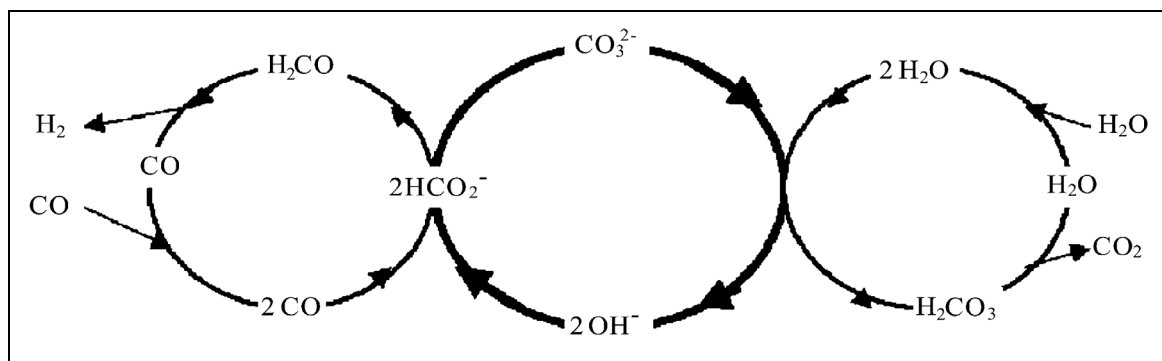


Figure 1.10 – A suggested mechanism for the catalyzed water-gas shift reaction in high temperature pressurized aqueous systems involving a dissolved salt [Elliott et al. 1983]

In this mechanism, any source of hydroxide ion (OH⁻) acts as a catalyst for the water-gas shift reaction. In addition, the mechanism indicates that the decomposition of the existing formate salt in the system is the rate-limiting step. The carbonate salt reacts completely with water on one hand. Simultaneously, formate is produced by the reaction of carbon monoxide CO with OH⁻, which originate from the carbonate salt. The formate then decomposes to carbonate and formaldehyde. Based on this mechanism, the released H₂ would originate from the decomposition of formaldehyde.

1.8. References (Chapter 1)

1. Akiya, N., Savage, P.E. 2002. Roles of Water for Chemical Reactions in High-Temperature Water. *Chemical Reviews*, **102**(8), 2725-2750.
2. American Society for Testing Materials (ASTM) - G173-03, Standard Tables for Reference Solar Spectral Irradiances: Direct Normal and Hemispherical on 37° Tilted Surface, ASTM International, West Conshohocken, PA, 2003, www.astm.org.
3. Andersen R.A. (ed.) 2005. Algal culturing techniques. Academic Press, Elsevier Science, San Diego, California. U.S.A. 596 p.
4. Basso, D., Patuzzi, F., Castello, D., Baratieri, M., Rada, E.C., Weiss-Hortala, E., Fiori, L. 2016. Agro-industrial waste to solid biofuel through hydrothermal carbonization. *Waste Manag*, **47**(Pt A), 114-21.
5. Bates, R.B., Ghoniem, A.F. 2012. Biomass torrefaction: Modeling of volatile and solid product evolution kinetics. *Bioresource Technology*, **124**, 460-469.
6. Behrendt, F., Neubauer, Y., Oevermann, M., Wilmes, B., Zobel, N. 2008. Direct Liquefaction of Biomass. *Chemical Engineering & Technology*, **31**(5), 667-677.
7. Beslin, P., Cansell, F., Rey, S. 1998. Thermodynamic Aspects of Supercritical Fluids Processing: Applications of Polymers and Wastes Treatment. *Oil & Gas Science and Technology - Rev. IFP*, **53**(1), 71-98.
8. Biller, P., Riley, R., Ross, A.B. 2011. Catalytic hydrothermal processing of microalgae: decomposition and upgrading of lipids. *Bioresource technology*, **102**(7), 4841-8.
9. Boukis, N., Diem, V., Habicht, W., Dinjus, E. 2003. Methanol Reforming in Supercritical Water. *Industrial & Engineering Chemistry Research*, **42**(4), 728-735.
10. Boukis N.; Galla, U.; Müller, H.; Dinjus E., Biomass gasification in supercritical water. Experimental progress achieved with the VERENA pilot plant. 15th European Biomass, Conference, Berlin, Germany; May 7–11, (2007).
11. British Petroleum Company – BP Statistical review of world energy, June 2016 (p. 42).
12. Brunner, G. 2009. Near critical and supercritical water. Part I. Hydrolytic and hydrothermal processes. *The Journal of Supercritical Fluids*, **47**(3), 373-381.
13. Bundesanstalt für Geowissenschaften und Rohstoffe (BGR) 2016: Energy Study 2016. Reserves, resources and availability of energy resources (20). – 180 p., Hannover, December 2016.
14. Cable News Network (CNN) Money: <http://money.cnn.com/2008/12/17/markets/oil/>
15. Calzavara, Y., Jousot-Dubien, C., Boissonnet, G., Sarrade, S. 2005. Evaluation of biomass gasification in supercritical water process for hydrogen production. *Energy Conversion and Management*, **46**(4), 615-631.
16. Castello, D. and Fiori, L. 2012. Kinetics modeling and main reaction schemes for the supercritical water gasification of methanol. *The Journal of Supercritical Fluids*, **(69)**, 64-74.
17. ChemicalLogic Corporation, Copyright © 1998 – Source of the curves: International Equations for the Pressure along the Melting and along the Sublimation Curve for Ordinary Water Substance, J. Phys. Chem. Ref. Data, Vol 23, No 3, 1994.
18. Cherubini, F., Peters, G.P., Berntsen, T., Strømman, A.H., Hertwich, E. 2011. CO2 emissions from biomass combustion for bioenergy: atmospheric decay and contribution to global warming. *GCB Bioenergy*, **3**(5), 413-426.
19. Chisti, Y. 2007. Biodiesel from microalgae. *Biotechnology advances*, **25**(3), 294-306.
20. Chisti, Y. 2008. Biodiesel from microalgae beats bioethanol. *Trends in biotechnology*, **26**(3), 126-31.

21. Chong, M.-L., Sabaratnam, V., Shirai, Y., Hassan, M.A. 2009. Biohydrogen production from biomass and industrial wastes by dark fermentation. *International Journal of Hydrogen Energy*, **34**(8), 3277-3287.
22. Clayton, B.C. 2015. *Market Madness: A Century of Oil Panics, Crises, and Crashes*, Oxford University Press, ISBN 978-0-19999-005-4, 248 p.
23. Crocker, M. 2010. *Thermochemical Conversion of Biomass to Liquid Fuels and Chemicals*, 1st ed., Energy and Environment Series, Vol. 1, Royal Society of Chemistry, Cambridge.
24. Dalarossa, Otávio. 2014. Oil Crisis Explained In 3 Minutes: <https://medium.com/@dalarossa/oil-crisis-explained-in-3-minutes-60c252fa96f7>.
25. Devi, L., Ptasinski, K.J., Janssen, F.J.J.G. 2003. A review of the primary measures for tar elimination in biomass gasification processes. *Biomass and Bioenergy*, **24**(2), 125-140.
26. Doucha, J., Straka, F., Lívanský, K. 2005. Utilization of flue gas for cultivation of microalgae (*Chlorella* sp.) in an outdoor open thin-layer photobioreactor. *Journal of Applied Phycology*, **17**(5), 403-412.
27. Elliott, D.C., Hallen, R.T., Sealock, L.J. 1983. Aqueous catalyst systems for the water-gas shift reaction. 2. Mechanism of basic catalysis. *Industrial & Engineering Chemistry Product Research and Development*, **22**(3), 431-435.
28. Elsayed, S. 2012. Scale-up studies of algal growth and hydrogen production using *Chlamydomonas reinhardtii* in closed Photobioreactors (Master thesis). Otto-von-Guericke University Magdeburg, Faculty of Process and Systems Engineering.
29. Energy and Climate Policies beyond 2020 in Europe. 2015. Danish Energy Agency.
30. Environmental protection Agency (EPA): Climate Change Indicators in the United States: Atmospheric Concentrations of Greenhouse Gases - www.epa.gov/climate-indicators - August 2016.
31. Erkonak, H., Söğüt, O.Ö., Akgün, M. 2008. Treatment of olive mill wastewater by supercritical water oxidation. *The Journal of Supercritical Fluids*, **46**(2), 142-148.
32. Erlach, B., Harder, B., Tsatsaronis, G. 2012. Combined hydrothermal carbonization and gasification of biomass with carbon capture. *Energy*, **45**(1), 329-338.
33. European Commission: <http://ec.europa.eu/energy/en/topics/energy-strategy-and-energy-union/2030-energy-strategy>, https://ec.europa.eu/clima/policies/strategies/2050_en
34. European Renewable Energy Council (EREC) 2011. Mapping Renewable Energy Pathways towards 2020, EU Industry Roadmap.
35. Furusawa, T., Sato, T., Sugito, H., Miura, Y., Ishiyama, Y., Sato, M., Itoh, N., Suzuki, N. 2007. Hydrogen production from the gasification of lignin with nickel catalysts in supercritical water. *International Journal of Hydrogen Energy*, **32**(6), 699-704.
36. Gabrielyan, L., Sargsyan, H., Trchounian, A. 2015. Novel properties of photofermentative biohydrogen production by purple bacteria *Rhodobacter sphaeroides*: effects of protonophores and inhibitors of responsible enzymes. *Microb Cell Fact*, **14**, 131.
37. Galbe, M., Zacchi, G. 2002. A review of the production of ethanol from softwood. *Applied Microbiology and Biotechnology*, **59**(6), 618-628.
38. Giuntoli, J., Agostini, A., Caserini, S., Lugato, E., Baxter, D., Marelli, L. 2016. Climate change impacts of power generation from residual biomass. *Biomass and Bioenergy*, **89**, 146-158.
39. Guan, Q., Wei, C., Savage, P.E. 2012. Kinetic model for supercritical water gasification of algae. *Physical chemistry chemical physics: PCCP*, **14** (9), 3140–3147
40. Guan, Q., Savage, P.E., Wei, C. 2012. Gasification of alga *Nannochloropsis* sp. in supercritical water. *The Journal of Supercritical Fluids*, **61**, 139-145.

41. Guo, L., Lu, Y., Zhang, X., Ji, C., Guan, Y., Pei, A. 2007. Hydrogen production by biomass gasification in supercritical water: A systematic experimental and analytical study. *Catalysis Today*, **129**(3-4), 275-286.
42. Guo, S., Guo, L., Yin, J., Jin, H. 2013. Supercritical water gasification of glycerol: Intermediates and kinetics. *The Journal of Supercritical Fluids*, **78**, 95-102.
43. Guo, Y., Wang, S., Huelsman, C., Savage, P.E. 2013. Products, pathways, and kinetics for reactions of indole under supercritical water gasification conditions. *The Journal of Supercritical Fluids*, **73**, 161-170.
44. Hallenbeck, P.C. 2011. Microbial paths to renewable hydrogen production. *Biofuels*, **2**(3), 285-302.
45. Heilmann, S.M., Davis, H.T., Jader, L.R., Lefebvre, P.A., Sadowsky, M.J., Schendel, F.J., von Keitz, M.G., Valentas, K.J. 2010. Hydrothermal carbonization of microalgae. *Biomass and Bioenergy*, **34**(6), 875-882.
46. Hena, S., Fatimah, S., Tabassum, S. 2015. Cultivation of algae consortium in a dairy farm wastewater for biodiesel production. *Water Resources and Industry*, **10**, 1-14.
47. Horne, A.J. & Goldman, C.R. 1930- (1994). *Limnology* (2nd ed). McGraw-Hill, New York.
48. Huang, G., Chen, F., Wei, D., Zhang, X., Chen, G. 2010. Biodiesel production by microalgal biotechnology. *Applied Energy*, **87**(1), 38-46.
49. IAPWS: International Association for the Properties of Water and Steam formulation for Industrial Use, 1997.
50. Inflation Data: https://inflationdata.com/Inflation/Inflation_Rate/Historical_Oil_Prices_Table.asp
51. James, A.K., Helle, S.S., Thring, R.W., Rutherford, P.M., Masnadi, M.S. 2014. Investigation of Air and Air-Steam Gasification of High Carbon Wood Ash in a Fluidized Bed Reactor. *Energy and Environment Research*, **4**(1).
52. Jazrawi, C., Biller, P., Ross, A.B., Montoya, A., Maschmeyer, T., Haynes, B.S. 2013. Pilot plant testing of continuous hydrothermal liquefaction of microalgae. *Algal Research*, **2**(3), 268-277.
53. Jiang, Y., Wang, X., Cao, Q., Dong, L., Guan, J., Mu, X. 2016. Chemical Conversion of Biomass to Green Chemicals. in: *Sustainable Production of Bulk Chemicals*, pp. 19-49.
54. Kabyemela, B.M., Adschiri, T., Malaluan, R., Arai, K. 1997. Kinetics of Glucose Epimerization and Decomposition in Subcritical and Supercritical Water. *Industrial & Engineering Chemistry Research*, **36** (5), 1552-1558.
55. Kambo, H.S., Dutta, A. 2015. Comparative evaluation of torrefaction and hydrothermal carbonization of lignocellulosic biomass for the production of solid biofuel. *Energy Conversion and Management*, **105**, 746-755.
56. Kıpçak, E., Söğüt, O.Ö., Akgün, M. 2011. Hydrothermal gasification of olive mill wastewater as a biomass source in supercritical water. *The Journal of Supercritical Fluids*, **57**(1), 50-57.
57. Kruse, A., Dinjus, E. 2007. Hot compressed water as reaction medium and reactant. *The Journal of Supercritical Fluids*, **41**(3), 361-379.
58. Kruse, A., Gawlik, A. 2003. Biomass conversion in water at 330-410 °C and 30-50 MPa. Identification of key compounds for indicating different chemical reaction pathways. *Industrial and Engineering Chemistry Research*, **42**(2), 267-279.
59. Kruse, A., Henningsen, T., Smag, A., Pfeiffer, J. 2003. Biomass gasification in supercritical water: Influence of the dry matter content and the formation of phenols. *Industrial and Engineering Chemistry Research*, **42**(16), 3711-3717.
60. Küçük, M.M., Demirbaş, A. 1997. Biomass conversion processes. *Energy Conversion and Management*, **38**(2), 151-165.
61. Larina, O.M., Sinelshchikov, V.A., Sytchev, G.A. 2016. Comparison of thermal conversion methods of different biomass types into gaseous fuel. *Journal of Physics: Conference Series*, **774**.

62. Le Quéré, C., Andres, R.J., Boden, T., Conway, T., Houghton, R.A., House, J.I., Marland, G., Peters, G.P., van der Werf, G.R., Ahlström, A., Andrew, R.M., Bopp, L., Canadell, J.G., Ciais, P., Doney, S.C., Enright, C., Friedlingstein, P., Huntingford, C., Jain, A.K., Jourdain, C., Kato, E., Keeling, R.F., Klein Goldewijk, K., Levis, S., Levy, P., Lomas, M., Poulter, B., Raupach, M.R., Schwinger, J., Sitch, S., Stocker, B.D., Viovy, N., Zaehle, S., Zeng, N. 2013. The global carbon budget 1959–2011. *Earth Syst. Sci. Data*, **5**(1), 165-185.
63. Liu, Z., Balasubramanian, R. 2014. Upgrading of waste biomass by hydrothermal carbonization (HTC) and low temperature pyrolysis (LTP): A comparative evaluation. *Applied Energy*, **114**, 857-864.
64. López Barreiro, D., Prins, W., Ronsse, F., Brilman, W. 2013. Hydrothermal liquefaction (HTL) of microalgae for biofuel production: State of the art review and future prospects. *Biomass and Bioenergy*, **53**, 113-127.
65. Matsumura, Y., Minowa, T., Potic, B., Kersten, S.R.A., Prins, W., van Swaaij, W.P.M., van de Beld, B., Elliott, D.C., Neuenschwander, G.G., Kruse, A., Jerry Antal Jr, M. 2005. Biomass gasification in near- and super-critical water: Status and prospects. *Biomass and Bioenergy*, **29**(4), 269-292.
66. Minowa, T., Sawayama, S. 1999. A novel microalgal system for energy production with nitrogen cycling. *Fuel*, **78**(10), 1213-1215.
67. Modell, M. 1985. Gasification and Liquefaction of Forest Products in Supercritical Water. in: *Fundamentals of Thermochemical Biomass Conversion*, (Eds.) R.P. Overend, T.A. Milne, L.K. Mudge, Springer Netherlands. Dordrecht, pp. 95-119.
68. Mohd Azhar, S.H., Abdulla, R., Jambo, S.A., Marbawi, H., Gansau, J.A., Mohd Faik, A.A., Rodrigues, K.F. 2017. Yeasts in sustainable bioethanol production: A review. *Biochemistry and Biophysics Reports*, **10**, 52-61.
69. Morweiser, M., Kruse, O., Hankamer, B., Posten, C. 2010. Developments and perspectives of photobioreactors for biofuel production. *Applied microbiology and biotechnology*, **87**(4), 1291-301.
70. Muñoz, R., Guieysse, B. 2006. Algal–bacterial processes for the treatment of hazardous contaminants: A review. *Water Research*, **40**(15), 2799-2815.
71. Onsager, O.-T., Brownrigg, M.S.A., Lødeng, R. 1996. Hydrogen production from water and CO via alkali metal formate salts. *International Journal of Hydrogen Energy*, **21**(10), 883-885.
72. Perez-Garcia, O., Escalante, F.M.E., de-Bashan, L.E., Bashan, Y. 2011. Heterotrophic cultures of microalgae: Metabolism and potential products. *Water Research*, **45**(1), 11-36.
73. Posten, C. 2009. Design principles of photo-bioreactors for cultivation of microalgae. *Engineering in Life Sciences*, **9**(3), 165-177.
74. Qiang, H., Zarmi, Y., Richmond, A. 1998. Combined effects of light intensity, light-path and culture density on output rate of *Spirulina platensis* (Cyanobacteria). *European Journal of Phycology*, **33**(2), 165-171.
75. Organization of the Petroleum Exporting Countries (OPEC) monthly oil market report 2008: http://www.opec.org/opec_web/en/publications/461.htm.
76. Renewables 2017 - Global Status Report, Renewable Energy Policy Network for the 21st Century (REN21), Paris - REN21 Secretariat. ISBN 978-3-9818107-6-9.
77. Renewables Information: Overview (2017 edition). International Energy Agency (IEA), ISBN PRINT 978-92-64-27776-2.
78. Resources for the future: <http://www.rff.org/blog/2009/2008-oil-price-shock-markets-or-mayhem>
79. Richmond, A. 2004. Principles for attaining maximal microalgal productivity in photobioreactors: an overview. *Hydrobiologia*, **512**(1), 33-37.

80. Richmond, A., Cheng-Wu, Z., Zarmi, Y. 2003. Efficient use of strong light for high photosynthetic productivity: interrelationships between the optical path, the optimal population density and cell-growth inhibition. *Biomolecular Engineering*, **20**(4), 229-236.
81. Rönnlund, I., Myréen, L., Lundqvist, K., Ahlbeck, J., Westerlund, T. 2011. Waste to energy by industrially integrated supercritical water gasification – Effects of alkali salts in residual by-products from the pulp and paper industry. *Energy*, **36**(4), 2151-2163.
82. Sasaki, M., Kabyemela, B., Malaluan, R., Hirose, S., Takeda, N., Adschiri, T., Arai, K. 1998. Cellulose hydrolysis in subcritical and supercritical water. *The Journal of Supercritical Fluids*, **13**(1), 261-268.
83. Shaw, R.W., Brill, T.B., Clifford, A.A., Eckert, C.A., Ulrich Franck, E. 1991. Supercritical water a medium for chemistry. *Chemical and Engineering News*, **69**(51), 26-39.
84. Sinağ, A., Kruse, A., Schwarzkopf, V. 2003. Key Compounds of the Hydrolysis of Glucose in Supercritical Water in the Presence of K₂CO₃. *Industrial & Engineering Chemistry Research*, **42**(15), 3516-3521.
85. Singh, S.P., Singh, P. 2015. Effect of temperature and light on the growth of algae species: A review. *Renewable and Sustainable Energy Reviews*, **50**, 431-444.
86. Susanti, R.F., Veriansyah, B., Kim, J.-D., Kim, J., Lee, Y.-W. 2010. Continuous supercritical water gasification of isooctane: A promising reactor design. *International Journal of Hydrogen Energy*, **35**(5), 1957-1970.
87. Talebnia, F., Karakashev, D., Angelidaki, I. 2010. Production of bioethanol from wheat straw: An overview on pretreatment, hydrolysis and fermentation. *Bioresour Technol*, **101**(13), 4744-53.
88. Toor, S.S., Rosendahl, L., Rudolf, A. 2011. Hydrothermal liquefaction of biomass: A review of subcritical water technologies. *Energy*, **36**(5), 2328-2342.
89. U.S. Energy Information Administration – Spot prices of crude oils and products: www.eia.gov/dnav/pet/PET_PRI_SPT_S1_M.htm
90. Valdez, P.J., Nelson, M.C., Wang, H.Y., Lin, X.N., Savage, P.E. 2012. Hydrothermal liquefaction of *Nannochloropsis* sp.: Systematic study of process variables and analysis of the product fractions. *Biomass and Bioenergy*, **46**, 317-331.
91. Verardi, A., De Bari, I., Ricca, E., Calabro, V. 2012. *Hydrolysis of Lignocellulosic Biomass: Current Status of Processes and Technologies and Future Perspectives*.
92. Weyer, K.M., Bush, D.R., Darzins, A., Willson, B.D. 2010. Theoretical Maximum Algal Oil Production. *BioEnergy Research*, **3**(2), 204-213.
93. Williams, P.T., Onwudili, J. 2006. Subcritical and Supercritical Water Gasification of Cellulose, Starch, Glucose, and Biomass Waste. *Energy & Fuels*, **20**(3), 1259-1265.
94. World Energy Resources: Full report 2016. World energy council. ISBN: 978-0-946121-62 5.
95. Yakaboylu, O., Harinck, J., Smit, K., de Jong, W. 2015. Supercritical Water Gasification of Biomass: A Literature and Technology Overview. *Energies*, **8**(2), 859-894.
96. Yanik, J., Ebale, S., Kruse, A., Saglam, M., Yuksel, M. 2007. Biomass gasification in supercritical water: Part 1. Effect of the nature of biomass. *Fuel*, **86**(15), 2410-2415.
97. Yanik, J., Ebale, S., Kruse, A., Saglam, M., Yuksel, M. 2008. Biomass gasification in supercritical water: II. Effect of catalyst. *International Journal of Hydrogen Energy*, **33** (17), 4520-4526.
98. Yoneda, K., Honda, Y., Momiyana, N., Abe, R. 1943a. Water-Gas Shift Conversion Under High Pressure and Temperature in Potassium Carbonate Solutions. *Journal of the Chemical Society of Japan*, **46**, 554.
99. Yoneda, K., Kondo, S., Abe, R. 1943b. Behavior of Water-Gas in Aqueous Potassium Bicarbonate and Formate Under-High Pressure and Temperature. *Journal of the Chemical Society of Japan*. **46**, 667.

100. Yoneda, K., Kondo, S., Abe, R. 1944a. Thermal Decomposition of Potassium Formate Solution and the Behavior of Water Gas with K_2CO_3 below the Decomposition Temperature. *Journal of the Chemical Society of Japan*, **47**, 5.
101. Yoneda, K., Kondo, S., Abe, R. 1944b. Mechanism of Conversion. *Journal of the Chemical Society of Japan*, **47**, 7.
102. Zhang, S., Bi, X.T., Clift, R. 2015. Life cycle analysis of a biogas-centred integrated dairy farm-greenhouse system in British Columbia. *Process Safety and Environmental Protection*, **93**, 18-30.

2. Literature and Technology Review

2.1. Introduction

This chapter highlights part of the research activities in the field of hydrothermal conversion in near- and supercritical water. In general, there are a variety of applications when dealing with fluids at elevated temperatures and pressures, depending on the work conducted and its objectives. An example is applying supercritical CO₂ as a solvent for the extraction of other compounds, due to its non-toxicity, environmental safety and availability at low cost [Díaz-Reinoso *et al.* 2006, Zhang *et al.* 2010]. It is also used as a solvent in other applications that include the production of fine particles on the submicron level, by the rapid expansion of system mixtures from supercritical state [Türk *et al.* 2006]. On the other hand, supercritical water can be used in the synthesis of nanoparticles such as copper or nickel oxides, a technique where a fine tuning of process conditions allows the control of particle size formation or nucleation [Hayashi and Hakuta 2010]. These interesting fields, however, are mentioned only as examples of application versatility and will not be the focus of this study.

2.2. Feedstock materials and process objectives

As pointed out in the previous chapter (Ch. 1 Introduction), the gasification in supercritical water or the hydrothermal conversion generally utilizes the unique properties of water that only exist in the vicinity of its critical region. The idea of utilizing water in this manner was first introduced by Modell *et al.* 1978 and Modell 1985. These early works demonstrated that a gaseous mixture of H₂, CO₂ and CO can be obtained from model compounds (glucose) as well as cellulosic materials (forest products) using supercritical water without char formation. Since then, the exploitation of wet materials under comparable conditions has started and continued.

Typically, the conversion of carbonaceous materials under high temperatures and pressures can be conducted on catalytic or non-catalytic basis. Depending on the mechanism of feed delivery to the system and product discharge, continuous and batch processes can be distinguished. Elliott *et al.* 1989 developed a process for the conversion of high-moisture biomass (cellulose, sucrose and sorghum) to CH₄, CO₂ and H₂, in a continuous-flow reactor under a reduced temperature (350 °C) and using a Ni-based catalyst.

In general, numerous kinds of materials can be used in different processes of hydrothermal conversion. This depends in the first place on the scope of work or the product targeted from each process. Standard chemicals or model compounds are widely used under sub- and supercritical conditions on different scales of operation. Examples of such compounds include glucose, ethanol, glycerol, formaldehyde, benzene, isooctane and phenol. Some experiments are designed to investigate the influence of the feed's molecular structure on the process performance or the type of product formed [Chakinala *et al.* 2013]. Other experiments are conducted to generate a kinetic expression or suggest a reaction pathway that is valid or plausible at the corresponding operating conditions for a given compound [Kabyemela *et al.* 1997, Akgül *et al.* 2013, Guo *et al.* 2013, Abelleira *et al.* 2013]. These experiments are typically carried out in small scale systems such as batch autoclaves or continuous tubular reactors of small dimensions. These experiments usually include certain measures (ex.: conversion efficiencies, production rates or species concentration in a certain phase), which optimally describe the process performance depending on the objective of each work.

On the other hand, agricultural byproducts or crop residues and other waste materials have gained noticeable attention in the recent decades due to their vast amounts, treatment or disposal necessity, and their high content of moisture. Several works tend to focus on releasing the stored energy of the biomass in the form of a solid, liquid or gaseous biofuel. Erlach *et al.* 2012 presented a conceptual design, using balance calculations with the aid of *Aspen Plus* simulation, of an industrial-scale plant for the hydrothermal carbonization of wood. The goal was to provide a mean of treating this material to upgrade its heating value and decrease its water content prior to entrained flow gasification. This was conducted to compare carbon capture rates and the overall process efficiency with entrained flow and fluidized bed gasification of the raw wood.

Ro *et al.* 2007 evaluated wet gasification of animal wastes (manures) in a conceptual study based on energy content of both the feed and product gas as well as proposed reaction schemes. According to estimates, the work claimed that these wastes, especially swine manure, can be converted with a net positive energy return if an efficient heat recovery (90%) is achieved, at a threshold concentration of 8 wt%. Rice husk was used by Basu *et al.* 2009 for supercritical water gasification in a batch reactor. The influence of temperature (400 – 680 °C) and feed concentration (2 – 14 wt%) on the process efficiency was studied. Maximum gasification efficiency on carbon basis (defined as CGE and is explained in section 3.3 of the next chapter) of 70% was obtained at the lowest feed concentration and the work reported

linear increase of this value upon raising temperature. *Güngören Madenoğlu et al. 2011* tested several types of ligno-cellulosic biomass (cauliflower residue, acorn, tomatoes residue and hazelnut shell) for SCWG in a continuous-flow system at $T = 600\text{ }^{\circ}\text{C}$ and $P = 35\text{ MPa}$ using 8 wt% feed concentration. Potassium and sodium carbonate were added as catalysts and the values of CGE were improved by addition of these salts into the reacting system. Other feedstock materials were used for hydrothermal liquefaction or supercritical gasification in continuous-flow systems, such as fruit pomace [*Hammerschmidt et al. 2014*], corn silage, clover grass [*D'Jesús et al. 2005*, *D'Jesús et al. 2006*], potato-starch gels, pyroligneous acid [*Möbius et al. 2012*] and wood sawdust [*Antal et al. 2000*].

Several works discussed the utilization of black liquor, a chemical by-product from the pulping industry that consists of an aqueous solution of lignin residues, hemicellulose and inorganic compounds [*Magdeldin et al. 2015*, *Cao et al. 2011*]. This material contains about 40% inorganic chemicals that can be recovered using supercritical water gasification, where the organic fraction of black liquor is gasified and the inorganics are separated by precipitation. [*Sricharoenchaikul 2009*]. Black liquor is typically recovered by boilers on a large scale in preset or existing technologies, where it has to be concentrated before combustion [*De Blasio et al. 2016*]. In table 2.1, different types of carbonaceous materials are highlighted in terms of their content of moisture, energy and ash. The values listed in the table below may vary depending on the nature or conditions through which these materials evolved as well as the method of collection. Therefore, using a range of values would be acceptable to address these materials. Certainly, the degree or extent to which these materials exist varies depending on the country, its location, resources and the lifestyle of its population.

Table 2.1 – Different types of biomass and some of their basic analyses

	Moisture content wt%	Calorific value (HHV) MJ.kg ⁻¹	Ash content (550 °C) wt%
Microalgae (misc.) ^a	> 95 ^f	20 - 22	10 - 15
Sewage sludge (secondary) ^b	87	15.4	27.02
Cow manure (fresh) ^a	86 - 88	15 - 17	13 - 14
Rice husk ^c	7.9	14.87	19.9
Brewery spent grain (Malt) ^d	4 - 6	N/A	2.4 - 7.9
Wood pellets ^a	6.5 - 8.5	18.6 - 19.1	0.27 - 0.65
Wheat straw ^a	8.01 - 10.3	15.63 - 17.2	4.23 - 7.16
Corn silage ^e	62 - 70	3.9 - 4.5	18.3
Hazelnut shell ^a	12 - 13	17 - 20	1 - 3

^a Based on data collected from ECN *Phyllis* classification database, ^b Qian et al. 2015, ^c Basu et al. 2009, ^d Aliyu and Bala 2011

^e D'Jesús et al. 2005, ^f The values depend on the culture density during growth, moisture content can be significantly reduced upon harvesting.

2.3. Exploitation of algal biomass

Extensive efforts have been presented in several works to utilize microalgae, evaluate the given processes and define a systematic approach for describing the corresponding systems. The works conducted in these systems has covered the different thermochemical techniques referred to earlier (HTC, HTL and HTG) using different scales and modes of operation.

2.3.1. Hydrothermal carbonization

Heilmann et al. 2010 reported on hydrothermal carbonization of microalgae and the energetic content of the algal char produced. Two strains of microalgae were selected (*Chlamydomonas reinhardtii* and *Dunaliella Salina*) and put in a 450 ml stirred batch reactor under $T = 190 - 210$ °C, $P = 16.5$ bar. Certain concentrations of algal feed were used (5, 7.5, 15 and 25 wt%) and the residence time was varied between 0.5 to 3 h. The key outcome of the experiment was to measure the amount of recovered carbon in the algal char relative to aqueous filtrate and CO₂ evolved. About half of the carbon present in the feed was found, along with nitrogen in the aqueous filtrate in the form of reaction by-products. The char obtained from both strains was also compared with natural coal and char from a lignocellulosic material (Prairie grass). The quality, in terms of energy content, of the algal char produced was in the bituminous range according to the values presented. Also, the work stated the potential of a shift to continuous operation, given the relatively low residence time and mild conditions adopted.

2.3.2. Hydrothermal liquefaction

Increasing both temperature and pressure to values around the critical point of water provides a new dimension for operation in terms of product characteristics. Under these conditions, a liquid substance referred to bio-crude or bio-oil can be obtained and the process is then denoted as hydrothermal liquefaction. Several algal species or strains have been used for the conversion process. Some examples include *Spirulina*, *Chlorella vulgaris* and *Porphyridium cruentum* [*Vardon et al. 2011*, *Biller and Ross 2011*]. The majority of the works published in the category hydrothermal liquefaction deals with batch reactor [*Toor et al. 2011*]. In the work of *Valdez et al. 2012*, a mini batch reactor of 4.1 ml was used in the temperature range of 250 – 400 °C and residence time of 10 to 90 minutes to convert microalgae (*Nannochloropsis*) without the use of a catalyst. Operation pressure was not reported. Dichloromethane was used to separate the aqueous and organic phases. Two fractions of bio-crude, heavy and light, were distinguished and separated by the addition of n-Hexane.

Based on the results, the work concluded that the yield of total bio-crude (heavy and light) depends on system temperature at the first place. In addition, producing more of one fraction over the other is directly related to temperature and reaction time adjustment. These statements are generally supported in a different work [Barreiro *et al.* 2013] regardless of the strain used. According to the experiments, using higher feed concentration, from 5 up to 35 wt% at 350 °C and 60 min residence time, resulted in an increased oil yield from 36 to 46% respectively.

Nannochloropsis was also used by Toor *et al.* 2013 in a batch autoclave of larger volume (400 ml). Filtration was used to separate the aqueous phase and acetone was the chemical applied to extract the bio-crude. The bio-crude yield at the same temperature as in the work of Valdez *et al.* 2012 are similar (46 wt%) despite the difference in the biomass loading (25 wt%) and residence time (30 min) in the work of Valdez *et al.* 2012. The influence of high lipid-containing feedstock on the production bio-crude was supported in the two works along with other works (ex.: Biller *et al.* 2011). This, along with other process variable, gives an indication regarding the importance of species selection for hydrothermal liquefaction.

2.3.3. Gasification in supercritical water

Gasification of algal biomass in supercritical water proceeds at the highest temperature and pressure compared to other hydrothermal conversion systems. Here, the goal is to convert the organic stream into a combustible gaseous mixture of high energetic value along with carbon dioxide. The published works in this field have covered several species of microalgae, different systems of various sizes, under batch and continuous mode of operation. Of the early works processing algal biomass, Minowa and Sawayama 1999 presented. The work gave a brief analysis of the gasification of 12.6 wt% *C. vulgaris* in a 12 cm³ batch autoclave with a magnetic stirrer. A nickel-based catalyst on silica-alumina, heated using an electric furnace to 350 °C at a relatively reduced pressure (18 MPa).

The gaseous product consisted mainly of CO₂, H₂ and CH₄ and all the nitrogen content of the algal species was converted to ammonia in the aqueous effluent. As the catalyst loading was increased 3-folds, the CGE was doubled from 35% to 70% and the gas composition approached the equilibrium composition, but did not match it. They stated that a complete conversion is possible at a higher reaction temperature or with a larger amount of catalyst with no further investigations.

Stucki et al. 2009 conducted a catalytic gasification of *Spirulina platensis* in supercritical water with different feed concentrations (2.5 – 20 wt%). A complete gasification (100% CGE) in an unstirred batch reactor ($V = 30$ ml) at $T = 400$ °C and a $P = 30.8 - 34.5$ MPa to a methane-rich gas was reached. A ruthenium-based heterogeneous catalyst was loaded in the reactor. A feed-to-methane thermal conversion of 60 – 70% was achieved based on the calorific value of the algal biomass used. One run was conducted without a catalyst at the lowest feed concentration. This resulted in a very low CGE (10%) and a gas product, which consisted mainly of CO_2 and H_2 . This is a clear indication that implementing a metal-based catalyst has the advantage of operating at lower temperature and still reach good conversion.

In the work of *Chakinala et al. 2010*, *Chlorella Vulgaris* was tested for gasification in supercritical water using a batch system in the shape of quartz capillaries (ID = 0.2 cm, L = 15 cm). The study investigated the influence of reaction time (1 – 15 minutes), temperature (400–700 °C), feed concentration (2.9 and 7.3 wt%) and the use of several types of metal-based catalysts in some experiments. The goal was to evaluate the gasification efficiency (GE) and the composition of the gaseous products (H_2 , CO_2 , CO, CH_4 and some C_2 - C_3 hydrocarbons).

Using the lower and higher feed concentration at 600 °C resulted in a GE was 68% and 53% respectively. The work also referred to other experiments conducted, not reported in the work though, in algal concentrations lower than 2.9 wt%, where a complete gasification was achieved. It confirmed the significant impact of operating at higher temperature on the amount of gases produced, in particular when a GE of 83% was achieved with a 7.3 wt% feed concentration at the highest temperature applied (700 °C). These experiments were conducted non-catalytically and with a reaction time of two minutes.

Regarding the reaction time, the work concluded that 5 minutes (at $T = 580$ °C) resulted in a GE of max. 73% if no catalysts were used, even if the reaction time was increased beyond this value. As *Inconel*^{®1} powder and a nickel wire were used as a catalyst, the GE was improved to 84% compared with 53% at the same temperature mentioned earlier. *Inconel*[®] powder was introduced in this work as a mean to mimic the catalytic effect of the reactor walls (when *Inconel*[®]-based reactors are used) on gasification, which was discussed elaborately in earlier works [ex.: *Antal et al. 2000*, *Boukis et al. 2003*, *Potic et al. 2004*]. Furthermore, the experimental results showed that a complete conversion using a Ru/TiO₂ catalyst at 700 °C was possible, even at lower temperature (600 °C) if excess Ru/TiO₂ was used.

¹ *Inconel* refers to brand name which refers to a group of nickel-chromium based alloys

Continuous-flow systems for wet gasification have been presented in literature as well. Elliott et al. 2012 used a bench-scale tubular reactor, of 1-liter volume, at $T = 350\text{ }^{\circ}\text{C}$ and $P = 20\text{ MPa}$. Among several strains tested including macroalgae and mixed strains, *Spirulina* and *Nannochloropsis salina* were relevant to highlight. They were fed at a concentration of 20 – 25 wt%. A simple separator for minerals (salts or ash) and a sulphur stripper were integrated in the system to reduce the risk of plugging and catalyst deactivation respectively. The minerals are removed batch-wise as they accumulate in the separator. The material used for sulphur removal was Raney nickel. Since the heat recovery was not planned for this scale of operation, heat was provided externally. A Ru/C-based catalyst bed was used for the experiments. Depending on the specific run, the system was operated at a continuous mode for a range of 6 – 10 hours. A direct indication of residence time was not referred to in the work, but a volumetric flow rate range of $1 - 1.5\text{ L}\cdot\text{h}^{-1}$ algal feedstock was stated and another term, liquid hourly space velocity (LHSV), in the range of $1.2 - 1.9\text{ h}^{-1}$ was used and was defined as the liters of slurry processed over the liters of catalyst bed at the designated operating temperature.

Detailed measurements and calculations of the CGE, COD conversion, trace elements in both solid minerals and aqueous phase as well as the spent catalyst were conducted. High CGE were obtained with *Spirulina* compared to *Nannochloropsis salina* (90% and 59% respectively). The authors suggested an explanation to the reduced conversion based on the high lipid content of *Nannochloropsis salina*, which resulted in incomplete gasification of the long chain fatty acids, leading carbon losses in the catalyst bed and aqueous byproduct. During some of the tests, several findings or challenges were reported. This includes the loss of a fraction of the carbon along with the separated minerals, evidences of catalyst deactivation during longer term operation, high levels of ammonia in the aqueous phase and while phosphate precipitation in the mineral separator.

Miller et al. 2012 addressed the gasification of algal biomass in their work. A tubular reactor heated via a three-zone split furnace was available for the continuous gasification of *Spirulina* at $T = 550 - 660\text{ }^{\circ}\text{C}$ and $P = 23.5\text{ MPa}$ without a catalyst. A two-streams configuration was applied by using supercritical water that is combined with the algal biomass at a mixing tee in a 1:1 ratio. Two high concentrations were used for the experiments (17.5 and 25 wt%) and a range of residence time of 1 – 40 seconds was tested. Two measures were used to express the efficiency of operation; the gasification efficiency, as the ratio between the total gaseous products obtained and the mass of dry algal biomass.

The second measure is the gasification rate, expressed in units of concentration per time. The work defined this metric as the amount of gas produced, relative to the feed volume, divided by the average residence time. A set of factorial experiments was conducted to investigate the interaction between the major process variables (temperature, feed concentration and residence time). A maximum gasification efficiency of 95% was achieved using the longest residence time ($\tau = 40$ s). The GE efficiency may sometimes exceed 100% in many cases, given the contribution of water as a reactant for the total gaseous products (refer to chapter materials and methods). No data on carbon balance (i.e. CGE) was presented.

Based on the interaction introduced by the factorial experiments, the impact of operation temperature was found to have the crucial significance. Further, changing the residence time was more effective at lower temperatures. In addition, the work covered other topics, demonstrating the reliable pumping of very concentrated slurry (paste-like) using a piston cylinder. It also provided a relation between the flow regime and gasification rate, indicating that the gasification rate peaks around the turbulent region of the pipe flow (Reynold's number, $Re = 4000$).

Another system for the catalytic gasification of *Phaeodactylum tricornutum* in a continuous-flow mode was described by *Bagnoud-Velásquez et al. 2014*. The laboratory unit contained a salt separator and the reactor (ID = 12 mm and L = 1.4 m) was packed with a Ru/C catalyst. The procedure was to pump a model compound (5 wt.% glycerol) first to preheat the system, followed by the 6.5 wt.% algal feed. Operating at 32.3 MPa, temperatures of 360, 470 and 420 °C for the preheater, salt separator and reactor respectively were applied. A weight hour space velocity of $0.42 \text{ g}_{\text{feed}} \cdot \text{g}_{\text{cat}}^{-1} \cdot \text{h}^{-1}$ was set.

Based on the results from one experiment using the algal feed, the effluent was not oily and not clear ($\text{TOC} = 8740 \text{ mg} \cdot \text{L}^{-1}$). A drop in CGE (from 100% down to 31.1%) as well as the rate of gas production was noticed after switching from glycerol to algae. Also, the switching resulted in a decreased of methane production, accompanied by an increase of H_2 , C_2H_6 and C_3H_8 . The software Aspen plus was used to calculate the thermodynamic equilibrium composition of gases (based on the minimization of the Gibbs free energy) at similar feed concentrations and operating conditions. The results, however, did not match with those obtained during the experiment at steady state. Some difficulties were pointed out in the work such as the catalyst poisoning by sulphur. The poisoning was faster or more severe compared to the work of *Elliott et al. 2012*, despite using a lower concentration of algal feedstock.

This indicates the significance of the sulphur removal system in the earlier work. Another challenge was the blockage of the active metal sites due to coke deposition. Added to that, the precipitation of some heteroatoms such as P, Mg and Ca on the catalyst was identified from the SEM-EDX analysis. One main message interpreted from this work is the variation or dependence of system performance and gas composition on the configuration, flow regime and mode of operation. This was supported by comparing the results obtained with those from several previous works.

The results discussed in this chapter demonstrate a broad range of approaches depending on the scope of each work. To conclude the varieties of the systems associated with hydrothermal conversion, the following figure (fig. 2.1) shows a schematic summary of basic units and operational sub-processes involved in such systems.

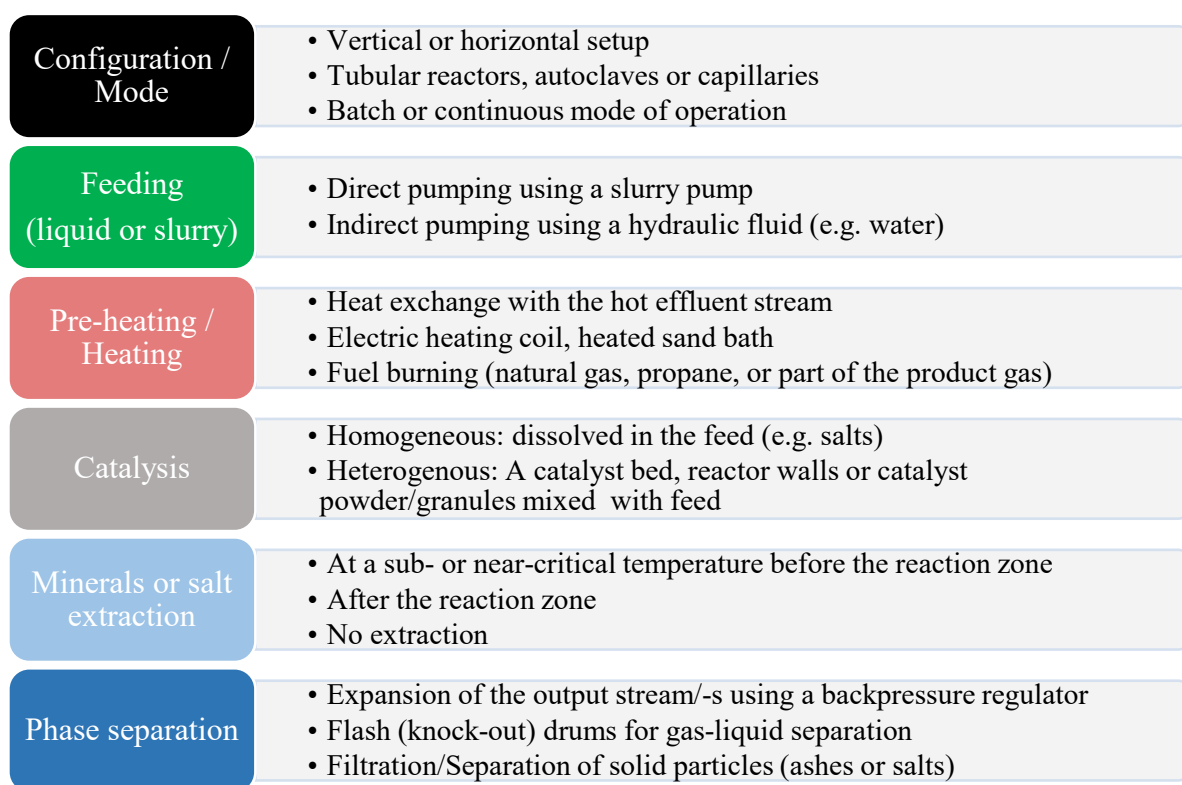


Figure 2.1 – Basic sub-processes involved in hydrothermal gasification (HTG).

At the end of this chapter, table 2.2 provides a quantitative summary of previous works related to hydrothermal gasification with the focus on algal biomass as a feedstock. Related to the works listed in the table, the collected data take into consideration the algal species, operating temperature, pressure, available catalyst for operation, feedstock concentration, system size, mode of operation, residence time as well as the efficiency of gasification.

2.4. Treatment of sewage sludge

Given the concept of utilizing renewable sources for continuous energy production, there is an emerging need to treat waste streams such as sludge or fecal matter to prevent the spread of pathogens and maintain acceptable quality of aquatic resources. This is of particular concern in poor communities, where a lack of proper sanitation and limited access to clean water is common [Arthurson 2008]. Sewage sludge has also drawn the attention as a promising feedstock in hydrothermal conversion. This is due to its energy content and the production in large amounts from wastewater treatment plants [Gong *et al.* 2014]. Developing hydrothermal conversion systems, such as the supercritical gasification of sewage sludge, would achieve a double benefit by generating energy-rich gas product and providing a safe disposal of this material at the same time [Gasafi *et al.* 2008].

Chen and co-workers investigated the gasification of secondary sludge in a 140 ml batch reactor under near- and supercritical conditions. Based on a solid concentration of 8.9 wt%, the work studied the influence of temperature variation (350 – 450 °C) and residence times of 5 to 25 minutes on the formation and distribution of the gaseous products, liquid intermediates as well as solids within the system. It was concluded that the organic constituents of sludge were almost completely dissolved and converted in water at 425 °C. The key message from the work was that temperature had the dominant influence over residence time in terms of gas yield, composition and product distribution [Chen *et al.* 2013].

In the work of *Boukis et al.* 2017, a catalytic process for the conversion of digested sludge (a by-product of anaerobic biogas production) under supercritical conditions was operated on pilot-scale using continuous flow. The work involved a ruthenium-based catalyst preceded by a bed of ZnO on top, in order to adsorb sulphur which exists in the feedstock and was not extracted in a salt separation system prior to the reactor. The gasification was conducted at a reaction temperature of 420 °C and pressure of 280 bar. Methane was the targeted or primary product of the process. In addition, the recovery of basic elements in the sludge such as nitrogen and phosphorus was demonstrated. The work showed the ability of processing as much as 334 kg of this material and recovering over 55% of the ash which makes up about 20 – 30 wt% of the raw sludge.

The influence of feed concentration and residence time on the gasification of primary sewage sludge was presented by *Wilkinson et al. 2012*. The gasification efficiency and gas composition was evaluated using a 9 ml batch reactor maintained at a temperature of 800 °C. Residence time was varied between 7, 10 and 14 minutes with solid concentrations of 3.84 and 21.3 wt%. Gasification efficiency reached 100% for both concentrations at this high temperature. However, the maximum value was achieved at lower concentration and shorter residence time (7 minutes) compared to 10 minutes using a concentration of 21.3 wt%. The frame work in which this study has been made was the comparison between supercritical water gasification and anaerobic digestion, giving an insight of the system size and energy requirement. In this context, it was concluded that SCWG is efficient in treating the organics and converting them to energy. Nevertheless, a minimum solid concentration of about 30 wt% was necessary for an auto-thermal or energy-neutral operation without heat recovery, according to the authors.

In another work, a combination of gasification, followed by oxidation of sewage sludge in supercritical water was presented [*Qian et al. 2015*]. A feed concentration of 13 wt% solids was adjusted; gasification temperatures of 450 to 600 °C were applied to the 0.6 liter reactor for 20 minutes. The produced effluent, liquid and solid residues, was treated using hydrogen peroxide (H₂O₂) as an oxidant under supercritical conditions. The results showed an impact of both the temperature and oxidation coefficient (n) on the gaseous products (yield and components), liquid effluent quality (TOC and NH₃-N) as well as solid residues in terms of its amount. The work alleges the feasibility of a combined process; SCWG at 450 °C and SCWO at 600 °C with an oxidation coefficient (n = 1), achieving enhanced effluent quality.

2.5. Toward process development

2.5.1. Slurry pumping

The ability of a reliable pumping of the feedstock to near- or supercritical pressures contributes significantly to the stability and success of the hydrothermal processes. Pressurizing water or any model compound is usually associated with no operational difficulties. The Pacific Northwest National Laboratory (PNNL) published an elaborate report on pumping biomass slurries (*Berglin et al. 2012*). The work consisted of several milestones to scale up a system that converts wet slurries to high-value hydrocarbon fuels. Several assessments based on information acquired from pumps vendors are available in this review. The study was focused on hydrothermal liquefaction. However, the details provided and the arguments made would be applicable for other hydrothermal conversions processes, where aqueous feed or slurry is involved. This is because pumping in these processes is conducted at high-pressure (near- / supercritical) and proceeds at ambient temperature in most of the cases.

The major factors influencing a reliable pumping are the feedstock nature of the pumped material and the scale of operation. Model compounds are pumped easily since they are simple liquid solutions. On the contrary, biomass and waste materials contain a variety of solid constituents, which can have fibrous structures, large particles, be sticky or viscous and contains insoluble inorganic fraction. This is in particular when pumping becomes an issue, especially as the concentration of these compounds increases.

Positive displacement equipment such as piston or screw pumps are widely applied to provide the desired operational pressure. These pumps are capable of delivering the feed at high pressures, can provide a stable and precise flow. On a laboratory scale, pumps similar to those used in liquid chromatography (HPLC) function properly. An example of these pumps includes those manufactured by *Eldex*[®] and *BISCHOFF*[®]. However, these pumps are only suitable at small scale, as they are mostly limited by low throughput ($< 2 \text{ L}\cdot\text{h}^{-1}$) and can handle diluted feed streams in case solids are considered. Upon the need to operate using higher solid concentrations, a pressurized cylinder can be integrated into the system. This has been available in some work groups (ex.: *D'Jesus et al. 2005*, *Miller et al. 2012*), where a floating piston inside a cylinder is driven by a working fluid, like water, on its other side. This enables a complete separation between the feed to be pressurized and the internal parts of the pump. Practically, this cylinder can be thought of as a form of a piston pump that is driven by another pump for pressure development.

When large-scale operation is planned, different pumps that are off-the-shelf are necessary. Pump selection should be made carefully depending on the desired throughput range of operation, maximum solid content or viscosity that the pump is able to handle. There are several manufacturers providing pumps that can operate reliably with slurry materials. Examples include *Serva*[®], *Weir minerals*[®] and *Feluwa*[®]. The double-hose diaphragm pumps from *Feluwa* are used in several workgroups (for example at the University of Cádiz, Karlsruhe Institute of Technology and Duke University) in the field of supercritical water on a pilot scale. An illustrative diagram of the equipment is shown in figure 2.2. The positive displacement pump allows no contact between the pressurized medium and the pump's internal parts. This is achieved by flowing the feed through a rubber cylindrical diaphragm (hose) that compresses the feed (in yellow) through a squeezing action across flow direction (green arrows).

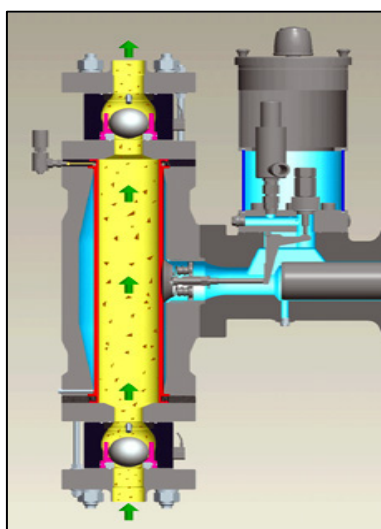


Figure 2.2 – Illustrative sketch of *Feluwa*'s hose diaphragm pump²

Pressure is developed on the surface of the hose via a piston that works against a hydraulic and actuation fluid (in blue), typically oil [*FELUWA hose diaphragm pumps - operation and maintenance manual 2014*]. Intake and discharge valves are located at the bottom and the top of the volume subjected to pressure. Valve operation is sometimes a concern when large, sticky or fibrous particles are present, causing the valve not to be fully sealed.

In practice, pre-processing or pretreatment is often required to prepare the slurry materials for pumping in continuous-flow systems. Typically, the slurry is preferred to be well-mixed to ensure homogeneity and avoid the formation of hot spots in the reaction zone due to the existence of agglomerates or large particles. Also, continuous mixing prevents settling of the solids and the formation of concentration gradients in the feed tanks.

² Credit: FELUWA: <http://www.mining-technology.com/contractors/pumps/feluwa-1/feluwa-11.html>

The other issue is associated with the particle size distribution of the slurry, which might hinder smooth pumping. Although some feedstock materials such as microalgae have fine particles, other sources of biomass feedstocks can contain particles or clumps of sizes up to 4-6 mm. Therefore, a limit for the tolerance of a given pump to particles' diameter or length should be predefined. Cutting or milling the slurry is practiced to control the particle size class of the feed input and ensure successful operation. Furthermore, viscosity is another factor that plays a role in pumping, beside the two issues mentioned above. Figure 2.3 shows the effect of varying slurry (secondary sludge) concentration on the viscosity. These measurements are usually conducted under different rates of shear stress, which gives a better insight when defining the suitable range, depending on the pipe sizing and velocities.

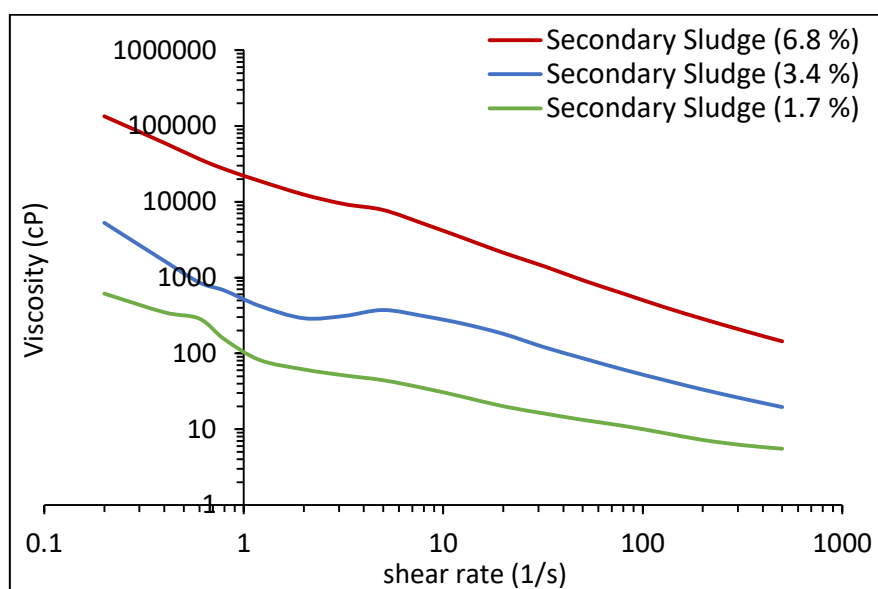


Figure 2.3 – Viscosity of different concentrations of milled secondary sludge at different shear rates³

The figure curves indicate that a viscosity increase of one to two orders of magnitude can be the result of using slurries of higher concentration. The feed material should be maintained in a pump-able or flow-able state to avoid any blockage or pipe failure. The composition of processed material, surrounding temperature as well as the degree of milling or mixing have an impact on the material's viscosity and therefore, these factors have to be taken into consideration, especially using thick or high concentrated slurries.

³ Data obtained at the laboratories of the Pratt School of Engineering, Duke University, June 2016

2.5.2. Recycling of natural resources

An important aspect that contributes to further development of hydrothermal processes is the utilization of byproducts. Referring to both mass and energy streams, the efficient use of these resources is a key milestone to scale-up and economic feasibility. In addition to energy management, the utilization of the minerals that exit the process in aqueous or waste streams has become a major concept of research works in the recent years. This concept was discussed on the different types of conversion systems presented in this chapter (HTC, HTL and HTC), demonstrating the potential to exploit these materials depending on the field of application.

Minowa and Sawayama 1999 provided a brief description, in which the recovered solution from catalytic gasification of *C. vulgaris* was used for gasification. The authors indicated that entire nitrogen content of the algal cells was converted into ammonia after conversion (NH_4^+ concentration in the effluent was 9000 mg.L^{-1}). As the effluent was separated from the catalyst, it contained low TOC (258 mg.L^{-1}). A dilution of 300-fold was needed to test the recovered effluent and compare it with a standard medium (Chlorella Ellipsoidea Medium) over a two-weeks cultivation batch. Despite the availability of nitrogen, the growth of microalgae was with the absence of other nutrients that were not found in the gasification effluent. Therefore, using this aqueous fraction solely resulted in a growth rate of one eighth of that measured in the standard medium. A mixture of gasification effluent and a standard medium having lower N concentration was successful and the growth rate was comparable to that of standard medium.

Haiduc et al. 2009 presented a conceptual idea with an integrated system referred to as SunCHem. The system is a combination of algal cultivation and the catalytic HTG of algal biomass in a batch reactor. As a first step of the concept proof, the two processes were tested separately. *Phaeodactylum tricornutum* was the feedstock for gasification. The major product was a gaseous mixture containing mainly methane and CO_2 , along with minimal concentrations of H_2 and $\text{C}_1\text{-C}_3$ hydrocarbons. Five other strains of microalgae and cyanobacteria were tested for cultivation using standard solutions.

The point of evaluation in the work was the influence of nickel, stemming from corrosion products on the algal growth. Certain levels of Nickel would exist due to a material loss of the reactor walls. They accumulate in the process effluent and tend to have a prohibitive role for the growth of microalgae. In this work, the HTG process effluent was not used for cultivation. Instead, a nickel solution was added to the culture medium in adjusted concentrations (1 - 25

ppm) to simulate the Ni levels expected in the HTG process effluent containing the nutrients. For all the species tested, the growth was negatively influenced by the presence of Ni even in the ppm concentration range (1 - 10 ppm). Ni concentrations above 25 ppm lead to a complete growth inhibition.

Few years later, *Biller et al. 2012* discussed a similar concept by establishing a closed-loop system between algal cultivation and hydrothermal liquefaction based on nutrient recycling of the aqueous phase. Several strains of both microalgae and cyanobacteria were processed in batch reactors at $T = 300$ and 350 °C. The process water was recovered from the bio-crude, analyzed for nutrients (ex.: NH_4^+ , PO_4^{3-} , K and Acetate). A number of cultivation experiments were performed for each of the strains in a standard growth medium, defined as media, and the growth behavior was compared to that using the nutrients-containing process water rates in a series of dilutions (50- to 600-fold) using distilled water. The Analysis of the uptake levels of different compounds during cultivation were conducted to the spent water.

Basically, the process water contained all the required nutrients for growth and doubling of the algal cells. However, they existed in much higher levels than they in standard growth media did. The work also mentioned the phenolic compounds, which evolve as intermediates during the process to levels up to 178 ppm, and one element, Nickel, and their potential of inhibiting algal growth. Therefore, the high dilution was necessary and that made the growth of tested strains possible in different degrees, in some cases better than the standard media due to the mixo-trophic nature of growth (i.e. by the existence of organic carbon in the process water). It was concluded that achieving optimum growth is controlled by adjusting the dilution ratio depending on the characteristics of growth behavior of each strain. A dilution of 200 and 400 folds was suggested based on these specific experiments.

An integrated part of the experiments conducted by *Bagnoud-Velásquez et al. 2014* discussed effluent recycling and the levels of its toxicity upon cultivation, as a goal to complete a closed cycle of nutrients. The study was carried out to assess the toxicity levels of soluble Aluminium on algal growth during cultivation. Aluminium may stem from system corrosion or catalyst leaching during hydrothermal conversion. Three species were selected for testing (*Chlorella sorokiniana*, *Chlorella vulgaris* and *Scenedesmus vacuolatus*). Low concentrations, as low as $25 \mu\text{g.L}^{-1}$, was found to create a toxic environment for algal growth due to the existence of Al-hydroxides. In general, the growth behavior showed different levels of tolerance to Aluminium (*S. vacuolatus* > *C. sorokiniana* > *C. vulgaris*).

Further efforts by *Bagnoud-Velásquez et al. 2015* continued to evaluate the feasibility of nutrient recycling. Here, *P. tricornutum* was liquefied hydrothermally ($T = 400\text{ }^{\circ}\text{C}$ and $P = 20\text{ MPa}$) in a batch autoclave. After separating the product mixture, the nutrient-containing aqueous effluent was used to grow microalgae in a flat panel photo-bioreactor of a relatively large size (5-L culture volume). The effluent solution was diluted by a factor 25. After dilution, the ammonium concentration was within the applicable range for algal cultivation [*Meiser et al. 2004*]. The effluent contained high levels of sodium concentrations, about 60 times higher than that in the standard medium. The low content of some elements' salts (S-, Mg-, Ca- and Fe-) were adjusted in the HTL effluent to be in the concentration vicinity of the standard medium.

Although a lag phase of four days was experienced at the beginning of cultivation with the HTL aqueous effluent, the algal cells were able to adapt to the medium change afterwards. The authors suggested possible explanation for the lag phase including the high sodium content in the HTL effluent compared to chloride, the existence of some organic compounds that would change the carbon uptake mode of microalgae, and the initial inhibition caused by some constituents that was overcome by the algal cells.

The results showed that a biomass productivity of ($0.5 - 1\text{ g DW}\cdot\text{L}^{-1}\text{d}^{-1}$) was reported in the work, a good value compared to those using the standard medium ($0.96 - 1\text{ g DW}\cdot\text{L}^{-1}\text{d}^{-1}$). The work stated that the productivity retained its good values even at high culture concentrations ($> 10\text{ g DW}\cdot\text{L}^{-1}$). The work concluded that the nutrient from hydrothermal conversion can replace to a certain extent the minerals needed to grow microalgae. A complete replacement would consequently mean a complete recovery from the high-temperature high-pressure process.

The effluent of HTC was also tested by *Du et al. 2012* for cultivating *Chlorella vulgaris*. Due to the high nutrients level in the effluent (especially Na and K), dilutions of 50-, 100- and 200-fold were applied and algal growth was compared with growth under standard conditions in a 150-ml culture volume. The culture showed an enhanced N and P removal rates with the diluted effluent compared to the standard medium. The algae produced from the effluent water cultivation contained high C (about 20% higher) and low N (about 8 7.8% lower) relative to that cultivated in the standard medium, which makes it superior if biofuels are to be produced from it.

The work demonstrated that the biomass productivities were higher using the diluted effluent, approximately 10 and 7 times higher for the 50- and 100-fold diluted effluent relative to the standard medium, respectively (0.160, 0.092 and 0.013 g.L⁻¹d⁻¹). The work argued that the effluent produced at higher temperatures conversion, comparing HTL, contains several compounds that lead to growth inhibition. In their explanation, the HTC-produced mono-sugars and amino acids in HTC can be harmlessly used by the algal cells for growth, C and N uptake.

2.5.3. System corrosion

Corrosion is an inherent phenomenon in high-temperature and high-pressure systems. A combination of supercritical condition and a corrosive environment is challenging for the selection of construction materials [Boukiss *et al.* 2001]. Several factors lead to corrosion under high temperature using aqueous solutions. This includes the existence and dissociation of reaction species such as acids or salts formed in the presence of some heteroatoms like S, Cl and N [Hodes *et al.* 2004], the solubility of gases (especially O₂ and H₂) and corrosion products (e.g. NiCl₂), as well as the stability degree of the protective oxide layers [Kritzer *et al.* 1999]. According to [Xiang *et al.* 1996, Kriksunov & Macdonald 1995 and Boukiss *et al.* 1998], corrosion during SCWO becomes more critical in the subcritical region, where both water's density and dielectric constant are relatively high; in other words, before the major changes to water's physical properties start to occur around the critical point.

Boukiss *et al.* 2011 demonstrated that materials such as stainless steel (316) in a solution containing mainly 600 ppm chlorides anions was subjected to stress corrosion cracking (SCC) and pitting in the subcritical temperature range (260–310 °C). This occurred in a continuous flow (1g.min⁻¹) tubular reactor (L = 1 m, ID = 0.75 cm) with an exposure periods (212 and 834 hours) and a pressure of 250 bar. At the higher temperature, general corrosion was also recognized through some solid corrosion products which exited the system. In the supercritical region, the presence of aqueous chloride solution also showed corrosion impact during the gasification of potassium chloride at a temperature of 700 °C and pressure of 300 bar [Boukiss *et al.* 2013]. A difference in corrosion rates between two different reactor materials which are made of nickel-based alloys was demonstrated in the presence of chloride solution and potassium hydrogen carbonate [Boukiss *et al.* 2008]. The two works related the corrosion rates to the change in the composition of each alloy, especially the alloy content of molybdenum, which played a role in the corrosion resistance.

Marrone and Hong 2009 discussed the challenges associated with corrosion in supercritical water systems. They summarized the efforts that has been made in this field and gave examples of the procedures necessary to control or minimize corrosion. A basic procedure is to have a corrosion-resistant construction material. Compared to stainless steel and carbon steel that are frequently used in a wide range of chemical processes, nickel-chromium-based alloys have a better performance in supercritical environments [*Boukis et al. 2010, Marrone and Hong 2007*]. The difference between these types is the variation or existence of some basic elements; Ni, Cr, Fe, Mo and Nb in the alloy.

Another procedure is to prevent the corrosive species from coming in contact with the reactor wall. This can be realized by separating the reaction zone from the metal surface, for example by flowing water in between to create a protective layer. Also, the water film helps preventing salt build-up inside the reaction zone. This design is defined in literature as the transpiring wall reactor (TWR). Such a technique has been presented in several works (ex.: *Abeln et al. 2001*). However, the use of large amount of clean water for the isolating film as well as the temperature fluctuations in the reaction zone was a challenge of applying this technique [*Chen et al. 2014*]. Other methods for corrosion control that were covered in the work of *Marrone et al. 2009* are adjusting process variables, applying a protective layer (coating) with high corrosion resistance and the use of a sacrificial surface (liner) as a shield on the reactor wall.

Table 2.2 – Summary of selected works in the field of hydrothermal gasification of algal feedstock

Author, year	Algal species	T (°C)	P (MPa)	Catalyst-/s used	Efficiency, % (CGE)	Mode (System size)	Residence time	Feed conc. (wt%)
Bagnoud-Velásquez et al. 2014	<i>Phaeodactylum tricornutum</i>	360-470	32.3	Ru/C	30.4 ± 0.9	cont. (158.3 ml) duration (ca. 5 - 6 h)	N/A	6.5
Miller et al. 2012	<i>Spirulina</i>	550-650	23.5	no catalyst	7 - 47.5 ^L (max. 95.2 ^{L,n})	cont. (13 ml) (6 - 90 min) ^k	1 - 40 s	17.5 & 25
Elliott et al. 2012	<i>Nannochloropsis salina</i> & <i>Spirulina</i>	350	20	Ru/C	90% (<i>Spirulina</i>) 59% (<i>N. salina</i>)	cont. (1 Liter) duration (6 - 10 h)	N/A	20 - 25
Chakinala et al. 2010	<i>C. vulgaris</i>	400-700 (600)	24	Ru/TiO ₂ , NiMo, CoMo, PtPd, Inconel [®] powder	max. 82% w/o cat. ^e 100% w cat. ^e	batch quartz capillaries (0.5 ml)	1 - 15 min (2 min)	2.9 & 7.3
Guan et al. 2012 (I)	<i>Nannochloropsis sp.</i>	410	-	Ru/C	45% (1 g/g cat. loading) 100% (2 g/g cat. loading)	batch (5 ml)	75 min	1.8 - 13.5
Guan et al. 2012 (II)	<i>Nannochloropsis sp.</i>	450-550	24	no catalyst	max. ~ 60	batch (10 ml)	75 min	1 - 15
Haiduc et al. 2009	<i>P. tricornutum</i>	400	30	Ru/C (Ru on granular coconut carbon catalyst)	4 - 8 w/o cat. 34 - 74 w cat.	batch (30 ml)	60 - 67 min	2.5 - 13
Stucki et al. 2009	<i>Spirulina platensis</i>	399-409	31 - 35	Ru/ZrO ₂ , Ru/C	60 - 70 ^f	batch (30 ml)	60 - 361 ^a	2.5 - 20
Minowa et al. 1999	<i>C. vulgaris</i>	350	18	Ni-based on silica alumina	35% (0.76 g/g cat. loading) 70% (0.25 g/g cat. loading)	batch (120 ml)	N/A	12.6
Onwudili et al. 2013	<i>C. vulgaris</i> , <i>S. platensis</i> , <i>S. latissima</i>	500	36	NaOH, Ni-Al ₂ O ₃	57.3 w/o cat. (<i>S. platensis</i>) 92.6 w cat. (<i>S. latissima</i>)	batch	30 min	6.66
Brown et al. 2010	<i>Nannochloropsis sp.</i>	500	35	no catalyst	90 ^s	batch (35 ml)	60	5.4 - 16.2

^a Reaction time at T > 374 °C (holding time)

^e GE here is the carbon-to-gas conversion, same as CGE

^l Gasification efficiency based on the total amount of gases produced and not carbon-based

ⁿ Based on one experiment at τ = 40 s

^f ECE: Energy conversion efficiency, based on the heating value of the produced gas to that of the dry algae

^s ECE: Energy conversion efficiency, based on the combined heating value of the product (HTL+HTG) to that of the dry algae

^k Based on the volume of feed cylinder with no refilling.

2.6. References (Chapter 2)

1. Abelleira, J., Sánchez-Oneto, J., Portela, J.R., Martínez De La Ossa, E.J. 2013. Kinetics of supercritical water oxidation of isopropanol as an auxiliary fuel and co-fuel. *Fuel*, **111**, 574-583.
2. Abeln, J., Kluth, M., Petrich, G., Schmieder, H. 2001. Supercritical water oxidation (SCWO): a process for the treatment of industrial waste effluents. *High Pressure Research*, **20**(1-6), 537-547.
3. Akgül, G., Kruse, A. 2013. Hydrothermal disproportionation of formaldehyde at subcritical conditions. *The Journal of Supercritical Fluids*, **73**, 43-50.
4. Aliyu, S., Bala, M. 2011. Brewer's spent grain: A review of its potentials and applications. *African Journal of Biotechnology*, **10**(3), 324-331.
5. Antal, M.J., Allen, S.G., Schulman, D., Xu, X., Divilio, R.J. 2000. Biomass Gasification in Supercritical Water†. *Industrial & Engineering Chemistry Research*, **39**(11), 4040-4053.
6. Arthurson, V. 2008. Proper Sanitization of Sewage Sludge: a Critical Issue for a Sustainable Society. *Applied and Environmental Microbiology*, **74**(17), 5267-5275.
7. Bagnoud-Velásquez, M., Brandenberger, M., Vogel, F., Ludwig, C. 2014. Continuous catalytic hydrothermal gasification of algal biomass and case study on toxicity of aluminum as a step toward effluents recycling. *Catalysis Today*, **223**, 35-43.
8. Bagnoud-Velásquez, M., Schmid-Staiger, U., Peng, G., Vogel, F., Ludwig, C. 2015. First developments towards closing the nutrient cycle in a biofuel production process. *Algal Research*, **8**, 76-82.
9. Basu, P., Vichuda, M., Leon, M.A. 2009. Gasification of rice husk in supercritical water. *8th World Congress of Chemical Engineering: Incorporating the 59th Canadian Chemical Engineering Conference and the 24th Interamerican Congress of Chemical Engineering*.
10. Berglin, E.J., Enderlin, C.W., Schmidt, A.J. 2012. Review and Assessment of Commercial Vendors/Options for Feeding and Pumping Biomass Slurries for Hydrothermal Liquefaction. PNNL-21981, Pacific Northwest National Laboratory, Richland, Washington, USA.
11. Biller, P., Riley, R., Ross, A.B. 2011. Catalytic hydrothermal processing of microalgae: decomposition and upgrading of lipids. *Bioresource technology*, **102**(7), 4841-8.
12. Biller, P., Ross, A.B. 2011. Potential yields and properties of oil from the hydrothermal liquefaction of microalgae with different biochemical content. *Bioresource technology*, **102**(1), 215-25.
13. Biller, P., Ross, A.B., Skill, S.C., Lea-Langton, A., Balasundaram, B., Hall, C., Riley, R., Llewellyn, C.A. 2012. Nutrient recycling of aqueous phase for microalgae cultivation from the hydrothermal liquefaction process. *Algal Research*, **1**(1), 70-76.
14. Boukis, N., Kritzer, P., Dinjus, E. 1998. Corrosion phenomena of alloy 625 in aqueous solutions containing sulfuric acid and oxygen under subcritical and supercritical conditions. Corrosion 98, National Association of Corrosion Engineers (NACE), Houston, TX, paper no. 415.
15. Boukis, N., Franz, G., Habicht, W., Dinjus, E. 2001. Corrosion resistant materials for SCWO-applications. Experimental results from long-time experiments, National Association of Corrosion Engineers (NACE), Corrosion, USA, paper no. 01353.
16. Boukis, N., Diem, V., Habicht, W., Dinjus, E. 2003. Methanol Reforming in Supercritical Water. *Industrial & Engineering Chemistry Research*, **42**(4), 728-735.
17. Boukis, N., Habicht, W., Hauer, E., Weiss, K., Dinjus, E. 2008. Corrosion behavior of Ni-base alloys and stainless steels in supercritical water containing potassium hydrogen carbonate. EUROCORR 2008: The European Corrosion Congress, 7-11 September, Edinburgh, GB
18. Boukis, N., Habicht, W., Hauer, E., Dinjus, E. 2010. Challenges of selecting materials for the process of biomass gasification in supercritical water. First International Conference on Materials for Energy, 4-8 July, Convention Center Karlsruhe, Germany, 348-350

19. Boukis, N., Hauer, E., Habicht, W., Dinjus, E. 2011. Corrosion behavior of stainless steels in pressurized hot water containing chloride and sulphate anions. *Papier EUROCORR*, 4-8 September, Stockholm, Sweden.
20. Boukis, N., Hauer, E., Habicht, W. 2013. Corrosion behaviour of Ni-base alloys in supercritical water containing alkali chlorides. *EUROCORR*, 1-5 September, Estoril, Portugal.
21. Boukis, N., Hauer, E., Herbig, S., Sauer, J., Vogel, F. 2017. Catalytic gasification of digestate sludge in supercritical water on the pilot plant scale. *Biomass Conversion and Biorefinery*, **7**(4), 415-424.
22. Brown, T.M., Duan, P., Savage, P.E. 2010. Hydrothermal Liquefaction and Gasification of *Nannochloropsis* sp. *Energy & Fuels*, **24**(6), 3639-3646.
23. Cao, C., Guo, L., Chen, Y., Guo, S., Lu, Y. 2011. Hydrogen production from supercritical water gasification of alkaline wheat straw pulping black liquor in continuous flow system. *International Journal of Hydrogen Energy*, **36**(21), 13528-13535.
24. Chakinala, A.G., Brilman, D.W.F., van Swaaij, W.P.M., Kersten, S.R.A. 2010. Catalytic and Non-catalytic Supercritical Water Gasification of Microalgae and Glycerol. *Industrial & Engineering Chemistry Research*, **49**(3), 1113-1122.
25. Chakinala, A.G., Kumar, S., Kruse, A., Kersten, S.R.A., van Swaaij, W.P.M., Brilman, D.W.F. 2013. Supercritical water gasification of organic acids and alcohols: The effect of chain length. *The Journal of Supercritical Fluids*, **74**, 8-21.
26. Chen, Y., Guo, L., Jin, H., Yin, J., Lu, Y., Zhang, X. 2013. An experimental investigation of sewage sludge gasification in near and super-critical water using a batch reactor. *International Journal of Hydrogen Energy*, **38**(29), 12912-12920.
27. Chen, Z., Wang, G., Mirza, Z.A., Yang, S., Xu, Y. 2014. Study of transpiring fluid dynamics in supercritical water oxidation using a transparent reactor. *The Journal of Supercritical Fluids*, **88**(Complete), 117-125.
28. Cherad, R., Onwudili, J.A., Williams, P.T., Ross, A.B. 2014. A parametric study on supercritical water gasification of *Laminaria hyperborea*: a carbohydrate-rich macroalga. *Bioresource technology*, **169**, 573-80.
29. De Blasio, C., Lucca, G., Özdenkci, K., Mulas, M., Lundqvist, K., Koskinen, J., Santarelli, M., Westerlund, T., Järvinen, M. 2016. A study on supercritical water gasification of black liquor conducted in stainless steel and nickel-chromium-molybdenum reactors. *Journal of Chemical Technology & Biotechnology*, **91**(10), 2664-2678.
30. Díaz-Reinoso, B., Moure, A., Domínguez, H., Parajó, J.C. 2006. Supercritical CO₂ Extraction and Purification of Compounds with Antioxidant Activity. *Journal of Agricultural and Food Chemistry*, **54**(7), 2441-2469.
31. D'Jesús, P., Artiel, C., Boukis, N., Kraushaar-Czarnetzki, B., Dinjus, E. 2005. Influence of educt preparation on gasification of corn silage in supercritical water. *Industrial and Engineering Chemistry Research*, **44**(24), 9071-9077.
32. D'Jesús, P., Boukis, N., Kraushaar-Czarnetzki, B., Dinjus, E. 2006. Gasification of corn and clover grass in supercritical water. *Fuel*, **85**(7-8), 1032-1038.
33. Du, Z., Hu, B., Shi, A., Ma, X., Cheng, Y., Chen, P., Liu, Y., Lin, X., Ruan, R. 2012. Cultivation of a microalga *Chlorella vulgaris* using recycled aqueous phase nutrients from hydrothermal carbonization process. *Bioresource technology*, **126**, 354-7.
34. Elliott, D. C.; Sealock, L. J., Jr.; Butner, R. S.; Baker, E. G.; Neuenschwander, G. G. 1989. Low-temperature conversion of high-moisture biomass: Continuous reactor system results, PNL-7126, Pacific Northwest Laboratory, Richland, WA.
35. Elliott, D.C., Hart, T.R., Neuenschwander, G.G., Rotness, L.J., Olarte, M.V., Zacher, A.H. 2012. *Chemical Processing in High-Pressure Aqueous Environments*. 9. Process Development for

- Catalytic Gasification of Algae Feedstocks. *Industrial & Engineering Chemistry Research*, **51**(33), 10768-10777.
36. Elliott, D.C., Biller, P., Ross, A.B., Schmidt, A.J., Jones, S.B. 2015. Hydrothermal liquefaction of biomass: developments from batch to continuous process. *Bioresource technology*, **178**, 147-56.
 37. Erlach, B., Harder, B., Tsatsaronis, G. 2012. Combined hydrothermal carbonization and gasification of biomass with carbon capture. *Energy*, **45**(1), 329-338.
 38. *FELUWA* hose diaphragm pumps - Operation & maintenance manual
 39. Gasafi, E., Reinecke, M.-Y., Kruse, A., Schebek, L. 2008. Economic analysis of sewage sludge gasification in supercritical water for hydrogen production. *Biomass and Bioenergy*, **32**(12), 1085-1096.
 40. Gong, M., Zhu, W., Xu, Z.R., Zhang, H.W., Yang, H.P. 2014. Influence of sludge properties on the direct gasification of dewatered sewage sludge in supercritical water. *Renewable Energy*, **66**, 605-611.
 41. Guan, Q., Savage, P.E., Wei, C. 2012. Gasification of alga *Nannochloropsis* sp. in supercritical water. *The Journal of Supercritical Fluids*, **61**, 139-145.
 42. Güngören Madenoğlu, T., Boukis, N., Sağlam, M., Yüksel, M. 2011. Supercritical water gasification of real biomass feedstocks in continuous flow system. *International Journal of Hydrogen Energy*, **36**(22), 14408-14415.
 43. Guo, S., Guo, L., Yin, J., Jin, H. 2013. Supercritical water gasification of glycerol: Intermediates and kinetics. *The Journal of Supercritical Fluids*, **78**, 95-102.
 44. Haiduc, A.G., Brandenberger, M., Suquet, S., Vogel, F., Bernier-Latmani, R., Ludwig, C. 2009. SunChem: an integrated process for the hydrothermal production of methane from microalgae and CO₂ mitigation. *Journal of Applied Phycology*, **21**(5), 529-541.
 45. Hammerschmidt, A., Boukis, N., Galla, U., Zevaco, T., Dinjus, E., Hitzmann, B. 2014. Influence of the heating rate and the potassium concentration of the feed solution on the hydrothermal liquefaction of used yeast and apple pomace under reducing conditions. *Biomass Conversion and Biorefinery*, **5**(2), 125-139.
 46. Hayashi, H., Hakuta, Y. 2010. Hydrothermal Synthesis of Metal Oxide Nanoparticles in Supercritical Water. *Materials*, **3**(7).
 47. Heilmann, S.M., Davis, H.T., Jader, L.R., Lefebvre, P.A., Sadowsky, M.J., Schendel, F.J., von Keitz, M.G., Valentas, K.J. 2010. Hydrothermal carbonization of microalgae. *Biomass and Bioenergy*, **34**(6), 875-882.
 48. Hirano, A., Hon-Nami, K., Kunito, S., Hada, M., Ogushi, Y. 1998. Temperature effect on continuous gasification of microalgal biomass: theoretical yield of methanol production and its energy balance. *Catalysis Today*, **45**(1-4), 399-404.
 49. Hodes, M., Griffith, P., Smith, K.A., Hurst, W.S., Bowers, W.J., Sako, K. 2004. Salt solubility and deposition in high temperature and pressure aqueous solutions. *AIChE Journal*, **50**(9), 2038-2049.
 50. Kabyemela, B.M., Adschiri, T., Malaluan, R.M., Arai, K. 1997. Kinetics of Glucose Epimerization and Decomposition in Subcritical and Supercritical Water. *Industrial & Engineering Chemistry Research*, **36**(5), 1552-1558.
 51. Kriksunov, L.B., Macdonald, D.D. 1995. Corrosion in Supercritical Water Oxidation Systems: A Phenomenological Analysis. *Journal of the Electrochemical Society*, **142**(12), 4069-4073.
 52. Kritzer, P., Boukis, N., Dinjus, E. 1999. Factors controlling corrosion in high-temperature aqueous solutions: A contribution to the dissociation and solubility data influencing corrosion processes. *Journal of Supercritical Fluids*, **15**(3), 205-227.

53. López Barreiro, D., Prins, W., Ronsse, F., Brilman, W. 2013. Hydrothermal liquefaction (HTL) of microalgae for biofuel production: State of the art review and future prospects. *Biomass and Bioenergy*, **53**, 113-127.
54. Magdeldin, M., Kohl, T., De Blasio, C., Järvinen, M.. 2015. *SuperCritical* Water Gasification of Black Liquor: Progress & Prospects. Nordic Flame Days 2015. International Flame Research Foundation (IFRF) and the Scandinavian-Nordic Section of the Combustion. 6-7 October, Copenhagen, Denmark.
55. Marrone, P.A., Hong, G.T. 2009. Corrosion control methods in supercritical water oxidation and gasification processes. *The Journal of Supercritical Fluids*, **51**(2), 83-103.
56. Marrone, P.A., Hong, G.T. 2007. Supercritical Water Oxidation. in: *Environmentally Conscious Materials and Chemicals Processing*, John Wiley & Sons, Inc., pp. 385-453.
57. Meiser, A., Schmid-Staiger, U., Trösch, W. 2004. Optimization of eicosapentaenoic acid production by *Phaeodactylum tricornutum* in the flat panel airlift (FPA) reactor. *Journal of Applied Phycology*, **16**(3), 215-225.
58. Miller, A., Hendry, D., Wilkinson, N., Venkitasamy, C., Jacoby, W. 2012. Exploration of the gasification of *Spirulina* algae in supercritical water. *Bioresource technology*, **119**, 41-7.
59. Minowa, T., Sawayama, S. 1999. A novel microalgal system for energy production with nitrogen cycling. *Fuel*, **78**(10), 1213-1215.
60. Modell, M., Reid, R.C., Amin, S.I. 1978. Gasification process US Patent 4 (113), 446, USA
61. Modell, M. 1985. Gasification and Liquefaction of Forest Products in Supercritical Water. in: *Fundamentals of Thermochemical Biomass Conversion*, (Eds.) R.P. Overend, T.A. Milne, L.K. Mudge, Springer Netherlands. Dordrecht, pp. 95-119.
62. Onwudili, J.A., Lea-Langton, A.R., Ross, A.B., Williams, P.T. 2013. Catalytic hydrothermal gasification of algae for hydrogen production: composition of reaction products and potential for nutrient recycling. *Bioresource technology*, **127**, 72-80.
63. Phyllis2 - Database for biomass and waste. Energy research Centre of the Netherlands (ECN): <https://www.ecn.nl/phyllis2/>
64. Potic, B., Kersten, S.R.A., Prins, W., Van Swaaij, W.P.M. 2004. A high-throughput screening technique for conversion in hot compressed water. *Industrial and Engineering Chemistry Research*, **43**(16), 4580-4584.
65. Qian, L., Wang, S., Xu, D., Guo, Y., Tang, X., Wang, L. 2015. Treatment of sewage sludge in supercritical water and evaluation of the combined process of supercritical water gasification and oxidation. *Bioresource technology*, **176**, 218-24.
66. Ro, K.S., Cantrell, K., Elliott, D., Hunt, P.G. 2007. Catalytic wet gasification of municipal and animal wastes. *Industrial and Engineering Chemistry Research*, **46**(26), 8839-8845.
67. Ross, A.B., Biller, P., Kubacki, M.L., Li, H., Lea-Langton, A., Jones, J.M. 2010. Hydrothermal processing of microalgae using alkali and organic acids. *Fuel*, **89**(9), 2234-2243.
68. Sricharoenchaikul, V. 2009. Assessment of black liquor gasification in supercritical water. *Bioresource technology*, **100**(2), 638-43.
69. Stucki, S., Vogel, F., Ludwig, C., Haiduc, A.G., Brandenberger, M. 2009. Catalytic gasification of algae in supercritical water for biofuel production and carbon capture. *Energy & Environmental Science*, **2**(5), 535.
70. Toor, S.S., Reddy, H., Deng, S., Hoffmann, J., Spangsmark, D., Madsen, L.B., Holm-Nielsen, J.B., Rosendahl, L.A. 2013. Hydrothermal liquefaction of *Spirulina* and *Nannochloropsis salina* under subcritical and supercritical water conditions. *Bioresource technology*, **131**, 413-9.
71. Toor, S.S., Rosendahl, L., Rudolf, A. 2011. Hydrothermal liquefaction of biomass: A review of subcritical water technologies. *Energy*, **36**(5), 2328-2342.

72. Türk, M., Upper, G., Hils, P. 2006. Formation of composite drug-polymer particles by coprecipitation during the rapid expansion of supercritical fluids. *Journal of Supercritical Fluids*, **39**(2), 253-263.
73. Valdez, P.J., Nelson, M.C., Wang, H.Y., Lin, X.N., Savage, P.E. 2012. Hydrothermal liquefaction of *Nannochloropsis* sp.: Systematic study of process variables and analysis of the product fractions. *Biomass and Bioenergy*, **46**, 317-331.
74. Vardon, D.R., Sharma, B.K., Scott, J., Yu, G., Wang, Z., Schideman, L., Zhang, Y., Strathmann, T.J. 2011. Chemical properties of biocrude oil from the hydrothermal liquefaction of *Spirulina* algae, swine manure, and digested anaerobic sludge. *Bioresource technology*, **102**(17), 8295-303.
75. Wilkinson, N., Wickramathilaka, M., Hendry, D., Miller, A., Espanani, R., Jacoby, W. 2012. Rate determination of supercritical water gasification of primary sewage sludge as a replacement for anaerobic digestion. *Bioresource technology*, **124**, 269-75.
76. Xiang, T., Johnston, K.P., Wofford, W.T., Gloyna, E.F. 1996. Spectroscopic Measurement of pH in Aqueous Sulfuric Acid and Ammonia from Sub- to Supercritical Conditions. *Industrial & Engineering Chemistry Research*, **35**(12), 4788-4795.
77. Zhang, S., Zu, Y.G., Fu, Y.J., Luo, M., Li, W.L., Efferth, T. 2010. Supercritical carbon dioxide extraction of seed oil from yellow horn (*Xanthoceras sorbifolia* Bunge.) and its anti-oxidant activity. *Bioresource Technology*, **101**(7), 2537-2544.

3. Materials and methods

3.1. Overview

In this chapter, the experimental procedures followed as well as the laboratory apparatuses used for the supercritical water gasification of algal biomass are illustrated. A detailed explanation of the algal growth techniques and the corresponding process variables is not the core of this work and therefore, only a brief overview on the cultivation system will be presented. Among the numerous algal species which can grow outdoors, *A. obliquus* (formerly *Scenedesmus obliquus*, reclassified to *Acutodesmus obliquus*) was selected for cultivation. The selection was mainly based on their tendency to a rapid growth, efficient carbon dioxide fixation [Sforza *et al.* 2014,] and high biomass productivities on large scale [Abomohra *et al.* 2013]. Cultivating other species and including them as a parameter in the gasification process was not part of this work.

3.2. Biomass production

A. obliquus was cultivated first in a pilot unit in Hamburg-Reitbrook [Hindersin *et al.* 2013] and, at a later stage, within the novel structure (BIQ-House, Hamburg-Wilhelmsburg) that is shown below in figure 3.1. This structure represents a closed cultivation system (photo-bioreactor) of a flat-panel configuration. The building itself offers 15 residential units of areas ranging between 50 and 120 m². Forming the exterior (façade) on two sides of the house (south-east and south-west), 129 vertical flat panels are fixed to face the surrounding, covering an area of about 200 m² that is subjected to sunlight, and holding a total culture volume of about 4 m³.

The cultivation is based on natural light as the energy source and carbon dioxide as the carbon source for biomass production. As mentioned previously (chapter 1), the performance of such systems is mainly a function of the light intensity, exposure, optical light path across the culture, mixing, aeration rate as well as process mode of operation [Hindersin *et al.* 2014, Grobbelaar 2007]. Each of the flat panel units has a width of 0.7 m and a height of 2.7 m, with a light path or thickness of 1.7 cm. The inner volume containing the aqueous algal culture is held between two layers of a clear laminated safety glass (LSG). This material is a protective type of glass which is capable of retaining the culture content between the panels in case of fracture through thin interlayers of polyvinyl butyral (PVB). The algal culture is kept in a continuous motion by mixing via compressed air and CO₂ coming upwards inside the panels.

In addition, small beads (scrapers) exist in continuous motion within the culture in order to inhibit the settling of biomass and prevent bio-pollution [Smart Material House BIQ, July 2013]. The culture density is kept at a constant level with the aid of optical density or turbidity measurements. This technique allows the required dilution through the addition of fresh medium when turbidity rises, so that an optimum growth environment is maintained during cultivation. Such a mode of operation is defined as turbido-stat [Kuenen *et al.* 2009, Najafpour 2007]. Using a compact air flotation system within the house's basement, the produced biomass is separated by concentrating part of the circulated culture.



Figure 3.1 – The novel construction (BIQ house) in Hamburg-Wilhelmsburg

[Photos Credit: S. Elsayed and J. Arlt]

The concentration reaches a factor of 10–20 depending on the existing cultivating conditions. Afterwards, the remaining liquid is pumped back into the flat panels for further use. In the case when higher biomass concentrations are necessary, centrifugation can be conducted offline. Circulating the culture, biomass separation, air and CO₂ supply as well as heat management are controlled automatically using adequate process equipment which are placed and operated on the ground level of the building.

The source of CO₂ that is added to the culture medium is the flue gas resulting a small combined heat and power unit (CHP) running on biogas. Nutrition is available through an aqueous solution containing the basic macro- and micro-elements needed for growth and biomass accumulation. Depending on the uptake level, the amount of nutrients is adjusted within the culture medium to keep an optimum growth behavior and avoid nutrients limitation. The basic components of the nutrient source (*Flory Basis 2*) used for cultivation are shown in table 3.1. Other trace elements such as Copper (Cu), Iron (Fe) and Zinc (Zn) are available in the nutrient. Due to the low percentage of nitrogen in *Flory Basis 2*, additional nitrogen source is supplied in the form of urea.

Table 3.1 – The composition of the nutrient applied for algal cultivation.

	N	P ₂ O ₅	MgO	K ₂ O	SO ₃
Flory Basis 2			wt%		
	3	15	5	35	23.5

Thermal or heat management is conducted depending on the weather conditions or temperature of the surroundings. During sunny summer days, the temperature of the culture medium can rise up to 35 – 40 °C. The elevated temperature can be reduced by running the culture through a set of heat exchangers to absorb the thermal energy originally falling on the surfaces of the flat panels. The excess thermal energy can be utilized for various purposes such as heating of the domestic water. The opposite thing occurs as temperature falls, for example below 5 °C. This is when the culture is heated up to maintain good algal metabolism. The biomass productivity, including the night losses due to respiration, ranged during all seasons from 5 g.m⁻².d⁻¹ up to 30 g.m⁻².d⁻¹ with a mean productivity of 9 ±7 g.m⁻².d⁻¹ [Hindersin et al. 2014].

3.3. Feed preparation

The feedstock to gasification was received from our project partner (Strategic Science Consult GmbH) in Hamburg, in the form of concentrated algal slurry (fig. 3.2). It had solids concentration ranging between 15 and 27 wt% depending on the delivered batch. The slurry was mixed with distilled water according to the concentration assigned to each experiment. An alkali metal salt (K_2CO_3 or $KHCO_3$) was dissolved in the feed as a homogeneous catalyst in an ion concentration (K^+) of 1500 ppm. The content of solids (dry matter, DM) in the slurry was measured before and after each experiment by drying for 24 hours at a temperature of 105 °C (*ULE 400, Memmert*). Additionally, a thickening agent (*Xanthan*) was added to the slurry in a ratio of 0.2 wt% to prevent settling of the particles and ensure a homogeneous mixture.

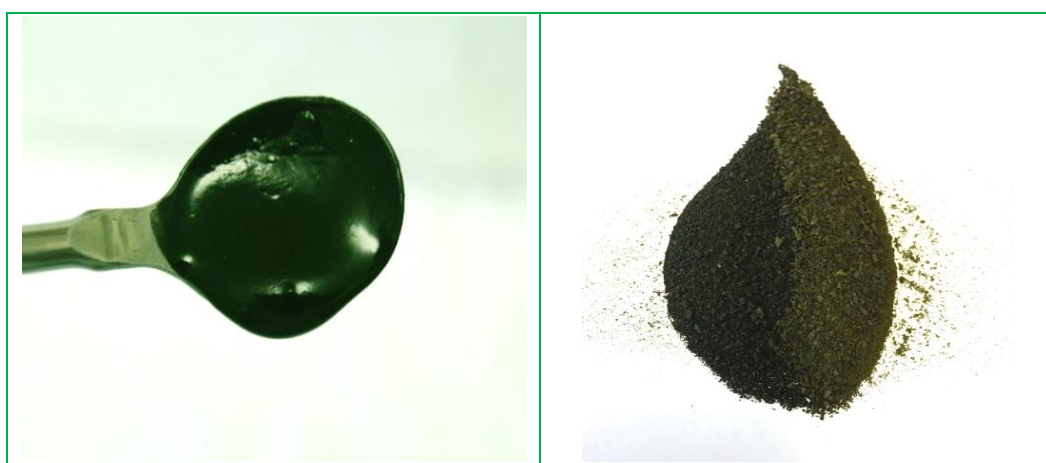


Figure 3.2 – Microalgae in the slurry form (left) and as a dried biomass (right)

An elemental analysis of the dried microalgae was conducted (*DIN EN ISO 11885, DIN EN 13137, DIN EN 15104, DIN 51721, DIN EN 51722-1, DIN 51732, LECO TruSpec CHN Makro, Agilent ICP-OES Vista Pro*) for several batches and is shown in Tab 3.2. Further analyses determined an ash content of 10 wt% at 550 °C (*DIN EN 14775, LECO TGA 701*) and an average higher heating value (HHV) of 23.2 MJ.kg⁻¹ DM (*DIN EN 14918, IKA C5000 control*). The description of these analytical methods can be found in the appendix (8.4).

Table 3.2 – Elemental composition of the algal biomass feedstock to gasification

Batch	TOC	O *balance*	H	N	P	K	S	Mg	Ca	Si	Na	Al	Fe	Cl
wt% (dry-basis)														
1	52.6	~ 27.3	7.1	8.7	1.6	0.9	0.7	0.5	0.2	0.2	0.06	0.06	0.10	0.02
2	50.7	~ 29.1	7.0	6.7	0.7	0.8	0.6	0.2	0.3	0.1	0.06	0.03	0.07	0.02
3	52.1	~ 30.3	7.3	6.9	0.8	0.9	0.6	0.6	0.3	0.1	0.06	0.03	0.02	0.02
4	48.6	~ 31.3	7.1	8.6	1.0	0.8	0.8	0.2	0.6	0.5	0.06	0.03	0.04	0.03

3.4. Process performance and product analysis

In order to evaluate the process in terms of efficiency and the nature of produced streams, the entire fractions obtained from each experiment were sampled and analyzed. The combustible gaseous mixture was analyzed using a gas chromatograph (*HP 5890*) to obtain its chemical composition. The solid precipitates were chemically analyzed (*DIN ISO 10694*) and physically examined by imaging (elemental mapping) using field emission scanning electron microscope (*FE-SEM, DSM 982 Gemini, Carl Zeiss Ltd., Oberkochen, Germany*). Analyses of the residual water from gasification were conducted and some values including total organic carbon, TOC (*DIN EN 1484*) and total nitrogen bound, TNb (*DIN EN ISO 12260*) were measured. Other measurements for the ions of certain elements (ex.: K, Mg, Na, Si, Al, Cr, Fe, Mo, Ni) were obtained using inductively coupled plasma optical emission spectrometry (*ICP-OES, DIN ISO 11885, Agilent 725*). An important value to calculate is the carbon gasification efficiency (CGE). This term is defined as the amount of carbon measured in the gaseous product divided by the total organic carbon in the dry biomass feedstock. Based on the following equation (Eq. 1), the carbon gasification efficiency can be calculated as the weight summation of carbon atoms existing in each component (*i*) of the gaseous species produced.

$$\text{Carbon gasification efficiency (CGE)} = \frac{\sum_i \alpha_i c_i n M}{w m} \quad \text{Eq. 1}$$

where:

- α_i : number of carbon atoms of component 'i' in the gas product, -
- c_i : concentration of component 'i' in the gas product, mol%
- n : total number of moles produced, -
- M : molar mass of carbon, g mol⁻¹
- w : weight fraction of total organic carbon in feed, -
- m : amount of feed, g

Using CGE is often preferred over gasification efficiency or gasification quotient, which uses the entire gas production, expressing efficiency in a percentage (GE) or fractional form (GQ) and is not based on the carbon balance. The performance of gasification can also be evaluated from a different perspective, if the quality of the aqueous phase has no less priority than the production of combustible gases. For example, another term which reflects the aqueous product quality and gives an indication of the process efficiency is the TOC removal efficiency. This term gives an indication of organic loading in the residual water, and it would be similar to CGE if no organic carbon was converted to inorganic carbon in the aqueous phase, or in case no precipitation containing organic carbon occurs.

3.5. Growth of microalgae using the residual water from gasification

The growth of *A. obliquus* was carried out by the cooperation partner (SSC GmbH and the university of Hamburg) using several batches of the residual water from gasification and a standard cultivation medium (control). This cultivation was conducted using the Multi-Cultivator (*MC1000-OD, Photon Systems Instruments, Czech Republic*). The supply of nutrients was available through the standard medium containing a concentration of 2 g.L⁻¹ *Flory Basis Fertilizer 1* (Euflor, Germany) and 446 mg N-NH₄Cl. And since this nutrient source does not contain nitrogen, the amount of nitrogen in the residual water was adjusted (diluted) by the addition of 2 g.L⁻¹ *Flory Basis Fertilizer 1*. This was done to compensate any possible nutrients losses during supercritical water gasification.

The culturing vessels contained 80 ml of inoculum or pre-culture in a water bath at a temperature of 30 °C. For energy supply, the vessels were irradiated continuously with a light intensity of 500 μmol photons m⁻² s⁻¹. The cultures were aerated using air bubbles enriched in CO₂ (4 vol%) and the pH of the growth medium was adjusted and kept at 7. Cell growth, measured in cell dry weight (CDW, g.L⁻¹) for the days of cultivation, was monitored by measuring the optical density at a wavelength of 750 nm (OD750) and the calculation of an OD-CDW correlation curve.

Treatment of the residual water to eliminate or reduce the effect of potentially toxic substances was conducted using two methods; activated carbon filtration and photo-degradation. An amount of five hundred milliliters of the residual water was filtrated four consecutive times using activated carbon in a 4 – 7 μm pore size filter with 50 g of activated carbon. Photo-degradation was achieved using a strong ultraviolet (UV) radiation. The same volume (500 ml) of the residual water was irradiated for 4 h and the amount of evaporated water was replaced with double distilled water.

The total organic carbon (TOC) and total nitrogen (TN) of the residual water treated using activated carbon filtration as well as UV-degradation were measured using a total organic carbon analyzer (*TOC-Vcpn*) as well as a total nitrogen measuring device (*TNM-1, Shimadzu, Japan*). The possible loss of these elements after treatment was determined. The sum parameter phenolic compounds or phenol index was analyzed using the photometric cuvette test (*LCK345, Hach Lange, Germany*). Further details with regards to the experimental procedures followed for cultivation using the residual water is available in the work of *Patzelt et al. 2014*.

3.6. Experimental setup (Supercritical water gasification)

The experiments included in this work were conducted in three laboratory units on a continuous mode of operation. Simplified flow diagrams of the process units are presented in this section. Basically, the systems include feed preheating, reaction and gasification in supercritical water as well as phase separation of the product mixture. The phase separation systems of the three units operate in the same manner. The hot gaseous mixture leaving the reactor was cooled down, filtered to remove any solid residues, its pressure was relieved using a backpressure regulator (*TESCOMTM, Emerson Electric*) and separated from the residual water at atmospheric pressure. The removal of salts or inorganic fraction of the biomass is achieved either before or after the reaction zone as explained in the following sections.

3.6.1. Laboratory unit I (LUI)

In this unit (refer to fig. 3.3), the gasification in supercritical water takes place in a tubular reactor (ID = 1.8 cm, L = 152 cm) made of a nickel-chromium-based alloy. Depending on the experiment, the reactor was maintained in a temperature range of 600 – 650 °C and a pressure of 280 bar. The algal biomass concentration in the feed stream was varied between 10 – 15 wt%. The feed was brought to the reactor using indirect pumping (*HPLC Pump, Bischoff*) in a feed cylinder via pressurized water on the other side of a cylinder piston.

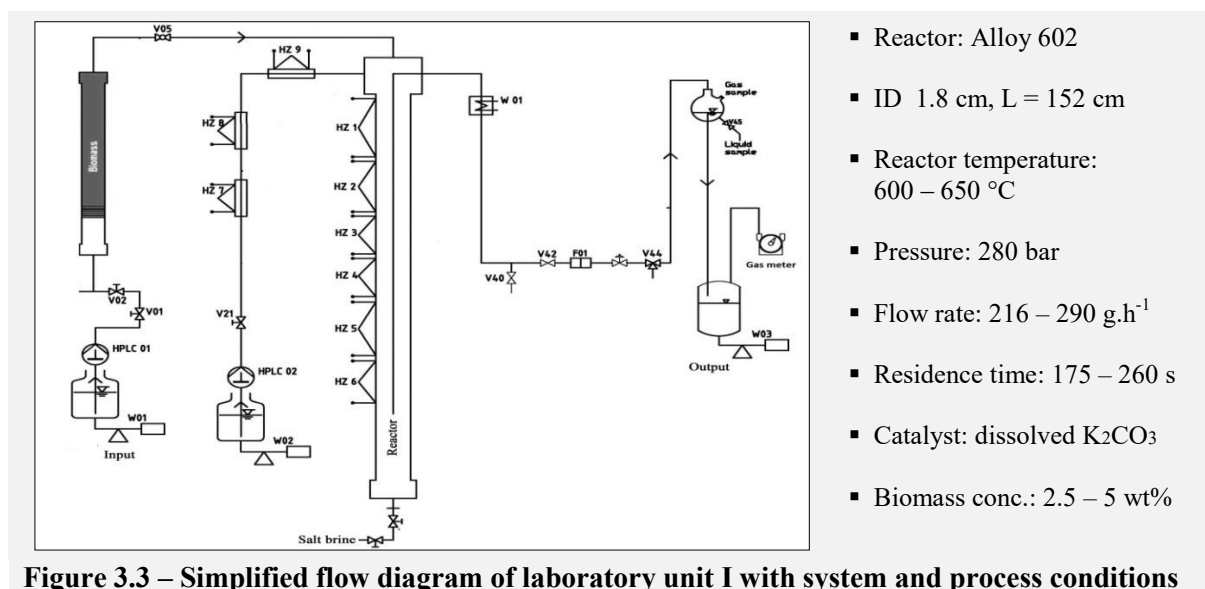


Figure 3.3 – Simplified flow diagram of laboratory unit I with system and process conditions

A second stream containing pure deionized water was pumped into the system from the top to preheat the feed stream at the reactor inlet. This stream was heated up in the range of 500 – 600 °C. As a result of this configuration, the feed stream is mixed with water at the reactor inlet in a mixing chamber. This resulted in a final concentration of 2.5 to 5 wt% in the reactor.

Depending on the conditions assigned to each experiment, a total flow rate ranging between 216 – 288 g.h⁻¹ was set for the combined biomass and water streams (total feed). Based on these values and given the density of supercritical water under these conditions, a mean residence time of about 175 – 260 seconds was calculated in the reaction zone. After exiting the reactor, the hot gaseous mixture is cooled down and separated from the residual water which was sampled, weighed and analyzed. The volume of produced gas was measured using a gas meter (*TG 3, Ritter Apparatebau GmbH*) and analyzed for chemical composition. The inorganic constituents or nutrients of algal cultivation which were left over from gasification were then extracted from the bottom of the reactor using a manually-operated valve at certain times during operation. This fraction was referred to as salt brine (SB).

3.6.2. Laboratory unit II (LUII)

The second set of experiments was carried out in the laboratory unit (II). In the configuration illustrated in figure 3.4, the system was operated using a one-stream feedstock input to the reactor. At the beginning, the feed is preheated up to 400 – 420 °C and then delivered to the reactor by indirect pumping in a similar technique as for LUI. The gasification took place in a tubular reactor (ID = 1.8 cm, L = 75 cm) made of alloy 602 at a reactor temperature in the range of 600 – 690 °C depending on the experiment, and pressure of 280 bar. The concentration of algal biomass was varied between 2.5 and 20 wt% for the experiments in this system. A mass flow rate of 150 g.h⁻¹ for the feed stream was kept constant and the mean residence time of 177 – 206 seconds was calculated under these conditions.

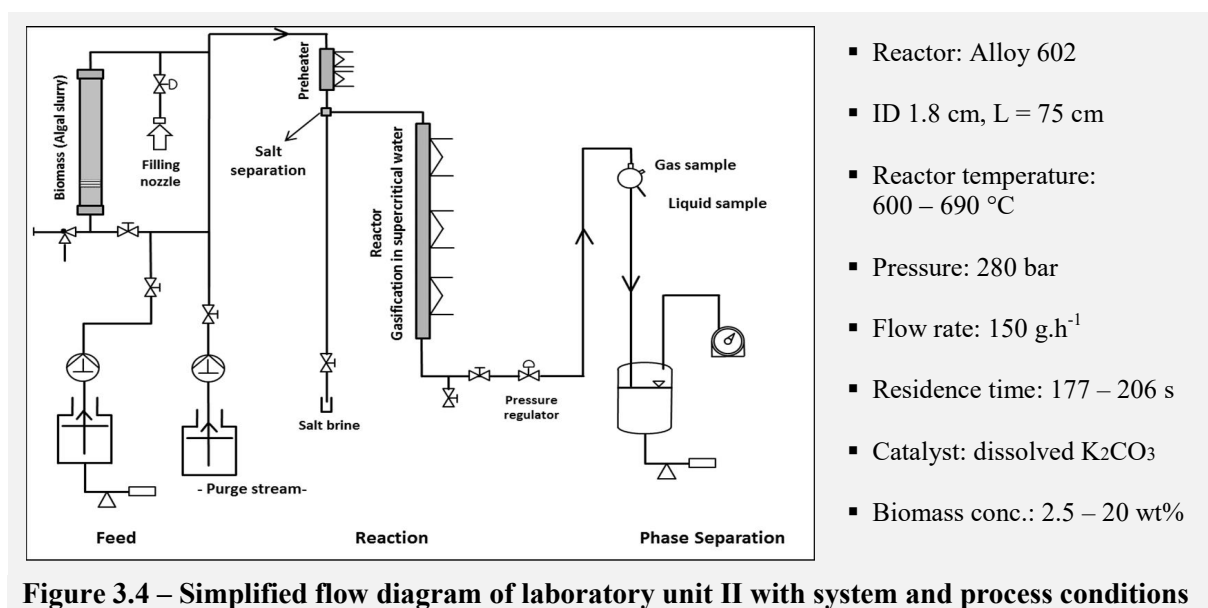


Figure 3.4 – Simplified flow diagram of laboratory unit II with system and process conditions

In order to extract the salts before hydrothermal conversion and decrease the load of inorganic constituents inside the reactor, a technique was applied by extracting some of these salts before entering the reactor using a vertical two-way connection (Tee-shaped) working as a by-pass for salts through a high-pressure valve. Using this technique, the salts, being almost separated due to their existence on the threshold of solubility near the critical point of water (370–400 °C), would be extracted and collected separately. This separated fraction, salt brine (SB), is then removed from the system at certain time periods during operation based on the biomass concentration.

3.6.3. Laboratory unit III (LUIII)

The third unit, illustrated in figure 3.5, has a comparable configuration to LUII. The major characteristic here is the size of the alloy 602 reactor which has a middle length (120 cm) compared to the first and second laboratory units. The other difference involved is the salt extraction technique, or the mechanism through which the salt brine is separated from the system before the reactor. In this unit, an automatically-operated valve for the extraction of salts was activated. This valve can be adjusted during operation using the software, to either open or seal for certain time intervals and in the desired frequency, depending on the experimental conditions and the feed concentration.

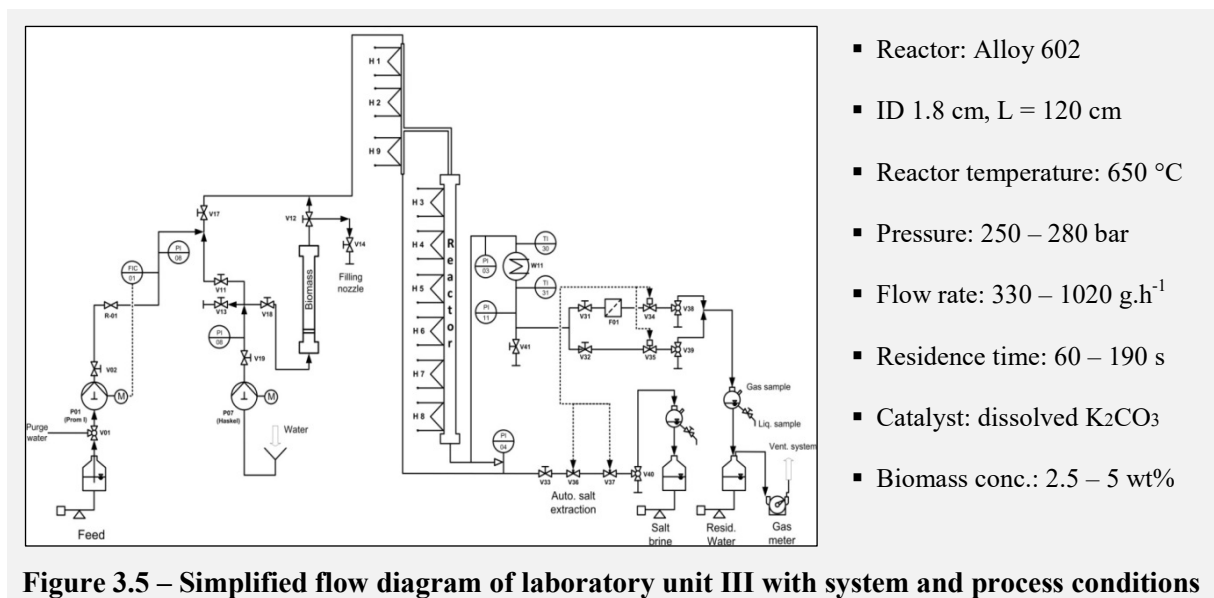


Figure 3.5 – Simplified flow diagram of laboratory unit III with system and process conditions

Similar to the second unit, two separate lines, one for the residual or process water and other for the salt brine, exit the hot zones of gasification and preheating respectively. After that, they are directed to the phase separation system, where their pressure is then relieved just before separation from the product gas mixture and being collected for measurements.

3.7. Pre-testing and system startup

Typically, a model compound such as ethanol (C_2H_5OH) was used during some early experiments for testing purposes prior to introducing the algal biomass in the system. This procedure is common and several compounds, especially alcohols, are used in other works for the same purpose. Ethanol was also used during the starting phase before switching to algal biomass. The aim of this procedure was to build up pressure in the system, reach a stable, steady-state operation and evaluate the system technical status before each experiment.

Ethanol has the advantage of having a comparable carbon mass fraction (52 wt%) to that of the microalgae available for gasification. Also, it can be converted easily into a combustible gas mixture under supercritical conditions due to its simple structure. Different concentrations of ethanol were used (5 – 11 wt%) and the balance calculations were conducted based on the mass of carbon atoms in the gaseous and aqueous phases. As the operational variables (T, P, flowrates, gas composition) were stabilized, a switch to biomass was activated.

3.8. Heat supply and temperature control

The thermal energy required to preheat the systems and maintain its temperature at the desired levels was provided through electric heating coils. To ensure a good temperature profile during the experiments, several measurements (fig. 3.6) were conducted to compare the inner and outer temperature profile along the reactor during a demonstration run with supercritical water at a temperature of 620 °C, pressure of 250 – 260 bar and flow rate of 150 g.h⁻¹.

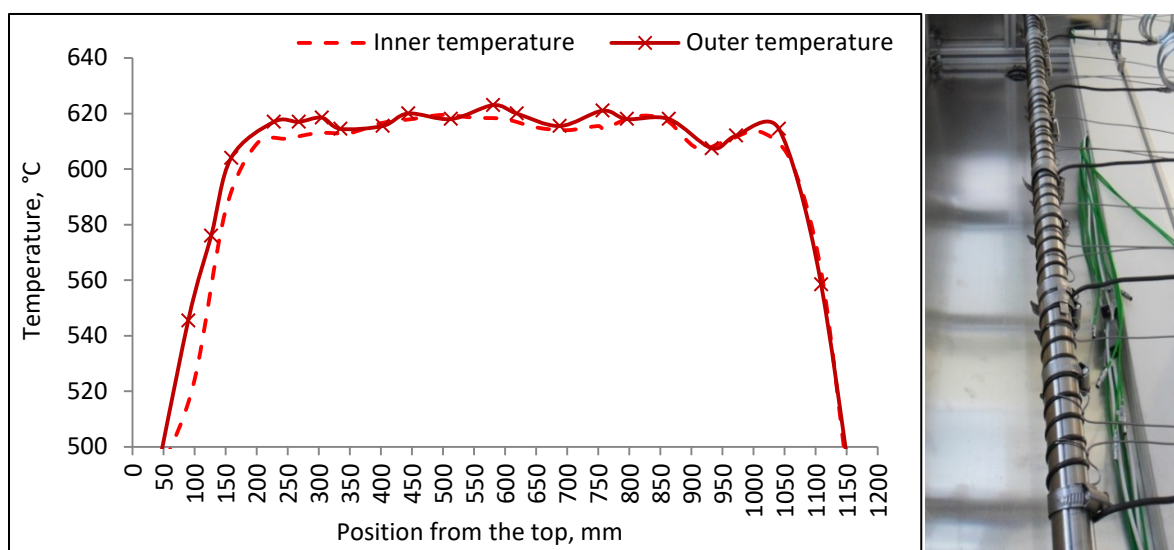


Figure 3.6 – Inner and outer temperature measurements for one of the tubular reactors (LUI)

A movable capillary thermocouple was inserted inside the reactor from the top, having the mixing chamber as the reference point, to measure the inner temperature at certain depths. These depths match the corresponding positions of the thermocouples on the outer surface of the reactor. A slight temperature offset was observed between the reactor's inner volume and its outer surface. Such a difference can be expected due to the heat losses across the reactor wall and the flow dynamics inside the reactor. Once the reactor is in operation, the incoming preheated fluid would maintain the reactor hot enough with the surplus of having the heating coils in case additional heating is needed.

Similar procedures were carried out to evaluate the inner and outer temperature measurements of the preheater before the reactor in the third laboratory unit. An example is demonstrated in figure 3.7, where several measurements were conducted at two temperature settings of the heating coils. The dashed lines represent the temperatures measured by the thermocouples on the outer surface along the 67 cm length of the preheater.

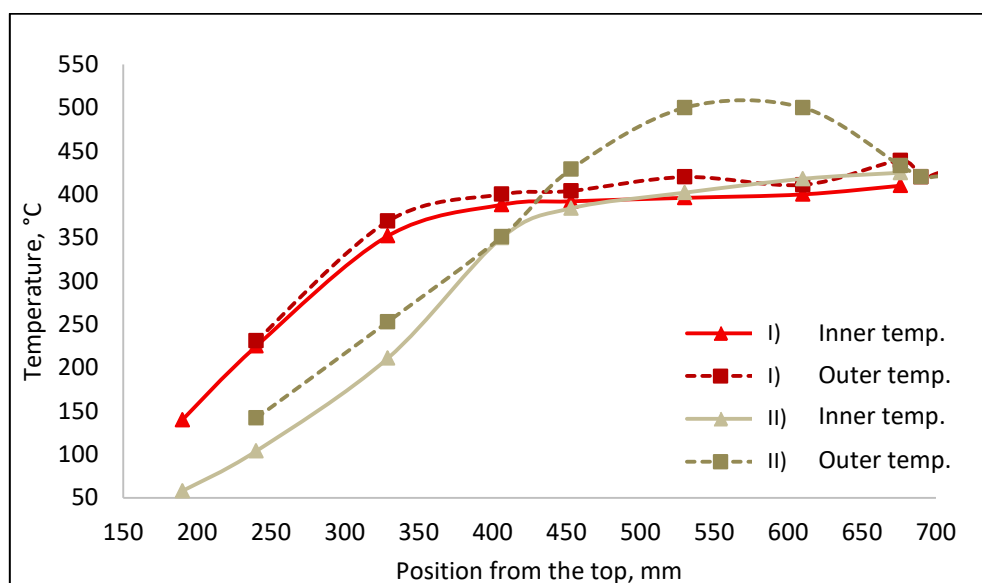


Figure 3.7 – Inner and outer temperature measurement along the preheater in LU11
Flowrate = 200 g.h⁻¹ and the following temperature settings for the hot zone:
I) min/max: 400/420 °C II) min/max: 400/500 °C – modified from [Stoll 2016]

The temperature along the preheater showed a very comparable profile at the lower settings applied (I). As the temperature of the middle section was increased (up to 500 °C) in the second setting (II), a difference between the inner and outer temperature, about 80 °C, was identified around this position. Despite the low flow rate applied, this offset might be thought of as a delay of response, if a measurement error is excluded. It may occur due to the cold temperature of the incoming feed or the heat losses on the outer surface.

3.9. References (Chapter 3)

1. Abomohra, A.EF., Wagner, M., El-Sheekh, M. Hanelt, D. 2013. *Journal of Applied Phycology*, **25**, 931-936.
2. Grobbelaar, J.U. 2007. Photosynthetic characteristics of *Spirulina platensis* grown in commercial-scale open outdoor raceway ponds: what do the organisms tell us? *Journal of Applied Phycology*, **19**(5), 591-598.
3. Hindersin, S., Leupold, M., Kerner, M., Hanelt, D. 2013. Irradiance optimization of outdoor microalgal cultures using solar tracked photobioreactors. *Bioprocess and Biosystems Engineering*, **36**(3), 345-355.
4. Hindersin, S., Leupold, M., Kerner, M., Hanelt, D. 2014. Key parameters for outdoor biomass production of *Scenedesmus obliquus* in solar tracked photobioreactors. *Journal of Applied Phycology*, **26**(6), 2315-2325.
5. International building exhibition Hamburg, *Smart Material House BIQ*, July 2013 (<http://www.biq-wilhelmsburg.de/>)
6. Kuenen, J.G., Johnson, O.J. 2009. Continuous Cultures (Chemostats) A2 - Schaechter, Moselio. in: *Encyclopedia of Microbiology (Third Edition)*, Academic Press. Oxford, pp. 130-147.
7. Najafpour, G.D. 2007. CHAPTER 2 - Dissolved Oxygen Measurement and Mixing. in: *Biochemical Engineering and Biotechnology*, Elsevier. Amsterdam, pp. 14-21.
8. Patzelt, D.J., Hindersin, S., Elsayed, S., Boukis, N., Kerner, M., Hanelt, D. 2014. Hydrothermal gasification of *Acutodesmus obliquus* for renewable energy production and nutrient recycling of microalgal mass cultures. *Journal of Applied Phycology*, **27**(6), 2239-2250.
9. Sforza, E., Gris, B., De Farias Silva, C.E., Morosinotto, T., Bertucco, A. 2014. Effects of light on cultivation of *scenedesmus obliquus* in batch and continuous flat plate photobioreactor, *Chemical Engineering Transactions*, **38**, 211-216.
10. Stoll, I.K. 2016. Vergasung von Biertreber unter den Bedingungen des überkritischen Wassers mit dem Schwerpunkt Salzabtrennung (Master thesis). Karlsruhe Institute of Technology, Institute of Catalysis Research and Technology (IKFT).

4. Results and Discussion¹

The experimental results from the three units of supercritical water gasification (SCWG) are presented in this section. The major product from the experiments was a combustible gas mixture which consisted of hydrogen, carbon dioxide, methane and ethane. In addition, minor amounts of carbon monoxide and light hydrocarbons (e.g. propane, propene and ethylene) were obtained in low concentrations during some experiments. The inorganic constituents of the biomass feedstock were found either in the aqueous phase (salt brine, residual water) or in the form of solid residues.

4.1. Summary of the results from the first laboratory unit I (LUI)

A summary of the operating conditions and corresponding results obtained from LUI are listed below in table 4.1. The plan to evaluate a stable and extended operation, depicted by steady-state and long-duration experiments was the main objective in this unit. As a result, a continuous operation, up to 50 hours, was achieved under supercritical conditions. The rates of gas production ranged between 7–8 L.h⁻¹ in average. The highest carbon gasification efficiency (CGE) for the 5 wt% feed concentration was 62.3%. This value increased significantly (up to 94 %) as a more diluted biomass (2.5 wt%) was used.

Table 4.1 – Summary of the experimental conditions and obtained results from LUI

Exp.	Feed conc.	Flow rate	T	Residence time	Avg. gas production	Duration	CGE	TOC conversion
-	wt%	g.h ⁻¹	°C	min	L.h ⁻¹	h	%	%
1	5	240	600	4.0	6.3	23	57.0	95.2
2			630	4.0	7.0	8.5	60.0	98.2
3		216		4.0	8.0	30	62.3	98.5
4			650	4.0	8.5	48	61.5	98.4
5	2.5	288	650	2.9	8.2	45	88.0	97.5
6				2.9	7.6	22	82.1	95.0
7			600	3.2	8.4	50	93	96.0
8				3.2	7.9	48	94	95.3

Moreover, high conversions of total organic carbon (TOC) were achieved for the entire experiments. This was reflected in the clarity of the residual water. The values of TOC conversion were even higher than CGE in some cases. Such a finding can be explained by the fact that part of the organic carbon in the algal biomass was converted to an inorganic form in the aqueous phase, which was measured in high concentrations in the residual water after gasification.

¹ Part of the results presented in this chapter appeared in earlier works (Elsayed et al. 2014, Patzelt et al. 2014 and Elsayed et al. 2016)

4.2. Summary of the results from the second laboratory unit II (LUII)

The set of experiments in this unit was conducted with the goal of assessing the process performance upon using algal biomass in several concentrations, reaching up to 20 wt%. Thicker biomass slurries were available, but they were not tested due to difficulties associated with pumping. The highest temperature (690 °C) was applied in this unit and an operating pressure of 280 bar was maintained. A summary of the operating conditions and the obtained results is provided in table 4.2. The maximum value of CGE (96.4 %) was achieved, when the lowest concentration of biomass was used (2.5 wt%). The average rate of gas production in LUII was comparable to that in LUI at the same temperature, feed concentration and operating pressure. However, there was a clear improvement in CGE in LUII. The highest rates of gas production, specifically 23.6 and 27.5 L.h⁻¹, were achieved with the highest concentrations of biomass in the feed streams, 20 and 15 wt% respectively. Minor concentrations of CO (less than 0.4 mol%) were also present in the gaseous product.

Table 4.2 – Summary of the experimental conditions and obtained results from LUII

Exp.	Feed conc.	Flow rate	T	Residence time	Avg. gas production	Duration	CGE	TOC conversion
-	wt%	g.h ⁻¹	°C	min	L.h ⁻¹	h	%	%
1	2.5	150	690	2.9	6.3	8.4	96.4	99.6
2	5		600	3.4	7.6	10.0	87.0	98.9
3			620	3.3	8.0	6.5	88.2	99.2
4			650	3.1	8.0	11.0	89.5	99.0
5			690	2.9	10.4	8.5	91.0	98.0
6	10		620	3.3	11.8	9.0	70.0	97.7
7			650	3.1	10.2	11.0	72.0	98.3
8			690	2.9	15.4	9.2	87.0	98.0
9			15	690	2.9	27.5	8.3	86.0
10	20		690	2.9	23.6	8.4	82.0	98.6

Using the highest biomass concentration, a value of CGE (82%) was achieved. Although it is difficult to directly compare these results with other systems of previous works, this is considered to be one of the highest CGE reported so far. This statement is made, given such a concentration of organic materials and a continuous flow SCWG system of this scale. Other results obtained in previous works included either systems of much smaller scales [e.g. *Miller et al. 2012*], less feed concentrations [e.g. *Cao et al. 2011*, *Güngören et al. 2011*, *Xiao et al. 2013*] or involved the use of a heterogeneous catalyst [e.g. *Bagnoud-Vela'squez et al. 2014*, *Elliott et al. 2012*]. The maximum duration of stable operation achieved in this unit was 11 hours. Experimental work based on extended operation was not planned in this unit.

4.3. Summary of the results from the third laboratory unit III (LUIII)

The focus here was to study the influence of three variables on the process performance and gasification products. These variables include the addition of salts in the input stream, operating pressure and residence time. The operating conditions and results summary from LUIII is listed below in table 4.3. The highest pressure of all runs (300 bar) was applied in this unit. However, pressure was not found to have a noticeable influence on the process in the range of experimental conditions tested. Two experiments were conducted without the addition of potassium bicarbonate in the algal biomass, whereas two other experiments were carried out using a maximum concentration of dissolved potassium of 3000 ppm K⁺.

Table 4.3 – Summary of the experimental conditions and obtained results from LUIII (T = 650 °C)

Exp.	Feed conc.	Flow rate	Residence time	P	Avg. gas production	Duration	Dissolved K ⁺	CGE	TOC conversion
-	wt%	g.h ⁻¹	min	bar	L.h ⁻¹	h	ppm	%	%
1	5	462	2.6	280	16.3	6.5	0	57.0	93.8
2		330	3.4	280	15.0	7.8	1500	65.0	96.0
3		462	2.6		20.0	7.0		66.3	97.0
4		667	1.9		33.0	7.0		66.2	86.0
5		1020	1.1		52.0	7.8		70	88.6
6		462	2.6		22.0	5.0	3000	74.0	97.0
7	2.5	462	2.6	280	13.8	7.0	0	72.0	-
8				250	13.4	7.0	1500	77.9	94.1
9				280	14.0	7.8		76.5	93.0
10				300	13.0	7.5		76.0	94.0
11				462	2.6	280		14.2	6.5

The temperature was kept at 650 °C during these experiments. Relatively higher flow rates (up to 1020 g.h⁻¹) were applied in this unit. This flow rate corresponds to a biomass loading of 51 g TS.h⁻¹. As a result of that, the mean residence time which was calculated based on these conditions was as low as one minute for the highest flow rate applied. This is considered as the shortest residence of the entire work included in the three units. Compared to LUII, the automated salts extraction system designed for this unit enabled a more frequent removal of the aqueous fraction defined as salt brine (SB). The values of CGE calculated here were lower compared to those from LUII. As a result, the concentrations of TOC in the aqueous fractions increased noticeably. This was reflected on the decreased values of TOC conversion in the residual water. An average gas production as high as 52 L.h⁻¹ was measured during operation with the highest biomass loading.

4.4. Influence of temperature

Based on the results obtained from the two laboratory units (LUI and LUII), the influence which temperature has on the process performance evaluated through carbon gasification efficiency, the concentrations of TOC in the residual water as well as the yield of the gas components was investigated. In LUI, the results indicated that a temperature increase from 600 to 650 °C contributed to a slight improvement in the CGE, by about 6% (see figure 4.1). This was calculated using biomass concentration of 5 wt%.

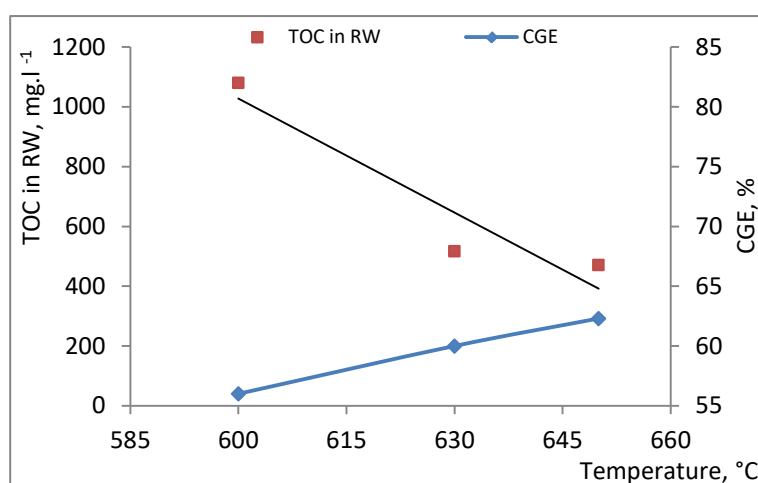


Figure 4.1 – Influence of temperature on the carbon gasification efficiency (CGE) and the TOC concentration in the residual water – Operating conditions: feed conc. 5 wt%, P = 280 bar (data from LUI)

The increase in CGE within this temperature range appeared to be linear, but its trend did not indicate a significant improvement for a further temperature rise anywhere close to 700 °C or higher, for instance. As a result of the improved gasification on carbon-basis under these conditions, the reduction of TOC concentrations in the residual water was clearly obvious starting 630 °C. A decrease in the TOC levels by approximately 50% (from ~ 1000 mg.L⁻¹ to ~ 500 mg.L⁻¹) was achieved upon rising the temperature from 600 °C to the 630 – 650 °C regions.

The experimental work conducted in LUII (figure 4.2) showed comparable findings in this context with regards to LUI. The influence of temperature was studied at two different concentrations (5 and 10 wt% TS) with increasing the temperature up to 690 °C. For the feed containing 5 wt% TS, increasing the temperature from 600 °C to 690 °C did not achieve a major change (improvement) in the gasification efficiency. A rise of 4 – 5 % in the value of CGE was the overall effect of the temperature rise in LUII. However, the absolute values of CGE were much enhanced than in LUI.

In numbers, CGE increased from 56 – 62% to 87 – 88.5% based on the "600 °C to 650 °C" temperature rise in LUI and LUII respectively. The different values of CGE in both units can be probably referred to the different rates of biomass loading in both cases, where higher biomass loading rates in LUI (10.8 g.h⁻¹ TS) compared to (7.5 g.h⁻¹ TS) in LUII would explain such a decrease. A clear enhancement in CGE was calculated using the 10 wt% concentration of biomass in LUII. By increasing the temperature from 620 °C to 690 °C, an increase from 70% to 87% was accordingly achieved. The improvement trend appeared much better compared to that using the 5 wt% concentration. Such a finding would give an indication that the gasification temperature has the upper hand, i.e. a more significant influence on CGE improvement at a higher concentration.

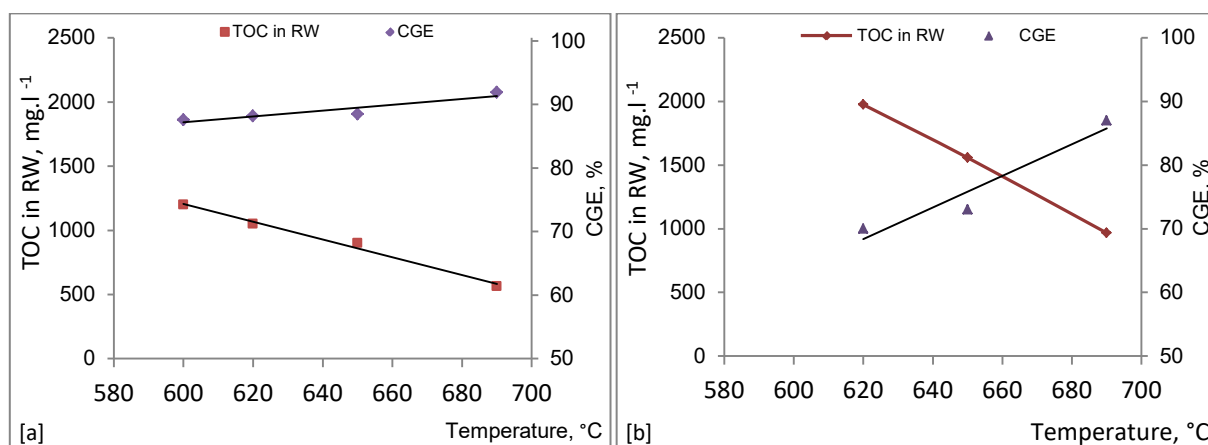


Figure 4.2 – Influence of temperature on the carbon gasification efficiency (CGE) and the TOC levels in the residual water

Operating conditions: P = 280 bar, feed conc. [a] 5 wt% and [b] 10 wt% (data from LUII)

The concentrations of TOC in the residual water continued to decrease in a similar manner as for LUI. Higher concentrations of TOC were expectedly detected in the residual water of the experiments with the higher feed concentration. In both cases, a decline of about 50% was measured between 620 °C and 690 °C for the two concentrations used. In LUII, the formation of inorganic carbon in the residual water was less compared to LUI, which led to a higher TOC for the same concentration (5 wt% TS).

The results obtained in this section come in compliance with previous works which discussed the influences of temperature, pointing out an increase in the gasification efficiency upon increasing temperature [e.g. *Boukiss et al. 2004, Chakinala et al. 2010*] regardless of the feedstock type and its concentration. The higher CGE at elevated temperatures is expected and can only make sense, given the endothermic nature of biomass decomposition or reforming in the supercritical medium.

Demonstrating the influence associated with temperature is quite interesting, despite the fact that the temperature change here did not cover a wide range. On the other hand, there was a change in the chemical composition and the yield of the major gas components (H_2 , CH_4 , CO_2 and C_2H_6) at the different temperatures applied. Figure 4.3 illustrates the changes which occurred regarding the major gas components of SCWG in the form of molar yield per 1 gram total solid or dry biomass. The yield of produced hydrogen and carbon dioxide increased at the higher temperatures. This was accompanied by a decrease measured in the yield of methane. Although ethane was found in concentrations below 10 mol%, it showed a decreasing trend at higher temperature. At the low temperatures, propane was also detected in minor concentrations (< 2 mol %) among the produced gas components in both units. Also, traces of ethene and propene (~ 0.4 mol %) were measured in LUI at lower temperatures. The maximum volumetric amount of the total gas yield was around $1.26 \text{ L.g}^{-1} \text{ TS}$ and it was obtained using the 5 wt% feed concentration at the highest temperature.

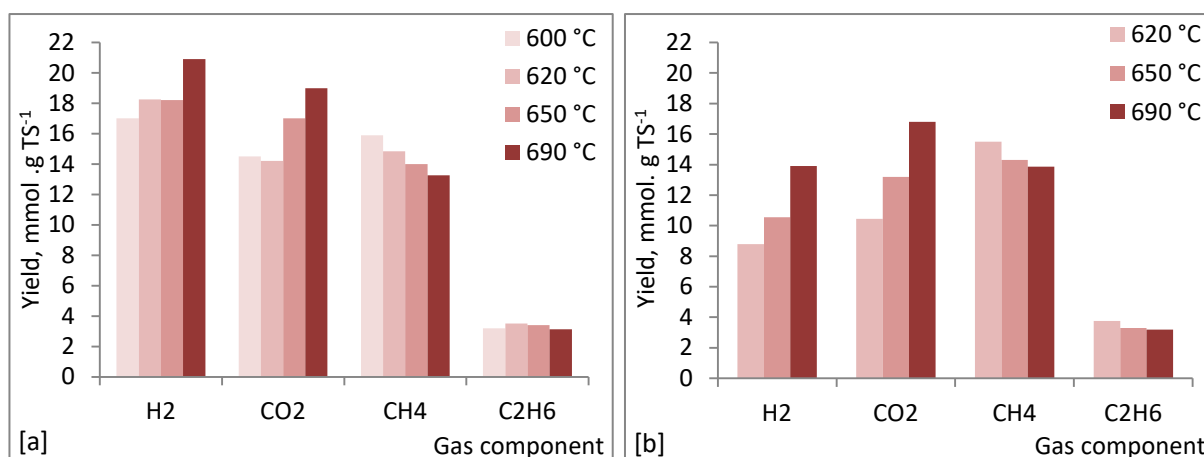


Figure 4.3 – Influence of temperature on the gas yield (data from LUI)

Operating conditions: P = 280 bar, feed conc. [a] 5 wt% and [b] 10 wt% (data from LUI)

Overall, the increased yield of hydrogen and carbon dioxide from the gasification of organic materials at supercritical conditions was reported in earlier works [e.g. *Lee et al. 2002*, *Garcia-Jarana et al. 2008*, *Ref3*, *Ref4*]. The increase of hydrogen and decrease of methane yield at elevated temperatures can be explained on a thermodynamic basis, according to the overall reactions contributing to their formation [*Kruse et al. 2008*]. In quantities, the absolute yield of the carbon-containing species, especially at lower temperatures, would have been higher than expected, if a complete gasification was assumed.

4.5. Influence of biomass concentration

The influence of changing biomass concentration on the carbon gasification efficiency and the concentrations of TOC in the residual water is demonstrated in figure 4.3. The results were obtained from operation with four biomass concentrations (2.5–20 wt% TS) in the feed stream. The reason behind selecting 690 °C for SCWG was to evaluate changing biomass concentration at the highest CGE which can be obtained, in accordance with the results of the previous section. Using the most diluted feed stream (2.5 wt% TS), the highest CGE (96.4 %) was achieved. The decrease in CGE showed a linear trend in the concentration range applied, despite the high temperature applied to the system.

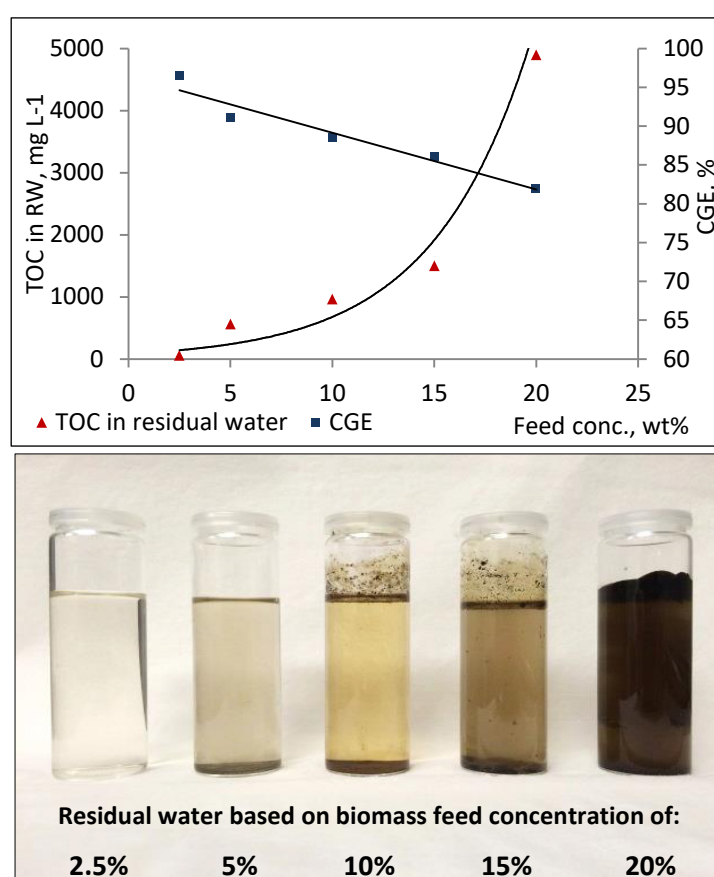


Figure 4.4 – Influence of biomass concentration on carbon gasification efficiency and the TOC levels in the residual water – Operating conditions: T = 690 °C, P = 280 bar (data from LUII)

The lowest value of CGE (82%), i.e. worst process performance in terms of gasification, was calculated while using the highest biomass concentration (20 wt% TS). The change of CGE was clearly reflected in the physical appearance as well as the TOC concentrations in the residual water exiting the system after cooling. In particular, the TOC increase was linear and started to have what seems to be an exponential trend with biomass concentrations above 15 wt% TS.

The value of TOC reached approximately 5000 mg.L^{-1} (the darkest aqueous fraction in fig. 4.3) using the highest biomass concentration, compared to a value below 100 mg.L^{-1} when 2.5 wt% feed concentration was used. On the other hand, the influence of biomass concentration on the yield of the major gas components is presented below in figure 4.4. The obvious trend here was the yield of hydrogen in the gas mixture, as it reached a maximum value during operation with the lowest biomass concentration. A major decrease, by approximately 4 folds, was measured as the biomass concentration was increased from 2.5 to 20 wt% TS.

Methane showed an increasing trend as the concentration of biomass in the feed stream was increased. The yield of methane was almost doubled between the lowest and highest feed concentrations. An increase in the yield of ethane, from 2.3 to 4 mmol.g TS^{-1} , was measured between the lowest and highest ends of feed concentrations. Except from a slight decrease at the higher concentrations, major changes in the amount of produced carbon dioxide was not observed during these experiments.

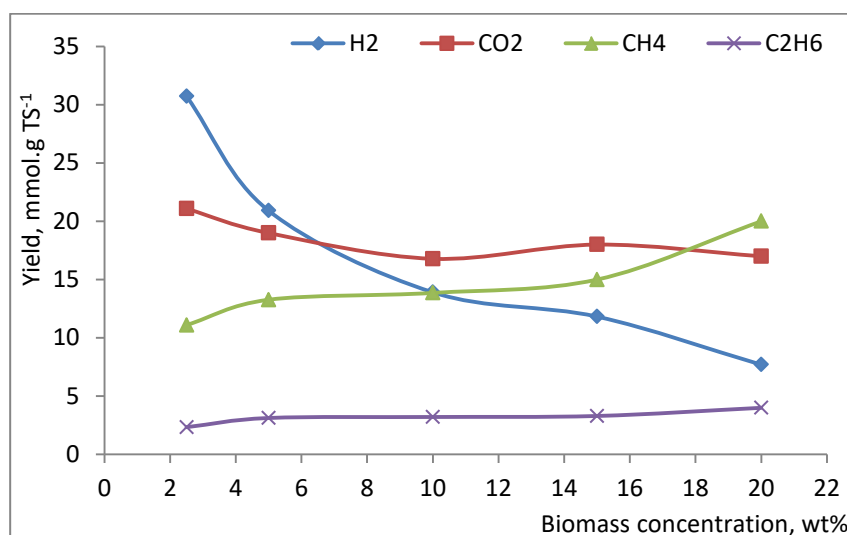


Figure 4.5 – Influence of biomass concentration on the molar yield of the major gas components at different biomass concentrations – Operating conditions: $T = 690 \text{ }^{\circ}\text{C}$, $P = 280 \text{ bar}$ (data from LUII)

The specific yield of the total gas product was negatively affected at higher concentrations. That was due to the reduction in CGE between the lowest and highest concentrations used. The maximum amount of the total gas product obtained per 1 gram of algal biomass was around 1.4 Liter with the 2.5 wt% feed concentration, compared to 1 Liter using the 20 wt%. In this context, an interesting finding regarding the contribution of water to the hydrogen production was concluded from the experimental work.

The results showed that at the lowest biomass concentration (2.5 wt%), the amount of hydrogen measured significantly increased, beyond the hydrogen content of the dry biomass being processed. In this case, the molecules of water contributed to the overall yield of hydrogen and around 45 to 50 % of the produced hydrogen originated from the water medium. The similar finding was also reported in previous works [e.g. *Boukris et al. 2003*, *Kruse and Dinjus 2005*] and it confirms the reactive role which water plays under supercritical conditions, especially at low concentrations.

The effect of feedstock concentration on the system performance in terms of the gas amount and composition was previously discussed in others works. Although these works included systems with different configurations (e.g. Quartz Capillaries: *Chakinala et al. 2010*), other types of feedstocks, or both (e.g. dewatered sludge in a batch system: *Xu et al. 2012*), it was reported that the specific gas yield or gasification efficiency was improved at lower feed concentrations, preferably in a combination with a higher temperature.

Caputo et al. 2016 reported a significant drop in CGE (from 77 to 23.8%) between 3 and 5 wt% feed concentrations of algal biomass respectively, despite a further dilution with a pure water stream before gasification. The operating conditions on continuous operation were: [T = 663 °C, P = 240 bar and residence time = 2.13 minutes]. Other results for obtained from a batch system [*Guan et al. 2012*] highlighted the influence of biomass concentration on hydrogen production at 500 °C. There, the molar yield of hydrogen decreased by almost three folds [from ~ 10 to ~ 3.3 mmol.g⁻¹ TS] as the loading of algal biomass was increased from 1 to 15 wt%. No major changes in the other evolved gaseous species (CO₂, CH₄, C₂H₆) was reported.

Similar to the influence of changing temperature, the composition of hydrogen and methane showed opposite trends at the different feed concentrations. The decomposition of biomass in the presence of water excess, i.e. diluted streams, have been shown to produce more hydrogen than methane. An argument for that was made by *Kruse et al. 2003* based on the competition between the formation of both gaseous species in the frame of thermodynamics and stoichiometry. The explanation indicated that water is necessary for the production of hydrogen through biomass reforming or the water-gas shift reaction. On the contrary, it is not directly contributing to the methanation reactions [the methanation of CO and CO₂ results in the production of water]. Therefore, and according to *Le Chatelier* principle of equilibrium, hydrogen production would be favored in the presence of more water, where the methane formation would then be promoted in a medium with less water content.

As mentioned earlier in this chapter, the levels of total inorganic carbon (TIC) in the aqueous phase of gasification were noticeably high. In particular, the concentration of TIC was even higher than the TOC for the same samples. According to the mass balance calculations, the share of TIC solely and compared to TOC for each experiment did increase at the higher concentrations of algal biomass (see table 4.4). Such a remark, given the fact that the elemental analysis of the dry algal biomass feedstock barely showed any contribution of inorganic carbon, indicates the conversion of organic carbon to an inorganic form during the process. The appreciable amount of TIC in the aqueous phase probably originated from the formation of dissolved carbonates from the several cation species of the converted microalgae.

Table 4. 4 – The share of carbon in the aqueous phase of supercritical water gasification

[Operating conditions: T = 690 °C and P = 280 bar (Data from LUII)]

Feed conc.	Measurements in the entire aqueous phase of SCWG as a percent of the total carbon in the feedstock:	
	Total organic carbon (TOC)	Total inorganic carbon (TIC)
2.5	0.49%	2.17%
5	3.51%	3.82%
10	3.12%	5.05%
15	4.60%	8.53%
20	5.60%	9.01%

An inclusive measurement such as the phenol index could not provide an evidence of significant amounts of phenolic compounds in the residual water. This basically refers to amounts which would be in concentrations that are high enough to cover the gap of carbon balance which is created from the reduced CGE at higher concentrations. Relatively, the existence of these compounds in the residual water was detected in minor concentrations compared to the extracted fraction (salt brine). This means that the majority of phenolic constituents were actually available in the subcritical region, in concentrations which are approximately one order of magnitude higher compared to that in the residual water. A good interpretation of this finding would imply that these evolved compounds were almost entirely destructed under supercritical conditions to form gaseous species as suggested by the reaction scheme presented in the first chapter of this work. Other unreacted intermediates or polymerized molecules from side reactions probably contributed to the increased TOC at higher biomass concentrations. No extensive or quantitative measurements of these substances were conducted.

4.6. Influence of the dissolved salts addition

Another variable introduced through the experimental work was the concentration of an alkali metal species (potassium) in the algal biomass feedstock. For this purpose, two sets of experiments were conducted at 650 °C in the third unit (LUIII), using two different concentrations of biomass in the feed stream (2.5 and 5 wt%) for each set. The flow rate was maintained at 462 g.h⁻¹ and the source of the alkali metal was a dissolved potassium bicarbonate (KHCO₃). The amount of this compound was added in different concentrations starting from zero (no addition), to 1500 ppm (used during the entire experimental work in the 3 units) reaching and 3000 ppm of the metal ion (K⁺).

The results presented in figure 4.6 relate the concentration of dissolved potassium to the two major indicators of process performance discussed beforehand (CGE and TOC). Gasifying both feed concentrations under these conditions demonstrated an improvement in CGE at increased concentrations of K⁺. This increase, as already highlighted in section 4.4 and 4.5, was moving hand-in-hand with the decrease of the TOC levels in the residual water for each experiment.

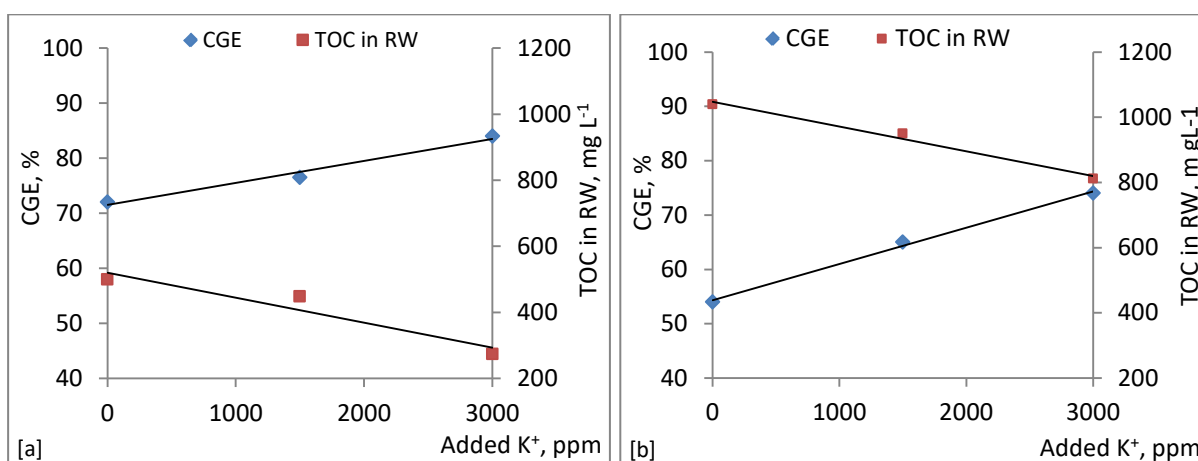


Figure 4.6 – Influence of the dissolved salts addition on the carbon gasification efficiency and the TOC concentrations in the residual water

Operating conditions: T = 650 °C, P = 280 bar, feed conc. [a] 2.5 wt% and [b] 5 wt% (data from LUIII)

An increase in CGE (from 72 to 84% and from 54 to 74%) was reflected in the TOC decrease (from 499 to 327 mg.L⁻¹ and from 1039 to 811 mg.L⁻¹) for the lower and higher biomass concentrations respectively. Analogous to the case of temperature influence, the gasification improvement in connection with the concentration of K⁺ seemed to be more significant at the higher concentration. This is despite the fact that better carbon gasification and less loading of organic carbon was obtained at lower biomass concentrations.

Some changes occurred to the gas yield as a response to the variation in the amount of dissolved salt. An overall increase of the total yield was experienced at each concentration (see figure 4.7). This increase, however, was in the range of 12% for the 2.5 wt% feed concentration referred to the case where no K^+ was added. Except from a slight increase in the yield of hydrogen and carbon dioxide, no major changes was observed. Using the 5 wt% concentration, the increase in the total gas yield was more than 62% with 3000 ppm of K^+ .

With an increase of about 40% in the yield of CO_2 at the 5 wt% feed concentration, the increase of hydrogen was quite obvious, being the main contributor to the rise in the total yield. The reduced CGE at the higher concentration can be concluded from the low absolute yields of methane and ethane compared to the 2.5 wt% feed, regardless of the effect of alkali metal. The increased yield of H_2 and CO_2 can be explained by the catalyzed water-gas shift reaction as presented earlier (Ch. 1, sec. 1.7.5). Through this reaction, the consumption of CO proceeds in the first place to yield CO_2 and H_2 . The simultaneous increase of CH_4 and CO_2 does not comply with the results in the previous sections of this chapter.

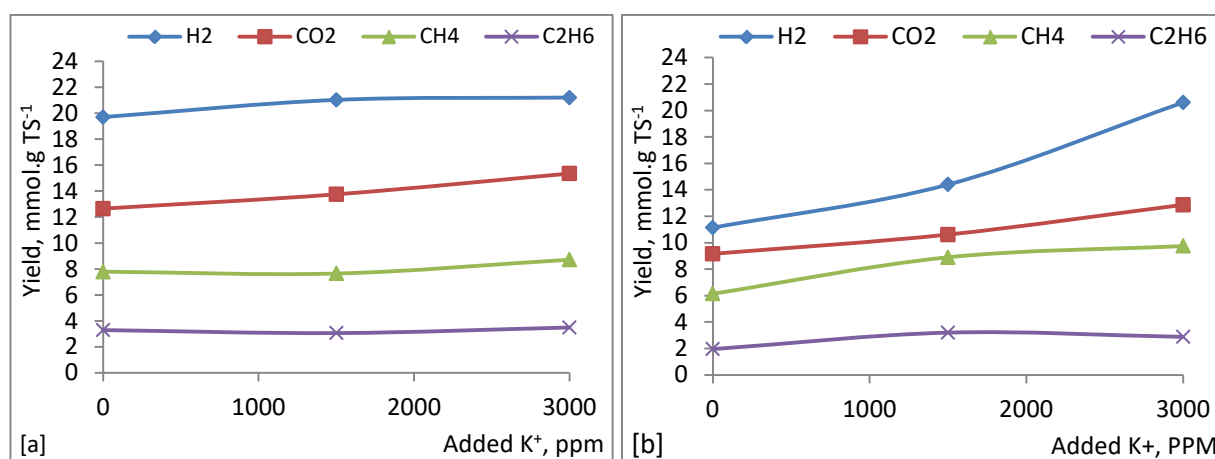


Figure 4.7 – Influence the of dissolved salt addition on the yield of the major gas components

Operating conditions: T = 650 °C, P = 280 bar, feed conc. [a] 2.5 wt% and [b] 5 wt% (data from LUIII)

A possible explanation for such a finding was suggested on the basis of the physical properties of water under supercritical conditions, promoting free radical reactions that leads to the formation of CH_4 [Sinag *et al.* 2003]. Other works which studied the influence of the addition of an alkali metal also demonstrated an increased yield of the produced gas mixture as a whole or specifically the yield of H_2 and CO_2 after the addition of potassium-based salt. Examples cover several types of biomass such as sunflower stalk and corncob [Yanik *et al.* 2008] or wastes including straw [Schmieder *et al.* 2000] or sewage sludge [Xu *et al.* 2013].

In another work, a concentration of 5 wt% corn starch was used for SCWG in a continuous flow system ($T = 700\text{ }^{\circ}\text{C}$, $P = 250\text{ MPa}$, $\dot{m} = 180\text{ g}\cdot\text{h}^{-1}$) at different concentrations of K^+ , from 0 to 3000 ppm [D'Jesus *et al.* 2005]. The work indicated improved carbon gasification (from 82% to 92%) between 0 and 500 ppm K^+ . The CGE almost plateaued beyond 500 ppm K^+ and the work concluded that no significant rise in CGE was obtained with further addition of potassium. No results regarding the specific yield of each gas component was available to compare the yield of major species.

Compared to the results obtained in this section, the higher temperature and the lower feed capacity may give a good explanation for the CGE increase in the work referred to. Besides, the different composition and structure of the materials selected as a feedstock would consequently allow a large spectrum of results at the same operating conditions. As an example, inorganic species such as metals usually exist in many aqueous feedstocks or waste streams. Their existence would probably have a catalytic role which might influence the composition or yield of the produced gas during hydrothermal conversion. For instance, the algal biomass used in this work has a potassium concentration of about 0.8–0.9 wt% in the dry form, which corresponds to values less than 100 ppm depending on the biomass concentration in the feed stream. Such differences would make comparing experimental results from different works challenging without a standardized basis for performance measurement and feedstock assessment.

4.7. Influence of residence time

To evaluate the influence of residence time in the reaction zone, some experiments were conducted in LUIII at constant temperature ($650\text{ }^{\circ}\text{C}$), feed concentration (5 wt% TS), pressure (280 bar) and fixed amount of added potassium (1500 ppm K^+). The residence time for these experiments was varied between approximately 1.1 and 3.4 minutes. This was practically achieved by feeding the biomass at different flow rates ($330 - 1020\text{ g}\cdot\text{h}^{-1}$).

As previously summarized in table 4.3, there was no significant change of the carbon gasification efficiency at the range of residence times investigated. However, a slight decrease in CGE, from 70 to 65 %, was calculated at the longer residence time. The decrease of CGE might be explained by the possible formation of a stable reaction intermediate which were not converted any longer even at higher residence time. In another possible description, the increase in CGE might be the result of possible enhancement in flow dynamics inside the reactor at higher flow rates.

Yet, this argument would require further experimentation at higher throughputs, smaller reactor volumes or a combination of both. Higher concentrations of total carbon (TC) were measured at the shortest residence time, despite the improved CGE. This is a direct result of the increased flow rate, and consequently, the higher biomass flow in the system.

With regards to the gas yield in the product mixture, only slight changes were recognized as illustrated in figure 4.8. An overall decreasing trend in the major gas components was observed as the residence time was increased. This slight decrease was more obvious in the case of hydrogen compared to the other carbon-containing species. The yield of some light hydrocarbons (in the order: $C_2H_6 > C_3H_8 > C_2H_4 > C_3H_6$) was relatively higher at the shortest residence time (by 5 – 6 folds), although their absolute amounts in the experiments were minor ($< 1 \text{ mmol.g TS}^{-1}$) compared to the major gas species.

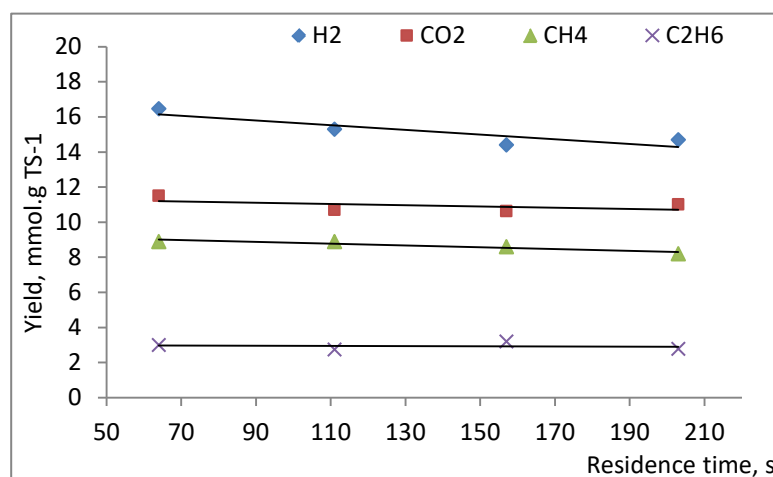


Figure 4.8 – Influence of residence time on the yield of the major gas components
Operating conditions: T = 650 °C, P = 280 bar, Feed conc. = 5 wt% (Data from LUIII)

The results of this section give an indication that when the residence time becomes outside a certain effective range, there may be low or no influence upon further changes. Operation at an optimum residence time, not too short for a complete gasification and not too long to avoid tar or char formation, is crucial for designing systems working under supercritical conditions, especially on a large scale where the precise reactor sizing is directly related to conversion efficiency.

Earlier works reported the influence of residence time on the process output in different ranges, from few seconds up to several minutes, on continuous operation. A decrease in CGE was reported using 5 wt% corn silage under a temperature of 700 °C and pressure of 250 bar in the range of 1 – 3 minutes on continuous operation [Boukiss *et al.* 2004]. The authors stated that the decrease might give an indication regarding the formation of tar or solids as side products.

On the other hand, an increase in CGE was demonstrated in the work of *D'Jesus et al. 2006* at a wide range of residence times [0.6 to 10 minutes] and temperatures (300 to 700 °C) using corn silage in a continuous flow system. In this work, a linear increase of CGE was observed upon increasing residence time until a region, where the highest CGE or a complete gasification was reached. Beyond this region, barely or no improvement in the gasification was measured. This region, however, was extended at lower temperatures, meaning that residence time was more effective at temperatures below 600 °C. Above this temperature, residence time was influential around ~ 0.6 to 2.2 minutes. At the highest temperature, the demonstrated composition of the major gas products (H_2 , CO_2 , CH_4 and C_2H_6) was stable and no changes were observed at residence times more than 1.5 minutes

Shorter residence times were also tested for the conversion of biomass in supercritical water. *Miller et al. 2012* reported high gasification efficiency (95.2%) of algal biomass at a temperature of 600 °C and pressure above 250 bar as indicated in the work. This value was obtained at the longest residence time which was in the seconds region (40 s) on continuous operation with lower loading (Feed flow rate < 48 g.h⁻¹). The process performance was described in terms of the gasification efficiency (GE) and not on carbon basis. It was clear from the work that shorter residence time (down to 1.1 s) resulted in a continuous decrease of the GE (min. 8.3%). Carbon monoxide was also present in the gas mixture in fractions that are compared to those of CO_2

Model compounds such as glucose were also used to test the influence of residence time. *Lee et al. 2012* reported that a complete CGE (100%) was achieved at 700 °C for a range of residence times (10 – 50 s), and flow rates (120 – 480 g.h⁻¹). The feedstock used in this work was 0.6 M glucose (~10.8 wt%) in a continuous flow reactor at 280 bar and temperatures of 600 – 700 °C. The total gas yield remained almost constant at 700 °C, and was not a function of the residence time past 10 seconds. In this region, the yield of hydrogen and methane were relatively stable. No data regarding the yield change of CO_2 versus residence time was presented at 700 °C. At the lower temperature (600 °C), an increase in the yield of H_2 , CO_2 and CH_4 , by approx. 5, 5.3 and 3.5 folds, respectively, was experienced. The maximum value of CGE was approximately 67% at the longest residence time. Also, appreciable amounts of CO (comparable to CH_4) were present, probably due to the short residence time applied.

4.8. Assessment of the aqueous phase and the potential of effluent utilization

The aqueous phase is the major fraction which exited the gasification process as a byproduct. This fraction corresponded to a range from 80 up to 97.5 wt% of the total output streams from all experiments conducted in the three units. The aqueous phase was divided into two fractions: The major fraction which left the reactor in the form of steam that was condensated after cooling (residual water, RW). The second fraction is a minor volume which represents the extracted salts and was defined as the salt brine (SB). The residual water ranged in color from yellowish, brownish to greyish (see figure 4.9) and it did have an aromatic odor that was clear to detect in some cases. In addition, small amounts of dark and tar-like sediments were identified from some experiments, especially as concentrated biomass was used.

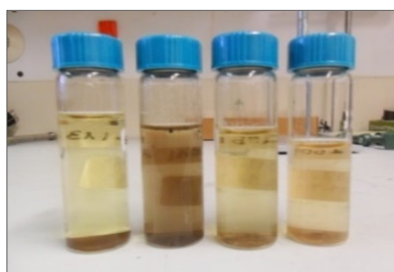


Figure 4.9 – Random samples of the residual water resulting from supercritical water gasification

The concentrations of ionic phosphorus (P) and nitrogen (N) which were measured in the aqueous phase is demonstrated in figure 4.10. The focus in this work was the existence of these elements in the aqueous phase, since they are the basic macronutrients for the growth of microalgae, given the potential of using the aqueous phase for that purpose as already stated. The measurements show that the majority of nitrogen (96 – 99 wt %) was found in the RW in the form of ammonium (NH_4^+), whereas the SB contained higher concentrations of phosphate ions (PO_4^{-3}) compared to the RW.

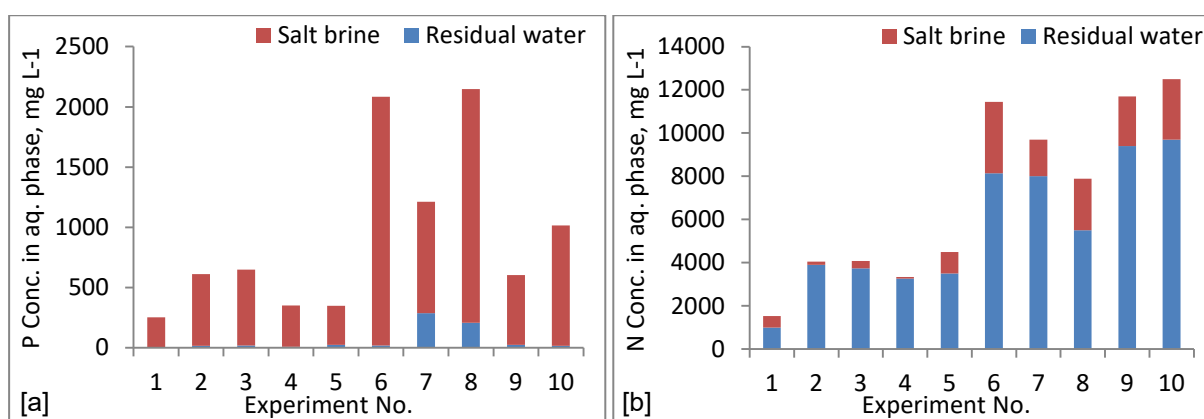


Figure 4.10 – Distribution of (a) ionic phosphorus and (b) nitrogen in the aqueous phase of gasification, between the residual water and salt brine (data from LUII)

The residual water of gasification is deemed as a valuable byproduct if its nutrient's content is utilized for cultivation. In this context, a list which provides a qualitative assessment of some compounds that were found in the residual water of gasification (table 4.5) was presented in the work of *Patzelt et al. 2014*. The assessment, made to several batches of residual water obtained at 600 – 650 °C, demonstrated the existence of twenty-eight substances (ex.: pyridines, aniline, quinolines, indoles) which are considered potentially toxic with respect to their impact in an algal culture.

Table 4.5 – List of existing compounds in the residual water of SCWG (source: *Patzelt et al. 2014*)

Aniline
Acetophenone
Quinoline
Isoquinoline
Indole
(p-Hydroxyphenyl) phosphonic acid
9H-Carbazole-9-methanol
3-Methylbenzenamine
3-Methylphenol
2-Methylquinoxaline
2-Methylquinoline
4-Methylquinazoline
5-Methylquinoline
4-Methylquinoline
4-Methyl-1H-indole
6-Methyl-1H-iIndole
9-Nitroso-9H-carbazole
2-Methylpyridine
3-Methyl-1H-pyrrole
3-Methy-pyridine
2,6-Dimethylpyridine
2-Ethylpyridine
2,5-Dimethylpyridine
2,3-Dimethylpyridine
3-Ethylpyridine
2,4,6-Trimethylpyridine
2,3,6-Trimethylpyridine
2,3-Cyclopentenopyridine

These compounds evolved during SCWG either as unreacted intermediates or through some side reactions. Therefore, the treatment of the aqueous phase was definitely necessary before applying it as the cultivation medium for microalgae. Carrying out such a treatment, the removal or reduction of the possible toxic compounds affecting the growth can be achieved.

For this purpose, treatment using activated carbon filtration (ACF) and ultraviolet (UV) degradation were implemented. To evaluate the influence of the two treatments approaches, measurements of phenol-index, content of total carbon (TC) and total nitrogen (TN) were conducted prior to using the residual water for cultivation. The activated carbon filtration was conducted four consecutive times (ACF1 to ACF4) and the UV degradation proceeded for four hours (UV4). The obtained measurements are listed in table 4.6. Changes in the three measured parameters were identified after treatment using the two approaches. In both cases, the total carbon of the residual water was reduced in a comparable extent. About 15% of the TC remained in the RW after treatment.

Table 4.6 – Influence of activated carbon filtration and ultraviolet treatment of the residual water on the phenol index, total carbon (TC) and total nitrogen (TN) (Data from Patzelt et al. 2014)

	Phenol index	TC	TN
	mg.L ⁻¹		
Untreated RW	190.0	1558.0	2913.0
ACF1	13.2	764.0	2748.0
ACF2	4.7	708.2	2632.0
ACF3	3.2	692.4	2462.0
ACF4	3.0	276.5	2529.0
UV4	58.3	238.5	595.7

The UV treatment resulted in about 80% elimination of the TN from the residual water. This was definitely an unwanted scenario, especially as the dominant species of the TN (NH₄⁺) is a required nutrient for algal cultivation. On the other hand, ACF did not contribute to a major removal of TN, as the levels were not significantly altered after treatment (over 86% of the TN remained in the RW). Activated carbon filtration succeeded in an almost reduction of the phenol index starting the second stage (ACF2). Such an efficient removal was not the case using UV treatment, since around 30% of the phenolic compounds remained in the treated residual water.

Despite the fact that the phenol index was reduced to different extents using the UV treatment and ACF, the chemical compound (Phenol) was present in the RW after both treatment methods. This is apparently because other phenolic compounds which were not assessed already existed in the RW before treatment. In all treatment steps, the pH of the RW, which is slightly alkaline (pH in the range of 8-10) remained relatively stable at upon ACF and decreased from 10 to 8.5 after UV treatment.

Furthermore, the assessment of the substances listed table 4.4 before and after treatment indicated that the majority of these chemicals were eliminated after treatment (successful removal of 23 and 26 compounds using UV and ACF respectively). Four new substances (1,8-Naphthyridine; Methylpyrazine; 2,5 Dimethylpyrazine and 3 Methylbenzenamine) were detected after UV treatment [Patzelt *et al.* 2014].

The formation of certain reaction intermediates or byproducts during hydrothermal conversion is normal. The uses or implementation of residual water differs according to the work orientation. The reaction intermediates of SCWG can be considered final products of hydrothermal liquefaction [Kruse *et al.* 2010]. Such compounds were also highlighted in other published works. A number of chemical substances were reported from the hydrothermal liquefaction of microalgae (*Nannochloropsis sp.*) at a temperature of 350 °C [Brown *et al.* 2010]. Indole was found with approximately 40 other compounds which were identified as products formed by major and minor existence. The author referred the formation of indole to the hydrolysis of the chlorophyll in microalgae to smaller fragments.

Chen *et al.* 2013 investigated the aqueous phase from the gasification of sewage sludge under near- and supercritical conditions (350 – 450 °C) in a batch reactor. Aniline, Indole, phenols and pyridine-based compounds were detected among many other substances including. The results of the two works mentioned in this section serve only as evidence that such chemicals are usually formed during hydrothermal conversion, despite the different range of operating conditions, under which these experiments were conducted.

4.9. Cultivation of microalgae using the residual water of gasification

In the next step, the residual water of SCWG was tested as a cultivation medium for the growth of microalgae. The growth of *A. obliquus* using three batches of the RW before applying the two treatment approaches is demonstrated in Figure 4.11a. Also, the UV- and ACF-treated fractions were tested for growth and compared to that untreated RW (Figure 4.11b). In both cases, the comparison was made in both cases with a reference or standard growth medium described in chapter 3. The growth of microalgae in these cases was measured by the cell dry weight (CDW) over the days of cultivation.

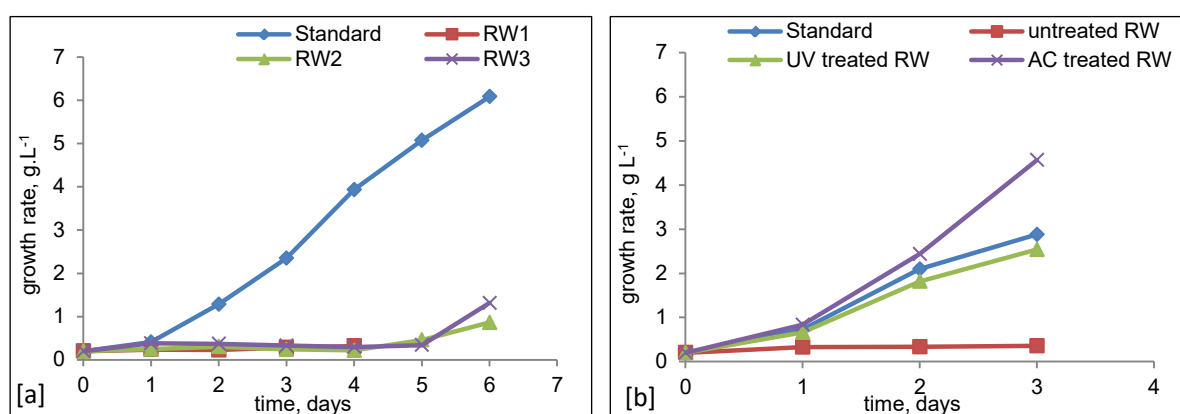


Figure 4.11 – Compared to a standard medium, the growth of *A. obliquus* in different batches of residual water from SCWG [a] and the effect of RW treatment on the algal growth [b]

[Modified from Patzelt *et al.* 2014]

From the growth curves, it can be observed that *A. obliquus* cultivated in the three different batches of the residual water showed a growth delay or inhibition for a period of four days, compared to the standard medium. Nevertheless, this was followed by a low growth rate, in the same time when standard medium culture was already in the linear growth phase (as of day 1). The growth behavior was in compliance with measurements of algal photosynthetic activity [Patzelt *et al.* 2014]. The growth inhibition was possibly a result of toxic substance present in the RW. Culture adaptation to an inadequate medium would occur and may explain the recovery which was in the form of an inefficient growth starting day 5.

The algal cultivation occurring in the treated fractions showed a comparable growth behavior to that of the standard medium. The toxicity of the chemical substance in the RW was eliminated or at least reduced noticeably using both treatment approaches. Growth started for all samples including the standard medium as of day 1. Interestingly, the ACF-treated fraction showed a higher growth rate than the standard medium, which might indicate the existence of organic substances in the RW that can be digested by microalgae for an enhanced growth.

4.10. Carbon distribution in the gasification products

In general, the distribution of carbon among the products of supercritical water gasification reflects the process performance by defining its efficiency and giving an indication of the extent, to which the output streams are loaded with organic or carbonaceous constituents. An elemental mass balance of the total carbon (TC) leaving the system in the gas, aqueous and solid phases was conducted and the results are demonstrated in figure 4.12. The balance calculations were obtained based on the experimental results from the two laboratory units LUII and LUIII. The operating conditions and corresponding results were summarized previously in table 4.2 and 4.3 of this chapter.

The fraction of carbon which is present in the gas phase with respect to that in the feed translates directly to the carbon gasification efficiency (CGE). This fraction varied depending on the process parameters set for each experiment and their influence on the process efficiency in terms of gas production (refer to previous sections 4.2 – 4.6). The term (n/d) or not detected designates the fraction of carbon which could not be traced in the balance calculations. This fraction probably stemmed from precipitations within the system fittings or pipelines, of which no recovery was possible.

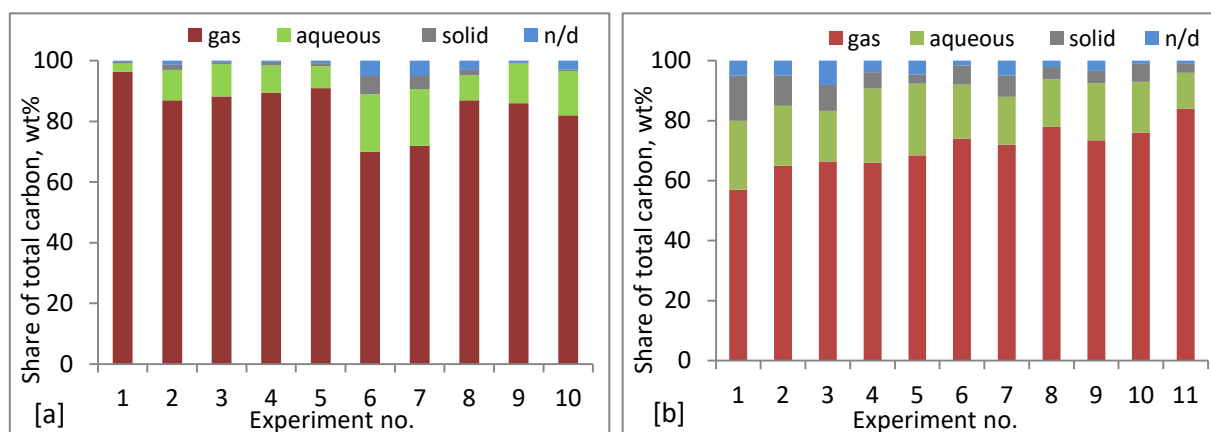


Figure 4.12 – Distribution of total carbon (TC) among the output streams of gasification from two laboratory units: [a] LUII and [b] LUIII

In the aqueous phase, the total carbon represented a combination of both the organic and inorganic carbon which are formed upon gasification. The high concentrations of inorganic carbon in the aqueous phase gives an indication of the organic to inorganic carbon conversion (CO_3^{-2}) in the residual water. For this reason, using the term (TOC conversion) to express the system performance may only be useful when the main objective of such processes is rather handling the aqueous phase or treating the organic content of wet streams and not obtaining a

gaseous product. Depending on the flow rate or biomass loading, this organic-to-inorganic conversion of carbon in the experiments presented was in the range of 5 to 15 wt% of the TOC found in the biomass feedstock. Consequently, the higher this organic-to-inorganic conversion becomes, the less the value of CGE is achieved.

The solid fraction which contains carbon represented the least amount of the three phases detected after gasification. The carbon in the solid phase was basically found in two forms. These forms depended on the system configuration or the laboratory unit which was used for the experiments. From the set of experiments conducted in the LUI, some char-like particles which precipitated on the inner walls of the reactor were identified in some experiments. In the two other laboratory units (LUII and LUIII), the form in which carbon appeared was different. This is due to the salts separation mechanism that was implemented in the preheating zone at the reactor inlet.

At the position of salts extraction in the temperature range of 350 – 420 °C, some of the biomass which was not gasified at this point left the system along with the salt brine. Consequently, carbon-rich phase, ranging in physical appearance between sticky substances to particle sediments evolved. The highest amount of total carbon present in the aqueous phase was measured during the two experiments with the highest flow rates, namely 667 and 1020 g.h⁻¹. This dark tar-like substance would represent complex intermediates or polymerized molecules that are usually formed during hydrothermal liquefaction at lower temperatures than that of SCWG. These materials were chemically analyzed and physically examined, showing high concentrations of carbon. In addition, an analysis using gas chromatography–mass spectrometry (GC - MS) gave an indication regarding the existence of high molecular mass compounds. Although the chemical structure of these compounds was difficult to determine as a result of molecular fragmentations, the existence of long chain alkenes such as hexadecene-based compounds was indicated.

Overall, the results obtained provide a quantitative indication for the system performance in terms of carbon distribution. When considering each reactor individually, temperature and biomass concentration had the major influence on the process efficiency and hence, the carbon distribution in the three phases. Comparing different process conditions, the higher biomass loading in LUIII, approximately 3 to 7 times higher than that in LUII, resulted in a clear decrease in CGE. A SCWG unit with an efficient performance would necessarily include the major fraction of carbon in the gas phase. Any deviation from this allows or increase the

tendency of the possibly un-gasified carbon in an intermediate form to find an its way through the aqueous phase or alternatively deposit in the form of solids. This becomes a significant operational challenge, especially in cases when the residence time is the limiting factor for a complete conversion, at higher biomass concentration in the feed stream, or at increased flow rates when the salt extraction mechanism is not finely adjusted.

4.11. Recovery of the nutrients after gasification

As presented in chapter one, the growth of microalgae depends mainly on the presence of macro- and micro-elements in the cultivation medium. These elements, or nutrients, are usually fed to the culture in the form of dissolved salts at certain concentrations that depend on the needs of the algal cells and the growth conditions. Part of these elements is usually taken up by the cells, contributing to its full structure. The excess elements are either consumed by the young fresh cells or left in the culture medium if the cells are mature enough and no longer growing.

Figure 4.13 demonstrates the average nutrient distribution of the dry biomass which was used for the gasification in supercritical water. Based on the ultimate analysis, the dominating components of these nutrients were nitrogen, phosphorus and potassium. Minor amounts of sulphur, magnesium, calcium, silicon as well as traces of iron, sodium, aluminum and chlorine were also measured. To achieve the recovery of natural resources and improve process economy, these elements are targeted for utilization through recycling from SCWG and re-using them in the algal cultivation.

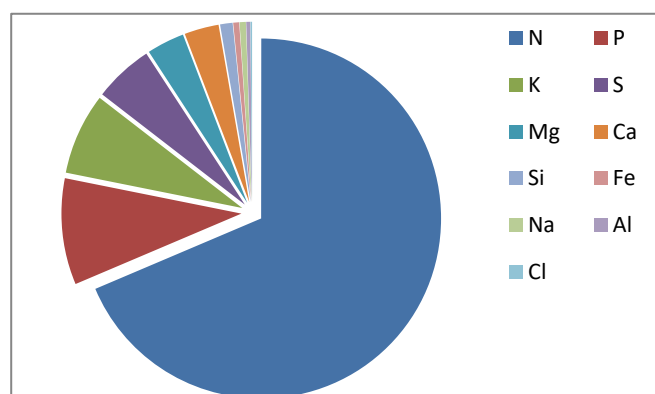


Figure 4.13 – Elemental distribution of the inorganic elements in the algal biomass

This means that these elements should be ideally extracted as a by-product from the gasification process and be fed into the culture medium in an aqueous form. Under near- and supercritical conditions, the availability of these elements takes a different form in the product streams. This is due to the destruction of algal cells and the carbon conversion during gasification. The distribution of the total nitrogen (N), phosphorus (P) and potassium (K) in the two phases (solid and liquid) resulted from SCWG are shown in figure 4.14. The data in the diagram represent average values from the mass balance calculations based on the experiments conducted from the two laboratory units LUII and LUIII. The total recovery of the three elements is shown in the diagrams as a reference. Mass fractions which are not detected are identified in the diagram with a dashed pattern and negative value.

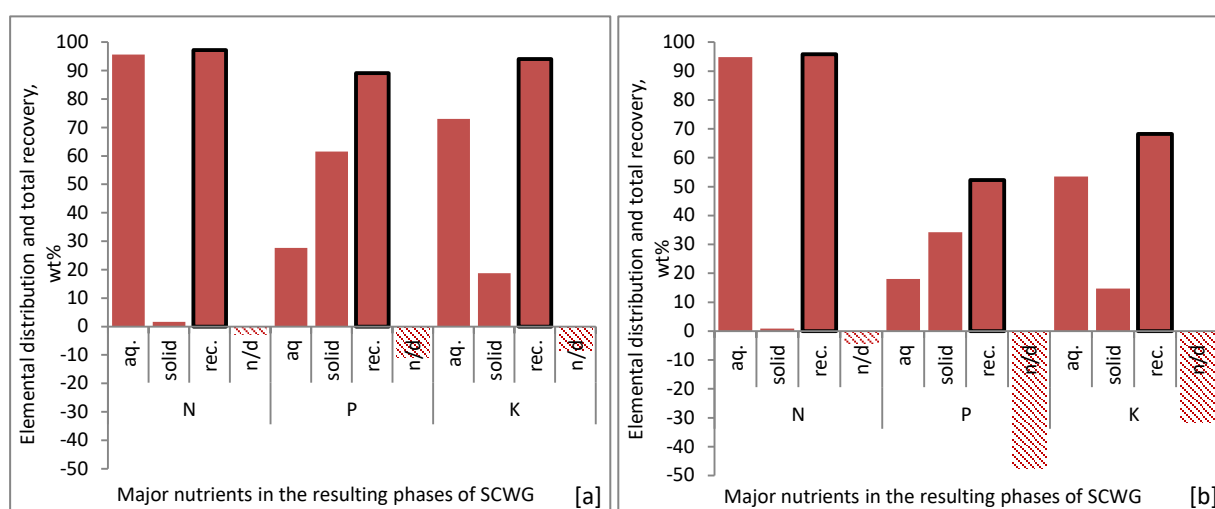


Figure 4.14 – Distribution and recovery of the macro-nutrients (N, P and K) from the gasification products for: [a] LUII and [b] LUIII [aqueous: aq.; recovery: rec.; n/d: not detected]

The recovery of total nitrogen in both cases was clearly high (97.3% and 95.8 for LUII and LUIII respectively) compared to phosphorus (LUII: 89.1% and LUIII: 52.3%) and potassium (LUII: 94.1% and LUIII: 68.2%). The vast majority of nitrogen was available in the aqueous phase in the form of ammonium. Minor amounts of nitrogen were also detected in the solid fraction of some experiments. On the other hand, both phosphorus and potassium showed an increased tendency to exist in the solid phase compared to nitrogen. The recovery of both P and K was clearly lower from the experiments that were conducted in LUIII. An explanation for the low recovery might be supported by the increased precipitations in this unit due to its configuration. Compared to the second unit, LUIII included longer pipelines between the reactor and phase separator which are both connected via separate product and salt extraction lines.

More losses were concluded with regards to the micro-nutrients after gasification. The recovery of these elements was calculated and found as follows for LUII (Mg = 84.5%, Ca = 79.2%, Si = 64.7% and S = 64.5%) and LUIII (Mg = 33.2%, Ca = 18%, Si = 22.1 and S = 40.2 %), with magnesium and calcium being detected in higher amounts in the solid phase. A similar graphical representation for these elements is found in the appendix (8.16). The trace elements (Cl, Al, Na and Fe) were also found in the output streams in very low concentrations compared to the other elements and therefore, they were difficult to trace and be included in the balance calculations.

Several works highlighted the migration of inorganic elements, sometimes referred to as heteroatoms in this context, to the solid phase under near- and supercritical conditions during the gasification of several feedstock materials as well as salt solutions. The works of *Leusbrock et al. 2012*, *Zhu et al. 2011*, *Yanagida et al. 2009* and *Acelas 2014* discussed this phenomenon with a special focus on phosphorus as a natural resource that has a limited availability. These works indicated the high tendency of phosphorus to precipitate in the solid phase under these conditions. It was found out that phosphorus migrates to the solid phase in the form of Phosphate (Ca-, K-, Mg- PO₄) salts, which was also observed based on X-ray diffraction (XRD) analysis conducted to one of the solid samples obtained from the experimental work. A possible method which can be applied for the recovery of phosphorus is extraction using acid or alkaline leaching, a method which was suggested in a previous work [*Stark et al. 2006*].

Typically, the accumulation or deposition of salts in the system possibly occurs during operation in the supercritical region. This could be problematic for the stability or durability of continuous operation. As mentioned earlier, chemical analyses and elemental mapping were conducted to the solid residues evolved during gasification in the framework of our experimental activity. These residues were extracted either from the unit after a routine maintenance of the system parts (reactor, filters, valves and connections) or from the sediment residues in both residual water and salt brine.

As shown in table 4.7, three major fractions of solid residues were distinguished. The first fraction was rich in salts (e.g. P-, Ca-, K- and Mg- salts). Its color was ranging between a white to bright grey color. The second fraction varied in color from dark grey to black and it contained high concentrations of coke or carbon which evolved through a complex intermediate during hydrothermal conversion. The third fraction contained corrosion products (e.g. Ni-, Cr- and Fe- oxides). A combination of these three fractions was found as well.

Table 4.7 – Solid residues from supercritical water gasification and their elemental composition

Element	Fraction I: salt-rich	Fraction II: carbon-rich	Fraction III: corrosion-rich
	wt%		
C	-	67.00	1.26
O	41.33	26.01	18.88
Na	0.16	-	-
Mg	6.11	-	0.41
Al	2.51	0.44	1.37
Si	2.75	-	0.10
P	16.71	-	0.44
K	13.92	-	0.76
Ca	16.50	-	-
S	-	2.58	0.18
Ni	-	3.26	35.48
Cr	-	-	28.73
Fe	-	-	12.39

This procedure was based on purging or flushing the system using water at the end of each experiment for a few hours. As a result, this procedure contributed to the recovery a major part of the salt precipitates within the unit. Figure 4.15 demonstrates the major influence of purging the system in some experiments which were carried out in LUII and LUIII. Purging was practically realized following two steps. The first step involved purging with hot water under supercritical conditions directly at the end of the experiment.

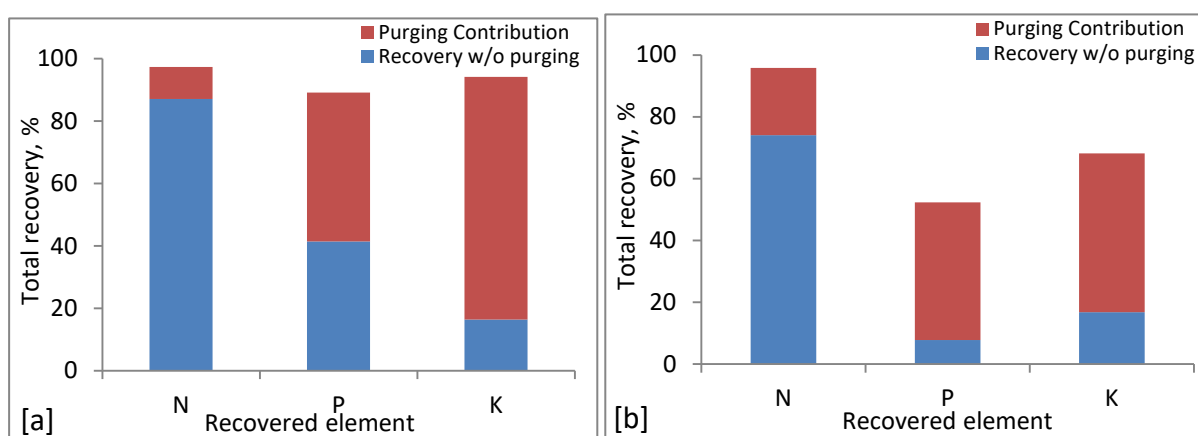


Figure 4.15 – Major contributions of purging to the recovery of N, P and K from supercritical water gasification for: [a] LUII and [b] LUIII

At this point, the system was still hot, but it was actually cooling down due to switching off the heating coils and the continuous flow of water without preheating. Consequently, this step contributed to recover some of the un-converted biomass residues inside the reactor and collect some of trapped gas within the system. After this, the system was purged under subcritical

conditions, by maintaining the high pressure at atmospheric temperature. The cold purging here helped in extracting some salts which have re-dissolved in water at low temperatures. At the last stage, the system was opened, water was circulated again across the unit and any remaining solids were finally separated. The aqueous phase resulted from this procedure was analyzed in the same manner as for the samples taken during the experiments. The balance calculations were conducted taken into account this additional fraction. Purging had a relatively low contribution to the recovery of total nitrogen due to its good recovery in the aqueous phase during the process. On the other hand, major contributions ranging between 50 and 75 wt% of the total recovered P and K was obtained from purging.

References (Chapter 4)

1. Acelas, N.Y., Lopez, D.P., Brilman, D.W., Kersten, S.R., Kootstra, A.M. 2014. Supercritical water gasification of sewage sludge: gas production and phosphorus recovery. *Bioresource technology*, **174**, 167-75.
2. Bagnoud-Velásquez, M., Brandenberger, M., Vogel, F., Ludwig, C. 2014. Continuous catalytic hydrothermal gasification of algal biomass and case study on toxicity of aluminum as a step toward effluents recycling. *Catalysis Today*, **223**, 35-43.
3. Boukis, N., Diem, V., Habicht, W., Dinjus, E. 2003. Methanol Reforming in Supercritical Water. *Industrial & Engineering Chemistry Research*, **42**(4), 728-735.
4. Boukis, N., Galla, U., Diem, V., D'Jesus, P., Dinjus, E. 2004. Hydrogen production from biomass in supercritical water. *Chemical Engineering Transactions*, ISBN 88-900775-3-0, 4, 131-136 and H₂-age: When, Where, Why Pisa, 16-19 May, Italian Association of Chemical Engineering.
5. Boukis, N., Galla, U., Diem, V., D'Jesus, P., Dinjus, E. 2004. Wasserstoffreiches Brenngas aus nasser Biomasse. Erste Ergebnisse mit der Pilot-Anlage VERENA. DGMK-Fachbereichstagung: Velen VI, "Energetische Nutzung von Biomassen", 289-296, 19 - 21 April, in Velen/Westfalen, Deutschland.
6. Brown, T.M., Duan, P., Savage, P.E. 2010. Hydrothermal Liquefaction and Gasification of Nannochloropsis sp. *Energy & Fuels*, **24**(6), 3639-3646.
7. Cao, C., Guo, L., Chen, Y., Guo, S., Lu, Y. 2011. Hydrogen production from supercritical water gasification of alkaline wheat straw pulping black liquor in continuous flow system. *International Journal of Hydrogen Energy*, **36**(21), 13528-13535.
8. Caputo, G., Dispenza, M., Rubio, P., Scargiali, F., Marotta, G., Brucato, A. 2016. Supercritical water gasification of microalgae and their constituents in a continuous reactor. *The Journal of Supercritical Fluids*, **118**, 163-170.
9. Chakinala, A.G., Brilman, D.W.F., van Swaaij, W.P.M., Kersten, S.R.A. 2010. Catalytic and Non-catalytic Supercritical Water Gasification of Microalgae and Glycerol. *Industrial & Engineering Chemistry Research*, **49**(3), 1113-1122.
10. Chen, Y., Guo, L., Jin, H., Yin, J., Lu, Y., Zhang, X. 2013. An experimental investigation of sewage sludge gasification in near and super-critical water using a batch reactor. *International Journal of Hydrogen Energy*, **38**(29), 12912-12920.
11. D'Jesús, P., Artiel, C., Boukis, N., Kraushaar-Czarnetzki, B., Dinjus, E. 2005. Influence of educt preparation on gasification of corn silage in supercritical water. *Industrial and Engineering Chemistry Research*, **44**(24), 9071-9077.
12. D'Jesús, P., Boukis, N., Kraushaar-Czarnetzki, B., Dinjus, E. 2006. Influence of Process Variables on Gasification of Corn Silage in Supercritical Water. *Industrial & Engineering Chemistry Research*, **45**(5), 1622-1630.
13. Elliott, D.C., Hart, T.R., Neuenschwander, G.G., Rotness, L.J., Olarte, M.V., Zacher, A.H. 2012. Chemical Processing in High-Pressure Aqueous Environments. 9. Process Development for Catalytic Gasification of Algae Feedstocks. *Industrial & Engineering Chemistry Research*, **51**(33), 10768-10777.
14. Elsayed, S., Boukis, N., Sauer, J. 2014. Hydrothermal gasification of microalgae - prospects and challenges. *DGMK Tagungsbericht*, 221-228.
15. Elsayed, S., Boukis, N., Patzelt, D., Hindersin, S., Kerner, M., Sauer, J. 2016. Gasification of Microalgae Using Supercritical Water and the Potential of Effluent Recycling. *Chemical Engineering & Technology*, **39**(2), 335-342.
16. García Jarana, M.B., Sánchez-Oneto, J., Portela, J.R., Nebot Sanz, E., Martínez de la Ossa, E.J. 2008. Supercritical water gasification of industrial organic wastes. *The Journal of Supercritical Fluids*, **46**(3), 329-334.

17. Güngören Madenoğlu, T., Boukis, N., Sağlam, M., & Yüksel, M. 2011. Supercritical water gasification of real biomass feedstocks in continuous flow system. *International Journal of Hydrogen Energy*, **36**(22), 14408-14415.
18. Kruse, A. 2008. Supercritical water gasification. *Biofuels, Bioproducts and Biorefining*, **2**(5), 415-437.
19. Kruse, A., Bernolle, P., Dahmen, N., Dinjus, E., Maniam, P. 2010. Hydrothermal gasification of biomass: consecutive reactions to long-living intermediates. *Energy Environ. Sci.*, **3**(1), 136-143.
20. Kruse, A., Dinjus, E. 2005. Influence of salts during hydrothermal biomass gasification: The role of the catalysed water-gas shift reaction. *Zeitschrift für Physikalische Chemie*, **219**(3), 341-366.
21. Kruse, A., Henningsen, T., Smag, A., Pfeiffer, J. 2003. Biomass gasification in supercritical water: Influence of the dry matter content and the formation of phenols. *Industrial and Engineering Chemistry Research*, **42**(16), 3711-3717.
22. Lee, I.-G., Kim, M.-S., Ihm, S.-K. 2002. Gasification of Glucose in Supercritical Water. *Industrial & Engineering Chemistry Research*, **41**(5), 1182-1188.
23. Leusbrock, I., Metz, S.J., Rexwinkel, G., Versteeg, G.F. 2010. The solubilities of phosphate and sulfate salts in supercritical water. *The Journal of Supercritical Fluids*, **54**(1), 1-8.
24. Miller, A., Espanani, R., Junker, A., Hendry, D., Wilkinson, N., Bollinger, D., Abelleira-Pereira, J.M., Deshusses, M.A., Inniss, E., Jacoby, W. 2015. Supercritical water oxidation of a model fecal sludge without the use of a co-fuel. *Chemosphere*, **141**, 189-96.
25. Patzelt, D.J., Hindersin, S., Elsayed, S., Boukis, N., Kerner, M., Hanelt, D. 2014. Hydrothermal gasification of *Acutodesmus obliquus* for renewable energy production and nutrient recycling of microalgal mass cultures. *Journal of Applied Phycology*, **27**(6), 2239-2250.
26. Stark, K., Plaza, E., Hultman, B. 2006. Phosphorus release from ash, dried sludge and sludge residue from supercritical water oxidation by acid or base. *Chemosphere*, **62**(5), 827-832.
27. Sinağ, A., Kruse, A., Schwarzkopf, V. 2003. Key Compounds of the Hydrolysis of Glucose in Supercritical Water in the Presence of K₂CO₃. *Industrial & Engineering Chemistry Research*, **42**(15), 3516-3521.
28. Xiao, P., Guo, L., Zhang, X., Zhu, C., & Ma, S. 2013. Continuous hydrogen production by biomass gasification in supercritical water heated by molten salt flow: System development and reactor assessment. *International Journal of Hydrogen Energy*, **38**(29), 12927-12937.
29. Xu, Z.R., Zhu, W., Gong, M., Zhang, H.W. 2013. Direct gasification of dewatered sewage sludge in supercritical water. Part 1: Effects of alkali salts. *International Journal of Hydrogen Energy*, **38**(10), 3963-3972.
30. Xu, Z.R., Zhu, W., Li, M. 2012. Influence of moisture content on the direct gasification of dewatered sludge via supercritical water. *International Journal of Hydrogen Energy*, **37**(8), 6527-6535.
31. Yanagida, T., Minowa, T., Shimizu, Y., Matsumura, Y., Noda, Y. 2009. Recovery of activated carbon catalyst, calcium, nitrogen and phosphate from effluent following supercritical water gasification of poultry manure. *Bioresource technology*, **100**(20), 4884-6.
32. Yanik, J., Ebale, S., Kruse, A., Sağlam, M., Yüksel, M. 2008. Biomass gasification in supercritical water: II. Effect of catalyst. *International Journal of Hydrogen Energy*, **33**(17), 4520-4526.
33. Zhu, W., Xu, Z.R., Li, L., He, C. 2011. The behavior of phosphorus in sub- and super-critical water gasification of sewage sludge. *Chemical Engineering Journal*, **171**(1), 190-196.

5. Process Simulation

5.1. Solution strategy

A model obtained through the software (*Aspen Plus*[®]) by *AspenTech* was developed to demonstrate the gasification of algal biomass in supercritical water with a computer-based simulation. The work was based on three major coordinates. At first, the possibility to provide a method to process a non-conventional feed such as microalgae in the software was analyzed. Then, the influence of major process variables (e.g. temperature and biomass concentrations) on the composition of the product gas was investigated. Finally, an energy assessment of the different sub-processes included in the system was carried out taking into consideration the energy sources and sinks of each process step. In this regards, two process configurations (1-stream and 2-streams operation) were simulated based on operation in the laboratory units where the experimental work was conducted.

Basically, the software uses a combination of state and transport equations to calculate the missing parameters at equilibrium. The results are then presented through a user-friendly interface with the aids of process diagrams, tables and graphical representation. There are two property methods included that were implemented in the calculations:

- PENG-ROB: This equation of state model (Peng–Robinson) is selected to describe the thermodynamic properties of the system given in this work. This model is suitable for hydrocarbon systems and can be applied to provide reasonable calculations in systems involving supercritical water [Tang and Kitagawa 2005, Letellier et al. 2010].
- IAPWS 95 (International Association for the Properties of Water and Steam, adopted in 1995): This method provides adequate steam table correlations and it is suitable for calculating the properties of water as the major component in several streams of the process (See values comparison with another method in Appendix 8.18).

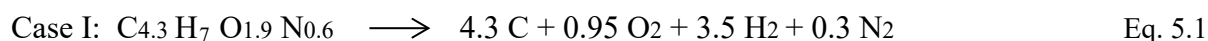
Some assumptions were made prior to establishing the model, in order to simplify or set a basis for the calculations. These assumptions state that:

- A temperature of 20 °C and a pressure of 1 bar were set as the reference conditions.
- The reaction system is operated under isobaric and isothermal conditions.
- Heat losses in the reaction zone are neglected.
- Calculations are made under steady state operation.
- The inorganic fraction of the feedstock which exits the system in the form of ash or salts is set as an inert component of the system and is not part of the equilibrium calculations.

5.2. Feedstock decomposition

Given the elemental analysis obtained from the experimental work and assuming a molecular mass of 100 kg.kmol^{-1} , a hypothetical formula ($C_{4.3} H_7 O_{1.9} N_{0.6} AFE_{0.08}$) was suggested for the feed on a dry basis. The ash forming elements (AFE) were added only for the sake of completeness. It includes the inorganic constituents of microalgae (e.g. P, K, Mg, Ca) which leave the process in the form of solid precipitates (ash or salts).

Due to the absence of biomass materials within the Aspen component database and the difficulty to process such components using the reactor models available in the software, one mean to overcome this issue is to implement a so-called pseudo-component, i.e. define a feedstock in terms of some input data such as elemental and proximate analysis as well as another property like the heat of combustion. Afterwards, one step prior to gasification in SCW should be carried out. This step includes the decomposition of microalgae to simpler molecules that can be further processed as conventional components in the reaction system of the model. Two cases were suggested based on this concept. The first assumes hypothetical decomposition of microalgae (Eq. 5.1) to its elemental constituents (C, H₂, O₂, N₂) and this case is referred to as feed decomposition to basic elements (FDE). The second case (Eq. 5.2) assumes the decomposition of biomass in water to produce a mixture of synthesis gas (CO and H₂) along with nitrogen. This case is defined as feed reforming to synthesis gas (FRS).



In both cases, the feedstock is processed in the reactor model *R-Yield* (figure 5.1). This is where the suggested decomposition to simpler molecules takes place based on a pre-defined yield that is calculated from the stoichiometry of each of the two reactions mentioned above. The produced mixture from *R-Yield* is then combined with water and delivered to the reaction system under supercritical conditions.

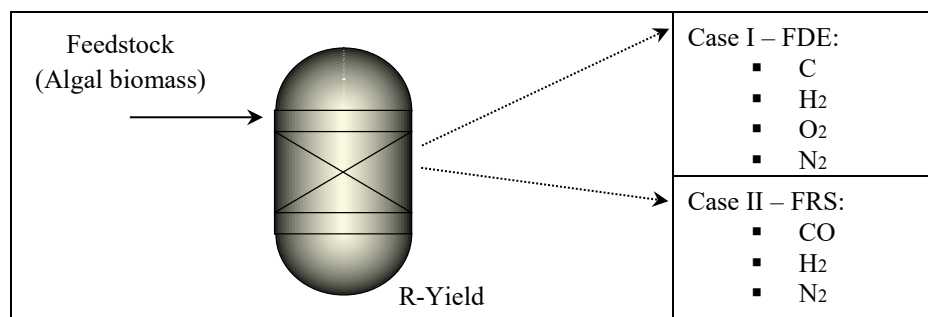


Figure 5.1 – Feed decomposition to simpler molecules in the R-Yield reactor model

5.3. Algal biomass simulant

Another method to simulate the biomass feedstock in the Aspen model is to create a mixture of standard or conventional compounds that are available in the software database. Using this method, the decomposition step which was applied in the previous section, for FDE and FRS, is eliminated and the model can be illustrated on a simpler basis for calculations.

From more than fourteen compounds, several combinations were made to create an optimum mixture that corresponds to the composition or weight fraction of the basic elements in the algal biomass. As a result, two combinations using four compounds were created and referred to as algal simulants (AS). The selected compounds, illustrated in table 5.1, were *Aminobutyric Acid*, *Furfuryl Alcohol*, *Methyl Acetate* and *Methyl Butyrate*. The combinations which resulted in a good match to microalgae were found to be in the ratios of 60 to 40 wt%.

Table 5.1 - A combination of conventional compounds achieving similar weight percentage of the basic elements in microalgae

Algal Biomass Simulant I (ASI)								
Aminobutyric Acid (60 wt%)		Elemental wt%		Furfuryl Alcohol (40 wt%)		Elemental wt%		Elemental wt% in mixture
Chemical Formula	C ₄ H ₉ O ₂ N	C	0.465	Chemical Formula	C ₅ H ₆ O ₂	C	0.612	0.524
Molar Mass	103.12	H	0.087	Molar Mass	98.10	H	0.061	0.077
		O	0.310			O	0.326	0.317
		N	0.136			N	0.000	0.081
Algal Biomass Simulant II (ASII)								
Methyl Cyanoacetate (60 wt%)		Elemental wt%		Methyl Butyrate (40 wt%)		Elemental wt%		Elemental wt% in mixture
Chemical Formula	C ₄ H ₅ NO ₂	C	0.484	Chemical Formula	C ₅ H ₁₀ O ₂	C	0.587	0.526
Molar Mass	99.09	H	0.050	Molar Mass	102.13	H	0.098	0.069
		O	0.323			O	0.313	0.319
		N	0.141			N	0.000	0.085

Having defined an expression for the feed using the methods explained above, two reactor models will be implemented in the different runs of simulation. The first model is the Gibbs reactor (*R-Gibbs*). This model is based on calculating an equilibrium composition which achieves a minimum level of the Gibbs free energy. For this model, a few input requirements are necessary, typically operation pressure and temperature. In the second model, the stoichiometric reactor (*R-Soich*), one or a series of reactions are provided in advance with a molar extent or fractional conversion of the input components. The model then calculates the enthalpy of reactions based on the given information. Both models are discussed elaborately in the following sections of this chapter.

5.4. Thermodynamic equilibrium

The chemical equilibrium calculations are commonly conducted through the use of equilibrium constants of known reactions, a procedure which is useful for simple tasks. However, such calculations tend to be complex when the equilibrium composition is determined by a number of simultaneous reactions, in which several species are involved. Therefore, another method for solving these kinds of problems is made by obtaining the equilibrium composition through minimization of the system's Gibbs free energy.

Typically, the Gibbs model does not require the determination of reaction stoichiometry. Only the system temperature and pressure, or alternatively the operation pressure and reaction enthalpy should be available as an input for calculations. To relate thermodynamic variables with the Gibbs free energy, a combination of the first and second law of thermodynamics takes the following differential form:

$$dU = TdS - PdV \quad \text{Eq. 5.3}$$

Using the definition of a system's enthalpy (Eq. 5.4) with its differential in terms of the pressure, volume and internal energy, and by applying equation 5.3, the following expression (Eq. 5.5) can be obtained:

$$H = U + PV \quad \text{Eq. 5.4}$$

$$dH = dU + (PdV + VdP) = (TdS - PdV) + (PdV + VdP)$$

$$dH = TdS + VdP \quad \text{Eq. 5.5}$$

By introducing the term (Gibbs free energy, G) and using equation. 5.5, the pressure and temperature dependence of the Gibbs free energy in a given system can be expressed by equation 5.7:

$$G = H - TS \quad \text{Eq. 5.6}$$

$$dG = dH - (TdS + SdT) = TdS + VdP - (TdS + SdT)$$

$$dG = VdP - SdT \quad \text{Eq. 5.7}$$

For a system under constant pressure and temperature, the change of Gibbs free energy equals to zero. In other words, the condition ($dG = 0$) occurs as the system's available energy reaches its minimum value. This state becomes valid when the system is at equilibrium [Nobel 2005].

In the systems which include reactive species, a chemical reaction proceeds in the direction of decreasing the Gibbs free energy until it stops as the chemical equilibrium is established. Under these conditions, an increase in the Gibbs free energy means a violation to the second law of thermodynamics. Limiting equation 5.7 to an isothermal condition with the assumption of an ideal gas behavior leads to the following equation:

$$\int_{P^0}^P dG = \int_{P^0}^P \frac{nRT}{P} dP = nRT \ln \frac{P}{P^0} \quad \text{Eq. 5.8}$$

The variable (P) in the adjusted Gibbs function (Eq. 5.8) refers to the set pressure of the system and (P⁰) is the pressure at a reference or standard condition. To specify this equation with respect to the number of moles of gases (n), the equation can be rearranged to:

$$\frac{G(P)}{n} = \frac{G(P^0)}{n} + RT \ln \frac{P}{P^0} \quad \text{Eq. 5.9}$$

The term (G/n) represents the Gibbs free energy per mole in a system comprising multi-components. This specific quantity is defined as the chemical potential and is mostly given the symbol (μ) in literature. The chemical potential is an expression which reflects the free energy change within the system per mole of any existing species [Perry 2008]. For a reactive system involving several components, the formula is simplified to:

$$\mu_i = \mu_i^0 + RT \ln \frac{P}{P^0} \quad \text{Eq. 5.10}$$

Once the gas involved is non-ideal, a new term (fugacity, f) substitutes the pressure in equation 5.10. This term can be considered as a pressure substitute for real gases at a certain temperature. The fugacity of a component (i) is a function of the molar concentration (y_i) and system pressure as written in equation 5.11. The term Φ_i is dimensionless and refers to the fugacity coefficient. Now, equation 5.10 would take the following form (Eq. 5.12):

$$f_i = \Phi_i y_i P \quad \text{Eq. 5.11}$$

$$\mu_i = \mu_i^0 + RT \ln \frac{f_i}{f_i^0} \quad \text{Eq. 5.12}$$

Where (μ_i^0) is the chemical potential of a given component at standard pressure. Now, for a system containing (N) number of species at a constant temperature and pressure, the expression of Gibbs free energy at equilibrium can be written as:

$$(dG)_{T,P} = \sum_{i=1}^N (\mu_i dn_i)_{T,P} = 0 \quad \text{Eq. 5.13}$$

Using an adequate equation of state such as that of Peng-Robinson, the fugacity coefficient can be determined. The Peng-Robinson equation of state (PR-EoS) relates temperature, pressure and molar volume (\tilde{V}) by putting them in terms of critical properties and an acentric factor (w) of the components found in this system. The general form of the PR-EoS is [Castello and Fiori 2011]:

$$P = \frac{RT}{\tilde{V}-b} - \frac{a\alpha}{\tilde{V}(\tilde{V}+b) + b(\tilde{V}-b)} \quad \text{Eq. 5.14}$$

The bulky parameters (a , b and α) are extensions of the following:

- $a = \frac{0.457 R^2 T_c^2}{P_c}$
- $b = \frac{0.078 R T_c}{P_c}$
- $\alpha = [1 + (0.3746 + 1.5422 w - 0.2699 w^2)(1 - \sqrt{\frac{T}{T_c}})]^2$

In the case when mixtures of different species are considered, the parameters a and b in equation 5.14 should be calculated with respect to the pure substances by the means of the *van der Waal* mixing rules as follows:

$$a_{mix} = \sum_i^N \sum_j^N y_i y_j \sqrt{a_i a_j} (1 - k_{ij}) \quad \text{Eq. 5.15}$$

$$b_{mix} = \sum_i^N \sum_j^N y_i y_j \frac{b_i + b_j}{2} \quad \text{Eq. 5.16}$$

The parameter k_{ij} is a binary interaction parameter that has a role in improving the phase equilibrium correlations of mixtures [Staudt and Soares 2012]. It can be predicted from the regression of equilibrium data, calculated using solver functions or by empirical correlations [Poling *et al.* 2007, Lwin 2000, Fateen *et al.* 2013]. These rules provide a good accuracy for equilibrium calculations of non-polar systems [Twu *et al.* 2002], which matches the nature of water under supercritical conditions. By applying the compressibility factor ($Z = P\tilde{V}/RT$) in equation 5.14, the following polynomial equation is obtained:

$$Z^3 - [1 - B] Z^2 + [A - 2B - 3B^2] Z - [AB - B^2 - B^3] = 0 \quad \text{Eq. 5.17}$$

where; $A = \frac{aP}{R^2 T^2}$, $B = \frac{bP}{RT}$

At this point and after determining the value of the compressibility factor, the fugacity coefficient and chemical potential can be obtained for each component in the mixture that corresponds to the equilibrium composition according to the following equation [Castello and Fiori 2011]:

$$\ln(\phi_i) = \frac{b}{b_{mix}}(Z - 1) - \ln(Z - B) - \frac{A}{2\sqrt{2}B} \left(\frac{2\sum_j y_j a_{i,j}}{a_{mix}} - \frac{b}{b_{mix}} \right) \ln \left(\frac{Z+(1+\sqrt{2})B}{Z+(1-\sqrt{2})B} \right) \quad \text{Eq. 5.18}$$

The entire calculations are conducted using an iterative technique in the model created by Aspen Plus. These calculations are based on the previous algorithm or sequence of equations, by achieving the conditions of the Gibbs free energy minimization. The molar concentration of each of the produced species is initially assumed and subsequently, the composition of the product mixture leading to the minimum value of Gibbs free energy is calculated.

5.5. Process Configuration

Two process schemes were suggested for the gasification of algal biomass in supercritical water. Adopted and modified from the experimental work, the schemes have taken into consideration two configurations. The first scheme is based on a 1-stream operation, where the entire feedstock is preheated and delivered to the reactor in a single stream. The second scheme has a 2-streams configuration. This is where the total input to the reaction system is divided into two fractions (pure water and algal slurry of higher-than-final concentration), preheated separately with the hot gaseous mixture before mixing and entering the reactor. The idea of demonstrating 1-stream and 2-streams schemes via Aspen simulation aims at investigating the heating mechanism and energy requirements for both cases.

In the 1-stream configuration (fig. 5.2a), the feed is brought to the operating pressure by pumping through (PUMP1). It is then preheated in the heat exchanger (HEX), where the thermal energy of the hot product stream is utilized. Further heating is required through (HEX-H), as a make-up for the heat losses occurring past the reaction zone, to bring the feedstock to the reaction temperature (FEED-RT). This is followed by supercritical water gasification, where the Gibbs reactor (SCWG) is used. The conversion of the decomposed or simulated feedstock results in a combustible gaseous mixture. Exiting the reactor, the hot product stream (PROD-H) is cooled down by heating the pressurized feedstock as pointed out earlier. Afterwards, it is directed to a high-pressure separation column (SEP), where the product gas is separated from the residual water. The pressure of the product gas can be

utilized through expansion (EXP) using a gas turbine and work can be generated. This may be considered as compensation for the energy consumed in pumping the feedstock.

The gaseous product is expanded to about 2-3 bar. Exploiting the product stream can be achieved thermally by burning. Hydrogen can be separated and used for other applications, but such a decision will depend in the first place on system performance and process economics. The major gas fraction (GF1) exits the process as the final product and part of it (GF2) is thermally utilized to preheat the feedstock using a gas burner (BURNER), where the hot exhaust gases is cooled down (HEX-C) against the preheated feed stream to make up for heat losses. The dotted line between HEX-C and HEX-H is hypothetical energy stream that reflects the duty required for the make-up heating.

In the two-streams configuration (figure 5.2 b), additional process equipment are involved as a result of splitting the total feed input. A stream of pure water is pressurized (PUMP2) along with the other stream containing the feedstock. The product mixture leaving the reactor at the operation temperature and pressure (PROD-HH) is split into two fractions (PROD-H1 and PROD-H2). Each fraction is used to preheat both feed and water streams. After preheating, the two streams (H2O-HOT and PROD-C) are combined and then heated further in HEX-H to the desired temperature before mixing and entering the reactor.

For both schemes considered in this study, the feedstock decomposition (FDE and FRS) proposed in section 5.2 is outlined in a separate block (DECOMP), to which the feed is pumped and heated to a temperature which matches that of the reactor. Since this step is hypothetical, the decomposed feedstock has to be cooled down back to ambient temperature before further processing. The decomposition block is omitted when the simulation is conducting using the two other feed types (ASI and ASII). The two reactor models, *R-Gibbs* and *R-Stoich*, were set for different simulation runs. The amount and composition of the product gas were calculated at different reactions temperatures (600, 650, 700 °C) and feed concentrations (2.5, 5, 10, 15, 20 wt%). With regards to the aqueous fraction of the process, the residual water (RES-HP) exits the process at the bottom of the phase separator and its pressure is relieved. Regardless of the salts extraction mechanism applied in the experimental work, no salts separation is taken into account in the calculations. As the gasification process was the major focus in this work, the units (treatment, algal cultivation) and aqueous streams with dashed lines at the bottom of each scheme were kept only for the sake of concept demonstration for coupling supercritical water gasification with the cultivation of microalgae.

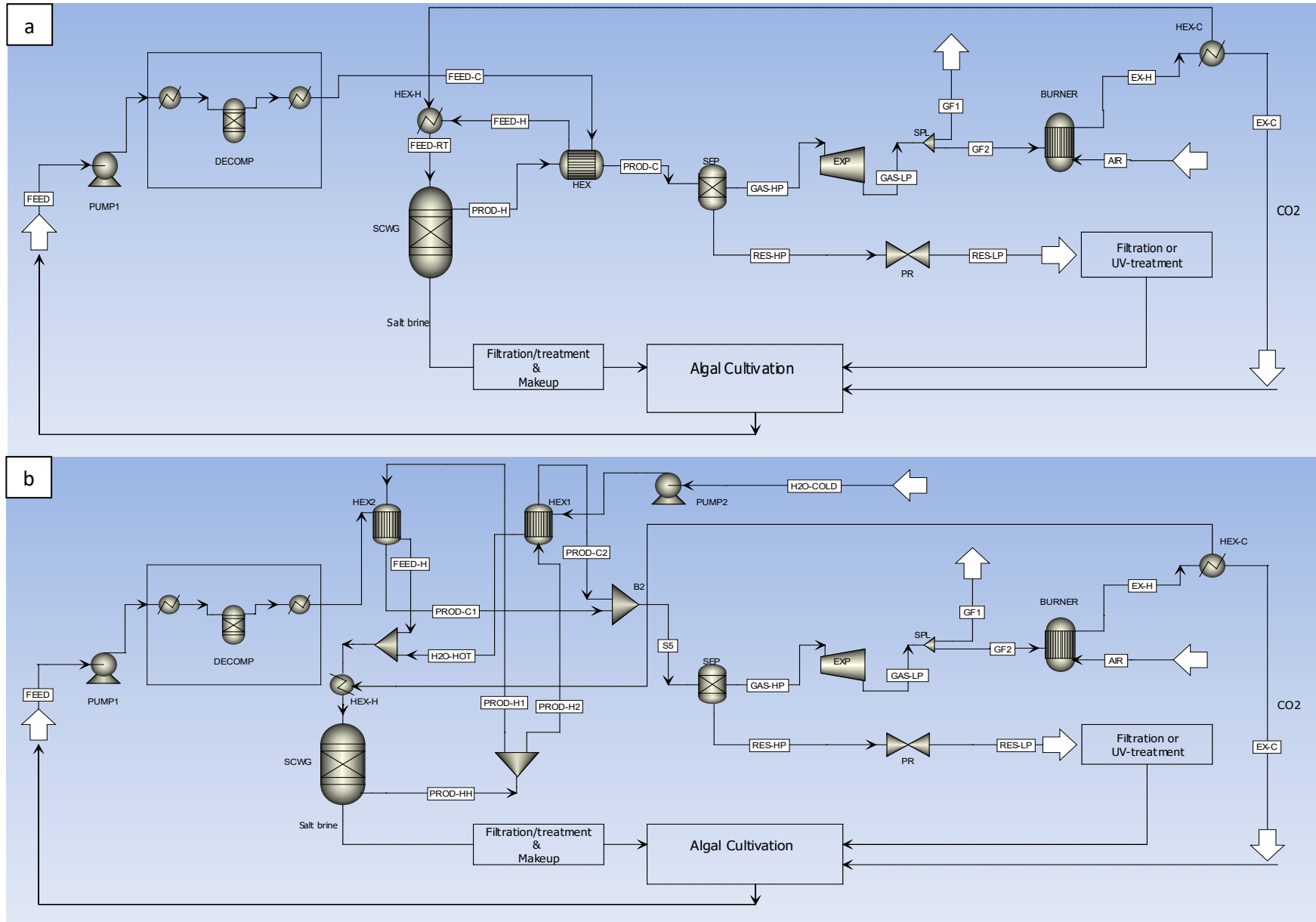


Figure 5.2 – Two suggested conceptual process schemes for the gasification of algal biomass in supercritical water

5.6. Results and Discussion (Process Simulation)

The created process models were run according to the different feedstock types presented earlier in this chapter. Two goals were set from conducting the simulation; the first goal was to investigate the influence of reaction temperature and biomass concentration on the gasification under supercritical conditions. The second goal was to evaluate the energy requirements of the different processes included in the proposed schemes.

A total flow rate of $100 \text{ kg}\cdot\text{h}^{-1}$ was set for the feed to and a sensitivity analysis was made by several combinations of temperature and biomass concentration. After quantifying the energy terms of the process, the thermal efficiency can be obtained under different operating conditions. This helps providing information regarding the potential of running an energy-neutral or auto-thermal process and provides a useful insight for designing such systems on larger scales.

From the four feedstock models proposed earlier in this chapter, two models (FDE and ASI) were selected as surrogates for the biomass in the process simulation. The selection was made based on the major constituents of the product gas (H_2 , CO_2 , and CH_4) and their molecular composition (fig. 5.3) from different simulation runs. The results were then compared to some of the experimental results at the same operating conditions, a reaction temperature of $650 \text{ }^\circ\text{C}$, an operating pressure of 280 bar and a biomass concentration of 10 wt%. Similar trends using the four models was observed under the same operating pressure, at biomass concentrations of 5 and 20 wt% at reaction temperatures of 650 and $690 \text{ }^\circ\text{C}$ respectively.

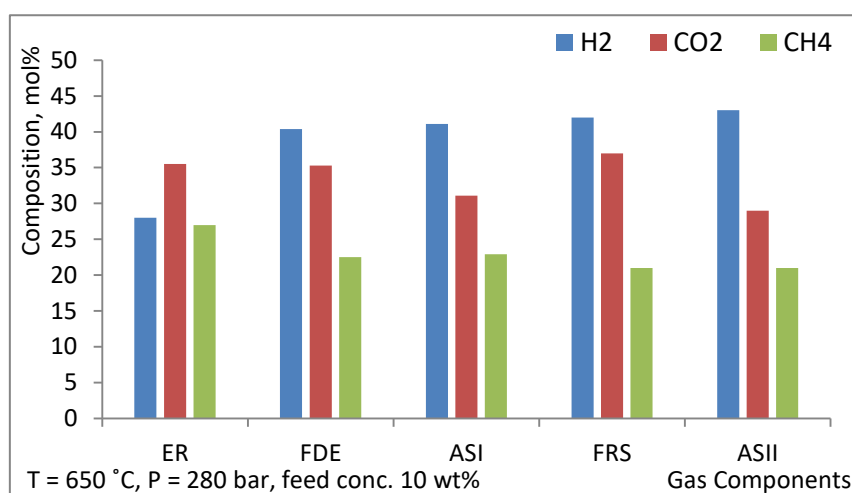


Figure 5.3 – Gas composition from supercritical water gasification of four simulated feedstock models compared to experimental results [ER: Experimental results, FDE: Feed decomposition to basic elements, FRS: Feed reforming to syngas, ASI&II: Algal Simulant]

According to the results from the models based on FDE and ASI, the gaseous mixture was found to have concentrations of hydrogen, methane and carbon dioxide which are relatively closer to those from the experiments than in the case of FRS and ASII. The difference, however, was that the simulation results showed for all models higher concentrations of hydrogen accompanied by lower methane levels, especially using low concentration of simulated feedstock (5 wt%). Nevertheless, the process simulation was still able to depict the influence of changing process variables on the gas composition as discussed in the following sections of this chapter.

5.6.1. Influence of reaction temperature

Running the process models at different temperatures provided a clear demonstration (fig. 5.4) of the influence this major variable has on the composition of the produced gaseous mixture. A wide range of temperatures (450, 550, 650 and 750 °C) compared to the experimental work was applied with a feed concentration of (10 wt%) and an operating pressure (28 MPa). The results generally show rising levels of hydrogen and a continuing decrease of methane upon elevating the reaction temperature.

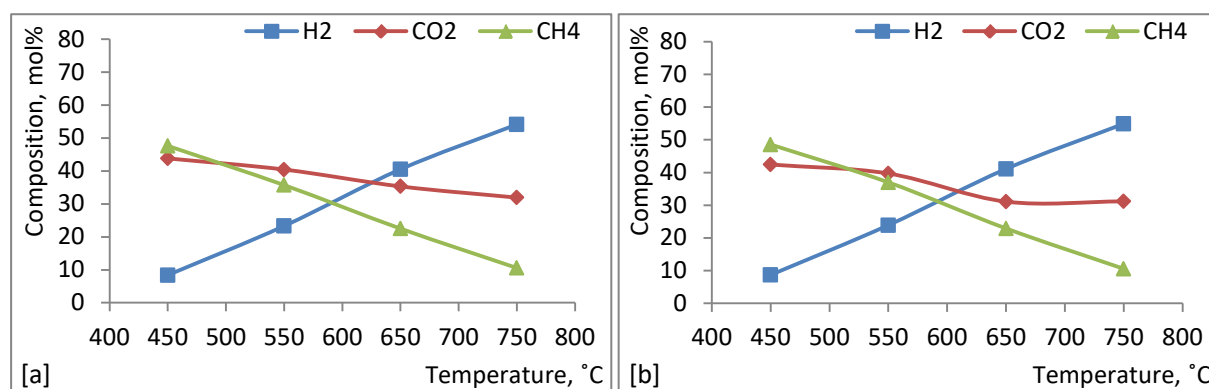


Figure 5.4 – Influence of reaction temperature on the composition of the major components in the produced gas for the two models based on FDE and ASI

Conditions: P = 280 bar, feed conc. 10 wt% [a] FDE model and [b] ASI model

According simulation, hydrogen increased by over 6 folds between 450 and 750 °C, accounting for about 55 mol% of the gas volume at the highest temperature. In a simultaneous response, the composition of methane dropped to its lowest level (~ 10 mol%), about one-fifth of its value at 450 °C. Carbon dioxide was found to have a higher stability over this temperature range. There was a slight decrease in the composition of carbon dioxide, but the change did not have a sharp course such as that of H₂ and CH₄, keeping its levels in the range of 32 to 43 mol% for both feed types at 750 and 450 °C respectively.

In addition to the major gas components, minor concentrations of carbon monoxide as well as traces of ethane, propane and propylene were calculated in the gaseous mixture from the simulated models. This does not come in accordance with the experimental results, where the levels of carbon monoxide were 0.3 mol% at maximum at the highest temperature applied (690 °C), and the measured ethane levels of about 9 mol% in a temperature range of 620 – 690 °C.

The increasing trend of hydrogen and decreasing trend of methane were previously concluded from the experimental results at the same feed concentration. Increasing the reaction temperature would probably favor some reactions over others according to thermodynamics. An explanation might be that at higher temperature, the methanation reactions which consume H₂ are slowed down due to the exothermic nature of these reactions. As a result, additional H₂ remains as a surplus in the gaseous mixture, raising its total levels in at such an elevated temperature. The concentration of CO would increase then as a result of its slowed-down methanation at higher temperature, which was better depicted through process simulation. However, the decreasing levels of CO₂ at elevated temperatures were not in compliance with the experimental work, where CO₂ were found to be increasing over the temperature range tested. One possibility for such a difference might be based on the fact that the equilibrium calculations would translate to more consumption of CO₂ during methanation. That might provide an explanation to the rise in the levels of CO (0.1 to 3 mol%) between 450 and 750 °C instead.

Generally, comparing the results obtained from process simulation with the relevant values obtained from the experimental work is a useful approach, as the influence of temperature on the trends of the major gas components was supported by process simulation. The fact that the values which were obtained during the experiments and those from simulation are not identical can be related to the different basis for calculations as well as the assumptions considered in the simulated models. The two models, based on FDE and ASI, have both demonstrated very little differences regarding the compositions of the three gas components in the temperature range applied. Nevertheless, the decision to use both models for the sake of demonstration continues in this chapter as a mean of double-checking or verifying the results.

5.6.2. Influence of feedstock concentration

As pointed out in chapter 4, the reaction temperature and feedstock concentration are the two major process variables which have the dominant influence on the gasification in supercritical water. Therefore, the simulation was run using a broad range of concentrations (2.5 – 20 wt%) at a reaction temperature of 690 °C and pressure of 280 bar. The molecular composition of hydrogen, methane and carbon dioxide was calculated and the results are shown in figure 5.5. The experimental results (ER) under similar operating conditions are plotted along with the results obtained from Aspen modeling and distinguished with dashed lines.

Both models (FDE and ASI) showed to very comparable results using the five concentrations, whereas the ASI-based simulation demonstrated a slightly lower H₂, higher CH₄ and CO₂ concentrations. Additionally, a bit more time was generally needed for the FDE models to achieve convergence due to the extra steps associated with feed decomposition. In a similar trend such as that of the experimental results, the concentration of H₂ in the product gas decreased by increasing feedstock concentration. The molar concentration of H₂ lost about 50% of its value referred to the most diluted feedstock (2.5 wt%), when the concentration was increased to the highest value.

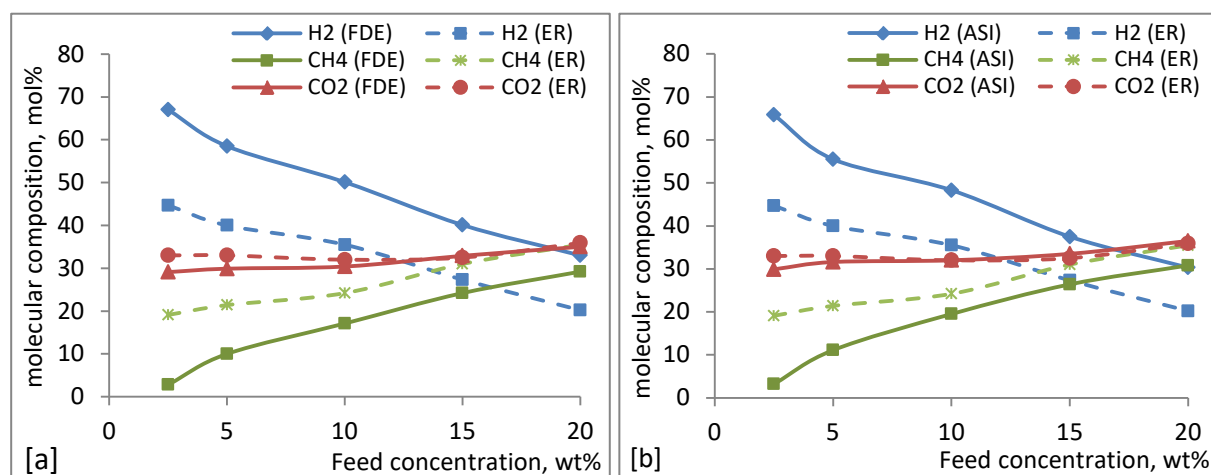


Figure 5.5 – Influence of feed concentration on the composition of the major components in the product gas, compared to experimental results (ER), for the two models based on FDE and ASI

Conditions: P = 280 bar, T = 690 °C [a] FDE model and [b] ASI model

A factor contributing to that is also the significant rise in the concentration of CH₄, which increased by almost 10 folds using the feedstock stream with the highest concentration. The molar composition of CO₂ was relatively stable over the range of feed concentrations simulated, staying in the range of approximately 30 – 35 mol% in the five cases for both feed models.

The simulated models continued to show clearly higher levels of hydrogen in the gas mixture compared to the experimental results, especially at the lower feedstock concentrations. There was an offset of approximately 15 to 20 % at the lower three concentrations used. The difference decreased to about 10–12% at the feed concentrations of 15 and 20 wt%. Such an observation may indicate that the equilibrium composition associated with the simulated models may have demonstrated a higher contribution of water to the overall hydrogen production under these conditions. This increase in the levels of hydrogen was reflected at the composition of methane in the gas mixture, obtaining over six times lower methane than what the experimental results showed for the lowest feed concentration. However, the offset was continuously decreasing until there results of the simulated models and the experimental results were quite comparable at the concentrations of 15 and 20 wt%. The composition of carbon dioxide in the gas mixture was the most component which was predicted by the Aspen models compared to the experimental results for all concentrations.

Additionally, the composition of the product gas mixture included minor amounts of carbon monoxide; with an increase from 0.8 to about 2.3 mol% between the lowest and highest feed concentrations respectively. The experimental results have only showed a slight rise in the molar composition, from 0.2 to 0.4 mol%, between 2.5 and 20 wt% respectively. Similar to what was indicated for the influence of reaction temperature, the models were not able to provide an adequate representation of ethane in the gas mixture compared to the experimental results, in which its molar composition was in the range 3 and 7.8 mol%. The models depicted an increase by 5 – 6 folds when raising the feed concentration from 2.5 to 25 wt%. Nevertheless, and despite being represented in trace concentrations (≤ 0.002 mol%) from simulation, the overall decrease supports the data obtained from the experimental results.

5.6.3. Gasification Quotient

This term (abbreviated as GQ) is a synonym for the gasification efficiency (GE) in a fractional form. It defines the total amount of gaseous products divided by the amount of feed input in a certain time period under a given process condition. The gasification quotient was introduced here to give another indication of the process performance other than carbon gasification efficiency or the removal efficiency of the total organic carbon. The value of GQ would typically exceed unity at conditions including combinations of high conversion efficiency, high temperature or diluted feed streams.

Figure 5.6 illustrates the change of GQ at different reaction temperatures and feed concentrations for the models based on FDE and ASI as well as the experimental results (ER). The term GQ would give an indication of water contribution to the overall gas production. As demonstrated in the figure, the GQ reaches maximum values at the highest reaction temperatures (690 °C for ER, 750 °C for FDE and ASI). Likewise, the highest values of GQ were observed clearly with the two lowest feed concentrations of those investigated.

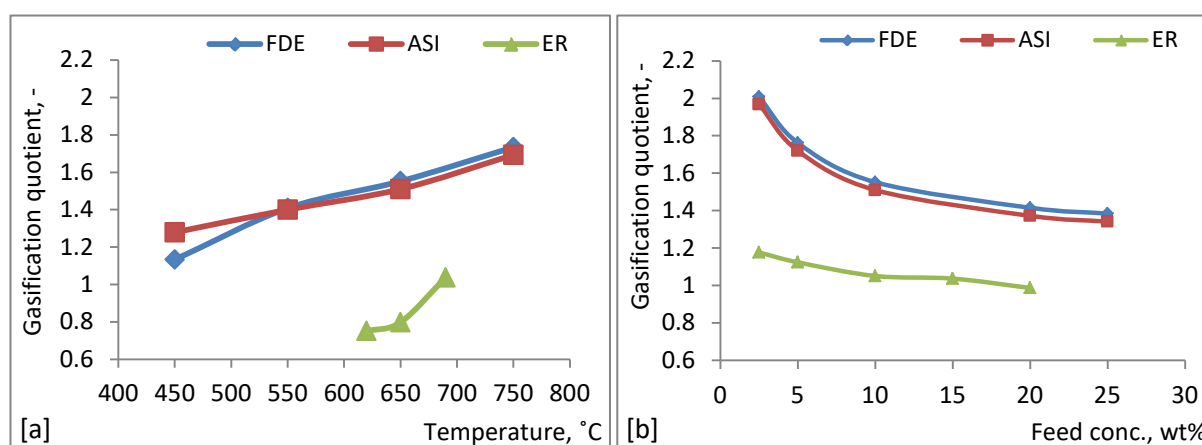


Figure 5.6 – Variation of gasification quotient versus temperature and feed concentration

Conditions: [a] Feed conc. 5 wt%, P = 280 bar, [b] T = 690 °C, P = 280 bar

The offset between the experimental results and those from the simulated models can be explained by a number of factors. The first factor is the already overestimated values of hydrogen in the gas product from simulation as previously mentioned. The second factor would definitely be the complete carbon conversion (CGE) that was assumed in process simulation, which would partly increase the gap between the simulated models and experimental results. The third factor is the percentage of inorganic elements existing in the algal biomass (ash) that consequently results in a lower gas yield compared to model compounds. In addition to these factors, the reaction kinetics, especially at higher feed concentrations, would have a role in creating the difference between the experimental and model-based results. As pointed out earlier, the thermodynamic equilibrium was the basis for model calculation. In other words, the simulated models only consider the changes to the Gibbs free energy of the system and its components. Reaction kinetics will logically undergo changes depending on the temperature and feed concentration, but the models were simplified and no input data were given for reaction kinetics, assuming it to be not limiting under these conditions.

5.6.4. Energy Assessment

The results obtained from the simulated models include an energy analysis during the process. These data (e.g. equipment duties, heat recovery) may provide an appreciable start basis for designing such systems especially at a large scale. The calculations presented in this section assumed a system with an operating capacity of $100 \text{ kg}\cdot\text{h}^{-1}$ total feed input. The concentrations of the feed stream was varied between 2.5 and 25 wt% and the reaction temperature was set to different values between 450 and 750 °C. Operating pressure was maintained constant at 280 bar.

Several runs were conducted using the two feed types selected, at a feed concentration of 10 wt%, a reaction temperature of 650 °C and pressure of 280 bar. Basically, the power sums which are included in the process are represented in figure 5.7. These terms are: 1) the enthalpy associated with gasification in supercritical water (D_{SCWG}); 2) the heat circulated within the system based on the thermal recovery of the hot product stream ($D_{\text{Heat Recovery}}$); 3) the duty required to preheat the feed stream further to the desired reactor temperature ($D_{\text{Additional heating}}$); 4) the power required for pumping (P_{Pumping}) and 5) the power which can be generated by expanding the pressurized gaseous product ($P_{\text{Gas expansion}}$).

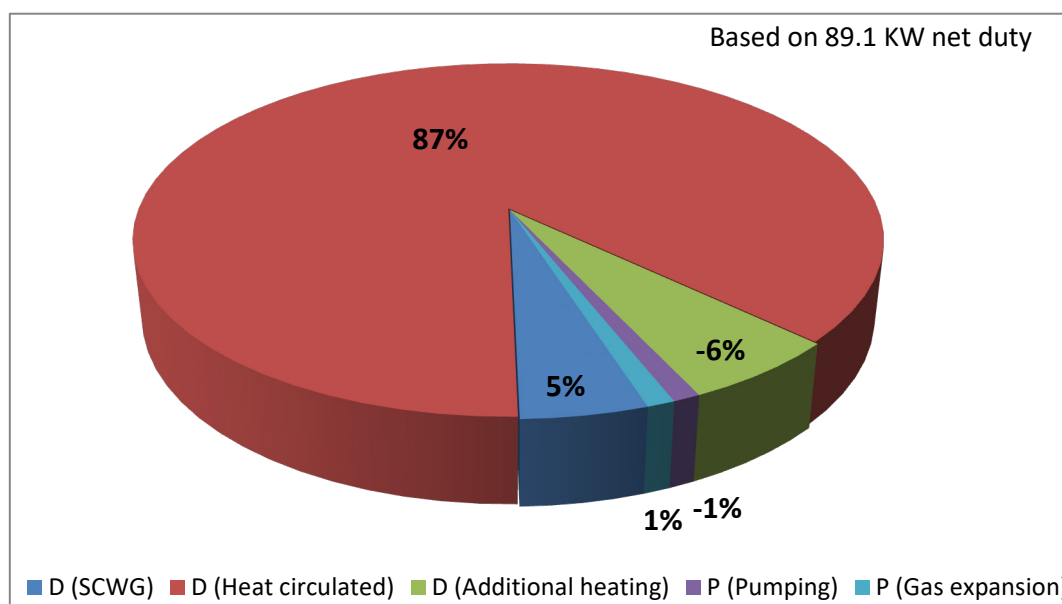


Figure 5.7 – Example of the duty shares (power) of supercritical water gasification (ASI model) [-ve for energy required] - Conditions: Flowrate $100 \text{ kg}\cdot\text{h}^{-1}$, Feed conc. = 10 wt%, $T = 650 \text{ }^\circ\text{C}$, $P = 280 \text{ bar}$

The simulation showed comparable results based on the 1-stream and 2-streams configurations implemented, in terms of the energy content of the product gas. According to the simulation, a slight decrease of the recovered heat for the 2-streams configuration resulted

in an additional energy for further preheating to the desired temperature at the reactor's inlet. Corresponding to operation, the 2-streams configuration would typically involve more piping and would have a decreased thermal efficiency due to increased heat losses compared to 1-stream-based operation. Still, the simulated models could not provide a clear influence upon introducing the 1- and 2-streams system on the gasification efficiency in terms of gas quantity or composition. From an energy-related point of view, adding more equipment (ex.: pump or a heat exchanger) to a process of the same capacity, given the energy consumption or efficiency of these equipment, would consequently result in an increased power demand. For this reason, the 1-stream configuration was selected to run the different models. This configuration would be also recommended for designing these systems unless significant benefits of the 2-streams configuration are proved. The results of the basic energy terms for the different process units included in the system are listed in tables 5.2 and 5.3.

The energy needed to decompose and gasify the feed under supercritical conditions varied depending on the feed model applied in the calculations. The term (DSCWG) represents the duty of the Gibbs reactor under supercritical conditions. Both feed models showed different results concerning the total energy related to gasification. The feed type FDE resulted in higher exothermic conditions than ASI. This is due to the hypothetical step of feed decomposition which was implemented in the FDE model, and which resulted in a major difference in the input streams to the reactor compared to the ASI models.

By increasing the temperature from 450 to 750 °C, a decrease in the energy release from the reactions by 6 and 8 KW was observed for ASI and FDE feed types respectively. As a result, more energy was required to maintain the reaction system at the elevated temperatures. This was reflected through the higher demand (duties) for preheating and the increased share of additional energy for further heating to reactor temperature. The increase of temperature in this range resulted in higher yield of the total gases. The theoretical power which can be obtained from the expansion of produced gas increased by 3 folds compared to the value at 450 °C.

In the case of changing feed concentration (table 5.3), the results showed that higher feed concentrations led to higher release of reaction enthalpy and lower duty for the overall preheating of the feed. However, additional heating was still required to reach the reactor temperature in this case (650 °C). Yet, the availability and amount of the product gas at higher concentrations would lead to an improved thermal efficiency for the process as a whole.

Table 5.2 - Energy requirements at different temperatures for the two feed types [Throughput 100 kg.h⁻¹ Feed, feed conc. = 10 wt%, P = 280 bar]*

Temperature, °C	450		550		650		750	
Power/Duty Equivalent (kW)	FDE	ASI	FDE	ASI	FDE	ASI	FDE	ASI
Duty equivalent of the feed stream (EF)	64.72	67.22	64.72	67.22	64.72	67.22	64.72	67.22
Reaction in supercritical water (DSCWG)	14.22	6.53	12.60	6.36	10.00	4.14	6.42	0.70
Duty of the major heat exchanger used for preheating (DH _x)	70.48	68.57	79.42	79.82	86.83	87.26	93.72	94.17
Duty related to additional heating (D _{Additional heating})	-6.35	-3.70	-6.50	-4.30	-7.12	-5.30	-7.90	-6.24
Duty equivalent of the gas product (D _{biofuel})	57.25	57.50	58.81	59.10	61.86	62.10	65.42	66.10
Power required for pumping (P _{Pumping})	-0.91	-0.90	-0.91	-0.90	-0.91	-0.90	-0.91	-0.90
Power equivalent of gas expansion (P _{Gas expansion})	0.43	0.43	0.57	0.57	0.93	0.95	1.35	1.35
Fraction of the gas product needed for additional heating (wt%)	11.10	6.80	11.20	7.25	11.50	8.50	12.10	9.51

Table 5.3 – Energy requirements at different feed concentrations for the two feed types [Throughput 100 kg.h⁻¹ Feed input, T = 650 °C, P = 280 bar]*

Feed concentration (wt%)	2.5		5		10		20		25	
Power/Duty Equivalent (kW)	FDE	ASI	FDE	ASI	FDE	ASI	FDE	ASI	FDE	ASI
Duty equivalent of the feed stream (EF)	16.18	16.81	32.36	33.61	64.72	67.22	129.44	134.44	161.8	168.06
Reaction in supercritical water (DSCWG)	0.55	-0.94	3.20	0.236	10	4.1	24.6	13.1	32.0	17.7
Duty of the major heat exchanger used for preheating (DH _x)	92.49	93.14	90.83	91.1	86.83	87.3	79	79.5	75.1	76
Duty related to additional heating (D _{Additional heating})	-4.88	-4.32	-5.72	-4.72	-7.115	-5.3	-9.60	-6.31	-10.76	-6.81
Duty equivalent of the gas product (D _{biofuel})	17.56	17.48	33.1	32.8	61.86	62.1	118.9	118.4	148.1	145.8
Power required for pumping (P _{Pumping})	-0.91	-0.90	-0.91	-0.90	-0.91	-0.90	-0.91	-0.90	-0.91	-0.90
Power equivalent of gas expansion (P _{Gas expansion})	0.45	0.45	0.67	0.67	0.93	0.95	1.24	1.25	1.36	1.37
Fraction of the gas product needed for additional heating (wt%)	28	25	17.5	14.3	11.5	8.5	8	5.4	7.2	4.7

* Negative sign refers to energy requirements or energy input

The heat recovery of the product stream is very crucial in such high temperature process, as it represents the highest share of energy which maintains the process performance stable. Theoretically, it is introduced in the process once and is then circulated during operation. Hence, this term does not contribute to the total energy output of the system. The absolute amount of heat recovery typically increases upon raising the reaction temperature. On the contrary, the decrease of heat requirements at higher concentrations is due to the increase of feed amount that is converted to a gas mixture given an exothermic condition. The additional energy required to further heating arises from the heat transfer efficiency, which was assumed to be around 87–90 % based on the calculations included in the models. This term is provided through burning part of the product gas mixture and recovering its heat. This fraction is illustrated along with the power equivalent calculations in both tables of the previous page.

The term related to gas expansion shows that the phase change associated with supercritical water gasification can result in a positive power in case a gas turbine is used for electricity generation. The results show that as of 10 wt% feed concentration, the gas expansion can contribute with an equivalent power to that required for feed pumping. Above this concentration and with a temperature as high as 650 °C, the energy resulted from expansion can theoretically exceed that which is used for pumping. In practice, these values would differ due to the losses or conversion efficiencies that lead to an increased power consumption for pumping and also a decreased power produced from expansion. Another phenomenon occurs upon expansion is the major temperature drop of the gas mixture after throttling. In the simulated models, the temperature dropped down to low values (-40 / -60 °C) at the turbine exit. Such a low temperature might be utilized, for example, to cool down some equipment during operation. One drawback is the fact that moist gas streams would lead to ice formation on the blades of the turbine causing damage of the equipment. In all cases, the contribution of these steps (fig. 5.8) to the overall efficiency is minor as illustrated earlier and much attention should be given to the management of thermal energy within the process.

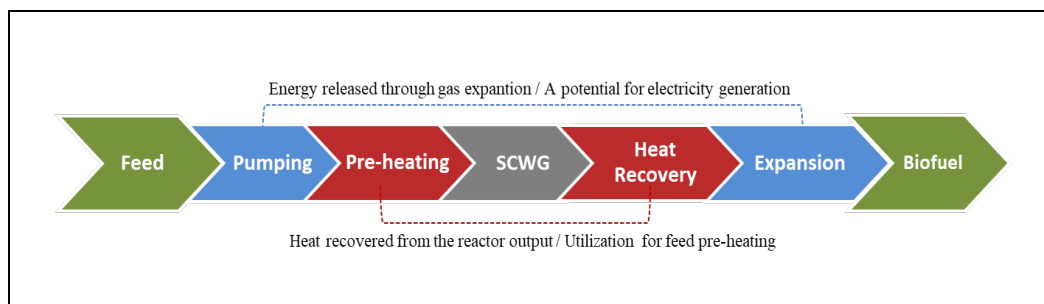


Figure 5.8 – Overall process steps for the gasification of biomass in supercritical water

5.6.5. Overall process efficiency

The formula presented in equation 5.19 was used to calculate the overall efficiency of the simulated system. The formula took into consideration the total energy required for or released through supercritical water gasification, the energy required for additional heating, the energetic content of the combustible gas mixture (i.e. biofuel), the energy required for pumping and the potential energy which would be available through the expansion of the high-pressure gas.

$$\eta = \frac{\pm E_{SCWG} - E_{additional\ heating} + E_{Biofuel} - E_{Pumping} + E_{Exp.}}{E_{feed}} \quad \text{Eq. 5.19}$$

The calculations explained earlier in this chapter were based on the R-Gibbs reactor model for the core process of gasification. This have demonstrated the dependence of gas composition on temperature and feed concentration and enabled to compare the influence of these two variables with the results obtained from the experiments. However, the simulated models were based on a complete carbon conversion in the feed stream to a gaseous mixture. That is why an overestimation of the gas amount (seen from GQ in section 5.6.3) was present. This has in turn an influence on the energy terms in the process and would lead to exaggerated values from simulation. For that reason, the reactor model R-Gibbs was replaced by the model (*R-Stoich*) in this section and several runs were made under different process conditions.

A series of basic reactions were set up according to table 5.4. In the *R-Stoich* reactor model, more information has to be defined before solving. This includes temperature, pressure, number of reactions with their corresponding stoichiometric coefficients and molar conversion. The molar conversion of each reaction was adjusted, so that a similar gas composition is achieved (e.g. H₂: 35.5 mol%, CH₄: 24.2 mol%, CO₂: 32 mol%, C₂H₆: 7.9 mol%, CO: 0.3 mol%) compared to that of an experiment conducted at the same operating conditions (P = 280 bar, feed conc. = 10 wt%, T = 650 °C, P = 280 bar).

A feed conversion of 90% was assumed, allowing the rest of algal simulant (ASI) to exit the process in the residual water. The results, indicating the different energy terms discussed earlier and represented in the overall process efficiency, were then compared to those obtained using the R-Gibbs model using the two feed types.

Table 5.4 – Suggested reaction scheme with the corresponding molar conversion for ASI model

Reactions	Equation	Mol. conversion
$[(X_1) C_4 H_9 O_2 N + (X_2) C_5 H_6 O_2] + (X_3) H_2O \rightarrow (X_4) CO + (X_5) H_2 + (X_6) NH_3 + (X_7) H_2O$	Eq. 5.20	0.9
$(A) CO + (B) H_2O \rightarrow (C) CO_2 + (D) H_2 + (E) H_2O$	Eq. 5.21	0.81
$(L) CO_2 + (M) H_2 \rightarrow (N) CH_4 + (O) H_2O$	Eq. 5.22	0.39
$(P) CO + (Q) H_2 \rightarrow (R) CH_4 + (S)H_2O$	Eq. 5.23	0.95
$(T) CH_4 \rightarrow (U) C_2H_6 + (V) H_2$	Eq. 5.24	0.39

Figure shows the course which the overall efficiency takes upon changing feed concentration (figure 5.9a) and reaction temperature (figure 5.9b). The results indicate a stronger influence of feed concentration on the overall efficiency. A maximum efficiency of 93.5 % for the feed type ASI and 82.4 % for FDE was relatively stable in the concentrations starting 10 wt%. The model (*R-Stoich.*) showed a quite similar trend to the feed type FDE.

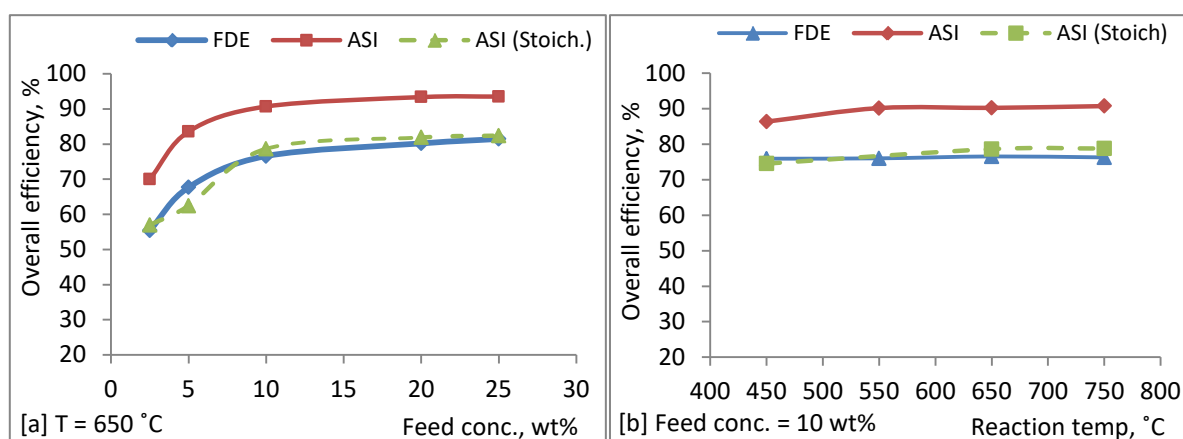


Figure 5.9 – Overall process efficiency at different feed concentrations [a] and temperatures [b] of the *R-Gibbs* models (for FDE and ASI) compared to the *R-Stoich.* model using ASI

A feed concentration between 10 and 20 wt% seems to be the optimum for operation when these values are considered. Above this concentration, handling the feedstock in terms of mixing and pumping would lead to difficulties that would affect operation. Given the several assumption made at the beginning to simplify the calculations, the actual efficiencies will be tend to be lower than those calculated. Therefore, operating at diluted feed stream would not allow a sustainable operation and lead to low overall process efficiency.

References (Chapter 5)

1. Brown, T.M., Duan, P., Savage, P.E. 2010. Hydrothermal Liquefaction and Gasification of *Nannochloropsis* sp. *Energy & Fuels*, **24**(6), 3639-3646.
2. Castello, D., Fiori, L. 2011. Supercritical water gasification of biomass: Thermodynamic constraints. *Bioresource technology*, **102**(16), 7574-82.
3. Fateen, S.-E.K., Khalil, M.M., Elnabawy, A.O. 2013. Semi-empirical correlation for binary interaction parameters of the Peng–Robinson equation of state with the van der Waals mixing rules for the prediction of high-pressure vapor–liquid equilibrium. *Journal of Advanced Research*, **4**(2), 137-145.
4. Kruse, A., Gawlik, A. 2003. Biomass conversion in water at 330-410 °C and 30-50 MPa. Identification of key compounds for indicating different chemical reaction pathways. *Industrial and Engineering Chemistry Research*, **42**(2), 267-279.
5. S. Letellier, F. Marias, P. Cezac, J. Serin. 2010. Gasification of aqueous biomass in supercritical water: a thermodynamic equilibrium analysis, *The Journal of Supercritical Fluids*, **51**, 353–361.
6. Lwin Y. 2000 Chemical Equilibrium by Gibbs Energy Minimization on Spreadsheets, Int. J. Engng Ed., **16**(4), 335-339.
7. Nobel, Park S. 2005. Appendix IV - Gibbs Free Energy and Chemical Potential. In: *Physicochemical and Environmental Plant Physiology* (3rd Edition), Academic Press. Burlington, pp. 545-553.
8. Patzelt, D.J., Hindersin, S., Elsayed, S., Boukis, N., Kerner, M., Hanelt, D. 2014. Hydrothermal gasification of *Acutodesmus obliquus* for renewable energy production and nutrient recycling of microalgal mass cultures. *Journal of Applied Phycology*, **27**(6), 2239-2250.
9. Perry, R.H. 2008. Ch. 4: Thermodynamics. In: *Perry's Chemical Engineers' Handbook*, (8th Edition), McGraw-Hill, New York.
10. Poling, B.E., Prausnitz, J.M., O'Connell, J.P. 2007. *The properties of gases and liquids* (5th Edition), McGraw-Hill, Singapore.
11. Staudt, P.B., Soares, R.d.P. 2012. A self-consistent Gibbs excess mixing rule for cubic equations of state. *Fluid Phase Equilibria*, **334**, 76-88.
12. Tang, H., Kitagawa, K. 2005. Supercritical water gasification of biomass: thermodynamic analysis with direct Gibbs free energy minimization, *Chemical Engineering Journal* **106**, 261–267.

6. Conclusions and prospects for future works

The results demonstrated in chapter two and the experimental results of this work give an indication that the efficiency of the systems implementing hydrothermal conversion depends to a major extent on the configuration, capacity and mode of operation. A large spectrum of results was obtained according to the objective of each study, nature of the feedstock (moisture content, physical and chemical properties) and the different operating conditions.

From this study, the results show that the gasification of algal biomass in supercritical water can be conducted with high efficiency on continuous operation. This experimental work demonstrated that the efficiency of supercritical water gasification (SCWG) is directly influenced by the major process variables, specifically the temperature and biomass concentration of the feedstock. The highest carbon gasification efficiency (CGE) or the highest specific gas yield was achieved at the highest temperature applied (690 °C).

Similar finding related to the solid content in the feedstock was concluded using the most diluted biomass of all concentrations tested. The contribution of water to the overall gas production was significant at low feed concentrations, which confirms the reactive role of water under supercritical conditions and the benefit of the high moisture content for an improved gasification efficiency with respect to carbon conversion. The quantity and composition of the produced gas can be controlled through the process variables, which allows adjustable conditions based on the desired component in the gas product.

Regarding the process configuration (1-stream and 2-streams), a less complex system with lower power consumption promotes the 1-stream process. Despite the reported improvement of the 2-streams configuration with regards to the fast heating rate and the prevention of char formation, the performance of the 1-stream configuration can be optimized by adjusting some variables such as residence time and flow dynamics in order to achieve a high conversion.

As a valuable byproduct, utilizing the residual water from SCWG for cultivation helps in recycling natural resources. This provides an important step forward considering the eco-balance and the economics of cultivation. Treating the residual water was deemed necessary to remove some substances which have a growth-inhibiting effect during cultivation. Unlike activated carbon filtration, the UV-treatment reduced the amount of total nitrogen in the aqueous phase and could not remove the phenolic compounds entirely. Yet, the two methods were able to remove the majority of the growth-inhibiting substances from the residual water.

Solid precipitations, especially those of Phosphorus salts, can be minimized by further optimization of system design and the fine-tuning of process conditions. This would be achieved in a way that increases the solubility of these solids in the aqueous phase, or enables an efficient extraction mechanism before or after gasification without disturbing operation. Eventually, this will reduce the risk of plugging, lead to longer operation and directly translate to a stable system performance. It would also increase the availability of these inorganic constituents as a target for the coupled systems.

Process simulation is a very useful and handy tool to optimize system variables and produce a wide range of information for the gasification process. Even though the calculations made using *Aspen Plus* were mainly based on thermodynamic equilibrium and no kinetic expressions were implemented in the models, similar trends were obtained compared to the experimental results. This contributes to a major cut-off in time and efforts associated with conducting experiments, especially on a large scale of operation.

Despite the lack of non-conventional compounds (biomass) in the input databank of *Aspen Plus*, several methods, some of which were presented in this work, can be adopted to provide an acceptable description of the feedstock as a first step before the simulation runs. The simulated models could give useful information regarding the influence of temperature and feed concentrations on the composition of the gaseous products. Another benefit was the obtained results of the major energy sources and sinks in SCWG, giving a possible start basis for the design of these systems especially if process scale-up is considered. Compared to the experimental work, some deviations in the simulation results were noticed. Such a remark was expected and can be explained by the assumptions made in process simulation and the gasification efficiency in the real systems. Also, the heat losses in the high-temperature zones were not represented in the models and therefore, these factors should be taken into account before considering any projection that is based on the simulation results.

From an energy-efficiency perspective, the gasification of biomass in supercritical water should be preferably conducted at the highest possible feed concentration and the lowest possible supercritical temperature. Practically, there may be a limit regarding the biomass concentration depending on the nature of the feedstock. For example, the processing a feedstock by the means of mixing and pumping can be challenging using a 20 wt% feed concentration (i.e. 80% moisture content). This is particularly the concern, given the high pressure of supercritical systems and the need of a reliable pumping on continuous operation.

Hence, biomass concentrations above this value would not be recommended. In addition, a feedstock with high content of organic matter and less ash would be preferred. Despite the reported improvement of CGE at higher temperatures, a temperature limit should be set depending on the optimized gasification through adjusting other process variables. The experimental work in this study concludes that temperatures below 650 °C are not sufficient for an efficient SCWG on continuous operation. This value may also differ depending on the system configuration, feedstock nature and throughput applied.

As for the prospects of future works, scaling up coupled systems such as the one discussed in this work will be challenging considering the costs associated with algal cultivation. Process economics which include fixed costs (e.g. fabrication of photobioreactor panels) and operating costs (e.g. culture harvesting and aeration) would remain a hurdle even at larger scales, especially if the produced biomass is only used for gasification. This is also the case for process economics, given the variation of biomass productivities in outdoor cultivation. Algal biomass can be rather used for the extraction of high-value molecules (e.g. omega-3, β -carotene) which are sold commercially. The spent culture (algal residues) can be utilized, along with other organic waste streams, for hydrothermal conversion.

Supercritical water gasification is a flexible process in terms of the feedstock type. In other words, the process can be used to convert a wide range of biomass materials with high moisture content. Therefore, the tendency to apply the already-available materials, such as waste streams including sewage sludge or agricultural crop residue, would allow better process economics by omitting the production costs of a feedstock such as microalgae. By exploiting these organic wastes, SCWG can be economically feasible at larger scales (e.g. total throughput $\geq 500 - 1000 \text{ kg.h}^{-1}$). Coupling algal cultivation and SCWG would still be achievable. This can be realized if the algal biomass is simply replaced by a waste stream as the feedstock for gasification. All other by-products from the SCWG of wastes (CO_2 , nutrients from wastes) can then be recovered and directed to cultivation. By designing such a system, the cultivation of microalgae can benefit from the wastes that are converted via SCWG to a combustible mixture. At the same time, treatment of the waste streams can be simultaneously achieved.

7. List of scientific contributions

- Elsayed, S., Boukis, N., Sauer, J. 2014. Hydrothermal gasification of microalgae - prospects and challenges. *DGMK Tagungsbericht*, 221-228.
- Elsayed, S., Boukis, N., Kerner, M., Hindersin, S., Patzelt, D. 2014. Gasification of Microalgae in Supercritical Water: Experimental Results from the Gasification of the Algal Species *Scenedesmus Obliquus* Cultivated in the BIQ-House in Hamburg. In: 22nd European Biomass Conference and Exhibition, 23-26 June, 573 - 578. Hamburg, Germany
- Patzelt, D.J., Hindersin, S., Elsayed, S., Boukis, N., Kerner, M., Hanelt, D. 2014. Hydrothermal gasification of *Acutodesmus obliquus* for renewable energy production and nutrient recycling of microalgal mass cultures. *Journal of Applied Phycology*, 27(6), 2239-2250.
- Elsayed, S., Boukis, N., Sauer, J., Patzelt, D., Kerner, M., Hindersin, S. 2015. Algal Cultivation and Hydrothermal Gasification: Biomass and Energy Production, *Energiewirtschaftlichen Tagesfragen*, 65 (Heft 1-2), 104-106.
- Patzelt, D.J., Hindersin, S., Elsayed, S., Boukis, N., Kerner, M., Hanelt, D. 2015. Microalgal growth and fatty acid productivity on recovered nutrients from hydrothermal gasification of *Acutodesmus obliquus*. *Algal Research*, 10, 164-171.
- Elsayed, S., Boukis, N. and Sauer, J. 2015. Gasification of microalgae in supercritical water. In: European Symposium for Chemical Reaction Engineering (ESCRE), 27 – 30 October 2015, Fürstfeldbruck, Germany
- Elsayed, S., Boukis, N., Patzelt, D., Hindersin, S., Kerner, M., Sauer, J. 2016. Gasification of Microalgae Using Supercritical Water and the Potential of Effluent Recycling. *Chemical Engineering & Technology*, **39**(2), 335-342.
- Duba, K., Yedro, F., Elsayed, S., Busick, A., Jacoby, W., Beckwith, W., Jooss, K., A. Deshusses, M. 2017. Supercritical water oxidation of fecal sludge: A neighborhood scale solution. In: 16th European Meeting on Supercritical Fluids (EMSF), 25 – 28 April 2017, Lisbon, Portugal
- Duba, K., Yedro, F., Elsayed, S., Busick, A., Jacoby, W., Beckwith, W., Jooss, K., A. Deshusses, M. 2017. Optimization of supercritical water oxidation process using *Aspen Plus*. In: European Meeting on Supercritical Fluids (EMSF), 25th – 28th April, Lisbon, Portugal

08. Appendix

8.1. Thermo-physical properties of water under sub- and supercritical conditions

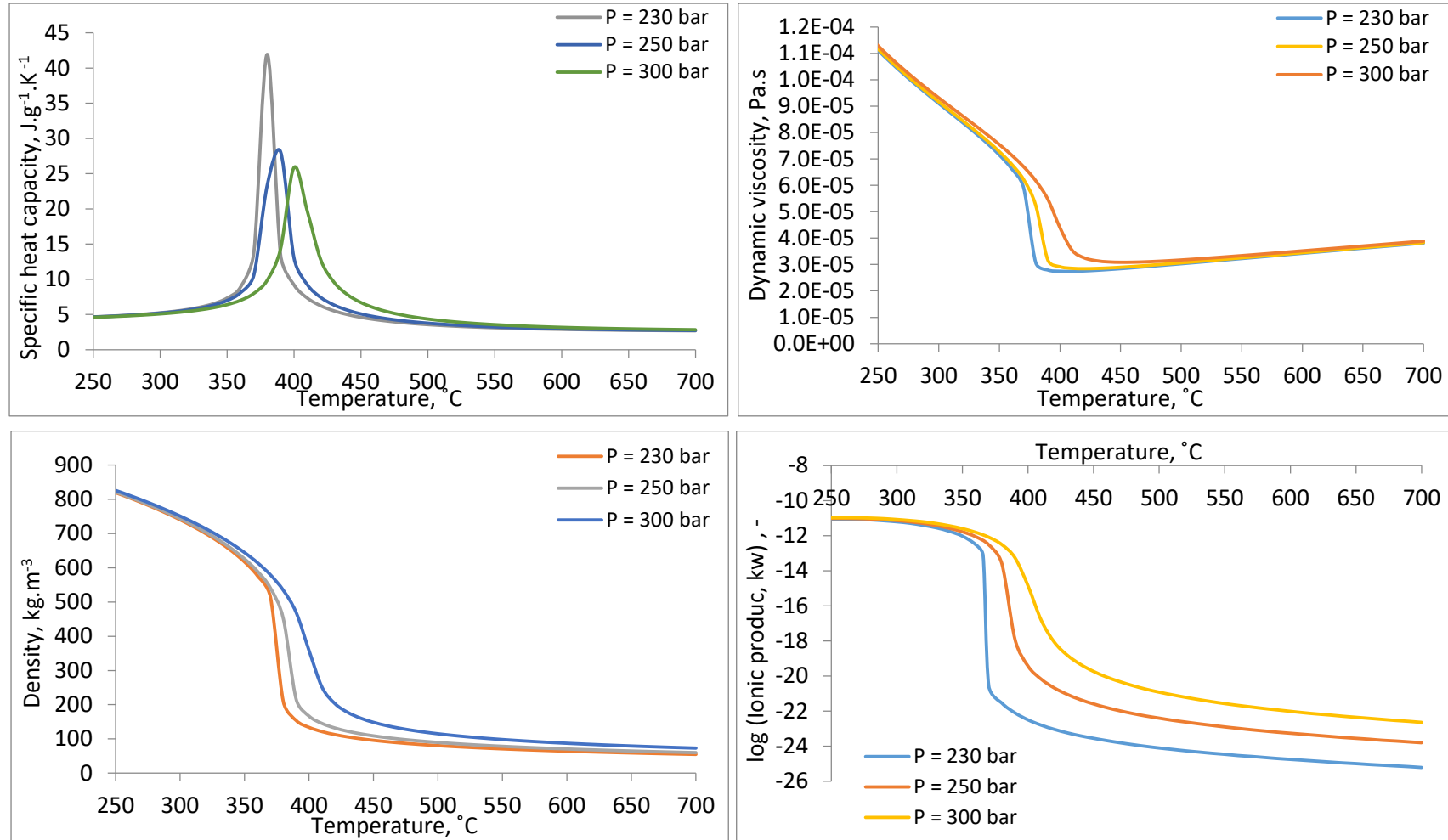


Figure A1.1 – Major changes which occur to water around the critical point at different pressures (Specific heat capacity, dynamic viscosity, density, ionic product) [Source: NIST Chemistry WebBook]

8.2. Cultivation systems

Microalgae grow in nature within open ponds or lakes. Extended man-made water bodies can also be designed for the same purpose. Those systems which have direct contact to the environment are defined as open cultivation systems. The major advantages of such systems are the relatively low capital cost, simple construction and operation. Photo-bioreactors (PBR) are cultivation systems which have no direct contact to the environment, can be operated indoors and are usually made up of transparent materials such as glass or plastic for light access. The major advantages of these systems are the well-controlled environment for cultivation which decreases the potential for contamination or unwanted species, flexibility of operation as well as the compact design. Basic PBR designs include the tubular, flat-panel and annular configurations. Table A1.1 provides a brief comparison between open and closed systems. These factors promote higher chances for the total process efficiency and higher productivities.

Table A1.1 – Qualitative Comparison between open cultivations systems and Photobioreactors

[Modified from: Brennan et al. 2010, Pulz and Gross 2004]

	Open cultivation systems	Photobioreactors
Area required	large (-)	relatively low (+)
Contamination risk	high (-)	low (+)
Evaporative losses	high (-)	low (+)
Operational costs	low (+)	high (-)
Control (ex.: Temp., pH)	difficult (-)	easy (+)
Investment cost	low (+)	high (-)
Surface-to-volume ratio	low (-)	high (+)
Light utilization	low (-)	high (+)
System cleaning	easy (+)	difficult (-)
Biomass productivities	low (-)	high (+)
Scale-up	easy (+)	difficult (-)
Shear stress on algal cells	low (+)	high (-)
Quality of biomass	low (-)	high (+)
Culture mixing	poor (-)	good (+)

The main challenge related to building up closed cultivation systems in large scales is the high capital and operating costs compared to open systems. Therefore, the adequate design of photo-bioreactors should contribute to a process which achieves high yield of biomass in order to compensate the high cost of the manufacturing. Also, having relatively high biomass concentrations in the culture contributes to making harvesting more economic [Carvalho et al. 2006].

8.3. BIQ house modules

The figure below shows how the modules or flat panels are mounted on a steel frame forming the façade of two sides of the BIO house (pictures on top). The picture on the bottom shows flow direction of culture medium and the continuous supply of compressed air (CO₂ included). This technique keeps the necessary elements of growth (air, CO₂; nutrients, light and temperature distribution) at good levels and prevent the deposition of algal cell during cultivation.

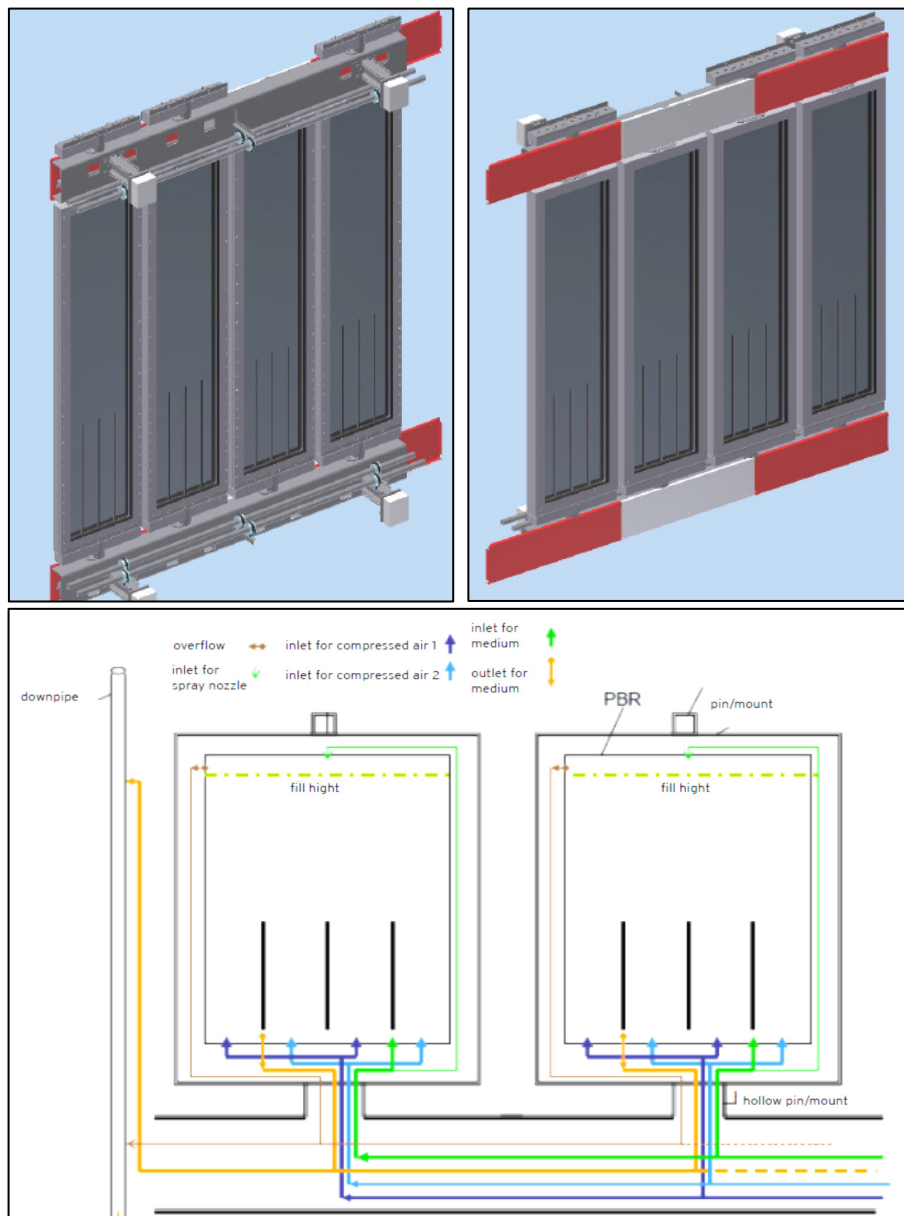


Figure A3.1 – Façade elements of the BIQ house: the flat panels reactor modules (PBR)

[Source: International Building Exhibition Hamburg, Smart Material House BIQ, IBA Hamburg GmbH, July 2013]

8.4. Methods applied for samples analysis

Table A3.1 – The methods applied for the analysis of the solid and liquid samples from supercritical water gasification

Analytical Method	Description of the measured parameter/s – phase
DIN ISO 10694: 1996-08	Determination of the total organic and total carbon (TOC, TC) after dry combustion – solid
DIN EN 13137: 2001-12	Determination of the total organic carbon (TOC) in waste, sludge and sediments – solid
DIN EN 15104:2011-04	Determination of the total content of carbon (TC), hydrogen and nitrogen – solid
DIN 51721:2001-08	Determination of the carbon content and hydrogen content – solid
DIN EN 51722-1: 1987-01	Determination of the nitrogen content (TN) – solid
DIN 51732:2007-08	Determination of the total carbon, hydrogen and nitrogen (C-H-N) – solid
DIN EN ISO 10304-1:2009-07	Determination of the dissolved anions by liquid chromatography of ions (Cl, NO ₃ ⁻ , NO ₂ ⁻ , PO ₄ ⁻³ and SO ₄ ⁻²) – aqueous
DIN EN ISO 11885:2009-09	Determination of selected elements (e.g. Al, Ca, Cr, Fe, K, Mg, Mo, Na, Ni, P, S, Si) by inductively coupled plasma optical emission spectrometry (ICP-OES) – aqueous
DIN EN 12260: 2003-12	Determination of the bound nitrogen (TN _b), following oxidation to nitrogen oxides – aqueous
DIN EN 1484: 1997-08	Determination of the total organic carbon (TOC) and dissolved organic carbon (DOC) – aqueous
DIN 38406-5:1983-10	Determination of ammonia-nitrogen (Ammonium-N) (E5) – aqueous

8.5. Significance of feed mixing

Figure A3.2 shows four different concentrations of algal biomass feedstock (from left to right: 2.5, 5, 10 and 15 wt%) without mixing for about 100 hours (~ 4 days) and the occurring particles settling. The figure can be described by other expressions such as phase separation or concentration gradient within the feed suspension. The settling is clearly observed at the two lower concentrations prepared.



Figure A3.2 – Particles settling without feed mixing at different concentrations after 100 hours

8.6. Analysis of the calorific value of the algal biomass:

Table A3.2 – Elemental analysis of a dried algal biomass sample

Sample associated with (Batch 4)	Unit	Value
Total organic carbon (TOC)	%	48.6
Aluminium (Al)	mg.kg ⁻¹	2990
Calcium (Ca)		6030
Eisen (Fe)		420
Potassium (K)		8000
Magnesium (Mg)		2020
Sodium (Na)		597
Phosphorous (P)		10030
Sulphur (S)		8040
Silicon (Si)		5030
Chlorine (Cl)		315

Table A3.3 – Determination of the calorific value of the algal biomass

Parameter	Unit	Value
Higher heating value (HHV)	kJ.kg ⁻¹	20.993.1; 21.086.0; 20.788.2
Analysis humidity ^a	wt%	9.8
HHV (based on 100% dry biomass)	kJ.kg ⁻¹	23.273.8; 23.376.9; 23.046.6
Hydrogen content in microalgae	wt%	7.1
Lower heating value (LHV) ^b	kJ.kg ⁻¹	19.184.4; 19.277.4; 18.979.4

^a These samples were conditioned with constant value of humidity for analysis. This was conducted to improve the accuracy of the measurements.

^b An expression used to relate the high heating value (HHV) to the lower heating value (LHV), taking into consideration the heat of vaporization of the moisture content and the heat released by the combustion of the hydrogen content of the biomass, can be written as:

$$\text{LHV} = \text{HHV} - 2454 (\text{W} + 9\text{H})$$

where:

- W = water or moisture content of the sample in percent (wt%) and
- H is the hydrogen content in percent (wt%)

This expression is derived from the international flame research foundation (IFRF) combustion handbook.

8.7. Supercritical water gasification of a model solution (Ethanol) at different concentrations

As indicated in chapter (3), conducting pre-experiments was a procedure that was followed in order to prepare the unit before switching to the algal biomass. Some data were collected based on the experiments carried out with a solution of ethanol in three concentrations (5, 9 and 11 wt%). Since no regular pattern for these experiments was the scope of work, it was added in the appendix to demonstrate that these model solutions containing no slurry or solid particles are simpler or easier to convert to a gaseous mixture under supercritical conditions with high carbon gasification efficiency (CGE). This can be identified from table A4.1 through the high rates of gas production as well as the carbon gasification efficiency. Carbon represents about 52 wt% of the ethanol molecule, which is comparable to the algal biomass. However, the algal biomass contains around 10 wt% inorganic constituents in the form of salts or ash. Therefore, it is expected that higher gas production and enhanced CGE can be achieved with a solution such as ethanol.

Table A4.1 – Summary of the pre-experiments conducted with an ethanol solution

Feed concentration	T	P	Flow rate	Duration	Maximum gas production	CGE
wt%	°C	bar	g.h ⁻¹	h	L.h ⁻¹	%
9	600	250	150	5.8	26	98.2
9	620	250	150	4.9	30	99.8
11	600	250	288	5.0	45	96.8
5	650	280	580	6.3	55	97.4
5	650	280	600	5.0	58	99.3
5	650	280	700	6.5	57	98.6

8.8. Quality of the residual water from SCWG

Table A4.2 – List of the qualitatively detected substances in the aqueous phase of SCWG and the influence of the two treatment methods applied on the removal of these substances [Patzelt et al. 2014]

Compounds	In residual water	after UV-treatment	after AC filtration
2-Methylpyridine	x		
3-Methyl-1H-pyrrole	x		x
3-Methy-pyridine	x		
2,6-Dimethylpyridine	x		
2-Ethylpyridine	x		
2,5-Dimethylpyridine	x		
2,3-Dimethylpyridine	x		
3-Ethylpyridine	x		
Aniline	x		
(p-Hydroxyphenyl)-phosphonic acid	x	x	x
2,4,6-Trimethylpyridine	x		
2,3,6-Trimethylpyridine	x		
Acetophenone	x		
3-Methylbenzenamine	x		
3-Methylphenol	x	x	
2,3-Cyclopentenopyridine	x		
Quinoline	x	x	
Isoquinoline	x		
Indole	x	x	
2-Methylquinoxaline	x		
2-Methylquinoline	x		
4-Methylquinazoline	x	x	
5-Methylquinoline	x		
4-Methylquinoline	x		
4-Methyl-1H-indole	x		
6-Methyl-1H-iIndole	x		
9H-Carbazole-9-methanol	x		
9-Nitroso-9H-carbazole	x		
1,8-Naphthyridine		x	
Methylpyrazine		x	
2,5-Dimethylpyrazine		x	
3-Methylbenzenamine		x	

8.9. Conductivity of the salt brine

Some measurements of conductivity to salt brine resulting from supercritical water gasification was made as an indicator of the salt existence in the aqueous phase. The higher the amount of ionized salts in the medium, the more its tendency to conduct electricity. The results of these measurements are listed below in figure A4.1. They are based on the salt brine from the experiments conducted in LU II at a temperature of 690 °C and flow rate of 150 g.h⁻¹. The measurement unit is presented in the form of milli-siemens per centimeter (mS/cm). The electrode was calibrated in reference to distilled water (1 – 3 $\mu\text{S}\cdot\text{cm}^{-1}$). This is a qualitative measure in terms of the entire ionic species that are found in the aqueous sample.

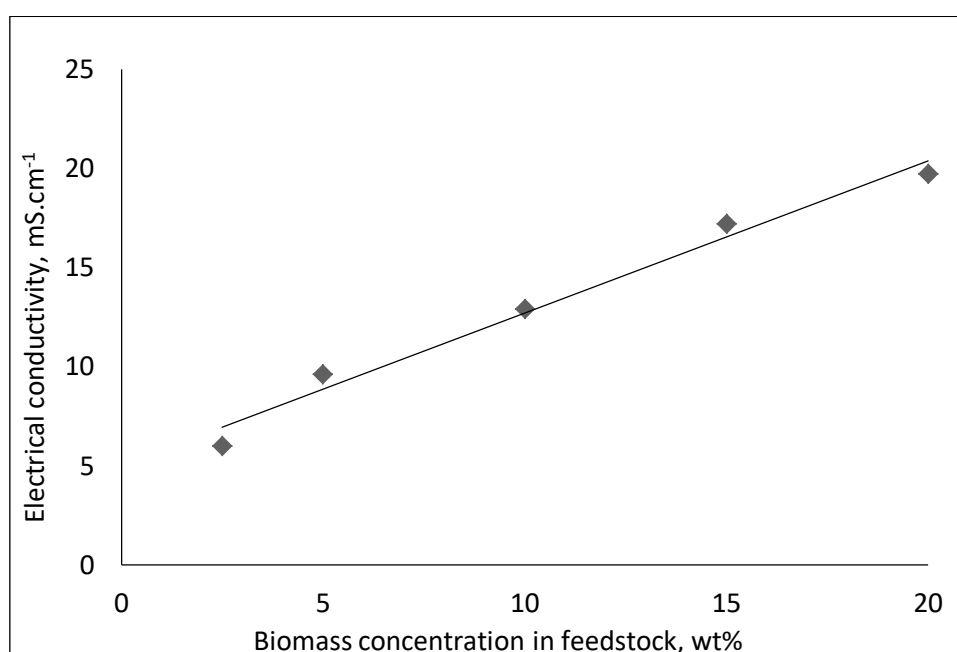


Figure A4.1 – Measurements of the conductivity of some samples of the salt brine resulting from supercritical water gasification of algal biomass (LU II)

8.10. Energy content of the gas product from SCWG

Based on the specific yield of the gas product from SCWG, the energy content (lower heating value, LHV) is listed below in the following table:

Table A4.3 – Energy content of the gas product from SCWG [Data from LUII]

Exp. No	Yield	H ₂	CH ₄	CO ₂	C ₂ H ₆	LHV, MJ.kg ⁻¹ TS
1	ml.g ⁻¹ TOC	1218.56	521.87	899.75	78.39	15.8
	ml.g ⁻¹ TS	622.93	266.78	459.95	40.07	
2	ml.g ⁻¹ TOC	896.72	375.83	698.77	123.45	18.2
	ml.g ⁻¹ TS	450.15	188.67	350.78	61.97	
3	ml.g ⁻¹ TOC	804.75	580.17	583.91	183.29	23.0
	ml.g ⁻¹ TS	412.03	297.04	298.69	94.20	
4	ml.g ⁻¹ TOC	1036.82	689.04	875.06	227.80	20.0
	ml.g ⁻¹ TS	520.48	345.90	439.28	114.36	
5	ml.g ⁻¹ TOC	893.17	567.51	789.84	133.24	17.7
	ml.g ⁻¹ TS	458.20	291.13	405.19	68.35	
6	ml.g ⁻¹ TOC	362.16	344.89	458.93	115.18	18.5
	ml.g ⁻¹ TS	181.80	173.13	230.38	57.82	
7	ml.g ⁻¹ TOC	565.83	642.62	674.14	179.62	20.0
	ml.g ⁻¹ TS	284.08	322.63	338.46	90.18	
8	ml.g ⁻¹ TOC	386.29	399.47	470.58	141.95	21.2
	ml.g ⁻¹ TS	193.74	200.36	236.02	71.19	
9	ml.g ⁻¹ TOC	600.28	598.49	692.41	139.01	18.5
	ml.g ⁻¹ TS	311.54	310.61	359.36	72.15	
10	ml.g ⁻¹ TOC	355.35	623.72	631.04	137.64	18.8
	ml.g ⁻¹ TS	184.43	323.71	327.51	71.44	

8.11. Analysis of a complex intermediate of hydrothermal conversion

This analysis was conducted to a tar-like sample resulted that was extracted from the preheating section at $T = 390\text{ }^{\circ}\text{C}$. The same was dissolved in acetone and analyzed via gas chromatography mass spectroscopy (GC-MS). The analytical procedures were as followed [GC-MS column: Stabilwax, $1\mu\text{L}$ injected, injection temperature $250\text{ }^{\circ}\text{C}$, temperature prog.: 5 min at $40\text{ }^{\circ}\text{C}$, heating rate $8\text{ }^{\circ}\text{C}/\text{min}$ until $250\text{ }^{\circ}\text{C}$, 10 min at $250\text{ }^{\circ}\text{C}$, detector temperature $260\text{ }^{\circ}\text{C}$]. The sample was partially soluble in acetone and several peaks were detected (see figure A4.2).

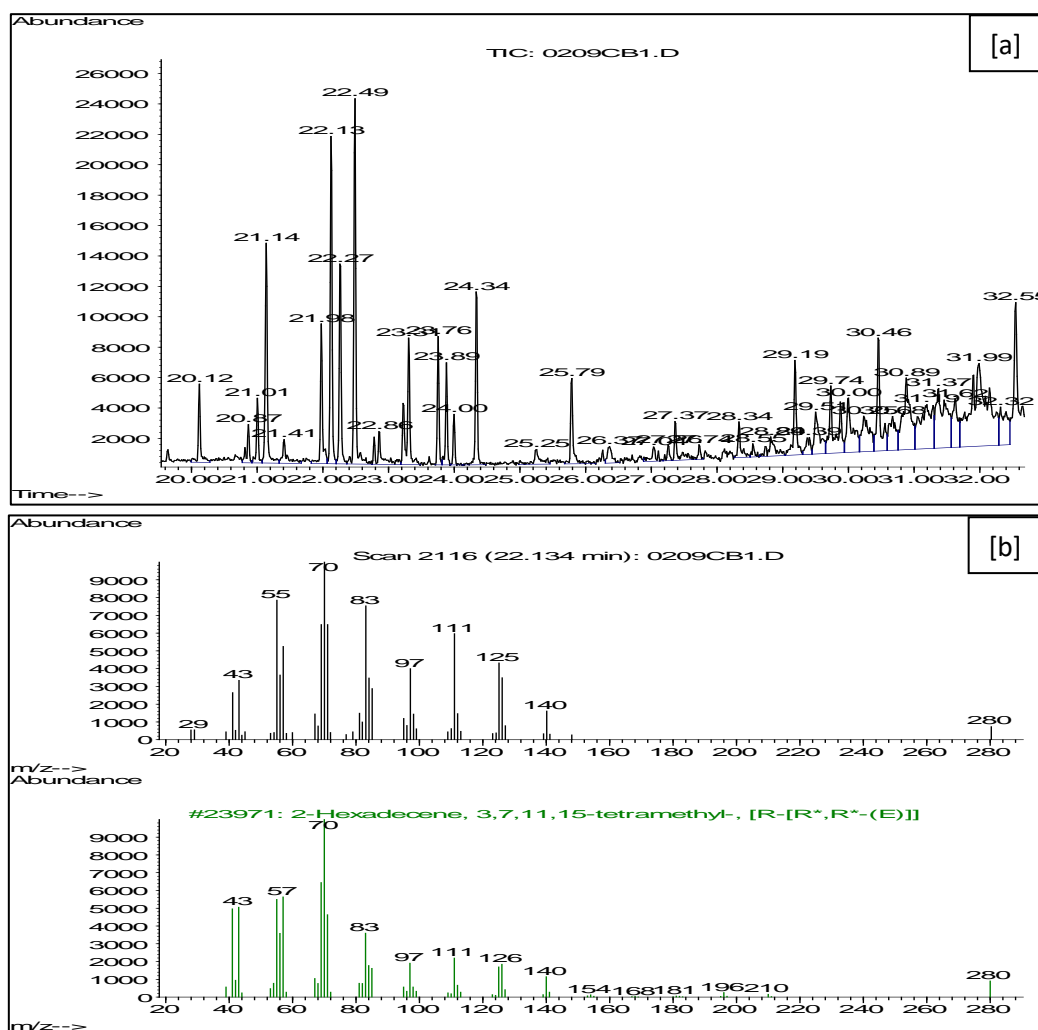


Figure A4.2 – [a] GC-MS chromatogram (with indicated retention time) of a sample extracted from LUIII in the preheating section at a temperature of $390\text{ }^{\circ}\text{C}$ and [b] fragmentation peaks of the compound detected at 22.13 min of retention time.

In Table A4.4, the major peaks with their corresponding retention time were reported. When possible, the assignment of the mass spectra with a database and the quality of the assignment was made. Otherwise, the detected peak of the mass fragmentation with the higher mass to charge ration (m/z) was provided. The analysis could not provide an accurate identification of the compounds in the sample, as they were not matched with any compound in the database. This can be possibly explained by the fact that the sample contained mainly of fragments or partially decomposed molecules that $-CH_2$ units for instance.

For the molecular peak at 280 m/z , an indication of a high molecular mass component is presumed, but it is more difficult to determine its structure. For the sake of comparison, the mass spectra of 2-hexadecene, 3,7,11,15 tetramethyl is reported. The two spectra are quite similar, not identical though, and the quality match is relatively high.

Table A4.4 – Retention time of the chromatogram with possible assignment of few compounds - When it was not possible, the peak with higher mass to charge ration (m/z) is indicated.

Retention time	Name	Quality	Peak observed at higher (m/z)
20.12	Possibly an alkane	-	127 (122; 113; 99;85;71;57;43) ¹
22.13	Possibly: 2-hexadecene 3,7,11,15 tetramethyl or isomer	86	280
22.27	Possibly: 2-hexadecene 3,7,11,15 tetramethyl or isomer	86	280
22.49	Possibly: 2-hexadecene 3,7,11,15 tetramethyl or isomer ²	95	280

¹ Other main fragmentation peaks.

² It is obvious that this is a compound relatively similar to the one reported in the database. However, a different compound is ideally identified for each retention time. Another possibility is that these detected compounds are long chain alkanes with some degree of instauration.

8.12. Analysis of a solid particle using X-ray diffraction (XRD)

These results (Figure A4.3 and table A4.5) were obtained using a diffractometer system to analyze a solid particle from one extended experiment (duration 22 hours). The sample (color: bright grey) was extracted from the system after operation. It was concluded that the sample contained high concentrations of inorganic elements such as phosphorus and potassium. The existence of these elements was also confirmed using elemental mapping (scanning electron microscopy, SEM).

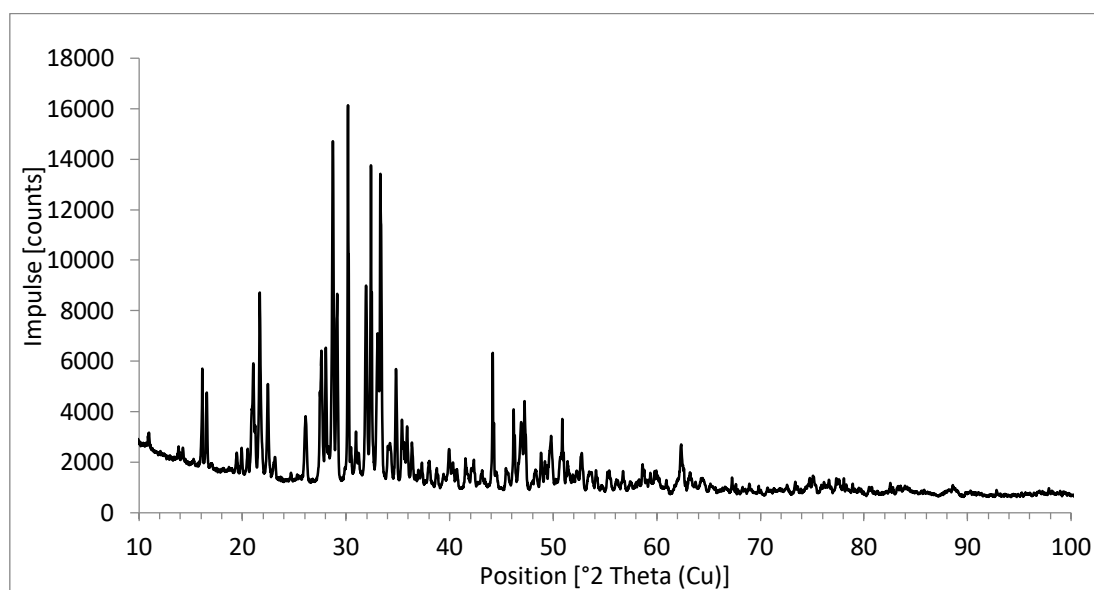


Figure A4.3 – X-ray diffraction analysis of a solid sample extracted after SCWG [Data from LUI]

(Operating conditions: T = 650 °C, P = 280 bar, Feed conc. = 2.5 wt% - Duration = 22 h)

Table A4.5 – Chemical formulas matching the structures detected in the XRD analysis

Power diffraction file (PDF)-No.	Score	Name	Scale factor	Chemical Formula
01-089-4675	44	Potassium Magnesium Phosphate	0.478	KMg (PO ₄)
00-011-0232	41	Calcium Phosphate	0.374	Ca ₄ P ₂ O ₉
01-087-0089	21	Berlinite, syn	0.082	Al (PO ₄)
01-087-1707	46	Kalsilite	0.277	K Al (SiO ₄)
00-048-0367	25	Aluminum Oxide	0.151	Al ₂ O ₃
00-015-0047	22	Leucite	0.078	K Al Si ₂ O ₆

8.13. Determination of the gas composition

The data obtained in this section (Figure A4.4 and Table A4.6) is an example of a regular gas sampling which was conducted every 30 minutes during operation under steady-state conditions.

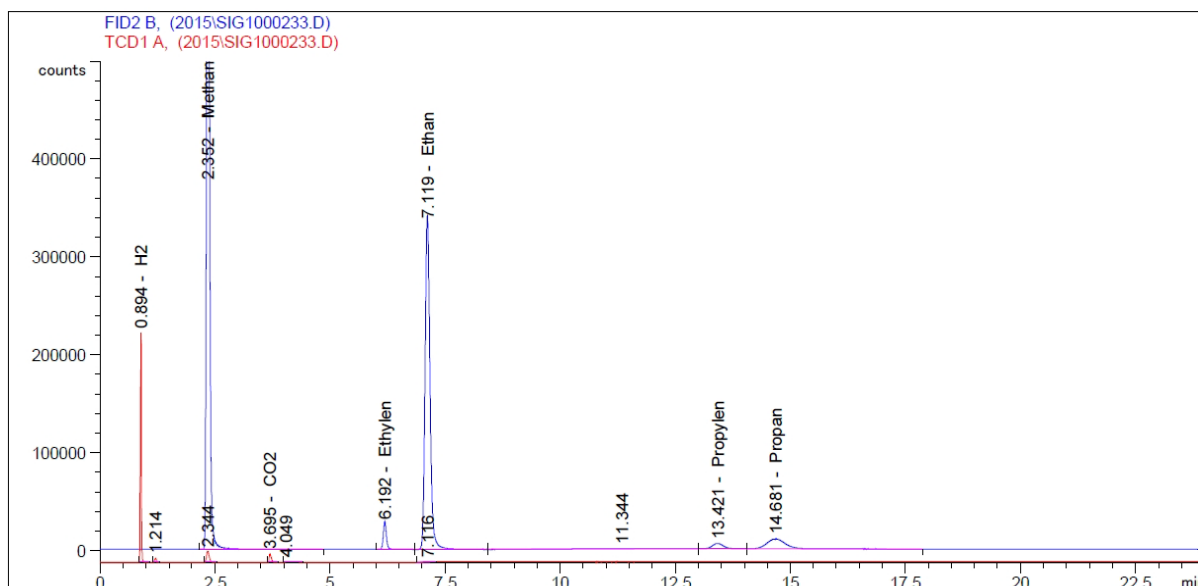


Figure A4.4 – Gas chromatogram [Exp. code ESL13-G7] [Date from LUIII]

(Operating conditions: T = 650 °C, P = 280 bar, Feed conc. = 2.5 wt%)

Table A4.6 – Retention time, composition and component detection based on gas chromatography

Retention time min.	Composition vol%	Gas component -
0.894	42.84502	Hydrogen
2.352	13.57464	Methan
3.695	34.75010	Carbon dioxide
6.192	2.49843e-1	Ethylen
7.119	5.19854	Ethan
13.421	1.32954e-1	Propylen
14.681	3.81393e-1	Propan

8.14. Elemental mapping using scanning electron microscopy (SEM)

Figure A4.5 and Table A4.7 provide the results of the elemental mapping that was conducted to some precipitates (grey powder) that evolved during gasification in supercritical water. The analysis of this precipitate indicates high concentrations phosphorus, calcium, magnesium and potassium.

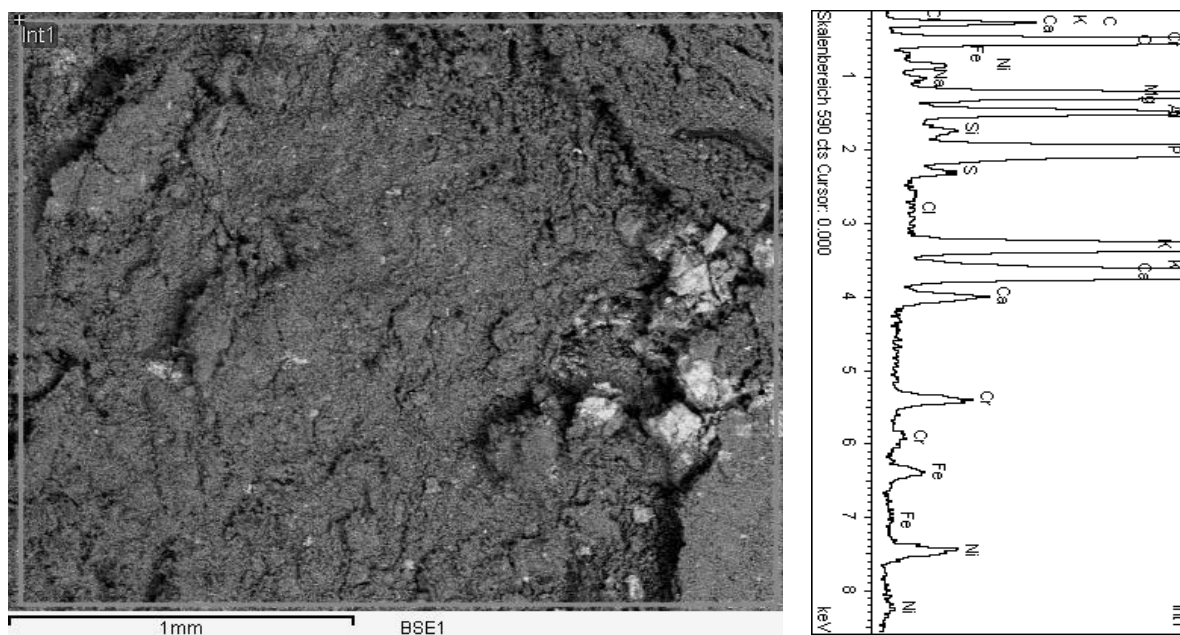


Figure A4.5 – Elemental mapping using scanning electron microscope (SEM) [Data from LUI]
 (Operating conditions: T = 650 °C, P = 280 bar, Feed conc. = 5 wt% - Duration = 30 h)

Table A4.7 – Results of the SEM analysis (weight and atomic percentages of the detected elements)

Element	wt%	Atom%
C	15.09	24.39
O	41.67	50.56
Na	0.21	0.18
Mg	6.88	5.50
Al	2.08	1.50
Si	0.22	0.15
P	13.83	8.67
S	0.42	0.26
Cl	0.07	0.04
K	6.43	3.19
Ca	7.45	3.61
Cr	1.67	0.63
Fe	1.04	0.36
Ni	2.93	0.97

8.15. Salt extraction mechanisms during supercritical water gasification

The simplified figure below (fig. A4.6) shows a basic demonstration of the extraction mechanism of inorganic elements (salts) during operation under near- and supercritical water conditions. Two methods were conducted based on the experimental work; a method of removing the salts at the bottom of the reactor after gasification (LUI). The other mechanism for salt extraction is applied under near-critical conditions before gasification (LUII and LUII).

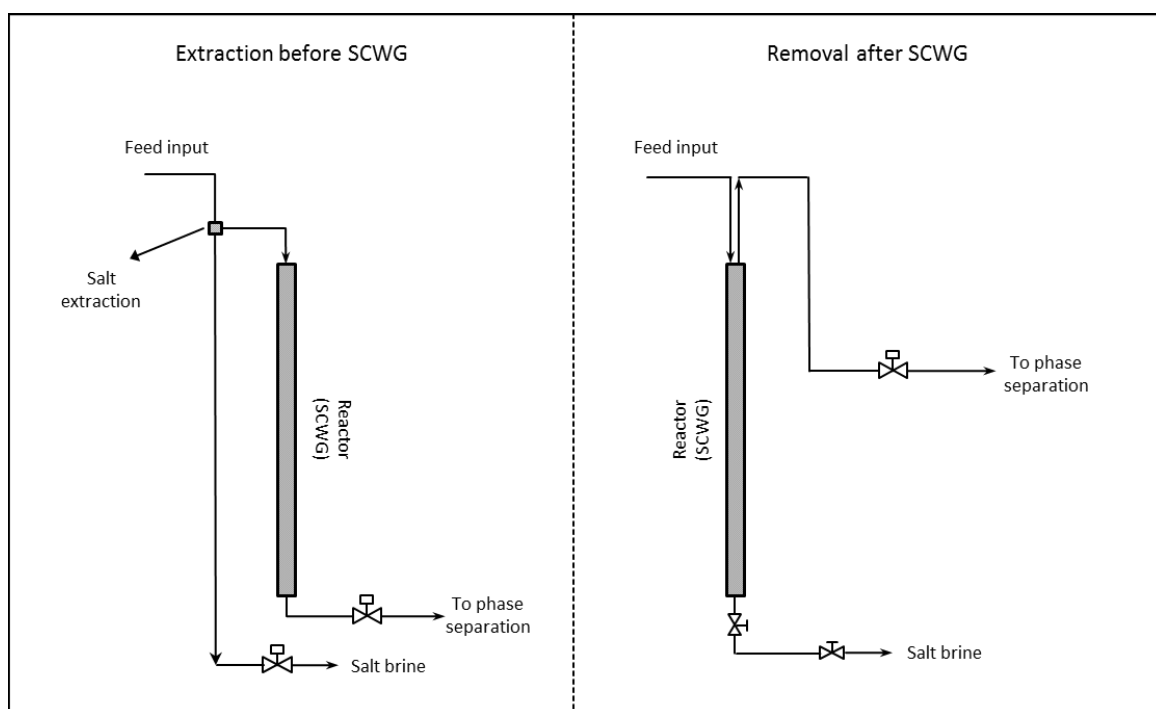


Figure A4.6 – Extraction of inorganic constituents during supercritical water gasification

8.16. Recovery of the micro-nutrients from supercritical water gasification

From the different phase of gasification under supercritical conditions, the distribution and percent recovery of the micro-nutrients for algal growth is shown below in figure A4.7.

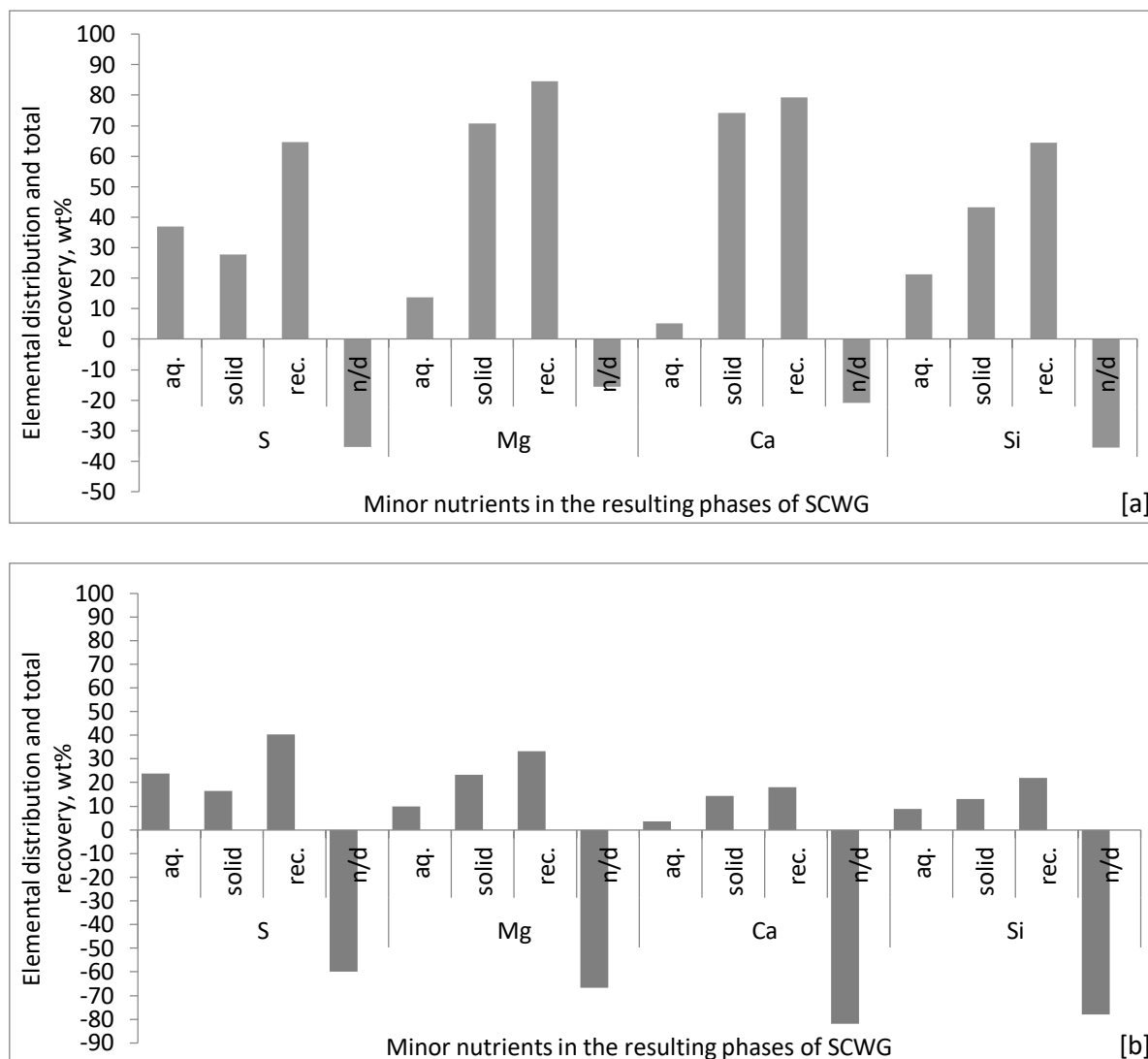


Figure A4.7 – Distribution and recovery of the micro-nutrients (S, Mg, Ca and Si) from the gasification products for: [a] LUH and [b] LUHIII [aqueous: aq.; recovery: rec.; n/d: not detected]

8.17. Process Simulation using Aspen Plus (Selected database components)

Table A5.1 – List of the components which were selected from the Aspen database for process simulation

Component ID	Type	Component name	Alias
H2O	Conventional	WATER	H2O
MICROALGAE	Nonconventional	MICROALGAE	-
H2	Conventional	HYDROGEN	H2
CO	Conventional	CARBON-MONOXIDE	CO
O2	Conventional	OXYGEN	O2
CO2	Conventional	CARBON-DIOXIDE	CO2
N2	Conventional	NITROGEN	N2
CH4	Conventional	METHANE	CH4
C2H4	Conventional	ETHYLENE	C2H4
C2H6	Conventional	ETHANE	C2H6
C3H6	Conventional	PROPYLENE	C3H6-2
C3H8	Conventional	PROPANE	C3H8
ETHANOL	Conventional	ETHANOL	C2H6O-2
NH3	Conventional	AMMONIA	H3N
2MP	Conventional	2-METHYLPYRIDINE	C6H7N-D1
N-MET-01	Conventional	N-METHYLPYRROLE	C5H7N
3-MET-01	Conventional	3-METHYLPYRIDINE	C6H7N-D2
2:6-D-01	Conventional	2,6-DIMETHYLPYRIDINE	C7H9N-D2
ANILI-01	Conventional	ANILINE	C6H7N-1
PHENO-01	Conventional	PHENOL	C6H6O
2:4:6-01	Conventional	2,4,6-TRIMETHYLPYRIDINE	C8H11N-D1
METHY-01	Conventional	METHYL-PHENYL-KETONE	C8H8O
N:N-D-01	Conventional	N,N-DIMETHYLANILINE	C8H11N
3-MET-02	Conventional	3-METHYL-4-METHYLETHYL-PHENOL	C10H14O-D4
QUINO-01	Conventional	QUINOLINE	C9H7N-D2
ISOQU-01	Conventional	ISOQUINOLINE	C9H7N-D1
8-MET-01	Conventional	8-METHYLQUINOLINE	C10H9N-N5
QUINA-01	Conventional	QUINALDINE	C10H9N
1-PEN-01	Conventional	1-PENTADECENE	C15H30-2
N-HEP-01	Conventional	N-HEPTADECANE	C17H36
METHY-02	Conventional	METHYL-MYRISTATE	C15H30O2-N1
METHY-03	Conventional	METHYL-PALMITATE	C17H34O2-N1
OLEIC-01	Conventional	OLEIC-ACID	C18H34O2
STEAR-01	Conventional	STEARIC-ACID	C18H36O2
BETA--01	Conventional	BETA-CHOLESTEROL	C27H46O
C	Solid	CARBON-GRAPHITE	C
CALCI-01	Solid	CALCIUM-OXIDE	CAO
POTAS-01	Solid	POTASSIUM-OXIDE	K2O
CALCI-02	Solid	CALCIUM-PHOSPHATE	CA3(PO4)2
POTAS-02	Solid	POTASSIUM-CARBONATE	K2CO3
AMMONIUM	Conventional	NH4+	NH4+
1-NIT-01	Conventional	1-NITROBUTANE	C4H9NO2-D1
A-AMI-01	Conventional	A-AMINOBTYRIC	C4H9NO2
FURFU-01	Conventional	FURFURYL-ALCOHOL	C5H6O2
METHY-01	Conventional	METHYL-CYANOACETATE	C4H5NO2
ISOPR-01	Conventional	ISOPROPYL-ACETATE	C5H10O2-D2
METHY-02	Conventional	METHYL-BUTYRATE	C5H10O2-5

8.18. Calculation of water properties

Table A5.2 shows a comparison between some of water's properties that are calculated based on the International Association for the Properties of Water and Steam (IAPWS) as well as the National Institute of Standards and Technology (NIST). The objective here is to show that the values used in the property method in the Aspen simulation (IAPWS) is quite similar to the same properties obtained with the NIST-based calculations.

Table A5.2 – Three properties of water under near and supercritical conditions, given by two references of calculations (NIST and IAPWS) at a pressure of 280 bar

Temperature (°C)	Density (kg.m ⁻³)		Cp (kJ.Kg ⁻¹ .K ⁻¹)		Viscosity (μPa.s)	
	NIST	IAPWS	NIST	IAPWS	NIST	IAPWS
300	747.68	748.00	5.12	5.12	92.56	92.63
320	709.68	709.75	5.49	5.51	85.49	85.51
340	664.17	663.85	6.10	6.15	78.29	78.24
360	605.36	605.03	7.34	7.05	70.24	70.19
380	512.21	511.51	11.70	12.04	59.20	59.12
400	259.44	261.65	26.92	26.99	35.51	35.68
420	169.41	169.13	10.1	9.93	30.42	30.41
440	140.40	140.42	6.79	6.75	29.90	29.91
460	123.99	124.07	5.38	5.30	30.13	30.14
480	112.84	112.95	4.60	4.52	30.63	30.63
500	104.51	104.64	4.10	4.04	31.25	31.25
520	97.94	98.06	3.76	3.71	31.93	31.93
540	92.54	92.64	3.51	3.48	32.64	32.65
560	87.98	88.07	3.33	3.30	33.38	33.39
580	84.05	84.12	3.19	3.17	34.13	34.13
600	80.60	80.67	3.08	3.06	34.88	34.89
620	77.54	77.60	2.99	2.98	35.64	35.64
640	74.78	74.84	2.92	2.92	36.39	36.39
660	72.29	72.34	2.87	2.87	37.14	37.14
680	70.02	70.07	2.82	2.83	37.89	37.89
700	67.93	67.97	2.78	2.80	38.63	38.64

8.19. Reaction intermediates in the residual water

As pointed out in chapter 4, the residual water from SCWG contained traces of several reaction intermediates, including alcohols, cyclic compounds such as aniline, pyridine and phenols as well as ketones. In the work of *Patzelt et al. 2014*, a qualitative list which involves 28 substances measured in the RW was presented. These substances, with other possibly occurring substances which are reported in literature, were inserted in the Aspen database before simulation and their existence in the RW stream after was investigated. A list including some of these compounds is shown in table 5.2. Of the 28 substances, the models predicted the presence of nine substances.

Table A5.3 – List of the reaction intermediates found in the residual water of gasification

Component calculated from the simulated models	Feed model (FDE)				Feed model (ASI)			
	Feed concentration, wt%							
	5		25		5		25	
	Reaction temperature, °C							
	450	750	450	750	450	750	450	750
Substances predicted by the models and reported in the RW								
2-Methylpyridine	x	x	x	x	x	x	x	x
3-Methylpyridine	x	x	x	x	x	x	x	x
2,6-Dimethylpyridine	x	x	x			x	x	x
Aniline		x		x	x	x	x	x
2,4,6-Trimethylpyridine			x	x			x	x
Quinoline				x			x	x
Isoquinoline							x	x
3-Methyl-4-Methylethyl-Phenol								x
Phenol	x	x	x	x	x	x	x	x
Substance predicted by the models								
8-Mthylquinoline								x
Quinaldine								x
Methyl-Phenyl-Ketone		x	x	x		x	x	x
N-Methylpyrrole		x		x	x	x	x	x
Ethanol	x	x	x	x	x	x	x	x

Also, the existence of five additional substances was predicted by the models. In both models, increasing feed concentration and temperature resulted in the presence of more intermediates. Despite their existence in trace amounts, compounds such as ethanol and phenol were found at relatively higher levels than the others. Quantitative trends were difficult to conclude. However, the existence of such intermediates was reported in literature [e.g. *Brown et al. 2010*, *Kruse et al. 2003*], where they were presented as products of pre-gasification (liquefaction) or the result of polymerization or side reactions at high temperatures.

8.20. Coupling algal cultivation and SCWG

8.20.1 Conceptual basis

The idea of coupling both cultivation and gasification stems basically from the fact that both systems benefit from the aqueous nature mutually; one system through the growth of microalgae, where nutrients, O₂ and CO₂ are available. The other system is where having water under supercritical conditions is the key concept to gasification and conversion to a combustible gas mixture. Figure A6.1 outlines a conceptual scheme that represents the two integrated systems described earlier. The scheme demonstrates how a successful coupling of both cultivation and SCWG can be realized.

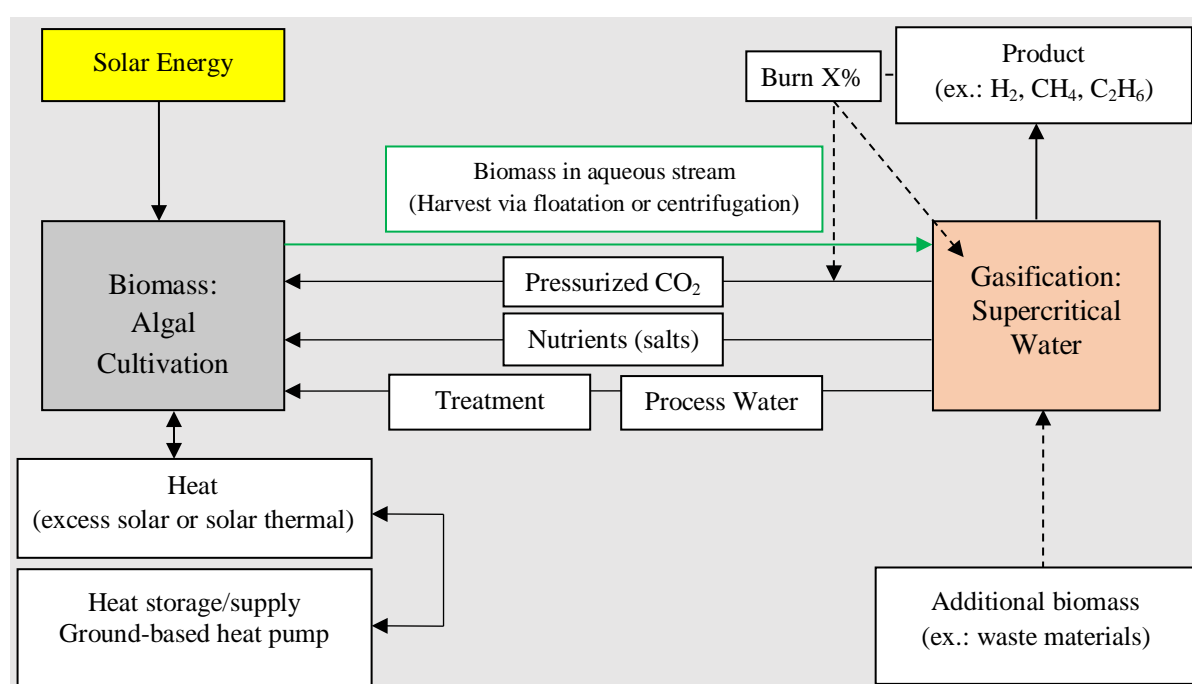


Figure A6.1 – Schematic representation of integrating algal cultivation and supercritical water gasification with the potential of nutrients and energy recovery³

Here, an ideal strategy prioritizes the efficient management of materials and energy streams in both systems. Such a strategy can be realized by designing heat networks or thermal looping between hot and cold streams, storing any surplus thermal energy that would be available for reuse when needed. In the case of cultivation, the ambient temperature shows a noticeable variation depending on the seasonal and day time at a given location. During sunny summer days, the temperature of the culture medium rises to levels, where growth inhibition might be possible. To the contrary, as the temperature drops below 10 °C at night

³ This figure was modified from the grant application of the project (PHYKON) – SSC Strategic Science Consult, Dr. habil. Martin Kerner, November 2012

or during winter, warming the culture becomes necessary to keep the algal cells at a warm and an acceptable level of activity for growth. As proposed, the excess thermal energy absorbed by the culture medium can be collected and stored using a heat pump in a geothermal well, where the temperature is relatively constant irrespective of seasonal time. This way, a mean of cooling the culture down to an optimum level for growth is provided.

The stored heat would be available to warm up the culture medium at low temperatures. The requirements of carbon dioxide for cultivation can be fulfilled entirely from SCW gasification by two routes. One route can be achieved by separating CO₂ from the combustible product of gasification under high pressure after cooling. Another route for supplying CO₂ is by burning the combustible mixture of gasification partially as previously discussed in Chapter 5 (Process Simulation) to make-up the heat losses in the SCWG system. This is a simple approach and the available CO₂ in this case would need to be pressurized before delivering to the culture medium. Both routes will probably be necessary for supplying the culture with this carbon source as long as a photoautotrophic growth is pursued. In any case, the decision of CO₂ separation, buffer storing and possible make-up will depend mainly on the cultivation system configuration, performance as well as process economics.

The degree of utilizing the concentrated salts in aqueous or solid form plays a role in the success of the coupling concept, as it helps establishing a closed loop of natural resources and decrease the operating costs associated with nutrients supply for cultivation. Beside the salts, the residual or process water from gasification will have to be treated either by filtration or using UV light to eliminate any toxic intermediates before recycling for cultivation. Moreover, the experimental results of this work along with other data available in literature (Ch. 2 Literature review) demonstrated the need to dilute the process water prior to the reuse for algal growth.

8.20.2 Biomass Productivity

As pointed out earlier (Ch. 1 Introduction), the major advantage of algal cultivation is the possibility of utilizing sunlight and using it as the source of energy for growth. By ensuring a proper access to light through adequate exposure and mixing, the culture can be maintained healthy, provided that other growth parameters are adjusted and kept at optimum conditions for a given species.

Since the suggested system of photo-bioreactors is operated outdoors, the major hurdle for cultivation becomes the variation of culture growth at different solar irradiance. The variation of irradiance or light intensity is practically a function of geographic location, seasonal and daytime. Added to that, the existence of clouds and their intensity usually results in a fluctuating irradiance on a given day. Considering the availability of sufficient solar energy for cultivation over the course of one day, optimum months for cultivation can be distinguished. Therefore, it would be difficult to generate a term that describes the productivities of an algal culture outdoors without using mean or average values. In addition to these factors, the productivity of outdoor cultivation also depends on the PBR configuration.

In this regard, an important term to highlight is the photosynthetic conversion efficiency (PCE). The term itself depends on several variables governing the performance of cultivation systems and biomass accumulation. At ideal or non-limiting growth conditions, the maximum PCE is calculated to be in the range of 9–10% [Bolton and Hall 1999, Stephens et al. 2010]. According to Melis 2009, this value can be translated into a biomass yield of approximately $77 \text{ g.m}^{-2}.\text{d}^{-1}$ for an average irradiance of $35 \text{ mole photons.m}^{-2}.\text{d}^{-1}$. Another work showed that maximum average productivities of $40 \text{ g.m}^{-2}.\text{d}^{-1}$ can be obtained in outdoor PBR systems [Williams and Laurens 2010]. Despite the lower value of mean annual productivity obtained in the work of Hindersin et al. 2014 ($\sim 10 \text{ g.m}^{-2}.\text{d}^{-1}$), the authors indicated that by optimizing growth conditions and sunlight utilization, a biomass productivity of $22 \text{ g.m}^{-2}.\text{d}^{-1}$ can be calculated. Given these data on biomass productivity, two mean values (20 and $40 \text{ g.m}^{-2}.\text{d}^{-1}$) were assumed in order to form a basis for this study. These values would correspond to a system or an arrangement of outdoor Photobioreactors with a flat panel configuration.

8.20.3 Layout of the cultivation system

Some assumptions (listed in table A6.1) were made to help designing the suitable cultivation system in terms of its size specifically. The assumptions were set in conjunction with the feed requirement for SCWG using three different capacities (50, 100 and 200 kg.h⁻¹) at concentrations of 5, 10 and 15 wt% DM. Combinations of these two variables are made. Accordingly and based on the two productivities values suggested earlier, the overall surface area subjected sunlight can be obtained. As a result, the numbers of panels for cultivation and the land area needed for cultivation can be calculated.

Table A6.1 – Scenarios based on two biomass productivities and different SCWG throughputs

Biomass productivity, 20 g.m⁻².d⁻¹	Cultivation area, m ²	Number of flat panels	culture volume, m ³	Land dimension L x W, m
- SCWG feed (5 wt% DM) - Throughputs: 50, 100, 200 kg.h ⁻¹	3000	1500	60	92 x 40
	6000	3000	120	-
	12000	6000	240	-
- SCWG feed (10 wt% DM) Throughputs: 50, 100, 200 kg.h ⁻¹	6000	3000	120	-
	12000	6000	240	-
	24000	12000	480	-
- SCWG feed (15 wt% DM) - Throughputs: 50, 100, 200 kg.h ⁻¹	9000	4500	180	-
	18000	9000	360	-
	36000	18000	720	-
Biomass productivity, 40 g.m⁻².d⁻¹	Cultivation area, m ²	Number of flat panels	culture volume, m ³	Land dimension L x W, m
- SCWG feed (5 wt% DM) - Throughputs: 50, 100, 200 kg.h ⁻¹	1500	750	30	-
	3000	1500	60	-
	6000	3000	120	-
- SCWG feed (10 wt% DM) - Throughputs: 50, 100, 200 kg.h ⁻¹	3000	1500	60	-
	6000	3000	120	180 x 40
	12000	6000	240	-
- SCWG feed (15 wt% DM) - Throughputs: 50, 100, 200 kg.h ⁻¹	4500	2250	90	135 x 40
	9000	4500	180	-
	18000	9000	360	-

The selection can be refined and limited to three cases by setting a limit for the size of the cultivation system. Using algal feedstock to SCWG of concentrations above 15 wt% was not considered in this study. The reason for that is the effort associated with dewatering the algal culture to high concentrations, the difficulty to handle and pump thick slurries and the decrease in gasification efficiency upon hydrothermal conversion.

The combinations listed include several scenarios with numbers of flat panels up to 18000. Large culture volumes (max. 720 m³) would result from using such extended sets of cultivation units. This excessive number of units would lead to difficulties due to the high total investment cost, despite the cost reduction associated with fabrication and operation. Therefore, conservative scenarios are suggested by applying certain limitations, such as considering the systems with a number of flat panels ≤ 3000 . Three cases can be selected (table AT7.1). The area of the land dedicated for building up a cultivation system will depend on the arrangement of the photo-bioreactors. The numbers of flat panels and total culture volume are based on flat panel units having a height, width and thickness (light path) of 2 m, 1 m, and 0.02 m respectively.

Through stacking or arranging the flat panels (figure A6.2) with an acceptable spacing between the units (ex.: 1-2 m) and by adjusting them to an optimal tilt angle (ex.: 5 - 20°) for an optimum utilization of solar irradiance, the total land area required to construct this system would be reduced. For example and given the three cases selected in this study (1500, 2250 and 3000 flat panels), the algal cultivation systems can be constructed on a land area of 3465, 5198 and 6930 m² respectively. This can be achieved for a given land of rectangular dimensions of 40 meters width and lengths of 92, 135 and 180 meters respectively. For these suggested dimensions, a central space for equipment and instrumentations can be taken into consideration.

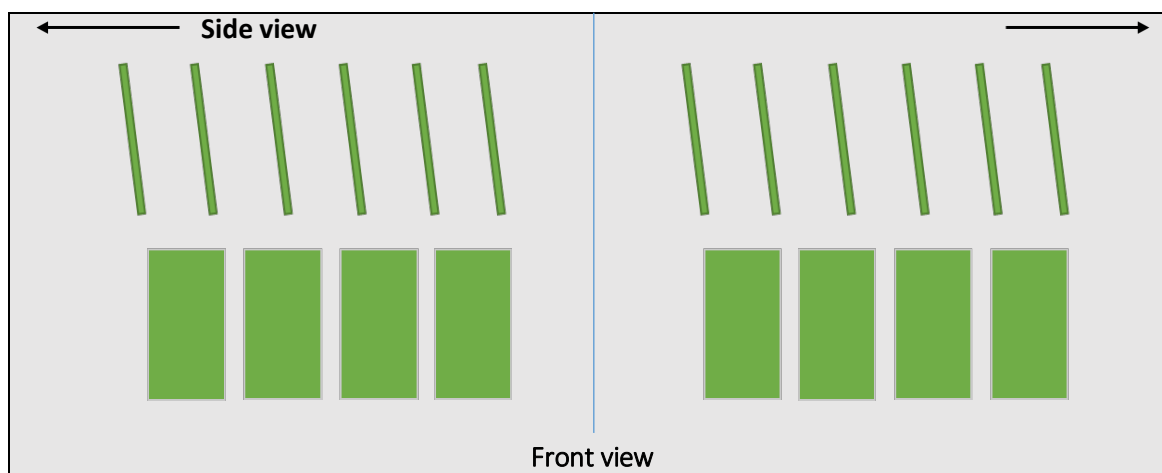


Figure A6.2 – Arrangement of flat panels for large scale cultivation of microalgae

8.21. References (Appendix)

1. Bolton, J.R., Hall, D.O. 1991. The maximum efficiency of photosynthesis. *Photochemistry and Photobiology*, **53**(4), 545-548.
2. Brennan, L., Owende, P. 2010. Biofuels from microalgae—A review of technologies for production, processing, and extractions of biofuels and co-products. *Renewable and Sustainable Energy Reviews*, **14**(2), 557-577.
3. Carvalho, A.P., Meireles, L.A., Malcata, F.X. 2006. Microalgal reactors: a review of enclosed system designs and performances. *Biotechnology Progress*, **22**(6), 1490-506.
4. Hindersin, S., Leupold, M., Kerner, M., Hanelt, D. 2014. Key parameters for outdoor biomass production of *Scenedesmus obliquus* in solar tracked photobioreactors. *Journal of Applied Phycology*, **26**(6), 2315-2325.
5. Linstrom, P.J. and Mallard, W.G. Eds., NIST Chemistry WebBook, NIST Standard Reference Database Number 69, National Institute of Standards and Technology, Gaithersburg MD, 20899, doi:10.18434/T4D303
6. Melis, A. 2009. Solar energy conversion efficiencies in photosynthesis: Minimizing the chlorophyll antennae to maximize efficiency. *Plant Science*, **177**(4), 272-280.
7. Patzelt, D.J., Hindersin, S., Elsayed, S., Boukis, N., Kerner, M., Hanelt, D. 2014. Hydrothermal gasification of *Acutodesmus obliquus* for renewable energy production and nutrient recycling of microalgal mass cultures. *Journal of Applied Phycology*, **27**(6), 2239-2250.
8. Pulz, O., Gross, W. 2004. Valuable products from biotechnology of microalgae. *Applied Microbiology and Biotechnology*, **65**(6), 635-48.
9. Stephens, E., Ross, I.L., King, Z., Mussgnug, J.H., Kruse, O., Posten, C., Borowitzka, M.A., Hankamer, B. 2010. An economic and technical evaluation of microalgal biofuels. *Nature biotechnology*, **28**(2), 126-8.
10. Williams, P.J.L., Laurens, L.M.L. 2010. Microalgae as biodiesel & biomass feedstocks: Review & analysis of the biochemistry, energetics & economics. *Energy & Environmental Science*, **3**(5), 554-590.